Role of intertissue mechanical interactions in the construction of the zebrafish olfactory circuit

P. Monnot

Sorbonne Université

Ecole doctorale Complexité du Vivant (ED515)

Institut de Biologie Paris Seine / Laboratoire de Biologie du Développement /

Equipe Forces mécaniques et développement du système nerveux

Institut Curie / Laboratoire Physico-Chimie Curie /

Equipe Physico-Biologie aux mésoéchelles

Rôle des interactions mécaniques entre tissus dans la mise en place du circuit olfactif du poisson-zèbre

Role of intertissue mechanical interactions in the construction of the zebrafish olfactory circuit

Par Pauline Monnot

Thèse de doctorat Sciences de la Vie

Dirigée par Marie Breau et Isabelle Bonnet

Présentée et soutenue publiquement le 17 juin 2021

Devant un jury composé de :

BONNET, Isabelle, Maitre de Conférences Sorbonne Université, Co-directrice de thèse

BREAU, Marie, Chargée de recherche INSERM, Directrice de thèse

DAVID, Nicolas, Chargé de recherche CNRS, Rapporteur

DEL BENE, Filippo, Directeur de recherche CNRS, Examinateur

FRANZE, Kristian, Professeur University of Cambridge (UK), Rapporteur

SUZANNE, Magali, Directrice de recherche CNRS, Examinatrice

Pour Aurélien, Catherine et Vincent,

« Je suis de ceux qui pensent que la science est d'une grande beauté. Un scientifique dans son laboratoire est non seulement un technicien mais il est aussi un enfant placé devant des phénomènes naturels qui l'impressionnent comme des contes de fées. »

Marie Curie

Acknowledgements

First, I would like to thank the members of my PhD jury: Nicolas David, Filippo Del Bene, Kristian Franze and Magali Suzanne for accepting to evaluate my work.

I am deeply grateful to Marie and Isabelle for choosing me to work on their project, for teaching me and training me on the techniques I used, for guiding me during three years and a half and for their support in my project but also in my career.

Thank you Marie for being greatly patient during my first months in the lab, when I was discovering almost everything from the zebrafish model to developmental biology. All along my PhD, you have been extraordinarily supportive and available for me, despite the huge amount of work you had as a young group leader. Participating in the genesis of your team has been a great human and scientific experience. You are really inspiring both as a researcher for your scientific skills but also as a team leader for your managerial qualities, listening to those you are working with.

Thank you Isabelle for all your help and encouragement during my PhD, and especially at times when I needed them the most. You have the ability to make physical concepts clear and simple, which really helped during the project and during the present manuscript writing.

I would like to show my greatest appreciation to all the past and present members of Marie's team. I want to express my gratitude to Karen for her contagious wonder at the living world and especially at the little beasts that surround us and for the passionate discussions we had on the best way to cycle from our neighbourhood to the lab. I also received generous support from Marion in the conceptualization of the project but also on the positive state of mind to keep. Thank you for your fighting spirit that you were able to transmit to me when I was downcast. I would like to thank Pénélope for her continuous support, for her good mood and for her permanent smile. It was great to know that I always had someone to count on to comfort me, to share a beer with or to chat on my latest silliness. I am also particularly grateful for the assistance given by Oxane during her internship on my project. Training and leading her has been a challenging but rewarding experience. Thank you to Girish and Bidesh for their work that paved the way for my project. Finally, I want to thank Melina for her amazing cakes, Camille for humming the Aristocats every day and Clara for making me laugh when she "lost her fishes" in the lab.

I want to thank our “sister” team at the IBPS, the team of Sylvie Schneider-Maunoury. Thank you Sylvie for your constructive comments, Christine for all your relevant questions that made me improve, Isabelle and Pierre-Luc for fighting to make the institute greener, Aline for your encouragements to combine private and professional life, Cécile for our interesting discussions, Antoine for defending the vegetarian cause, Morgane for your funny gif software and your great friendship. Thanks also to Martin, Ludovica, Diego, Hélène, Thassadite, Abraham and Alice.

I also want to thank the whole LBD and all the great people I met in the corridors, in the seminars or at the cafeteria. In particular, I would like to express my gratitude to the “Pôle gestion” for their efficiency and to the “Laverie” for their kindness. Thank you Séréna for sharing all the stressful and joyful moments of the PhD together. Thank you Alexis for distracting me all day long but also for helping me with all my technical issues on PCR gels or on my Fairphone and for putting up with all my stress.

I want to thank my team in Curie directed by Pascal Silberzan and Axel Buguin for integrating me even if I was most of the time at the IBPS. Special thanks to Nastassia and Mathilde for their support and their karaoke skills as we practiced at the Labex retreat.

I also thank the imaging platform of the Institut de Biologie Paris-Seine, in particular France, Suzanne and Jean-François, the Cell and Tissue Imaging core facility of the Institut Curie, and the IBPS aquatic platform for fish care, in particular Alex, Stéphane, Edouard and Jérémy.

I would like to thank the members of my “Comité de Suivi de Thèse”: Elisa Migliorini, Jean-Léon Maitre and Laurence Goutebroze for their constructive comments and for making me plan my future career.

Finally, I would like to thank my friends and family for showing all their support even if they did not fully understand what I have been studying for the last three years. Thank you for sending me postcards during the manuscript writing: Grand-père, Grand-mère, Mageo, Céline, Matthieu, Marie, Charlotte, Amélie, Lili, Luana, Marc-Antoine, Agathe, Céline G., Aude, Cathy you are wonderful. I would particularly like to thank my parents for encouraging me, inspiring me and for welcoming me whenever I needed to study in their office. Last but not least, I would like to thank Aurélien for supporting and encouraging me on a daily basis. I am glad that the last few months locked in the apartment with me writing did not discourage you to spend the rest of your life by my side.

Table of contents

Acknowledgements 5

Table of contents 7

List of abbreviations 9

Introduction 10

I. State of the art 12

A. Neuronal circuit formation and role of mechanical cues 13

1. Role of chemical cues in neuronal circuit formation 15

2. Role of mechanical cues in neuronal circuit formation *in vitro* 22

3. Role of mechanical cues in neuronal circuits formation *in vivo* 30

B. The zebrafish olfactory placode 36

1. Development of cranial placodes 36

2. Zebrafish olfactory circuit 44

3. Morphogenesis of the zebrafish olfactory placode 48

C. Intertissue mechanical interactions 63

1. Direct contact between the two tissues 65

2. Interactions mediated by the ECM 73

3. Key techniques 79

D. Zebrafish eye morphogenesis 85

1. General description of eye morphogenesis 85

2. Optic vesicle evagination 88

3. Optic cup invagination and RPE spreading 96

4. Lens coalescence 103

5. Extrinsic influences of surrounding tissues on eye morphogenesis 106

II. Goals 110

III. Results 112
A. Scientific article 112
B. Additional results 159
1. Additional results on the *rx3*$^{-/-}$ genetic condition 159
2. Perturbation of eye mechanical forces with additional conditions 163
3. Additional Material and Methods 168
IV. Discussion and perspectives 169
A. Which steps and parameters of eye morphogenesis are critical for OP formation? 170
B. The mechanical nature of the OP/eye interaction 176
1. Mechanical *vs.* chemical interaction 176
2. Measuring mechanical forces *in vivo* 183
3. Comparison with other examples of intertissue interactions 186
~~4.~~ Cooperation of traction forces with chemokine signalling 188
C. Role of the eye/OP interface 191
1. Role of the NCCs 191
2. Role of the ECM 192
D. Functional neuronal circuit formation 196
1. Mechanisms of stretch-induced axon growth 196
2. Olfactory circuit formation in the absence of eye 198
Conclusion 201
Bibliography 204
List of Figures 221
List of Tables 234

List of abbreviations

AFM: atomic force microscopy

AIS: axon initial segment

AP: anteroposterior

BMP: bone morphogenetic factor

CA: constitutively active

CAMs: cell-adhesion molecules

CNS: central nervous system

DN: dominant negative

dpf: days post-fertilization

DV: dorsoventral

ECM: extra-cellular matrix

ER: endoplasmic reticulum

EVL: enveloping cell layer

FGF: fibroblast growth factor

FRET: Förster resonance energy transfer

GFP: green fluorescent protein

GnRH: gonadotropin-releasing hormone

hpf: hours post-fertilization

HUA: hydroxyurea and aphidicolin

ML: mediolateral

MMP: matrix metalloproteinases

MZ: maternal zygotic

NC: neural crest

NCC: neural crest cell

Ngn1: Neurogenin 1

NR: neural retina

Omp: olfactory marker protein

OP: olfactory placode

OR: odorant receptor

OSN: olfactory sensory neurons

POM: periocular mesenchyme

PNS: peripheral nervous system

PPR: panplacodal region

PSM: presomitic mesoderm

RB: Rohon-Beard

RGC: retinal ganglion cell

RGD: arginylglycylaspartic acid

RPE: retinal pigmented epithelium

s: somites

TAAR: trace amine-associated receptor

TJ: tight junctions

UAS: upstream activation sequence

VR: vomeronasal receptor

wt: wild-type

YSL: yolk syncytial layer

1D, 2D, 3D: respectively one, two or three dimension(s)

Introduction

The generation of complex, multicellular organisms from a single cell is a fascinating biological process. An intricate and critical structure that forms throughout development of animals is the nervous system: a highly complex network of cells, functioning together to encode, process, store and transmit information to and from different parts of the body. The function of the nervous system is vital as it controls animal behaviours and coordinates them with external sensory inputs.

The correct wiring of the nervous system is essential for its proper function and relies on the ability of neurons to move to their final position and to grow neurites towards their appropriate synaptic partners. Brain heterotopia, lissencephaly or sublobar dysplasia are examples of brain malformation associated with abnormal neuronal migration (Barkovich et al., 2012), resulting in a wide range of clinical phenotypes often associated with mental retardation and severe neurodevelopmental delay. How do developing neurons migrate to their proper location, extend their axon in the correct direction and reach their target through their complex *in vivo* environment?

While neuronal circuit formation has been well studied from a chemical point of view, with numerous studies focusing on the chemical cues driving neuronal migration and axon growth, recent studies uncovered a crucial role of mechanical signals (including the mechanical properties of the environment such as stiffness, or the mechanical stresses applied to the growing neurons) in neuronal development. As most of these studies were conducted *in vitro*, there is a lack of information on the role of mechanical cues *in vivo*. My PhD project lies at the interface between biology and physics and is dedicated to investigate how mechanical forces influence neuronal movements and axon elongation to shape neuronal circuits *in vivo*.

To do so, I use the zebrafish olfactory circuit as a model. This circuit forms during the morphogenesis of the olfactory placode (OP). OP progenitors are initially located in two paired elongated domains surrounding the brain and coalesce into compact and spherical neuronal clusters. In each domain, cells from the extremities converge towards the centre of the placode by migrating along the brain wall (convergence movements), while central cells move laterally, away from the brain surface (lateral movements). During this second movement, cell bodies move away from their axon tips that remain attached to the brain's surface, thus inducing the

retrograde extension of OP axons. The lateral displacement of cell bodies away from axon tips appears to be a passive, non-autonomous process driven by extrinsic mechanical forces. In parallel, the underlying eye tissue undergoes drastic morphogenetic movements (evagination and invagination) during OP morphogenesis and represents a good candidate to exert these extrinsic forces. What is the mechanical contribution of eye morphogenesis in OP lateral movement and axon elongation?

My PhD project aims at answering this question and this manuscript presents the work I carried out during three years and a half under the supervision of Marie Breau and Isabelle Bonnet. The first chapter presents the state of the art and focuses on the scientific literature on four main topics: chemical and mechanical cues in neuronal circuit development, the zebrafish olfactory circuit and its development, intertissue mechanical interactions during morphogenesis, and the known mechanisms of zebrafish eye formation. The second chapter presents in detail the three specific goals of my PhD project designed to study the contribution of eye morphogenesis to olfactory circuit formation. The third chapter details the results obtained as presented in our research article “Intertissue mechanical interactions shape the olfactory circuit in zebrafish” as well as additional, unpublished results. Finally, the fourth chapter discusses these results and suggests future perspectives to pursue the present study.

I. State of the art

Our work on the mechanical contribution of eye morphogenesis to olfactory circuit formation in zebrafish is based on numerous previous studies in developmental biology. The first chapter of this manuscript (I) is dedicated to the state of the art and is divided in four sections. In the first section of this chapter (I.A), chemical and mechanical cues known to influence neuronal migration and axon growth during development will be presented, with a specific focus on recent studies investigating the role of mechanical cues in neuronal circuit formation *in vivo*. The second section (I.B) will describe our model system: the zebrafish olfactory circuit and its development within the OPs. At the end of this section, we will see that previous work from Breau and colleagues suggests that extrinsic mechanical forces drive neuronal migration and axon elongation in the developing OPs. These forces may come from surrounding tissues and the third section (I.C) focuses on known examples in the literature that describe such mechanical intertissue interactions contributing to morphogenesis. In particular, we will review key techniques used to examine how the forces generated by a tissue can shape a second, neighboring tissue. In our case, a potential generator of the extrinsic forces exerted on the placode is the adjacent eye tissue, which undergoes morphogenesis at the same time. The fourth and final section (I.D) is a brief overview of the main cell movements and cell shapes changes driving zebrafish eye morphogenesis.

A. Neuronal circuit formation and role of mechanical cues

The animal nervous system is a complex network of neurons, glial cells and their surrounding matrix that encodes, processes, stores and transmits information to and from different parts of the body. In vertebrates, the nervous system is divided in two main parts: the central nervous system (CNS) composed of the brain and the spinal cord and the peripheral nervous system (PNS) composed of numerous ganglia and nerves in the body periphery (Suter and Jaworski, 2019). In order to coordinate the external signals with animal behaviour, the nervous system processes information through three main steps: the collection of environmental information through sensory neurons and associated nerves, the evaluation of their relevance and of the required action into the brain, and the transmission to convey the decision to the motor unit through motor nerves (Maiorana and Van Valen, 2020).

Such an organization to allow the processing of high amount of information requires an exceptionally complex network of neurons. The nervous system is built from two broad categories of cells: neurons, which process and transmit information, and glial cells, which form a cellular framework that permits the development of the rest of the nervous system, and regulate neuronal survival and differentiation (Jessen, 2004). Neuron cell bodies (or soma) occupy well-defined locations within the organism and are connected with each other through polarised cytoplasmic projections called neurites. The term neurite refers to the axon, the dominant process which propagates the information in the circuit and transmits it to its target(s), and to dendrites which receive the information and transmits it to the soma. Inter-neuronal communication takes place at specialised contact areas called synapses (Figure 1).

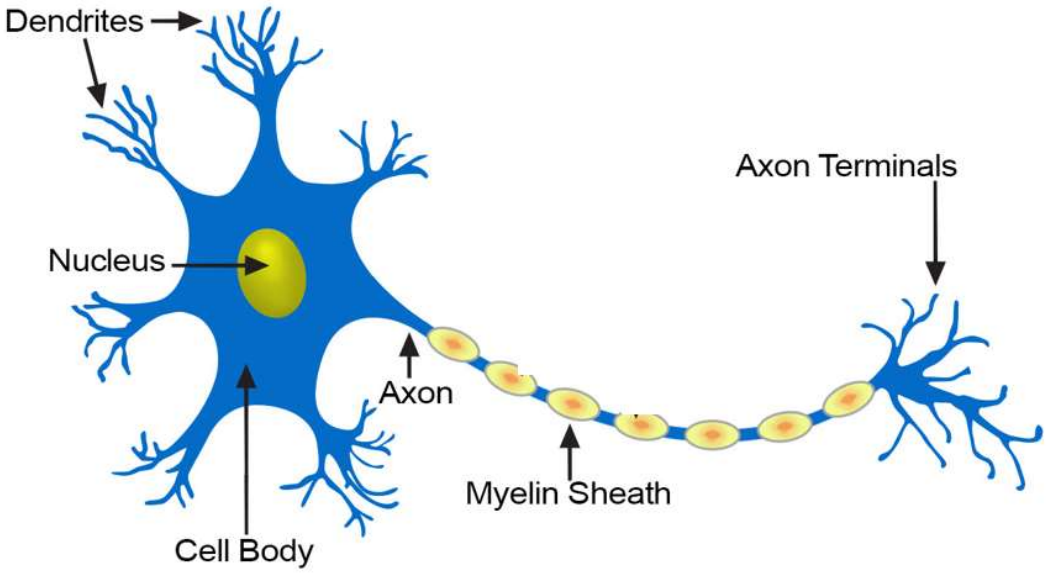

Figure 1: **Structure of a typical neuron** with the cell body (soma) and the neurites, comprising the dendrites and axon covered with myelin sheaths. (NIH-Website, 2021)

To illustrate the complexity of the nervous system with numbers, an average adult human brain contains 100 billion neurons making around 1.5 x 10^{23} synaptic connections (Herculano-Houzel, 2009; Pakkenberg et al., 2003). At 7 days post fertilization (dpf), the zebrafish larva contains already around 100 000 neurons (Hill et al., 2003). The correct wiring of the nervous system is essential for its proper function and relies on the ability of neurons to migrate to their final position and to grow neurites towards their appropriate synaptic partners. How do developing neurons extend their axon and dendrites in the correct direction and reach their target through their complex *in vivo* environment?

In this section, we will see that axonal protrusions read and follow a series of different guidance cues in order to grow and make synapses with the right partners during the development of neuronal circuits. We will first take a look at the well-studied chemical cues governing axon pathfinding. We will then discuss *in vitro* studies showing the importance of mechanical cues in addition to this chemical signalling, through mechanical properties of the substrate on which the axons migrate, or *via* mechanical forces applied to the growing axons. We will finally focus on what is currently known about the role of mechanical cues in shaping neuronal circuits *in vivo*.

1. Role of chemical cues in neuronal circuit formation

• Diversity of neuronal guidance mechanisms

After neuronal progenitors have migrated to their final location in the organism, they start to emit multiple and undifferentiated protrusions. One of them will specify into the axon and extend in the direction of its target, to which it will connect and form a synapse. Chemical cues driving this process of axon elongation and guidance have been studied since the late 19th century when Cajal first discovered "a cone-like lump with a peripheral base" at the tip of the extending axon. He called this specialized, dynamic, and cytoskeletal-rich structure the growth cone. As an attempt to explain how a nerve cell develops, forms its connections and displaces its cell body, he hypothesised that the growth cone might be guided by chemical cues in the extracellular environment (Cajal, 1909; Garcia-Marin et al., 2009).

Over a 100 years of research confirmed the hypothesis that growth cones are able to select the correct path towards their target by responding to the appropriate set of cues, and revealed a variety of axon guidance mechanisms (as illustrated in Figure 2). Chemical cues can operate either at short or long range: short range guidance requires direct contact between the growing axon and the cells that provide the guidance cue (Brankatschk and Dickson, 2006) while the distance between the source of long range cues and their target may vary between a few cells to a whole tissue (Wu et al., 2019). Chemical guidance cues can be either chemoattractive or chemorepulsive. They are capable of regulating interactions between axons and their underlying substrates but also of influencing the bundling or unbundling of axons together into nerves, through fasciculation or defasciculation processes (Kolodkin and Tessier-Lavigne, 2011).

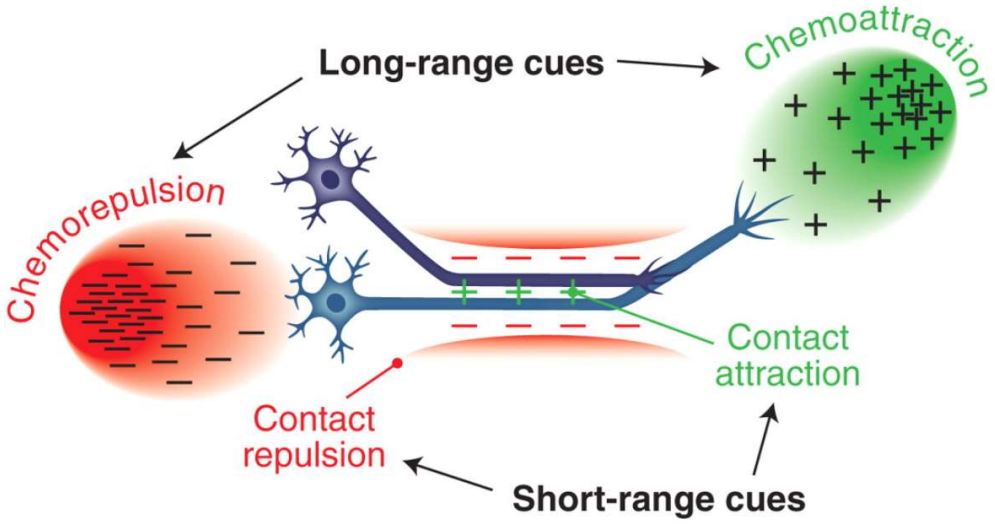

Figure 2 : **Schematic illustration of the diversity of neuronal guidance mechanisms**. Neuronal processes are guided by chemical cues that can function at long and short distances to mediate either attractive or repulsive guidance. (Kolodkin and Tessier-Lavigne, 2011)

This variety of mechanisms is associated with a range of axon guidance molecules among which Netrins, Slits, Semaphorins, and Ephrins represent conserved well-known families of proteins (Dickson, 2002; Kolodkin and Tessier-Lavigne, 2011).

- **Conserved families of guidance molecules**

Netrins are a small family of phylogenetically conserved secreted proteins. They have initially been identified as chemo-attractants for commissural axons in chick embryos and rat explants (Kennedy et al., 1994) and for circumferential axon guidance in *Caenorhabditis elegans* (Hedgecock et al., 1990). Recent studies showed that Netrins can function as both short-range and long-range guidance cues, even within the same system (Wu et al., 2019). Netrin receptors DCC and Unc5 participate in both attraction and repulsion, or only in repulsion, respectively.

Slits are large secreted proteins that signal through Roundabout (Robo) family receptors. Slits have been first implicated in axon guidance when searching for an axon repulsive cue in *Drosophila* midline (Kidd et al., 1999). Slits, like Netrins, are bifunctional, since they are also involved in promoting axon elongation in other contexts, as shown *in vitro* (Wang et al., 1999).

Semaphorins are a large, phylogenetically conserved family of proteins divided into eight classes, on the basis of their structure: classes 1 and 2 are found in invertebrates, classes 3 to 7 in vertebrates, and class V semaphorins in viruses (V for virus, not represented in Figure 3A).

As shown in Figure 3A, some semaphorins are secreted guidance molecules while others are transmembrane proteins. Semaphorin role in axon guidance has been first shown in grasshopper (Kolodkin et al., 1992). Many Semaphorins can function as both attractive and repulsive cues, and even the same Semaphorin may under certain circumstances serve in both capacities (Dickson, 2002). Semaphorins signal through multimeric receptor complexes during the establishment and maintenance of neuronal connectivity. The variability of potential receptors suggests that the function of Semaphorins, either as repellents or attractants, could actually depend on the use of different receptor complexes and thus the activation of distinct intracellular signalling pathways within the growing axon (Kolodkin and Tessier-Lavigne, 2011).

Ephrins are cell-surface signalling molecules divided into two classes: Ephrin-As, which are anchored to the membrane by a glycosylphosphatidylinositol linkage and bind EphA receptors; and Ephrin-Bs, which have a transmembrane domain and bind EphB receptors. Their role in axon growth and axon pathfinding has been first discovered in cultures of vertebrate retinal ganglion cells (RGCs) where Ephrin induced growth cone collapse and repulsion of RGC axons (Drescher et al., 1995). Like the other three families of chemical cues, Ephrins can mediate either attraction or repulsion. Because Ephrins do not appear to be active when not bound at the cell surface, they probably function only as short range guidance cues, which is not the case for the three other families that have been found to function both as short-range signals, staying in close proximity with the cells that produced them, and as long-range signals, diffusing from their source (Kolodkin and Tessier-Lavigne, 2011).

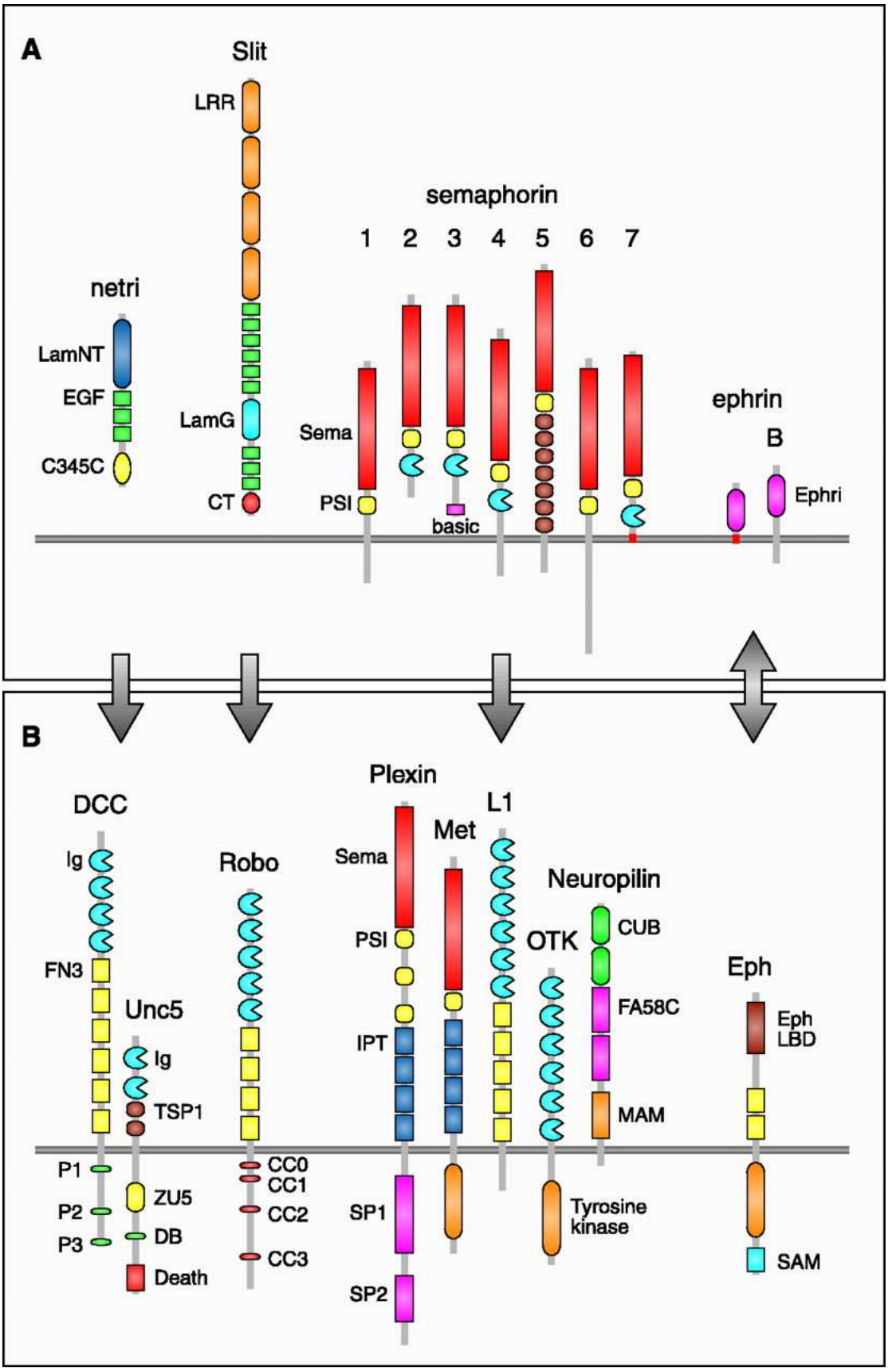

Figure 3: **Conserved families of guidance molecules (A) and their receptors (B)**. (Dickson, 2002)

The four families described above illustrate the diversity of chemical cues driving axon growth, pathfinding and fasciculation. When the axon meets these guidance molecules, different signalling pathways are activated, most of them involving the small RhoGTPase proteins, RhoA, Rac and Cdc42, which in turn control the cytoskeleton organization (Lowery and Van Vactor, 2009). The recognition of these molecules, the activation of the downstream signalling cascades and finally the direction change mainly occurs in the axon tip, the growth cone (Mortimer et al., 2008; Short et al., 2021).

- **The growth cone**

Not only does the growth cone translate environmental signals into directional movement – a function called "navigator" in (Lowery and Van Vactor, 2009) – but it also acts as a motor for the rest of the axon as it propels the axon shaft forward – a function called "vehicle". To give a picture, the growth cone can be seen as both the steering wheel and the engine of the extending axon.

In order to achieve these functions, the growth cone is composed of dynamic cytoskeletal components that determine its shape and movement on its journey. At its distal edges are finger-like filopodia, narrow cylindrical membrane extensions capable of extending tens of microns from the periphery of the growth cone. They are separated by sheets of membrane called lamellipodia-like veils (Lowery and Van Vactor, 2009) (Figure 4a). The growth cone can be separated into three domains based on the cytoskeletal distribution: the peripheral (P) domain, composed primarily of lamellipodia and filopodia; the central (C) domain, invested by stable, bundled microtubules that enter the growth cone from the axon shaft, in addition to numerous organelles and vesicles, and the transitional (T) domain at the interface of the P domain and the C domain (Dent and Gertler, 2003) (called periphery, transition zone and central zone on Figure 4a).

In response to attractive or repulsive chemical cues, axons exert mechanical forces on their environment in order to move: this is the vehicle function of the growth cone. K. Franze reviewed the intrinsic forces driving growth cone motility and suggested the following model (Figure 4). The addition of new actin monomers to the growing barbed ends of actin filaments in the filopodia results in a compressive polymerization force, F_P in the P domain (Figure 4b,c). At the same time, in the C domain, myosin II motors pull on the actin filaments, generating a contractile force F_C. The myosin-mediated contractile forces, F_C, and the actin-mediated

polymerization forces, F_P lead to a constant retrograde flow of actin filaments away from the P domain (where actin polymerizes) towards the C domain (where actin depolymerizes).

Moreover, actin filaments in the growth cone are coupled to the extracellular environment by so-called point contacts, composed of a large number of adaptor and signalling proteins such as cell-adhesion molecules (CAMs) serving as molecular clutches. It is *via* these clutches that the forces generated within the growth cone are transmitted to the surrounding environment. At low clutch engagement, there is a fast retrograde actin flow and the growth cone does not move much. At high clutch engagement, retrograde actin flow slows down, actin polymerization pushes the membrane forward, the traction force of the growth cone on its substrate, F_T, increases, and the growth cone advances. Thus, the growth cone advance depends on the level of clutch engagement, enabling fast adaptation to changes in the environment (Franze, 2020).

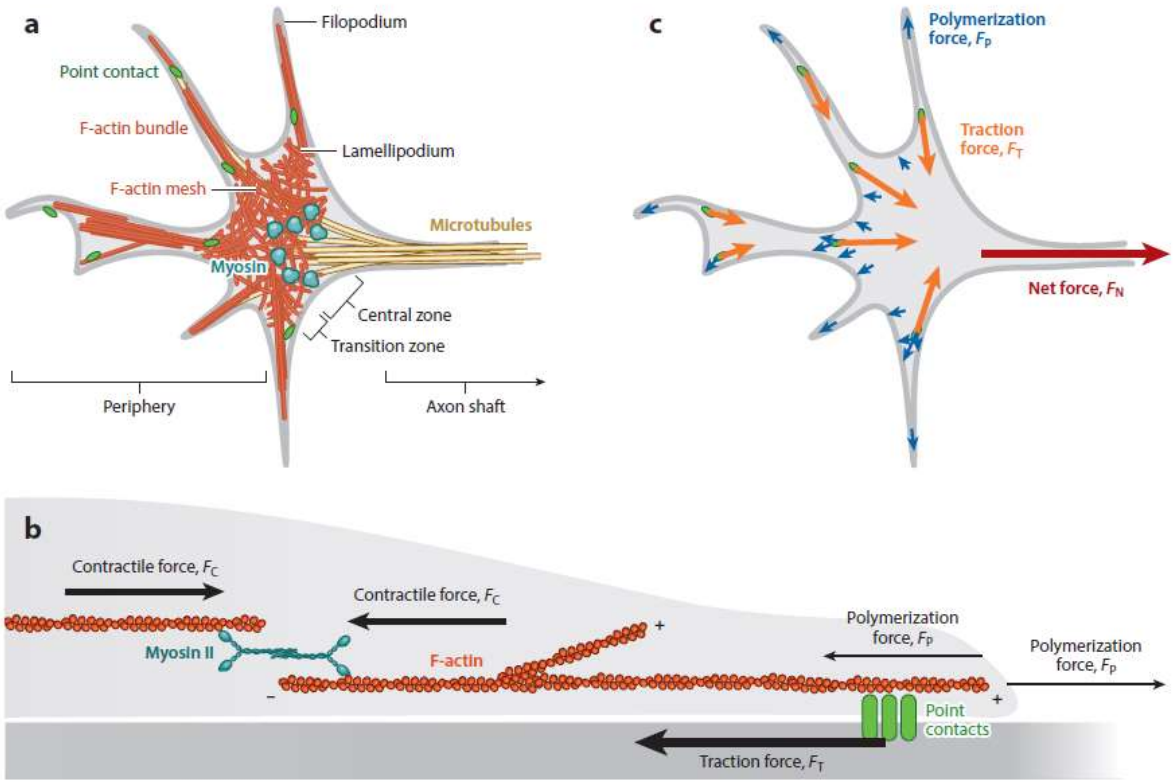

Figure 4: **Structure of the growth cone and origin of forces**. (a) Schematic drawing of a neuronal growth cone and its cytoskeleton divided in the P domain (periphery), the T domain (transition zone) and the C domain (central zone). "*Actin filaments (red) are connected to the extracellular environment via molecular clutches, which are assembled in point contacts (green). Point contacts are found mainly in the P domain, while myosin II motors (cyan) are*

localized in the C domain." (b) Schematic drawing of force generation within growth cones. (c) Schematic drawing of forces acting in growth cones. The length of the arrows correspond to the strength of the represented forces. (Franze, 2020)

In vivo, the journey of an axon towards its final target often involves several chemical cues that act sequentially. On one hand, fine-tuned expression of chemical cues in a particular location and at a specific developmental stage is required for selective guidance. On the other hand, sequential responses to several guidance cues encountered by axons as they extend are needed for complex pathways to develop. The axon cellular response itself evolves over time by abolishing its response to certain cues and acquiring responsiveness to others at key choice points (Kolodkin and Tessier-Lavigne, 2011). After reaching an intermediate target, changes at the transcriptional, the translational, or the protein/post-translational levels enable growth cone to modify its surface receptors for the next stage of its trajectory (as reviewed in (Stoeckli, 2018)).

- **Neurotaxis mediated by chemical or physical cues**

In this part, we have seen that chemical gradients mediate neuronal circuit formation by enabling axons to determine proper paths and grow towards their destination. Axon elongation can occur through chemotaxis, when the movement is induced by gradients of soluble molecules or by haptotaxis, when it is induced by gradients of substrate-bound molecules. However, describing neuronal network formation with only genes and biomolecules is "like you're trying to write a book with only half the letters of the alphabet" (Dance, 2021). In addition to these two chemical-taxis phenomena, the influence of physical cues, such as durotaxis (the motion is induced by rigidity gradient) and topotaxis (the motion is directed by topographical gradients) has been increasingly reported (Seo et al., 2020) (Figure 5). In the following parts, we will see processes in which mechanical cues can also play a role in shaping neuronal circuits, focusing on the rheological properties of surrounding tissues and on the forces exerted on the neurons.

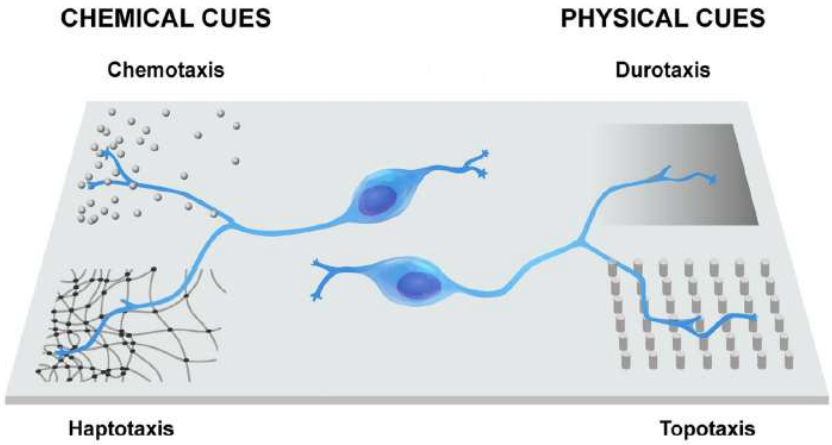

Figure 5: **Schematic representation for the neuronal movements in the environmental gradients**. (Seo et al., 2020)

2. Role of mechanical cues in neuronal circuit formation *in vitro*

Mechanical cues involved in neuronal migration and wiring include the mechanical properties of the surrounding environment in which the axons are migrating, and external or internal mechanical forces applied to these growing axons. *In vitro* studies enable to investigate independently the role of these two types of mechanical cues in rather simple systems compared to *in vivo* models and help determine what may be critical or not for neuronal development.

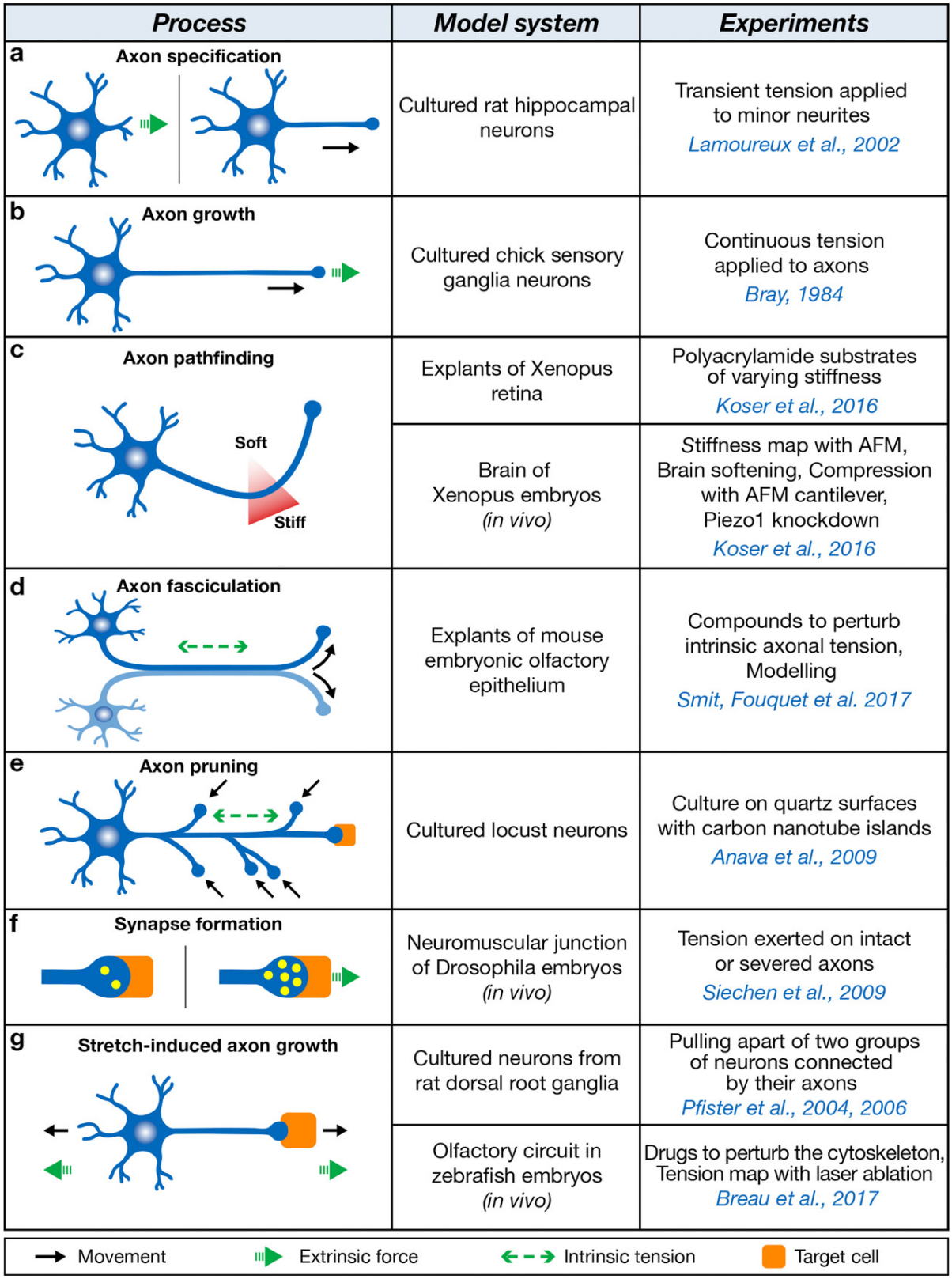

Figure 6: **Examples of mechanical cues involved in axon and synapse development**. (Gangatharan et al., 2018)

- **Mechanical properties of the environment**

First of all, we will briefly define a few terms used in rheology. Stress is the external force acting on an object per unit area, it is expressed in Pascal (Pa, 1 Pa=1 $N.m^{-2}$): the stress σ causes the deformation. Strain, the result of stress, measures the degree of deformation, it is dimensionless and often written with the greek letter ε (Franze et al., 2013). When materials are elastic, they have the property to return to their original shape if forces causing deformation are removed. For sufficiently small stress, strain will be proportional to the stress through the elastic modulus, whose value depends on the material being deformed but also on the nature of the deformation:

$$elastic\ modulus\ (Pa) = \frac{\sigma}{\varepsilon}$$

The module of elasticity in tension is called Young's modulus and is often denoted E: it characterizes how a linear elastic material reacts to tensile stress (tension or compression) (Petridou and Heisenberg, 2019). E is expressed in Pascal and relates the deformation of a material to the stress required to deform it: a stiff material needs more force to deform (and thus has a higher Young's modulus) compared to a soft material. As an example, 1 kPa is equivalent to 100 kg force per square meter.

Biological tissues exhibit a wide range of rigidities from stiff bone (around 20MPa for humans) to soft fat tissues (around 1kPa for humans), and brain tissues are among the softest ones (1-4kPa for humans) (Butcher et al., 2009; Handorf et al., 2015). Taking into account these variations in the rheological properties is highly important in order to have a complete picture of neuronal circuits formation.

Several *in vitro* studies shed light on the role of substrate stiffness in different steps on neuronal wiring. While most cell types spread more, migrate more and make larger focal adhesions on stiff substrates than on soft ones (as reviewed in (Gupta et al., 2016)), for cultured neurons, the lower the stiffness of the agarose gel is, the faster the neurites extend on its surface (Balgude et al., 2001). Moreover, neurons grown on softer substrates form more branches than those grown on stiffer gels, indicating that stiffness is also important for neurite branching (Flanagan et al., 2002). The stiffness also appears to control the balance between neuronal and glial populations as soft gels, (with elastic modulus of several hundred Pa), in the same range of stiffness as the one measured for intact rat brain, encourage attachment and growth of neurons while

suppressing astrocyte growth (Georges et al., 2006). These neuronal mechanosensing abilities were also confirmed dynamically when changing over time the stiffness of the substrate by using a DNA-crosslinked hydrogel (Jiang et al., 2010). On top of its role in neurite elongation, neurite branching and cell type balance, substrate stiffness has also be found *in vitro* to modulate synaptic activity and electrophysiological activity (Lantoine et al., 2016).

Neuronal mechanosensitivity appears well controlled albeit complex as comparison of different neuron populations, emanating from tissues with various rigidity properties, revealed differential behaviours and an adaptation of cytoskeletal dynamics to substrate stiffness in growth cones (Koch et al., 2012) (Figure 7). Altogether, these studies highlight the influence of the mechanical properties of the environment on neuronal navigation and wiring during embryonic development.

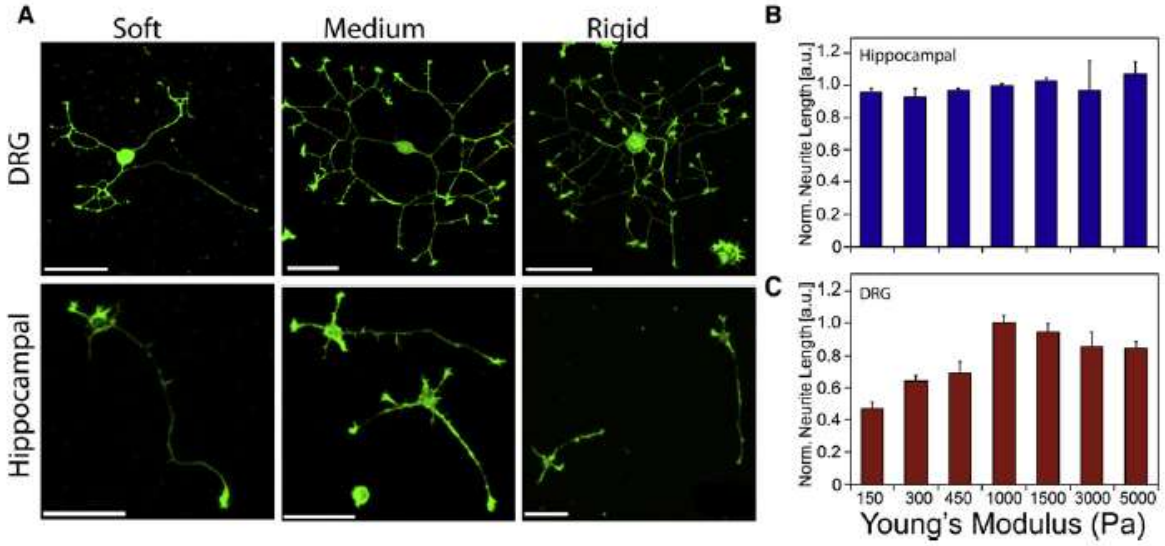

Figure 7: **Cultured neurons from different neuronal tissues respond differently to the stiffness of the substrate.** *"(A) Dorsal root ganglion (DRG) and hippocampal neurons grown on soft (300 Pa), intermediate (1000 Pa), and rigid substrates (5000 Pa), fixed and stained for actin filaments at 8 h (DRG) or 24 h (hippocampal). Scale bars are 10 mm. (B and C) Neurite outgrowth of hippocampal (B) and DRG (C) neurons on Laminin-coated polyacrylamide substrates of different stiffness. Total neurite length is normalized to the mean value at 1000 Pa to allow for comparison between independent experiments. Values represent the mean of at least three independent experiments. Error bars indicate the standard errors."* (Koch et al., 2012)

- **Mechanical forces**

Like environmental mechanical properties, the application of external forces can also control axon development and the role of external forces on axon specification, growth, and pruning has been assessed in neuronal cultures. The response of axons to mechanical stress has been hypothesised long ago by Paul Weiss who suggested that neurites respond to mechanical tension *in vivo*, during embryonic development, the tension being applied by the growth of the organism (Weiss, 1941). Around 40 years later, experiments on cultured sensory neurons from chick dorsal root ganglia showed that pulling on growing neurites changes their direction of extension to align with the direction of the applied force (Bray, 1979). This is accompagnied by an increase of the length and the volume of the pulled neurite (Figure 6B). Thus, neurons are able to detect exerted mechanical constraints and respond by stimulating the addition of novel material, membranes and cytoskeletal components: neurites respond to the force in a non-elastic fashion (Lamoureux et al., 2010). Unlike growth cone-mediated extension, where material is added in the protrusion at its distal end, the so called "towed" growth displays material addition in different regions all along the shaft of the neurite (Zheng et al., 1991).

Moreover, the application of a traction force on a rounded neuronal cell has been shown to be sufficient to initiate a neurite (Bray, 1984), a result later confirmed by pulling on small neurites in cultured rat hippocampal neurons (Anthonisen et al., 2019; Lamoureux et al., 2002) (Figure 8). The growth cone of these *de novo* initiated neurites were capable of normal motility (Zheng et al., 1991) and acquired axonal fate (Lamoureux et al., 2002). Indeed, when there is no more force applied, the neurites continued to elongate, showing axon features including rapid growth cone advance and expression of early axonal markers (Lamoureux et al., 2002). This was all the more surprising since it was previously thought that axonal fate was induced by neurite length (Dotti and Banker, 1987). Instead, Lamoureux and colleagues work suggests that mechanical tension and not length determines the specification of the axon among the multiple neurites (Figure 6A). In the absence of external pulling forces, axon specification could be due to an active internal tension within the neurite itself as several studies show that there exists a finite intrinsic tension in *in vitro* and *in vivo* neurons, which is generated by the cytoskeleton (Bernal et al., 2010; Bernal et al., 2007; Lamoureux et al., 1989; Rajagopalan et al., 2010; Tofangchi et al., 2016; Van Essen, 1997).

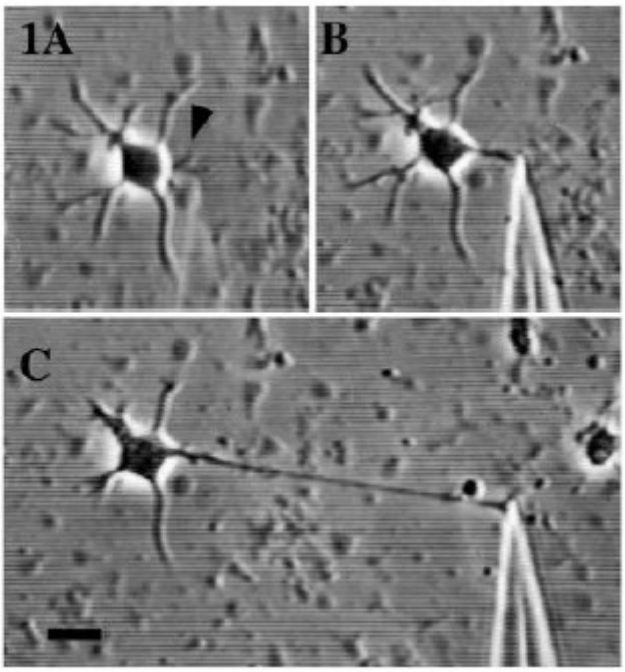

Figure 8: **Elongation of a minor process induced by experimentally applied tensile force**. *"(A) Neuron immediately before needle application. Arrowhead marks short process to which needle was attached. (B) Same neuron 30 min later during early stage of neurite towing. (C) 5 h 40 min after B, at the end of towing. The scale bar is 20 µm."* (Lamoureux et al., 2002)

Beside its role in defining the axon among multiple neurites, mechanical tension may also be critical in another phase of neuronal wiring: the removal of redundant neuritic branches, a process called axonal pruning. This role was uncovered in locust neurons cultured on surfaces with isolated anchoring sites to which the cells and the neurites could mechanically attach. This culture system led to the straitening of developing axons as their growth cone attaches to the substrate or to the neurites of a target neuron, suggesting a build-up of intrinsic mechanical tension. This increase of tension was further followed by the retraction of the unattached axonal collateral branches (Anava et al., 2009) (Figure 6E). Thus, mechanical tension could serve as a signal for the maintenance of the axonal branch and perhaps for the subsequent formation of synapses, but further experiments allowing the estimation of the tensile stresses in parallel to the examination of synapse functionality are needed to confirm this hypothesis (Gangatharan et al., 2018).

In many organisms and especially in vertebrates, there is a high number of neurons generated in various locations in the organism, which need to project collectively from one area to another. Growing as a fasciculated bundle enables large numbers of axons to navigate collectively

through the system and to eventually separate in order to target specific cells. Thus, control of axon fasciculation and defasciculation is essential in shaping neuronal circuits in complex organisms. Using explants of mouse olfactory epithelium, it has been observed that axons dynamically interact with each other through their shafts, leading to zippering and unzippering behaviours that regulate their fasciculation. Surprisingly, this zippering and unzippering occurred without any involvement of the growth cones, which were previously thought to be the sole regulators of fasciculation and defasciculation (Honig et al., 1998). Pharmacological treatments, tensile force measurements, and biophysical modelling, revealed that axon zippering, and by extension fasciculation, is favoured by axon–axon adhesion whereas an increase in mechanical tension within the axons promotes unzippering, and thus defasciculation (Figure 6D). This study brought to light the role of mechanical tension in regulating axon fasciculation (Smit et al., 2017).

Following the formation of a synapse between the axon and the target cell, the animal usually continues to grow, which irremediably results in an increase in the distance between the cell body and the synapse. This second phase of axon elongation, which is synchronized with the expansion of the growing body, is crucial since it contributes to an important proportion of the final axon size. The axon stretcher system developed by Pfister *et al.* enables to study this stretch-induced axon growth by pulling apart the two sides of neurons that have already established synapses with target cells (Pfister et al., 2004). The axons could be stretch-grown without rupture or disconnection with the target, and at much higher rates (8 mm/day) than the ones reported for growth cone-mediated axonal growth (~1 mm/day) (Figure 9). Remarkably, the stretched axons exhibit larger diameter than the non-stretched axons while the density of cytoskeletal constituents and organelles was not affected (Figure 6G). The stretched axons also appeared fully functional with the maintenance of the same resting potential and the ability to propagate action potentials (Loverde and Pfister, 2015; Pfister et al., 2006). Transcriptional analysis of control *vs.* stretched axons revealed an adaptive cellular stress response with gene regulation induced by the application of traction force (Loverde et al., 2020). Similarly, forces as small as 10 pN, generated by moving magnetic nanoparticles anchored to the cells with a magnetic field, were sufficient to induce axon growth. These stretch-grown axons were also found to increase microtubule density and they exhibited stimulated axonal branching, glutamatergic synaptic transmission, and neuronal excitability (De Vincentiis et al., 2020a). Altogether, these studies demonstrated that the extreme “stretch growth” of axon tracts by mechanical stimuli does not affect their function and even more promotes a thickening of the

axon (Pfister et al., 2004) and an increase in ion channel density, probably to preserve the fidelity of neuronal signalling (Pfister et al., 2006). These properties enable the axon to accommodate and adjust to the continuous growth of the whole organism.

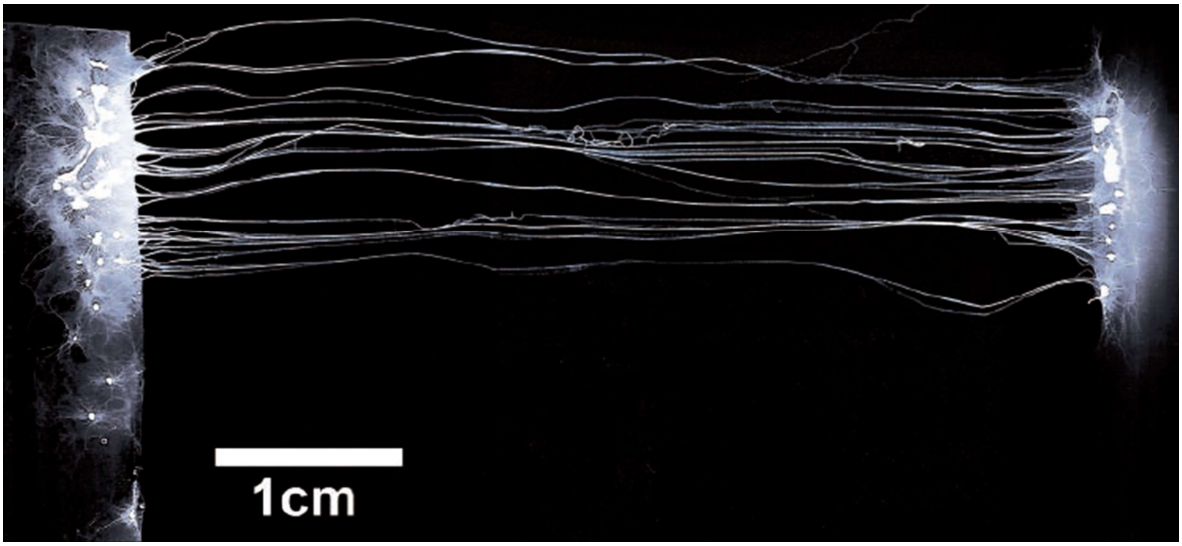

Figure 9: **Axon tracts grown to 5 cm long by artificial stretch growth.** *"Axon tracts (middle) bridge two populations of neurons (left and right). Before the initiation of stretch growth, the two populations of neurons were adjacent and the bridging axons were only about 100 µm long. Progressively separating the neuron populations induced mechanical tension on the axon tracts, resulting in enormous and rapid growth (colors are inverted to highlight axon tracts)."* Adapted from (Pfister et al., 2004)

The development of a range of technological devices to apply mechanical forces on developing neurons *in vitro* made possible the study of mechanical forces in neuronal circuit development. The examples described above show that the application of external force influences every phase of neuronal growth, such as specification, elongation, pruning and fasciculation of axon in neuron culture (Figure 10). Yet, what is the role of mechanical cues *in vivo*? How do the stiffness of the environment and mechanical forces mediate the shaping and the connectivity of neuronal circuits in developing organisms?

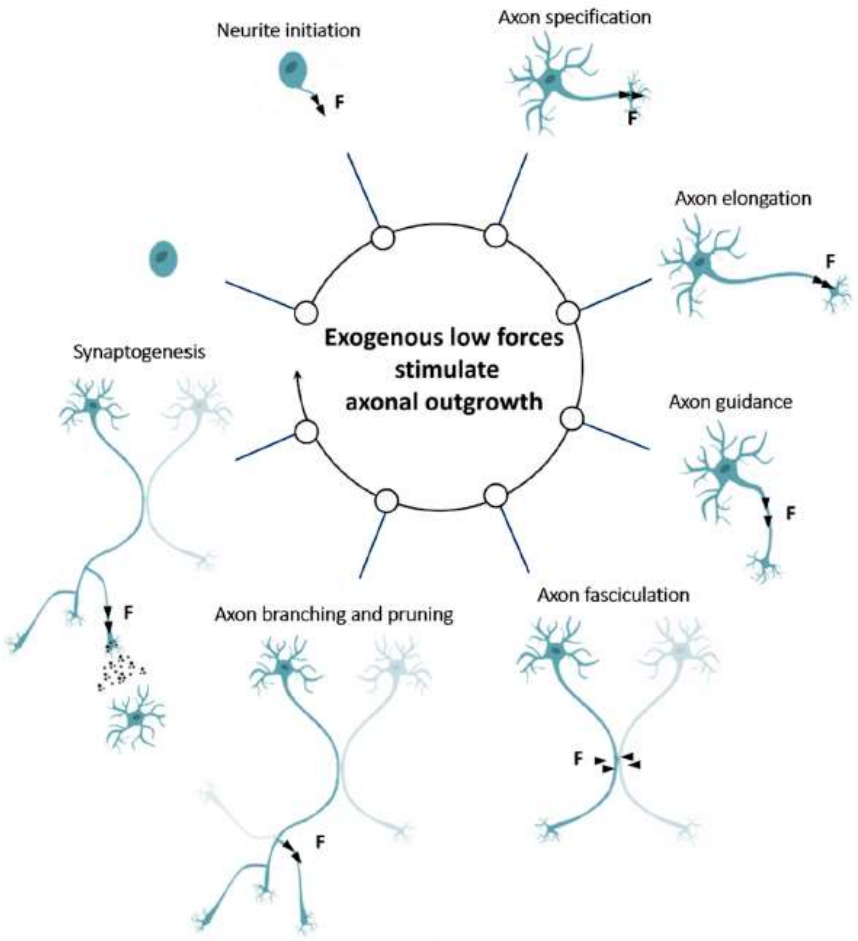

Figure 10: **Mechanical forces influence every phase of neuronal growth**. (De Vincentiis et al., 2020b)

3. Role of mechanical cues in neuronal circuits formation *in vivo*

As there are more and more *in vitro* studies on the role of mechanical signals in setting up neuronal circuits, there are much less *in vivo* studies, particularly because of the complexity of looking at a whole developing organism. Here we present three *in vivo* studies where neuronal circuit formation has been shown to be influenced by either the mechanical properties of the environment or by mechanical forces exerted by surrounding tissues.

- **Influence of the substrate stiffness**

Combining *in vivo* and *ex vivo* approaches, Koser *et al.* (2016) found that local substrate stiffness regulates axon pathfinding. They used the *Xenopus* optic pathfinding as a model, where RGC axons navigate in the brain to reach the optic tectum. Atomic force microscopy

(AFM), a classical tool used in material engineering, was used here to measure the rheological properties of the brain along the axonal path. The principle is the following: a nano-indenter, the cantilever, pushes on the sample across a small contact area and provides information on its mechanical properties such as stiffness. Measuring brain surface stiffness in live *Xenopus* embryos pointed out the presence of a stiffness gradient. The direction of the gradient coincides with the direction of the growth of RGC axons that turns towards softer tissues. This axon growth directed towards soft regions was reproduced *ex vivo* in the absence of chemical gradients. Stiffening of brain areas by applying a sustained compressive force using the AFM probe, and pharmacological inhibition and knock-down of the mechanosensitive ion channel Piezo1 resulted in aberrant axonal growth and pathfinding errors. However, as these two approaches are global perturbations, it will be important to further analyse whether Piezo1 functions specifically in the developing neurons and/or in the surrounding brain.

Based on these observations, the authors suggested a model of mechanical control of RGC axon growth (Figure 11). First, axons encounter stiff tissues and navigate with a straight trajectory. Then, a brain stiffness gradient leads to a differential speed within the axon bundle: the speed of axons on the softer side is reduced while the one on the stiffer side is increased, thus guiding axon turning toward softer tissues. Finally, softer tissues in the optic tectum facilitate axonal slowdown, unbundling and branching (Koser et al., 2016).

Focusing on the formation of this stiffness gradient in the brain, a follow-up study by the same group showed that local tissue stiffness changes significantly (with almost a 10-fold increase within 3 hours) during development and that this change correlates with the change in the angle of the axon path. The authors attributed the gradient of tissue stiffness to cell density as stiffer regions contained more cells than softer ones and perturbation of cell proliferation disturbed both stiffness gradient and axon pathfinding (Thompson et al., 2019). Altogether, these data suggest that local tissue stiffness, related to cell density, is sensed by neurons through mechanosensitive ion channels, which in turn influence axon pathfinding (Figure 6C).

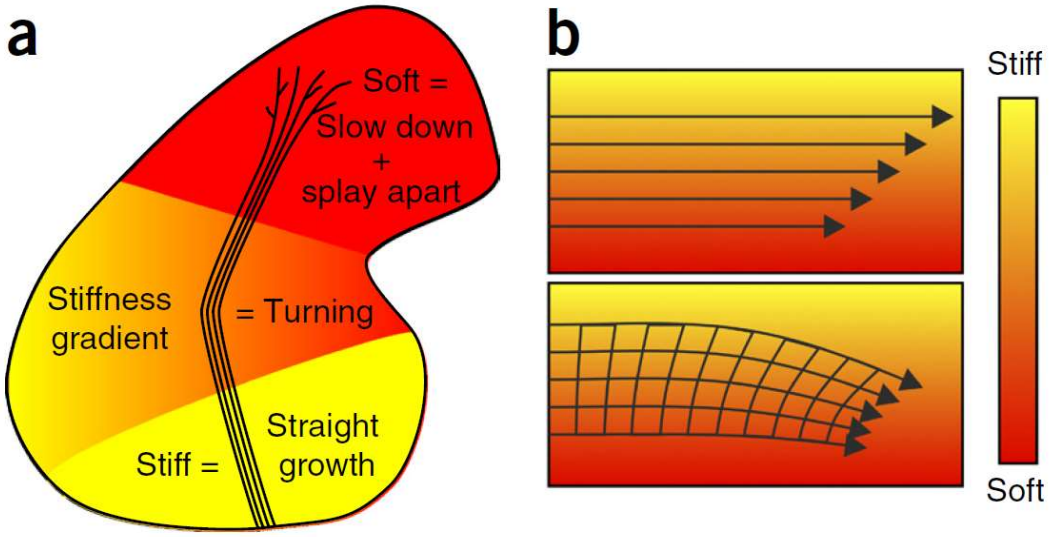

Figure 11: **Schematics of the proposed mechanism for axon pathfinding depending on surrounding brain stiffness.** (a) Outline of a Xenopus brain and the optic tract. (b) *"Schematic illustration of a mechanism by which axon bundles encountering a perpendicular stiffness gradient might turn toward the softer side of the substrate."* (Koser et al., 2016)

A remaining question is whether chemical signalling and mechanical signalling coordinate in order to guide axons during development. In this example, some brain cells in the vicinity of the optic tract secrete signalling molecules such as Semaphorin 3A or Slits (Campbell et al., 2001; Piper et al., 2006). We can imagine that these signalling molecules controlling axon pathfinding also influence the local mechanical properties of the tissues expressing them. Conversely, we can consider that rheological properties of the tissue could regulate specific pathways, leading to the expression or downregulation of chemical guidance cues. These hypotheses have not been addressed so far and further *in vivo* studies need to be carried out to fully grasp this potential crosstalk.

- **Influence of mechanical stresses**

Axon pathfinding appears to be also influenced by mechanical stresses exerted by surrounding tissues. For example, zebrafish muscle contractions are required for proper navigation of peripheral Rohon-Beard (RB) sensory axons (Paulus et al., 2009). Using several genetic conditions or simply embedding the embryos in agarose gave situations where muscle contractions were affected at different levels of severities. In all these conditions, axon pathfinding was defective and the severity of axon guidance defects scaled with the level of

muscle contraction loss. In the absence of muscle contractions, RB peripheral axons extend longitudinally instead of ventrally and made frequent contacts together while these neurons normally repel each other. These observations indicate that muscle contractions influence at least two aspects of RB axon guidance: ventral growth and mutual repulsion. Since RB axon guidance was analysed in multiple mutants or treatments that affect muscle cells in different ways and since the only common effect shared by all these manipulations is loss of muscle contractions or movement, it indicates that the defects observed are really specifically caused by the absence of muscle movements. Whether these defects are direct or indirect consequences of the loss of mechanical forces exerted by muscle is still a remaining question.

Mechanical forces seem to be also involved in later phases of neuronal wiring, when, for example, neurotransmitter vesicles cluster at the synapse. Vesicle clustering is required for efficient neurotransmission and is critical for a newly formed synapse to function. Siechen *et al* showed in *Drosophila* embryos that vesicle clustering at the presynaptic terminal of neuromuscular junction depends on mechanical tension within the axons during synaptogenesis (Siechen et al., 2009). They found that severing the axons from the cell body results in the loss of presynaptic vesicle clustering but strikingly, pulling mechanically on severed axons with the help of a micropipette restores vesicle accumulation. Moreover, clustering increased when intact axons were stretched mechanically by pulling the postsynaptic muscle. How can axonal tension induce vesicle clustering? In a follow-up study combining *in vivo* and *in vitro* approaches, Ahmed *et al*. presented a putative model linking mechanical perturbation, actin polymerization, and vesicle movement/accumulation (Ahmed et al., 2012) (Figure 12). In its normal state, the axon contains cross-linked microtubules along which molecular motors can transport vesicles. The actin scaffold in the synapse enables to trap some of these vesicles. Under compression, microtubules depolymerize and vesicle transport is disrupted. Under tension, actin polymerization at the synapse may allow more vesicles to attach to the scaffold leading to a higher accumulation of vesicles at the synapse. Further *in vitro* studies confirmed that tension in neurons actually modulates active transport of vesicles (Ahmed and Saif, 2014; Ahmed et al., 2013). Thus, intrinsic mechanical tension may be required for proper function of neurotransmission in newly formed synapses.

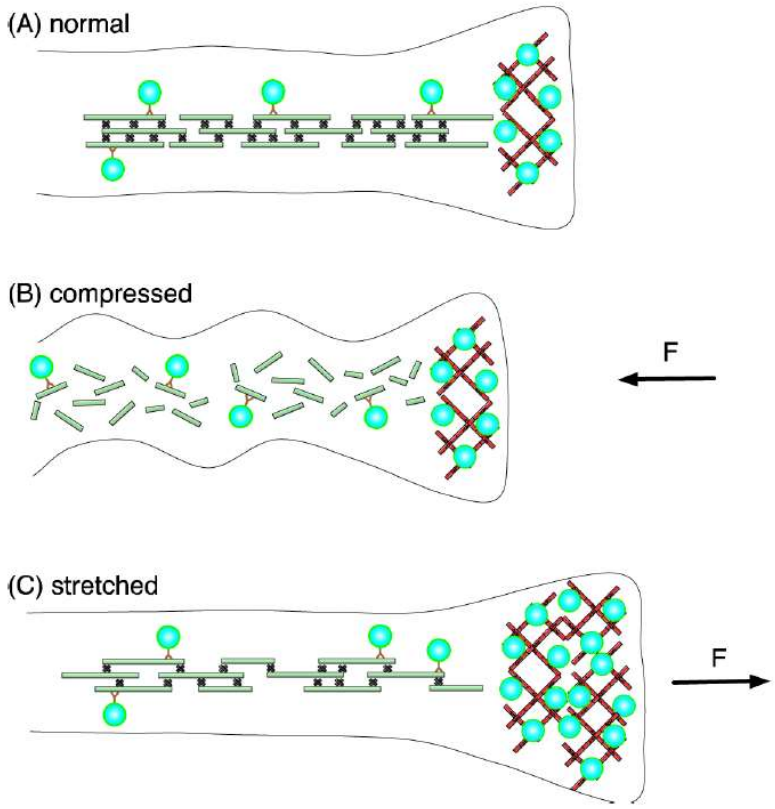

Figure 12: **Schematic view of the proposed mechanism connecting tension, cytoskeleton dynamics, vesicle transport and accumulation.** *"(A) A schematic diagram of an axon in its normal resting state. Microtubules (green) extend along the axon and are crosslinked (black) together to form a network. Vesicles (cyan) are attached to molecular motors (brown) that transport them along the microtubule network and some accumulate in the actin scaffolding (red) at the synapse. (B) Microtubules depolymerize under compression leading to disrupted vesicle transport while maintaining normal vesicle accumulation at the synapse. (C) A stretched axon exhibits increased vesicle accumulation at the synapse due to tension induced actin polymerization creating more vesicle binding sites."* (Ahmed et al., 2012)

- **Mechanotransduction in developing neurons**

Through all these examples, we saw how neuronal development is governed not only by chemical cues but also by mechanical cues. How are these mechanical signals transformed into biochemical signals inside the neurons and finally into cell responses?

Mechanotransduction is the molecular mechanism used by cells to sense and convert external forces into biochemical and biological responses to adapt their response to the environment (Javier-Torrent

et al., 2021). Probably the first mechanotransduction molecular players that comes to mind are membrane stretch-sensitive channels. These stretch-sensitive channels open and generate a cation influx when the plasma membrane is under tension (Ranade et al., 2015) and could be involved in sensing the environment stiffness or the tension exerted in the axon during different steps of neuronal circuit formation (Franze et al., 2013; Gangatharan et al., 2018). For example, global approaches of loss-of-function of Piezo-1 suggest that this mechanosensitive ion channel might be required in developing RGCs to sense the stiffness of their environment and to properly send their axonal protrusions to the optic tectum (Koser et al., 2016; Thompson et al., 2019). However, from these experiments, a role of Piezo-1 in surrounding brain cells, affecting the stiffness of these tissues and thus the axon pathfinding, cannot be excluded.

The detection and transduction of mechanical cues by neurons may also involve the cytoskeleton itself. Cytoskeletal components are involved in building internal axonal tension (Fan et al., 2019a; Fan et al., 2017) which, as we discussed earlier, acts as a mechanical cue driving several examples of neuronal circuit formation such as axon pruning (Anava et al., 2009), axon fasciculation (Smit et al., 2017), stretch-induced axon growth (Dennerll et al., 1989), and synaptic function (Siechen et al., 2009).

Finally, another general mechanism for mechanical signal detection relies on the interaction between cells and the surrounding extra-cellular matrix (ECM). Cell-ECM adhesion is mediated by complexes that anchor the inner cytoskeleton components, such as actin, to the outer ECM components through integrin receptors. *In vitro* studies on mouse embryonic fibroblasts showed that the actin–talin–integrin–fibronectin complex serves as a mechanosensor through which cells probe and respond to the rigidity of the environment (Elosegui-Artola et al., 2016). Moreover, as seen earlier (I.A.1), cell-ECM adhesion at contact points mediates the advance of the growth cone (Franze, 2020). This raises the possibility that adhesion complexes act as stiffness sensors in neuronal development and wiring. Here again, further studies are required to assess the role of adhesion sites in the different steps of neuronal circuit formation.

While most studies presented here were carried out *in vitro*, functional evidence demonstrating the *in vivo* importance of mechanical inputs has only started to emerge. The team of Marie Breau, involved in this exciting and growing interdisciplinary field, studies the zebrafish olfactory circuit in order to assess the role of mechanical forces in shaping neuronal circuits *in vivo*. In the following section, we will focus on the zebrafish olfactory circuit, which develops within the olfactory placodes (OPs).

B. The zebrafish olfactory placode

In the previous section, we have seen the emergence of both *in vitro* and *in vivo* studies illustrating the implication of mechanical cues in the different phases of neuronal circuit formation. In order to better understand the role of mechanical forces in the building of neuronal circuits *in vivo*, the lab uses the zebrafish olfactory circuit as a model.

First of all, unlike mammalian embryos, zebrafish embryos fully develop *ex utero*, which facilitates the study of neuronal migration and axon extension, which mainly occurs prenataly in mammals. Moreover, the transparency of these living organisms allows a wide range of live-imaging possibilities in combination with advanced techniques like optogenetics or laser ablation experiments. We focus more precisely on the sensory neurons that develop within the OP, a superficial tissue. Its location just underneath the skin makes it amenable to live-imaging and micro-manipulation. Finally, there is, in the zebrafish community, a broad panel of available transgenic tools to label specific tissues, cells or subcellular structures and an extensive array of embryological and genetic manipulations exists. Thus, the zebrafish olfactory circuit appears as an appropriate model to study neuronal circuit formation dynamically.

In the following section, we will first provide an overview of vertebrate cranial placodes and their developmental origin, then we will focus on the zebrafish olfactory circuit and finally we will present the known mechanisms driving OP coalescence.

1. Development of cranial placodes

- **General description of cranial placodes**

Cranial placodes are transient, discrete regions of thickened ectoderm, present in the head of vertebrate embryos. They are essential for the formation of much of the cranial sensory nervous system as they contribute to cranial sensory ganglia and to the paired sense organs that are the nose, the eyes, the ears and the lateral line in aquatic vertebrates. They give rise to a wide variety of cell types, including ciliated sensory receptors, sensory neurons, neuroendocrine and endocrine cells, glia and other supporting cells (Baker and Bronner-Fraser, 2001). From the most anterior to the most posterior, the cranial placodes include adenohypophyseal, olfactory, lens, trigeminal, otic, lateral line and epibranchial placodes (Figure 13 and Figure 14) (Schlosser et al., 2010).

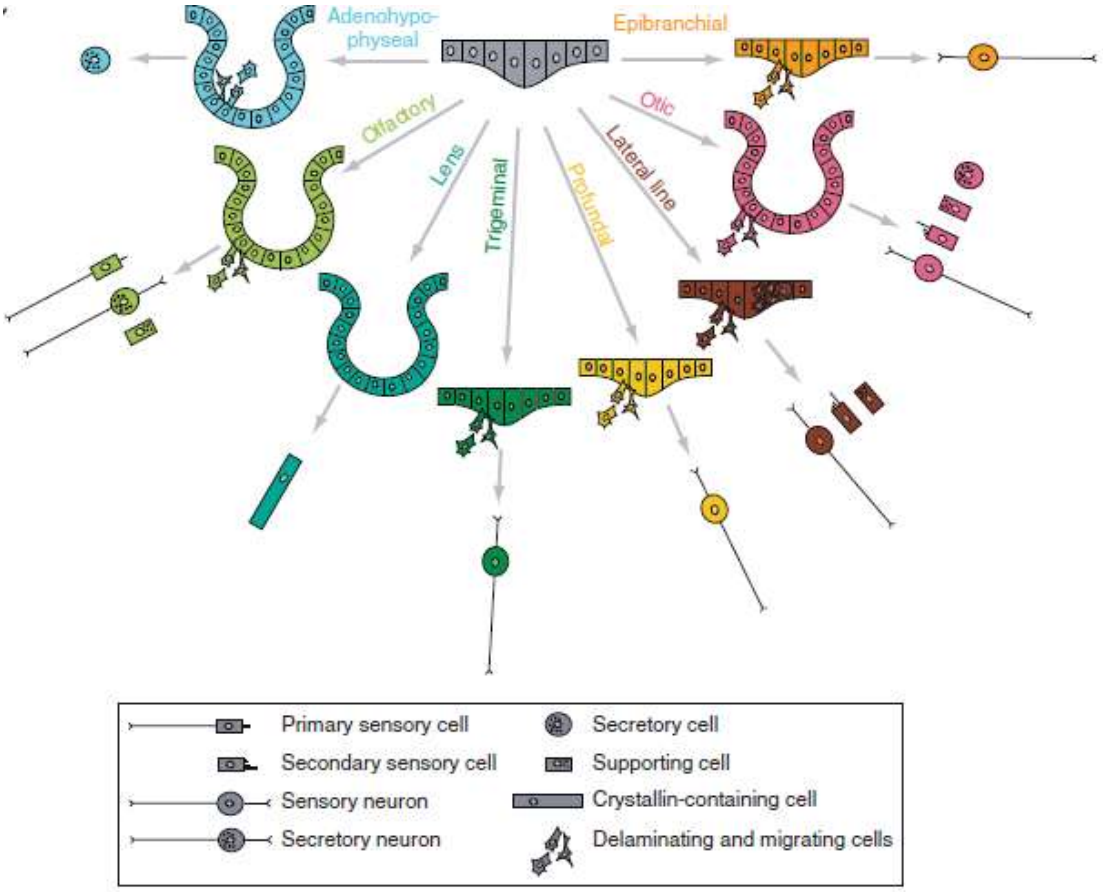

Figure 13: **Schematic illustrating the variety of vertebrate cranial placodes and of their cellular derivatives.** (Schlosser, 2010)

The adenohypophyseal placode gives rise to the adenohypophysis also called anterior pituitary, a major endocrine control organ composed of secretory cells. The two paired OPs form the olfactory epithelia constituted by olfactory neurons and supporting cells. The lens placodes also contribute to paired sense organs as they form the eye lens but unlike other cranial placodes they do not present a neural fate. Trigeminal placodes develop in two separate ganglia: the ophthalmic and the maxillomandibullar ganglia. In *Xenopus*, the ophtalmic complex remains partly unfused and thus is designated as profundal placode. Trigeminal placodes form primary sensory neurons that transmit somatosensory stimuli (touch, pain, temperature) from the skin of the face and jaws and the teeth (Baker and Bronner-Fraser, 2001). The otic placode generates the entire inner ear and the statoacoustic ganglion. Epibranchial placodes contribute to a set of sensory neurons relaying information from the face and viscera to the brain, such as heart rate, blood pressure, bronchial irritation, or gut distension. The lateral line placode forms the

mechanosensory lateral line used by aquatic vertebrates to detect movement, vibration, and pressure gradients in the surrounding water (Figure 13).

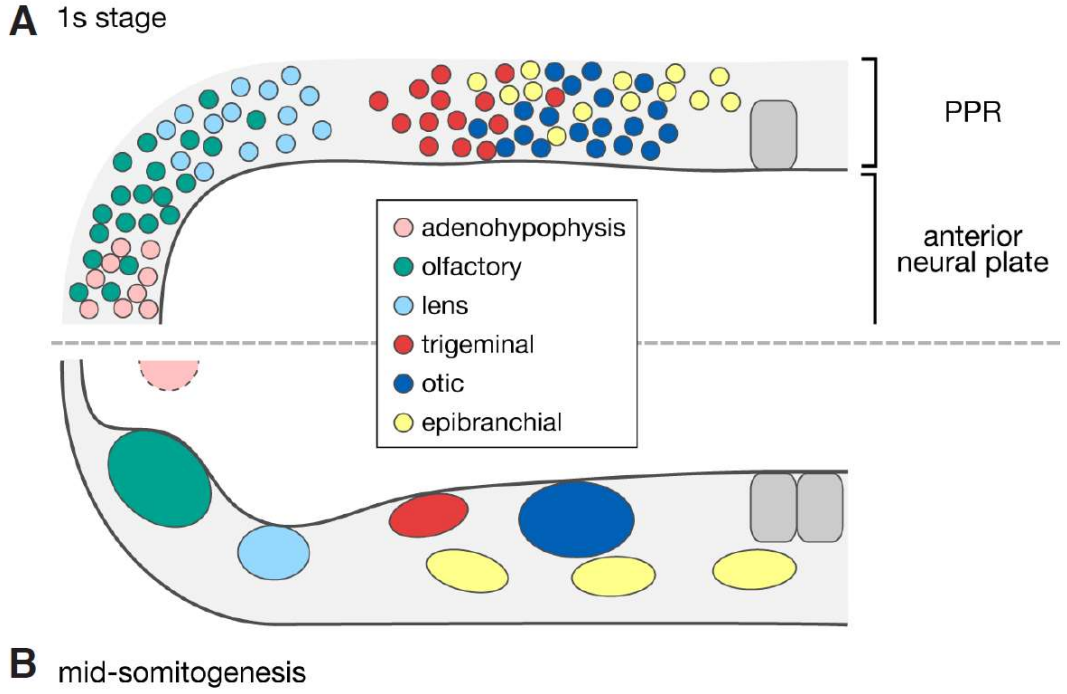

Figure 14: **Schematic representation of the position of placodal precursors and placodal structures respectively before and after placode assembly.** *"(A) Schematic view of placode progenitors scattered and intermixed within the pan-placodal region (PPR) surrounding the anterior neural plate at the 1s stage (dorsal view of a theoretical vertebrate). (B) Compact and individualised placodes occupying specific positions along the anteroposterior axis of the embryo from mid-somitogenesis stages onwards (dorsal view, the ventral position of the adenohypophysis is indicated by the dotted line surrounding the placode). Anterior to the left."* (Breau and Schneider-Maunoury, 2014)

In spite of the diversity of functions and cell types they are giving rise to, all the cranial placodes emanate from a common ectodermal domain (called pre-placodal region (PPR) or pan-placodal region or pre-placodal ectoderm), as shown by fate maps and lineage tracing in zebrafish, amphibian and chick (Bhattacharyya et al., 2004; Bhattacharyya and Bronner, 2013; Couly et al., 1998; Couly and Le Douarin, 1990; Dutta et al., 2005; Kozlowski et al., 1997; Pieper et al., 2012; Streit, 2002; Whitlock and Westerfield, 2000; Xu et al., 2008). This horseshoe-shaped territory surrounds the anterior neural plate by the end of gastrulation (Breau and Schneider-Maunoury, 2014) and is defined by the expression of the transcription factor Six1, its cofactor

Eya1, and other members of the Six and Eya families (Schlosser, 2014) (Figure 14). We will first see how this PPR is induced, then summarize how it subdivides into the different placodes and finally briefly discuss common mechanisms of subsequent placode individualisation.

- **PPR induction**

Sensory placodes arise from a crescent-shaped ectodermal territory located at the border of the neural plate at late gastrulation/early neurulation stages (Breau and Schneider-Maunoury, 2014). Like cranial placodes, the neural crest (NC) is also a transient cell population exclusively found in vertebrates and initially induced at the neural plate border. The NC is composed of multipotent stem cells, able to differentiate into many cell types and contributing to numerous organs such as the craniofacial cartilage, the cranial bones, the teeth, the cardiovascular system, the peripheral nervous system or the enteric nervous system (Shellard and Mayor, 2016).

Over the last decades, the induction of the PPR and the NC at the border of the neural plate has generated much debates among scientists (Ahrens and Schlosser, 2005; Brugmann et al., 2004; Glavic et al., 2004; Litsiou et al., 2005; Pieper et al., 2012). Two main models, apparently opposed, have been discussed (Figure 15). The neural plate border model suggests that both the PPR and the NC emerge gradually from a common neural plate border region (purple). The PPR (orange) and the NC (blue) progressively separate one from another as gene expression domains become refined in adjacent epidermis (yellow) and neural plate (green) to form two distinct populations at late neural plate stages. In the binary competence model, the ectoderm is initially subdivided into neural (light green) and non-neural (light yellow) territories and the NC arises from the lateral-most neuroectoderm while the PPR arises from the adjacent non-neuroectoderm (as reviewed in (Schlosser, 2014; Stundl et al., 2021; Thiery et al., 2020)).

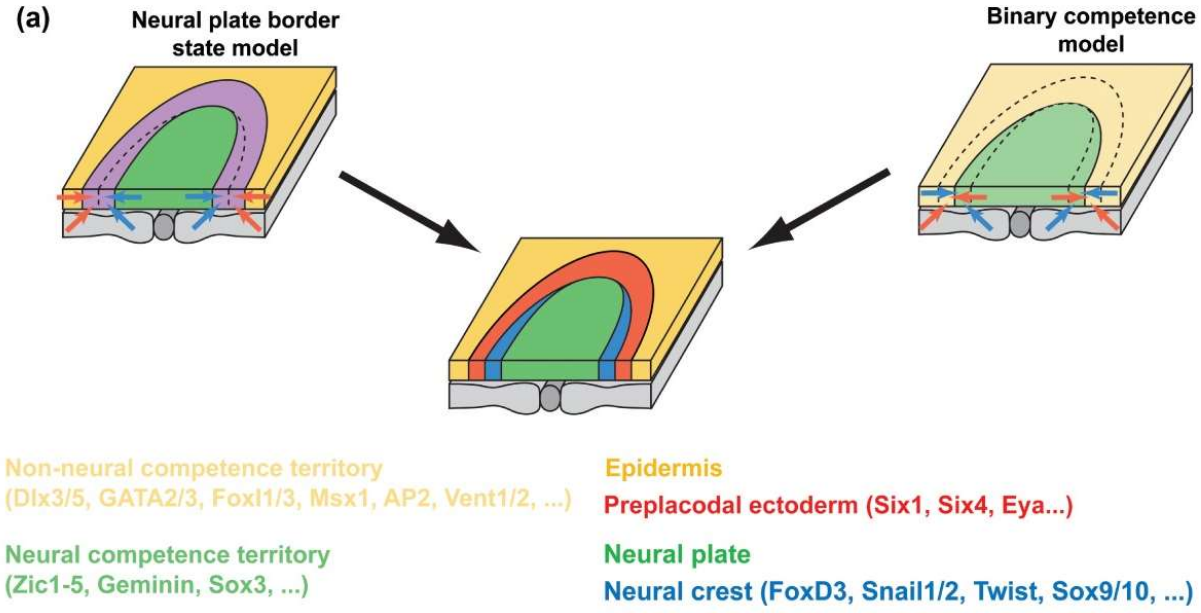

Figure 15: **Schematic representation of the two models for the induction of the PPR at the neural plate border.** (Left) Neural plate border model with the common neural plate border region represented in purple, the signals from adjacent epidermis by red arrows and the signals from the adjacent neural plate by red arrows. (Right) Binary competence model with neural and nonneural competence territory represented respectively in light green and light yellow. (Schlosser, 2014)

Recent studies on the complex gene regulatory network underlying PPR specification (Buitrago-Delgado et al., 2015; Maharana and Schlosser, 2018; Roellig et al., 2017; Trevers et al., 2018) tend to reconcile these two models. In their review, Thiery, Buzzi and Streit suggest that these two models are complementary when considering developmental time: at early gastrula stages, cells in the neural plate border are initially heterogeneous and have the competence to give rise to both NC and PPR, but as development proceeds, their potential is gradually restricted and the expression of preneural or non-neural factors becomes spatially confined due to signals from the adjacent neural and non-neural ectoderm (Thiery et al., 2020).

Subsequently, the PPR subdivides into specialized domains that prefigure the full range of cranial placodes during early neurulation, a process we will refer to as initial segregation as suggested in (Breau and Schneider-Maunoury, 2014). Then, coordinated morphogenetic movements within each placode domain lead to further compaction and give rise to discrete and condensed placodes separated by non-placodal tissues. This step is referred to as secondary coalescence (Breau and Schneider-Maunoury, 2014) (Figure 16).

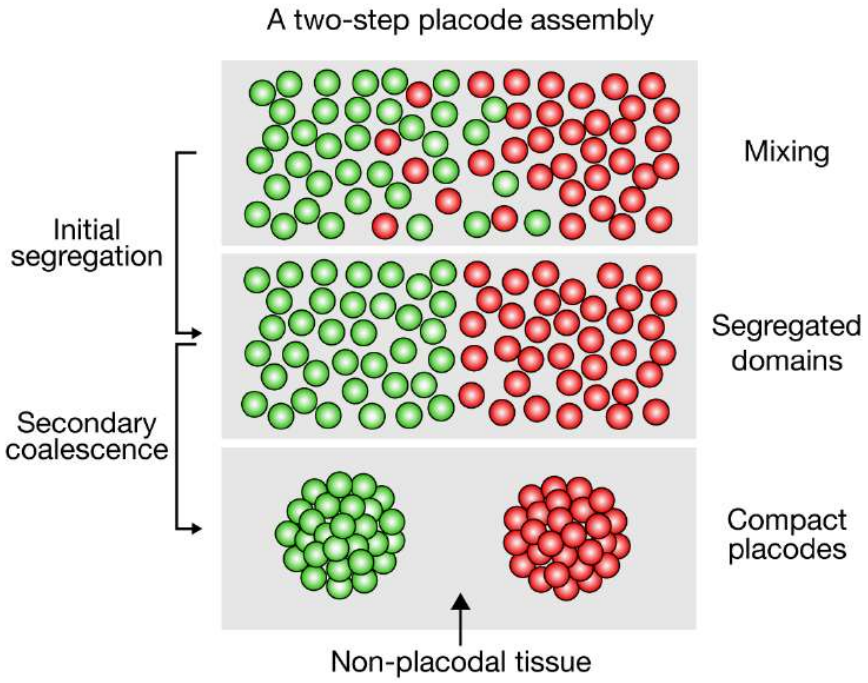

Figure 16: **Placode assembly seen as a two-step developmental process**. "*Fate map studies suggest two sequential steps in placode formation: segregation of intermingled placodal precursors into immiscible but still juxtaposed placodal domains (initial segregation), and further compaction resulting in discrete and condensed placodes separated by non-placodal tissues (secondary coalescence). In the upper panel, the coloured balls represent progenitors of adjacent placodes, whether or not they are specified."* (Breau and Schneider-Maunoury, 2014)

- **Initial segregation**

In 2014, M. Breau and S. Schneider-Maunoury suggested two models based on different mechanisms to explain how placodal precursors segregate into distinct embryonic domains from their scattered and intermixed distribution within the continuous PPR (Breau and Schneider-Maunoury, 2014). In the first scenario, placodal cells are already specified prior to segregation, which will confer similar properties to cells forming the same placode. These alike cells will then gather and sort out from other placodal cells due to differential intercellular adhesion or/and due to directional movements guided by local sources of cues that either attract or repel distinct placodal cell subpopulations. In the second model, unspecified placode precursors would be exposed to local gradients of environmental signals (Figure 17).

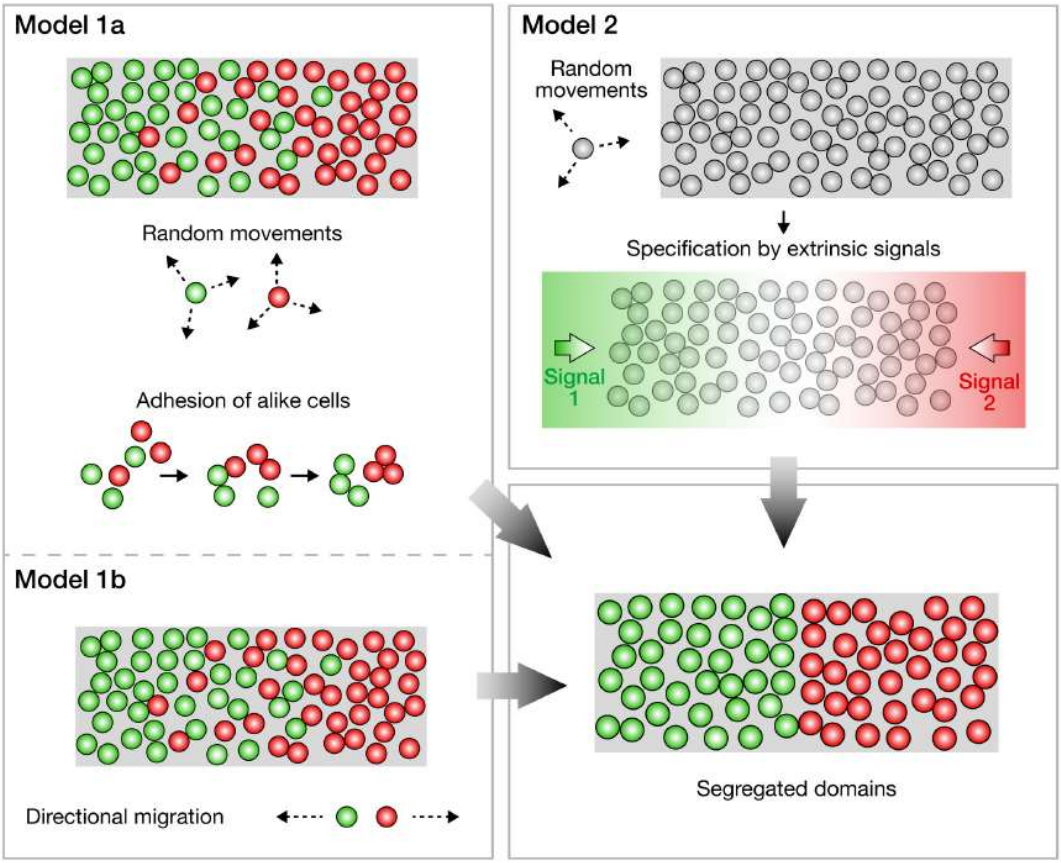

Figure 17: **Schematics describing the models that lead to initial segregation of the PPR domain.** *"(Model 1). Large-scale sorting out of early-specified intermingled placodal precursors. Specified placodal precursors initially present a high degree of intermixing and actively sort-out from each other by differential adhesion (Model 1a) or directional migration (Model 1b). (Model 2). Random movements preceding specification of placodal identities by surrounding signalling centres. Unspecified progenitors undergo random movements within the PPR before being specified by environmental signals. Further patterning mechanisms (cross-repression of transcription factors) lead to the formation of a sharp boundary between placodal domains. Grey and coloured balls represent unspecified and specified placodal progenitors, respectively."* (Breau and Schneider-Maunoury, 2014)

Despite the important number of studies on this process (Baker et al., 1999; Bhattacharyya and Bronner-Fraser, 2008; Groves and Bronner-Fraser, 2000; Rhinn et al., 2009; Schlosser, 2014; Steventon et al., 2012), the issue of initial segregation still deserves further investigation. The two models might complete each other with first a broad separation induced by extrinsic signals (as in the second model) and subsequently a fine separation of different placodal populations involving directed movements and adhesion-mediated cell-sorting (as in the first model).

- **Secondary coalescence**

After initial segregation of specific placodes in the PPR domain, placodal structures become more compact and clearly separated from each other by non-placodal areas (Figure 14 and Figure 16). From mid/end of somitogenesis, distinct morphogenetic processes will shape the final forms of the placodal derivatives (as reviewed in (Breau and Schneider-Maunoury, 2014)). The secondary coalescence relies on diverse cell behaviours. Delamination, the process by which cells detach from the ectoderm and migrate inward, occurs in zebrafish otic placode (Hoijman et al., 2017) and in chick trigeminal and epibranchial placodes (Graham et al., 2007). Coalescence also involves directional cell movements as reported subsequently in zebrafish trigeminal placodes (Bhat and Riley, 2011; Knaut et al., 2005) and also in the zebrafish lens placode (Kwan et al., 2012). Cell retention has been described in the zebrafish lateral line placode (Breau et al., 2012). This process consists in the active maintenance of cells in position by a chemotactic mechanism, in the absence of which they would migrate away from the site of placode formation (Breau et al., 2012).

Secondary coalescence also depends on molecular cues such as chemokine signalling or Fgf signalling (as reviewed in (Lassiter et al., 2014)). For instance, the chemokine pathway involving the ligand Cxcl12a (also known as stromal cell-derived factor 1 or Sdf1a) and its receptors controls the assembly of zebrafish OPs (Aguillon et al., 2020; Miyasaka et al., 2007), of zebrafish trigeminal placodes (Knaut et al., 2005; Lewellis et al., 2013) and *Xenopus* epibranchial placodes (Theveneau et al., 2013). In addition to its role in placode induction, specification and differentiation, Fgf signalling also controls some aspects of placode secondary coalescence. It has been shown in avians that Fgf signaling is essential for ophthalmic trigeminal placode cell delamination and differentiation (Lassiter et al., 2009). Interestingly, during the process of cell retention of lateral line placode described above, Sdf1α/Cxcr4b signalling and Fgf signalling act as opposite cues: Fgf activity is required for the maintenance of cells in the vicinity of the placode while Cxcr4b attracts cells posteriorly (Breau et al., 2012).

Finally, secondary coalescence also involves interactions of placodes cells with other cell populations such as neural crest cells (NCCs) or with the ECM. Probably the best example to illustrate the interplay between NCCs and placodes is the chase-and-run behaviour observed in *Xenopus*. NCCs chase epibranchial placodal cells by SDF1-mediated chemotaxis, and in turn, placodal cells run when contacted by NC, resulting in the coordinated migration of both cell

populations (Theveneau et al., 2013). These reciprocal interactions between NCCs and placodal cells illustrate the role of surrounding tissues in placode morphogenesis.

At the same time as these morphogenetic movements, neurogenesis starts in certain placodes to produce distinct neuronal subtypes, characteristics of the mature placode-derived organs (as reviewed in (Aguillon et al., 2016)). The coordination of both neurogenesis and morphogenesis might thus be critical for proper sensory circuit formation.

This section constituted a brief overview of vertebrate cranial placode formation with the induction of the PPR, the initial segregation into distinct placodal domains and finally the coalescence of the individualised placodes. In the following part, we will focus on the zebrafish OP, first by describing the olfactory circuit and then by deciphering the mechanisms of OP secondary coalescence.

2. Zebrafish olfactory circuit

• Zebrafish olfaction

Zebrafish olfaction mediates behaviours that are critical for survival, such as foraging, mating, social behaviour, and danger assessment (Kermen et al., 2013). In order to trigger such responses, the olfactory system is responsible for detecting and processing a wide range of odorants such as amino acids, bile acids, amines, nucleotides, sex pheromones or skin extracts (Yoshihara, 2014). Moreover, the olfactory system presents widespread plasticity mechanisms, which gives the animal its capacity to create new connections to adjust continuously in response to potential new odours (Calvo-Ochoa and Byrd-Jacobs, 2019; Cummings and Belluscio, 2010; Scheib et al., 2019).

Unlike mammals, teleost fish do not use sniffing to sense surrounding chemical compounds. Water enters the olfactory cavity through an incurrent nostril located at the anterior side of the nasal cavity and exits through an excurrent nostril located posteriorly (Figure 18) (Hansen and Zeiske, 1993). Water movement from the anterior to the posterior nostril is created by the movement of the fish through water or, when at rest, by water currents. Water is also moved into the olfactory chamber *via* actively beating cilia in the olfactory organ (Reiten et al., 2017). The olfactory epithelium containing olfactory sensory neurons (OSN) lies in the nasal cavity between these two nostrils (Kermen et al., 2013; Whitlock, 2006).

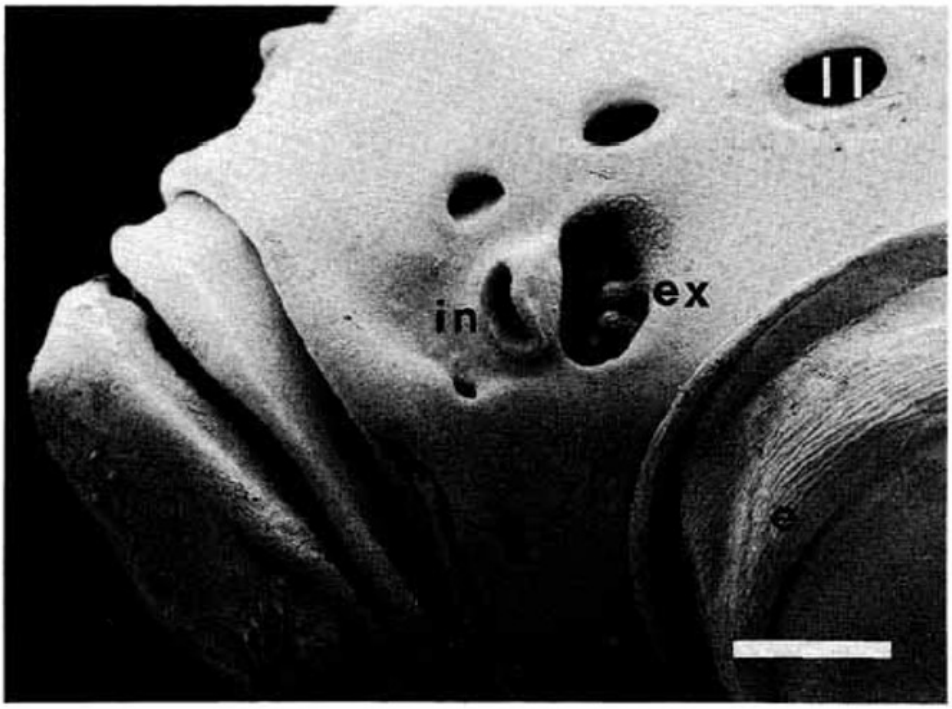

Figure 18**: Scanning electron microscopy image of the left side of an adult zebrafish head showing the eye (e), the incurrent (in) and excurrent (ex) nostril** and the openings of the cephalic lateral line system (l l). Scale bar = 0.5mm. (Hansen and Zeiske, 1993)

- **The olfactory epithelium**

The zebrafish olfactory system is primarily composed of two bilateral olfactory epithelia and two bilateral olfactory bulbs, and secondary by higher brain centres where the olfactory information is further processed (Figure 19A). The olfactory epithelium of the nasal cavity consists of several lamellae that converge in a central non-sensory raphe, forming a bilaterally symmetrical cup-shaped structure called the rosette (Figure 19B) (Calvo-Ochoa and Byrd-Jacobs, 2019). Lamellae are composed of a continuous sensory area and a surrounding non-sensory epithelium containing the goblet cells, ciliated nonsensory cells and epidermal cells with microridges (Hansen and Zeiske, 1998).

The rosette's sensory region is a characteristic pseudostratified columnar epithelium formed by OSNs and supporting cells. OSNs are bipolar neurons exposing their dendrite to external water on the apical side of the epithelium and projecting their axon through the basal lamina. There is a wide variety of OSNs allowing the fish to sense and discriminate among the broad range of odorant molecules. They can be divided in 5 classes: ciliated (cl); microvillous (mv); crypt (cr); kappe (kp) and pear (pr) neurons (Figure 19C). The soma of these OSNs are located at different

depths in the olfactory epithelium and they exhibit different morphologies and molecular markers.

Each mature OSN expresses receptors which will interact with a specific odorant. Odorant receptor (OR) is the most abundant type of receptor in terms of quantity of cells expressing it and around 102 different ORs genes are present in zebrafish. Trace amine-associated receptors (TAARs) detect volatile amines and they are around 109 zebrafish genes encoding for TAARs. Vomeronasal receptors (VRs) detect pheromones and it exists 50 different VR genes in zebrafish (Hashiguchi and Nishida, 2007; Shi and Zhang, 2009). Most OSNs only express one receptor but multiple receptors have been found for some specific subpopulations of OSNs as double *in situ* hybridization analysis demonstrated the co-expression of ORs in a small but significant population of OSNs (Sato et al., 2007).

The axons of OSNs project through the basal lamina, bundle within the brain to form the olfactory nerve and finally target the olfactory bulb, composed of discrete glomeruli (Calvo-Ochoa and Byrd-Jacobs, 2019). Even though OSNs expressing the same receptor or the same set of receptors are dispersed throughout the epithelium, they project their axons *via* the olfactory nerve to the same glomerulus in the olfactory bulb (Sato et al., 2005). During development, OSN axons initially target protoglomeruli regions which are specific to a group of receptors, before further sorting refining each protoglomerulus to give rise to glomeruli that are specific for each receptor (Shao et al., 2017).

Such a spatial projection within the brain of sensory stimulation from a PNS organ is referred to as sensory map. Sensory map features vary from one sense to another and depend on the specific sensory modality and the relevant information to be extracted from each sensory organ (Fritzsch et al., 2019). For example, for the sense of audition, a one-dimensional map of distinct frequencies projects from the organ of Corti to specific areas of the cochlear nuclei and auditory cortex (Schreiner and Winer, 2007). Regarding vision, the two-dimension (2D) surface of RGCs within the eye maps onto another 2D surface in the optic midbrain (Dhande and Huberman, 2014). In contrast to these continuous primary maps, distributed OSNs perceiving the same odorant stimuli project onto the same area of the olfactory bulb (Mori and Sakano, 2011), thus losing the spatial information of where an odorant has been sensed within the olfactory epithelium. An explanation for such specific sensory map could resides in the infinite nature of odorants that cannot be classified (Kaeppler and Mueller, 2013). Unlike other sensory stimuli that rely on clearly defined parameters such as the frequency and the loudness for

acoustic stimuli or the wavelength and the intensity for visual stimuli, olfactory stimuli cannot be defined depending on simple physical parameters and thus may require the so-called odotopic map, on which each glomerulus receives input solely from the precise group of OSNs expressing the same OR (Grabe and Sachse, 2018).

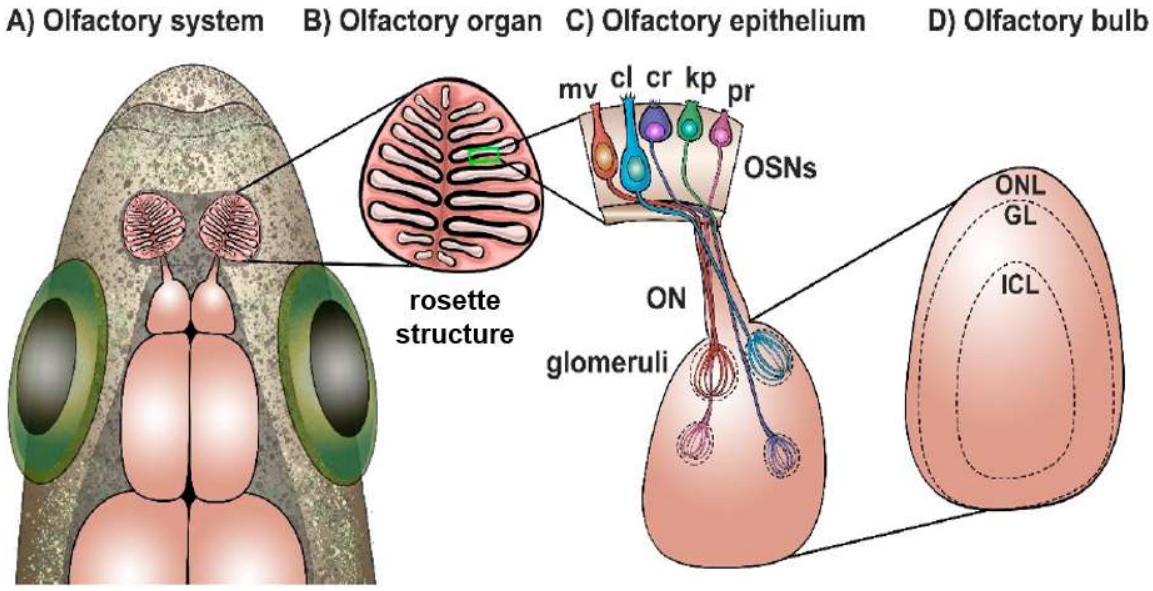

Figure 19: **Schematic representation of the organization of the zebrafish olfactory system.** *"(A) Localization of the olfactory system in zebrafish. Dorsal side is shown; rostral side is located upwards. (B) Olfactory organ morphology. Olfactory sensory epithelium forming a rosette structure arranged in lamellae is shown in black. (C) Olfactory epithelium (OE) composed of the following sensory neurons (OSNs): microvillous (mv), ciliated (cl), crypt (cr), kappe (kp) and pear (pr) OSNs. OSNs extend their axons to the olfactory bulb via the olfactory nerve (ON) to form discrete glomeruli. (D) olfactory bulb organization in three laminae: olfactory nerve layer (ONL); glomerular layer (GL) and intracellular layer (ICL).*" Adapted from (Calvo-Ochoa and Byrd-Jacobs, 2019)

- **The olfactory bulb**

The olfactory bulb is a paired brain structure that constitutes the first central relay of the olfactory system where olfactory information is processed and transmitted to olfactory-processing telencephalic areas (Calvo-Ochoa and Byrd-Jacobs, 2019).

The olfactory bulb can be divided into 3 main areas. From superficial to deep, these are: (1) the olfactory nerve layer, formed by OSN axons; (2) the glomerular layer, containing

approximately 140 spherical glomeruli formed by olfactory axons terminals and apical dendrites from their target cells, which are the mitral and ruffed cells (Braubach et al., 2012; Fuller and Byrd, 2005; Fuller et al., 2006) and (3) the intracellular layer, consisting of mitral and ruffed cell somas (Calvo-Ochoa and Byrd-Jacobs, 2019; Kermen et al., 2013) (Figure 19D). Odorant information is processed by olfactory bulb neuronal networks and then conveyed by the principal neurons, the mitral cells, to multiple higher brain areas (Miyasaka et al., 2013).

Zebrafish larvae are already able to detect amino-acids and adapt their behaviours straight after hatching (4-5 dpf), although their olfactory circuit development is not complete (Lindsay and Vogt, 2004). Thus the function of neuronal circuits is quickly established within 4 days and then subsequently refined. The development of the olfactory system requires multiple steps including the OP assembly, the specification of OSNs, the exit of OSN axons from the OP, the pathfinding towards the target glomeruli, the development of glomeruli, the assembly of neuronal circuits in the olfactory bulb and the establishment of higher-order projections (as reviewed in (Miyasaka et al., 2013)). In the following part, we will focus on the OP assembly and initial neurogenesis occurring during somitogenesis (11-24 hours post fertilization (hpf)).

3. Morphogenesis of the zebrafish olfactory placode

- **OP coalescence**

  - **Fate maps**

Single-cell labelling at the edge of the neural plate at 4-5 s (11-11.5 hpf) enabled to build a fate map of this region and revealed that OPs arise from two elongated fields of cells extending along the lateral edges of the anterior neural plate (Figure 20 A and B right). These fields reside within the Dlx3b-expressing region which also contains telencephalic precursors (Whitlock and Westerfield, 2000). Further studies from the same team suggested that the subdivision of this shared Dlx3b-expressing neurectoderm into OP and olfactory bulb domains is mediated by differences in the level of *dlx* genes expression (Torres-Paz et al., 2020; Torres-Paz and Whitlock, 2014). In the following parts, we will see how OPs change shape from these two elongated fields (Figure 20A) into two spherical clusters (Figure 20B).

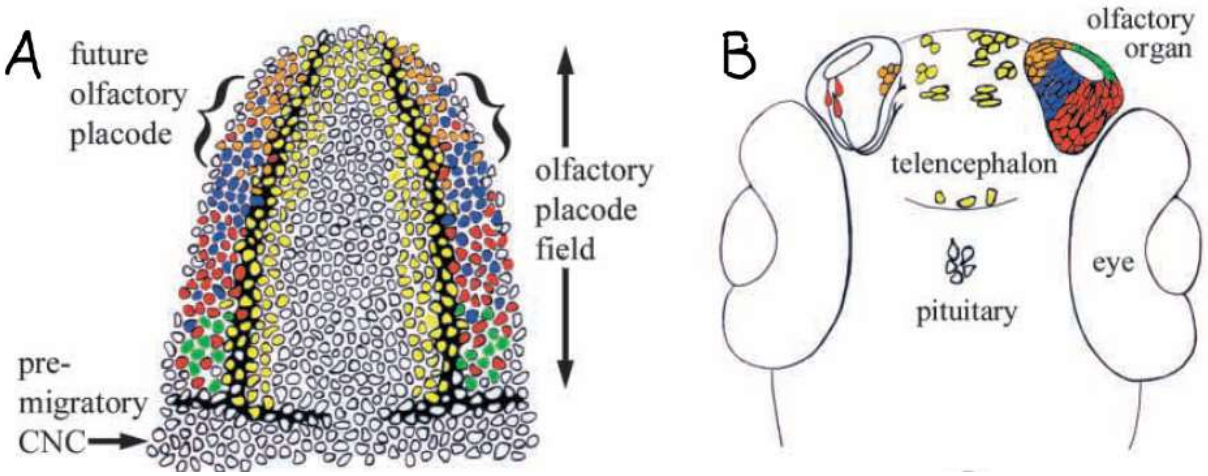

Figure 20: **Representation of the olfactory placode and telencephalon fields lineage tracing at 4-5 s (11-11.5 hpf) and the corresponding cell locations at 50 hpf.** *"(A) Schematized dorsal view of the anterior end of 12 h embryo with anterior towards the top of the page. The blackened border extending along the anteroposterior axis approximately represents the border between the fields of cells giving rise to olfactory organ and those giving rise to telencephalon. The transverse blackened border represents the anterior limits of premigratory cranial NC. (B) Schematized ventral view of a 50 h zebrafish head with anterior towards the top of the page. Right-hand olfactory organ: the olfactory organ has been subdivided into four coloured areas. Clones in these areas were colour coded in diagram A. Left hand olfactory organ: sensory neurons with axons extending into the CNS at 50 h come predominantly from red cells, pioneer neurons come from orange cells but only in the region abutting the telencephalic field anteriorly. The pituitary clones come from the non-coloured cells most anterior in the neural plate between the two blackened borders."* The cells are colour coded with respect to their future fates in the developing olfactory organ and bulb at 50 h: red, orange, green and blue cells contribute to the olfactory organ, yellow cells give rise to clones in the telencephalon. (Whitlock and Westerfield, 2000)

- **Role of cell division and apoptosis**

Cell division, cell death and cell rearrangements are recognized to be the elementary cellular behaviors participating in morphogenesis. Local cell proliferation or oriented cell divisions can induce tissue shape changes (Lecuit and Le Goff, 2007). Apoptosis contributes to morphogenesis either by simply removing the unnecessary cells or by generating mechanical forces that control tissue dynamics (Ambrosini et al., 2017; Monier and Suzanne, 2015). The planar polarized remodelling of cell junctions, also called T1 processes, can also induce tissue

shape changes and contribute to morphogenesis (Collinet et al., 2015; Lecuit et al., 2011; Rauzi et al., 2010).

During OP coalescence, cell division appeared to be rare as assayed with anti-phosphorylated Histone H3 antibody (Whitlock and Westerfield, 2000), and pharmacological perturbation of cell proliferation using hydroxyurea and aphidicolin (HUA) did not affect OP morphogenesis (Breau et al., 2017). The inhibition of apoptosis with a drug targeting caspases had no effect on final placode shape, indicating that neither cell proliferation nor cell apoptosis are required for the proper transformation of the two stripes of OP progenitor cells into spherical clusters (Breau et al., 2017). This suggests that the OP arises by converging cell movements of an initially antero-posteriorly extended field, rather than by local proliferation or local cell death.

- **Cell movements**

As placode assembly proceeds, the two stripes of OP progenitor cells progressively shrunk along the anteroposterior (AP) axis with a placode length decreasing from around 140 µm at 12 s to around 90 µm at 24 s, while getting larger along the mediolateral (ML) axis with a placode width from around 25 µm at 12 s to around 45 µm at 24 s (Breau et al., 2017). The OP coalescence into a compact cluster requires the chemical signalling pathway Cxcr4b/Cxcl12a. Initially, the *cxcr4b* receptor is expressed in the migrating OP cells, and its *cxcl12a* ligand in the abutting anterior neural plate. At the onset of OSN axon growth within the brain, the expression of *cxcr4b* persists in the OP while *cxcl12a* expression becomes restricted to the placode-telencephalon border and to the anterior tip of the telencephalon, prefiguring the route and target of OSN axons (Figure 21). Interfering with Cxcl12a by widespread ectopic expression, or with Cxcr4b using *cxcr4b*^{t26035} mutants (also called *ody* mutant) affects both OP morphogenesis and OSN axon pathfinding in the brain (Miyasaka et al., 2007). Whether Cxcr4b/Cxcl12a signalling is directly involved in the guidance of olfactory axons to the olfactory bulb or if the defects observed are simply a secondary consequence of an earlier OP morphogenesis defect remains unclear (Aguillon et al., 2016).

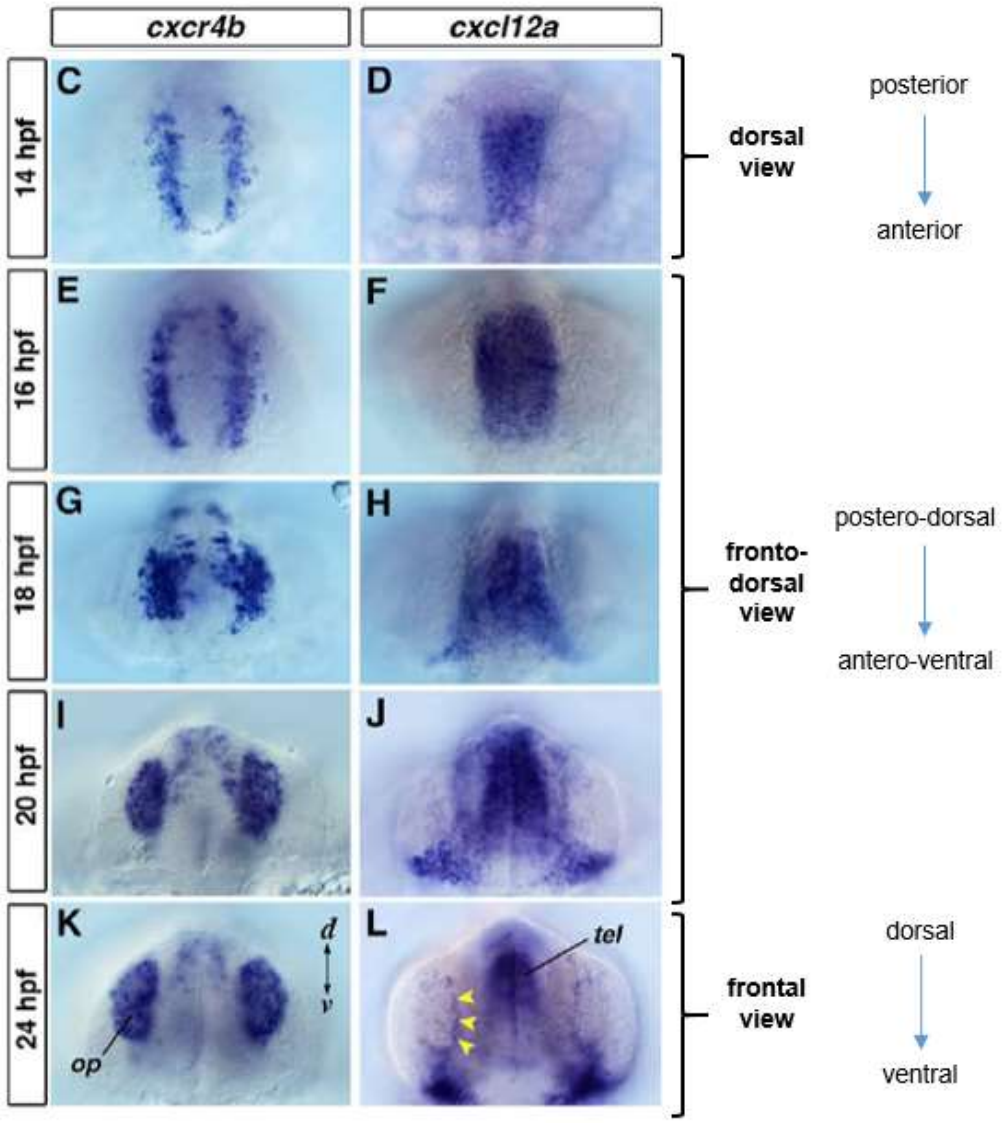

Figure 21: **Whole-mount *in situ* hybridization analysis of *cxcr4b* and *cxcl12a* expression during development of the OP in zebrafish**. From 14 to 16 hpf (10 s to 14 s), *cxcr4b* is expressed bilaterally along the lateral edge of developing neural tube (C,E), whereas *cxcl12a* is expressed medially, in the anterior brain (telencephalon), adjacent to the *cxcr4b*-expressing bilateral stripes (D,F). Progressive convergence of *cxcr4b*-expressing domains occurs between 16 and 20 hpf (14-22 s) (E,G,I) to form the OPs. *cxcr4b* expression in the OP persists during the initial phase of axon pathfinding (K). At the same period, *cxcl12a* expression is detected at the OP-telencephalon border (J, arrowheads in L), as well as in the anterior tip of the telencephalon. Adapted from (Miyasaka et al., 2007).

- **Retrograde axon extension**

The morphogenetic movements of OP cells underlying its shape change from an elongated domain into an ellipsoidal neuronal cluster have been further described using live imaging (Breau et al., 2017). Two main movements occurring between 12 s (15 hpf) and 24 s (21 hpf) have been identified (Figure 22). First, cells from the anterior and posterior extremities migrate actively along the brain towards the placode centre in a so-called convergence movement (represented by red arrows in Figure 22). The cell bodies are then displaced laterally, away from the surface of the brain, during the lateral movement (blue arrows). Central OP cells undergo lateral movements only, without clear anteroposterior displacement. Remarkably, axon growth initiates during lateral movements, whereby cell bodies move away from their axon tips that remain attached to the brain (the neurons extending axons are shown in blue). This process, referred to as retrograde axon extension, contrasts with the classical view of axon elongation through the active growth cone migration (as described in I.A.1).

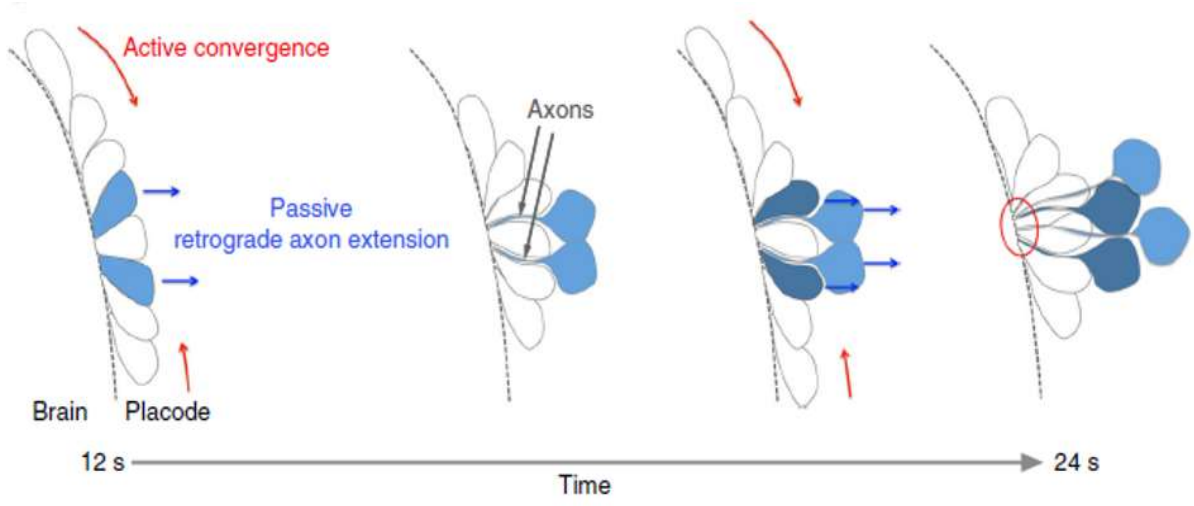

Figure 22: **Schematic description of the two movements sculpting OP morphogenesis.** *"Cells from OP extremities converge towards the centre through active migration along the brain surface (red arrows), while cell bodies of central cells passively move away from the brain (blue arrows). As they move laterally, central neurons keep contact with the brain surface through long cytoplasmic protrusions, thereby initiating the elongation of their axons (blue cells). Axons thus extend through movements of cell bodies away from static axon tips, a process referred to as retrograde axon extension. The red circle indicates the future entry point of axons in the brain."* Adapted from (Breau et al., 2017).

While the anteroposterior convergence represents active cell migration guided by Cxcr4b/Cxcl12a signalling (Aguillon et al., 2020; Breau et al., 2017; Miyasaka et al., 2007), the mechanisms driving the lateral phase of OP cell movements, during which axons elongate, remain elusive to date. Breau *et al*. propose that this process is non-autonomous, driven by extrinsic mechanical forces exerted on the cell bodies, based on the following findings: (1) the lack of protrusive activity and of polarised actomyosin in the moving cell bodies, (2) the absence of defects in their movements upon inhibition of microtubule polymerisation or upon cell-autonomous perturbation of actomyosin activity and (3) the lack of defects in cell body movements when the axons or their attachment to the brain were disrupted. Moreover, cell nuclei deformation patterns and laser ablation of cell/cell junctions suggest that central placodal cells undergo anisotropic mechanical stress: nuclei are elongated along the mediolateral axis and tension is higher in this direction (Breau et al., 2017), which reinforces the idea that mechanical tension plays a role in OP morphogenesis.

Altogether, these results suggest that lateral movements and retrograde axon elongation are driven by extrinsic mechanical forces exerted on the OP cell bodies by surrounding cells or tissues. The authors emit two different but non-exclusive hypotheses about the potential sources of these extrinsic forces: the actively converging placodal cells could squeeze and push the central cell bodies laterally (Figure 23, compression, red arrows) or the adjacent eye tissue, which undergoes morphogenetic movements at the same time, could exert traction forces on the OP and pull the cells bodies laterally (traction, green arrow) (Breau et al., 2017).

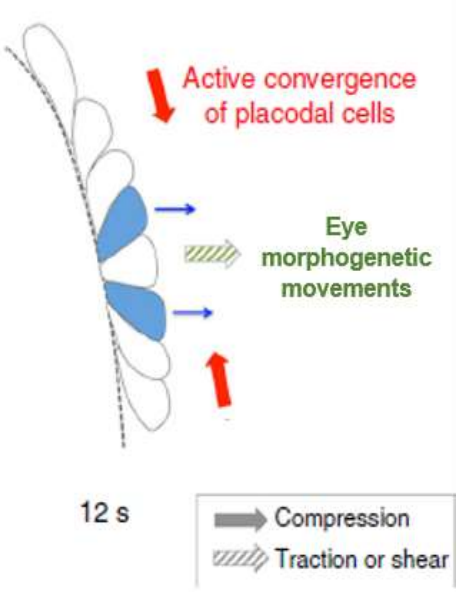

Figure 23: **Schematic representation of the suggested models for the mechanical forces driving passive retrograde axon extension in the OP** Compression exerted by actively converging cells from placode extremities is represented with red arrows while traction force exerted by eye morphogenetic movements is represented with cross-hatched green arrow. Adapted from (Breau et al., 2017).

- **Other examples of retrograde extension**

Axon elongation is classically seen as a growth-cone-driven process, in which the axon extremity (the growth cone) moves progressively further away from a cell body (Polleux and Snider, 2010). In contrast, Breau *et al.* described a different mode of axon extension, in which the axon grows by passive retrograde movement of the cell body away from the anchored axonal distal extremity. Interestingly, this process of retrograde neurite extension has also been observed in a sensory organ of *C elegans*: using time-lapse imaging, Heiman *et al*. found that sensory dendrites from amphid olfactory neurons form by stationary anchoring of dendritic tips and retrograde extension of the dendrite (Heiman and Shaham, 2009). First, the amphid neurons assemble into a multicellular rosette and their dendritic extremities attach to the overlaying epidermis at the centre of this rosette. As the epidermis migrates to enclose the head (Chisholm and Hardin, 2005), it pulls dendrite tips anteriorly which increases the distance between the tips and the neuronal cell bodies, resulting in dendrite elongation. Then, in a second phase, the neuron cell bodies migrate posteriorly, pulling further the dendrites as they move (Fan et al., 2019b). Several extracellular proteins have been identified as required for anchoring the

dendrite tips (Fan et al., 2019b; Heiman and Shaham, 2009) and dendrite tips remain attached to their target throughout both steps of epidermal migration and neuronal cell body migration. The authors refer to this entire process as 'retrograde extension' because during both processes, dendrite growth is driven by the increase in the distance between the dendrite endings and the neuronal cell bodies. This example also suggests that mechanical cues from the overlying skin can shape dendrites and enhances the importance of studying mechanical interactions between developing tissues.

The same team also described retrograde dendrite extension in other neurons: the two paired sensory neurons BAG and URX present in the worm head. They found that BAG and URX dendrites also develop by retrograde extension, in which the nascent dendrite endings anchor to the presumptive nose by forming specialized contacts with a single glial cell and then extend by stretching during embryo elongation (Cebul et al., 2020). While this work mainly focuses on the anchoring process of the neurons to the glia, little is known about the stretching process where the cell bodies move away from their dendrite tips. Interestingly, the two neuronal cells did not present the classical features of an active migratory cell (Cebul et al., 2020), raising the intriguing possibility that surrounding tissues that undergo morphogenetic movements elongating the embryo may exert external mechanical forces that push these cell bodies and contribute to retrograde dendrite extension. Further investigations are required to determine the mechanisms driving the cell bodies away from their dendritic tips.

Neurite elongation with fixed distal extremity also evokes the stretch-induced axon growth suggested to occur after the growth cone has reached its final target during animal body growth. As described previously in I.A.2, this process has been proposed to depend on mechanical forces imposed by tissue growth (Breau and Schneider-Maunoury, 2017; Franze et al., 2013; Gangatharan et al., 2018; Loverde and Pfister, 2015; Weiss, 1941). The retrograde extension described either in zebrafish OP axons, in *C elegans* amphid dendrites or in *C elegans* BAG and URX dendrites are good *in vivo* models to study how neurites extend by the increase in distance between the neurite tip and the cell body, as it may occur during animal growth.

- **Coupling between morphogenesis and neurogenesis**

Neurogenesis in the OP starts during coalescence movements. The *ngn1:gfp* transgenic line is commonly used to study the dynamics of morphogenesis and neurogenesis in the coalescing placode. The basic helix-loop-helix transcription factor Neurogenin 1 (Ngn1) is expressed in

multiple domains of the nervous system in zebrafish developing embryos, including the OP, demarcating the sites of primary neurogenesis (Blader et al., 1997). In the *ngn1:gfp* transgenic line, 8.4 kb of the *ngn1* upstream promoter controls the expression of the GFP reporter gene in a pattern which is similar to that of the endogenous *ngn1* gene (Blader et al., 2003). At 24 hpf, all *ngn1:gfp*$^{+}$ cells in the OP express the early marker of post-mitotic neurons HuC/D and are recognised by the Zns-2 antibody, previously described as a marker of pioneer neurons (Breau et al., 2017; Whitlock and Westerfield, 1998) (Figure 24A-F,M). At 48 hpf, the HuC/D^{+}; *ngn1:gfp*$^{+}$ cells are located in the OP centre and are called early-born olfactory neurons (EON) (Madelaine et al., 2011) while the cells in the outer cup of the OP express the olfactory marker protein (Omp), a commonly used marker for OSN (Celik et al., 2002) (Figure 24G-L,N).

However, *ngn1:gfp*$^{+}$ cells might as well give rise to OSNs and the exact fate of both *ngn1:gfp*$^{+}$ cells and *ngn1:gfp*$^{-}$ OP cells remain elusive. Lineage tracing experiments will be required to fill this gap of knowledge. To do so, several classical tools could be used such as single cell labelling with fluorescent dyes or photoconvertible proteins. Cells could also be marked permanently by genetic recombination using the Cre/LoxP system[1] to express a fluorescent reporter specifically in only a subset of cells. Alternatively, upcoming advances in automated cell tracking on time-lapse movies might enable to determine the specific fate of each cell of a given tissue. It is nowadays possible to automatically segment nuclei on 3D image (Nguyen et al., 2019; Ortiz et al., 2019) but the challenge lies on the capacity of following all the cells from one frame to the next one, especially in developing tissues where cell divisions and cell neighbour exchanges take place.

In *neurog1*^{hi1059} mutants, the absence of Ngn1 results in a partial EON specification and a delay of the early phases of OSN differentiation. The addition of a morpholino against a second basic helix-loop-helix transcription factor gene *neurod4* results in the double loss of function of *ngn1* and *neurod4* and in that case all EONs and OSNs are lost in the developing OP, indicating that *ngn1* and *neurod4* genes are redundantly required for OP neurogenesis (Madelaine et al., 2011).

[1] A fluorescent reporter is flanked by a *loxP-STOP-loxP* ("floxed" STOP) sequence and when Cre recombinase is expressed, it specifically activates the reporter by excising the STOP sequence. In order to obtain mosaicism, the Cre recombinase can be expressed under the control of a tissue- or cell-specific promoter or can be fused to human estrogen receptor which makes it active only in the presence of tamoxifen.
Kretzschmar, K., and Watt, F.M. (2012). Lineage tracing. Cell *148*, 33-45.

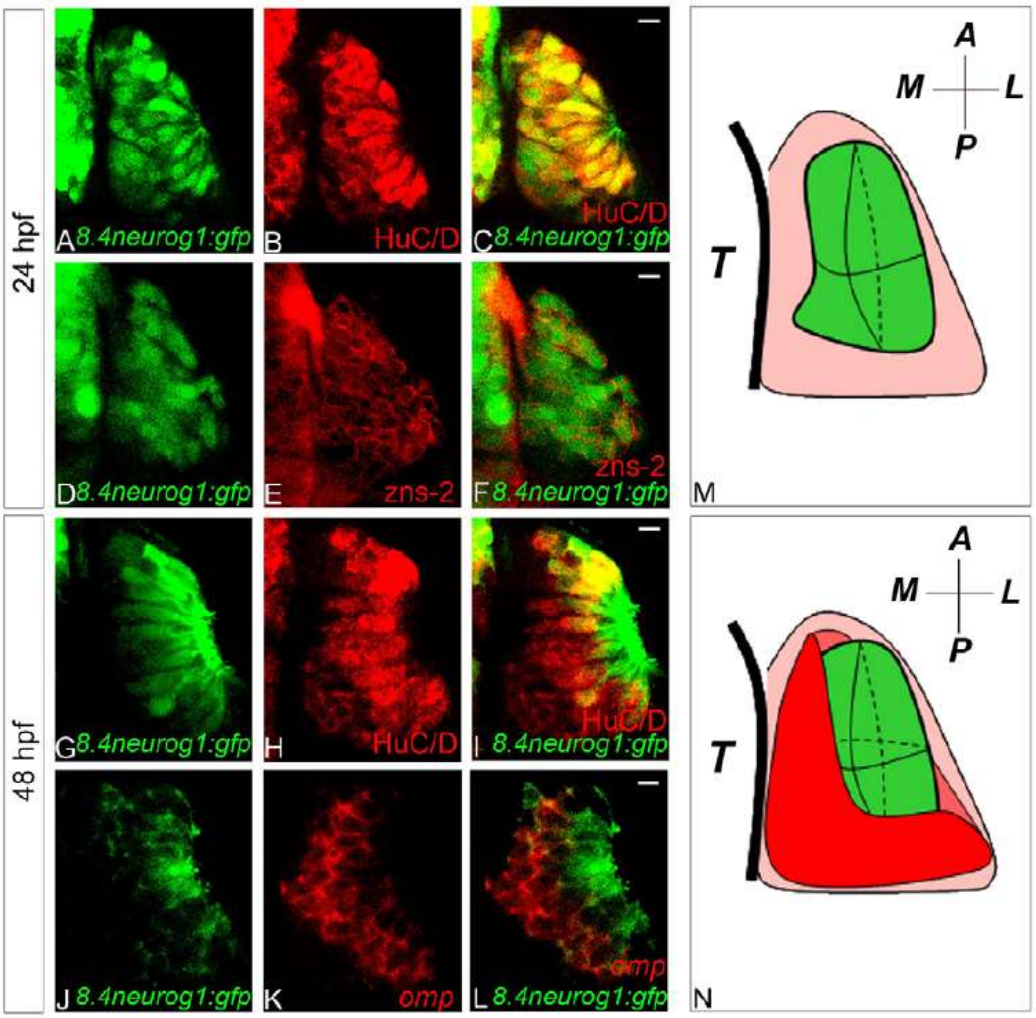

Figure 24: ***Tg(8.4neurog1:gfp)*** **line as a marker of a subpopulation of zebrafish OP neurons**. *"(A-F) Single confocal sections of OPs showing co-expression of HuC/D (A-C) or Zns-2 (D-F) with GFP from the Tg(8.4neurog1:gfp) transgene at 24 hpf. (G-L) Single confocal sections of OPs showing immunolabelling of HuC/D (G-I) or in situ hybridisation and immunolabelling of Omp (J-L) and GFP from the Tg(8.4neurog1:gfp) transgene at 48 hpf. Whereas all GFP-positive cells in the placode are HuC/D- and Zns-2-positive at 24 hpf, at 48 hpf HuC/D+/GFP– cells are present; little, if any, overlap is detected between the expression of omp transcripts and GFP at 48 hpf. (M,N) Schematics of OPs at 24 hpf (M) or 48 hpf (N). EONs are shown in green and OSNs in red. A, anterior; L, lateral; M, medial; P, posterior; T, telencephalon. The scale bars are 10 µm."* (Madelaine et al., 2011)

A study from the same lab further focused on how neurogenesis and morphogenesis are coordinated within OP by analysing the migratory behaviour of EONs in the absence of *ngn1*

(Aguillon et al., 2020). The authors found that OP coalescence movements in *neurog1*^{hi1059} mutants are spatially reduced, especially in anterior OP cells that migrate less posteriorly during OP coalescence. This defect of OP coalescence appears to be similar to the phenotype observed in *cxcr4b*^{t26035} mutants, lacking the receptor Cxcr4b (Aguillon et al., 2020; Miyasaka et al., 2007). Moreover, *cxcr4b* expression is dramatically reduced or even absent in EON progenitors of *neurog1*^{hi1059} mutants at the beginning of OP coalescence, and *cxcr4b*^{t26035} mutants caring the *Tg(-8.4neurog1:cxcr4b-mCherry)* transgene showed a rescued convergence phenotype, indicating that Cxcr4b is a downstream effector of Ngn1 during the early phase of OP morphogenesis. Using chromatin immunoprecipitation (ChIP)[2] and Cripsr/Cas9 experiments, the authors found that Ngn1 directly regulates *cxcr4b* through an E-box cluster located just upstream of the *cxcr4b* transcription start site. These results indicate that Ngn1 directly controls OP coalescence *via* its target gene *cxcr4b.* Thus, Ngn1 ensures the coordination of morphogenesis and neurogenesis in the peripheral olfactory sensory organ (Aguillon et al., 2020; Madelaine et al., 2011).

- **Pioneer neurons and axon growth towards the olfactory bulb**

Later on, OP neurons extend their axons from the OP towards the olfactory bulb. Whitlock *et al*. observed that the initial axon extension comes from a transient population of neurons labelled with the Zns-2 marker whose axons emerge from the OP at prim-5 (24 hpf) (Whitlock and Westerfield, 1998). These neurons are described as a different population than OSNs because they are unipolar, they cluster in the ventral-medial part of the OP and they undergo apoptosis at around 48 hpf as revealed with TUNEL assay (light green cells on Figure 25). On the contrary, OSNs progressively form a rosette in the dorso-lateral region of the placode, with their dendritic tips oriented towards the rosette centre and their axons on the other side (dark green and red cells on Figure 25). Moreover, surgical ablation of the ventro-medial unipolar neurons results in the misrouting of all olfactory sensory axons stained with the carbocyanine dye DiI (added to the surrounding water, this dye enters the cells in direct contact with the external medium). These results led the authors to suggest that these so-called pioneer neurons play a role in the correct glomeruli targeting of OSNs, acting as a scaffold for later born neurons

[2] Chip is a technique whereby a protein of interest is selectively immunoprecipitated from a chromatin preparation to determine the DNA sequences associated with it.

Collas, P. (2010). The current state of chromatin immunoprecipitation. Mol Biotechnol *45*, 87-100.

to project their axons towards the olfactory bulb. However, it seems likely that the proximal portion of OSN axons, which forms by retrograde extension within the OP (Breau et al., 2017), has been removed or perturbed during the surgical ablation of the ventro-medial unipolar neurons, and this may contribute to the later axon pathfinding defects. It would thus be important to revisit and clarify the fate, axonal projections and function of ventro-medial unipolar neurons versus rosette neurons.

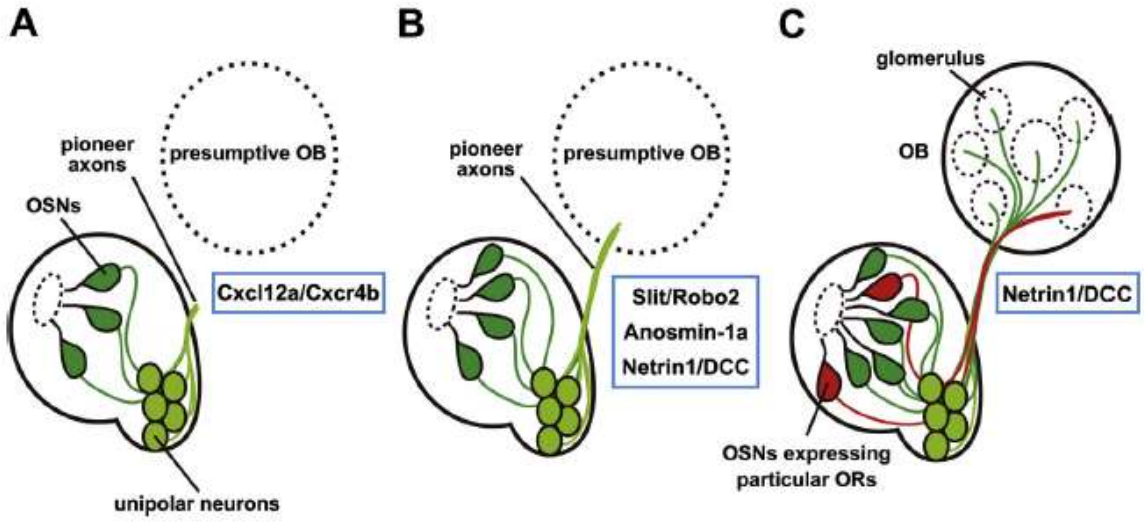

Figure 25: **Schematic representation of the OSN rosette and the pioneer neurons, and of the chemical cues involved in pathfinding of OSN axons towards their target glomeruli.** *"(A) Cxcl12a/Cxcr4b signalling guides the pioneer axons to exit the OP. (B) Slit/Robo2 repulsive signalling guides the pioneer axons toward the presumptive olfactory bulb (OB) by preventing them from entering into inappropriate area. Slit/Robo2 signalling and Anosmin-1a are required for fasciculation of olfactory axons before entering into the OB. Netrin1/DCC attractive signalling draws the pioneer/OSN axons into the OB. (C) Netrin1/DCC signalling guides the axons of OSNs expressing particular ORs to terminate on a specific glomerular cluster."* (Miyasaka et al., 2013)

Additionally, classical axon guidance molecules (see I.A.1), such as Slit ligands and Robo receptors (Miyasaka et al., 2005) or Netrin ligands and DCC receptor (Lakhina et al., 2012), have also been found to be implicated in the guidance and fasciculation of zebrafish olfactory neuronal projections within the brain territory (as reviewed in (Miyasaka et al., 2013)) (Figure 25).

- **Contribution of NCCs to neurons composing olfactory epithelium**

In addition to OSNs and supporting cells, the OPs have been proposed to generate a class of neuroendocrine cells secreting the gonadotropin-releasing hormone (GnRH) (Dubois et al., 2002). GnRH is a neuropeptide essential for the development of secondary sex characteristics in vertebrates. GnRH neurons are divided in two categories with two main functions: some have a direct endocrine role as the releasing hormone acting on the pituitary, while others act as a neuromodulator within the central nervous system. Whitlock *et al.* showed that endocrine and neuromodulatory GnRH cells arise respectively from the dorsally migrating cranial NC and from the adenohypophyseal placode, two separate non-olfactory regions in the developing neural plate (Whitlock et al., 2003).

Live imaging of double transgenic embryos with NCCs labelled in green (*sox10:EGFP*) and OP precursors in red (*six4b:mCherry*) enabled to further decipher the interactions between cranial NCCs and OP cells and showed that NCCs associate with and eventually surround the forming OP during OP coalescence between 10 s (14 hpf) and 20 s (19 hpf) (Figure 26). However, intermixing between the two cell populations remained limited during this process (Harden et al., 2012).

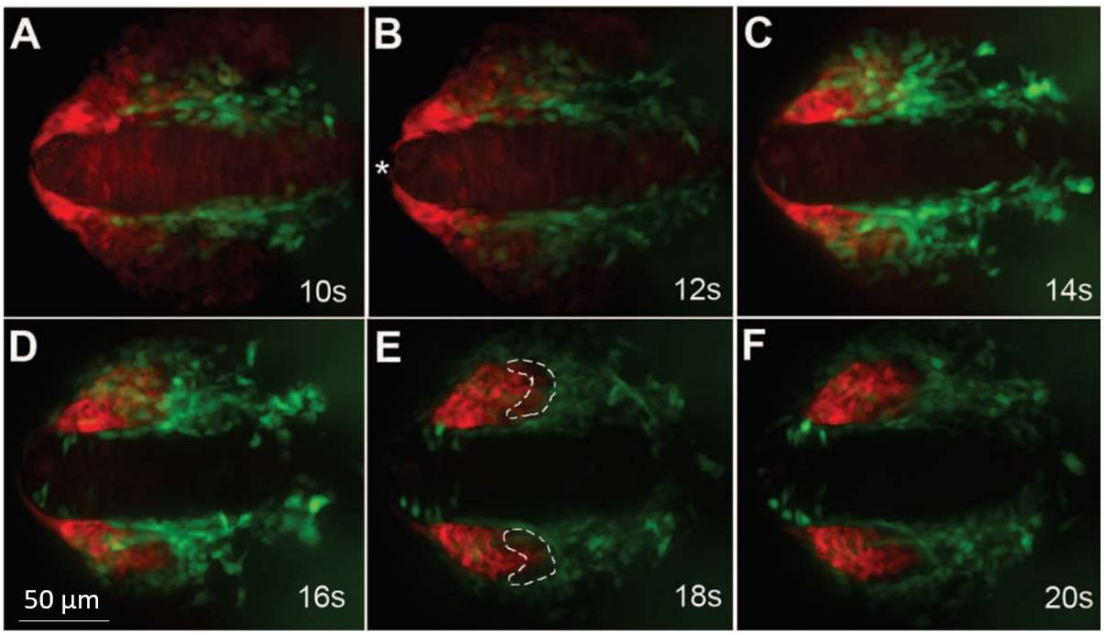

Figure 26: **Time lapse images showing the migration of cranial NCCs (sox10:EGFP line; green) and the coalescence of OP precursors (six4b:mCherry line, red).** Dorsal views with anterior to the left. (Harden et al., 2012)

Using photoconversion-based fate mapping and cell tracking, Saxena *et al.* found that a subset of NCCs expressing the transgene *sox10:eGFP* migrated into the olfactory epithelium and differentiated into microvillous sensory neurons. Moreover, laser ablation of the GFP+ NCCs present in the nasal cavity and morpholino-mediated knockdown of Sox10 inhibited microvillous neurogenesis, suggesting that these cranial NCCs are the primary source of microvillous sensory neurons within the olfactory epithelium (Saxena et al., 2010).

However, a recent study using cell backtracking in confocal movies and photoconversion experiments, questioned these scenarios. Using a novel marker for GnRH3 neurons, the GnRH cells present in the olfactory epithelium, Aguillon *et al.* found that most if not all GnRH3 neurons derive from the PPR. Similarly, they showed that microvillous sensory neurons have a placodal origin, rather than a NC one, arguing that the expression of the transgene *sox10:eGFP* observed in the olfactory epithelium (Saxena et al., 2010) does not reflect a NC origin for these cells but rather an ectopic site of transgene expression. These results support the idea of a common placodal origin for all the neuronal populations within the olfactory epithelium and argue against any NC contribution to the cell-type heterogeneity found in the olfactory epithelium (Aguillon et al., 2020).

- **Potential extrinsic forces exerted on the OP during its morphogenesis**

In this section, we have discussed the processes of cranial placode development with the induction of the common PPR, the subsequent segregation of the different placodes and finally the common mechanisms involved in individual placode coalescence. We have briefly described the function and the structure of the zebrafish olfactory circuit. At last, we have reviewed the mechanisms described so far to be involved in zebrafish OP coalescence and simultaneous neurogenesis and axon extension.

As described earlier, previous results from the team indicate that OP initial axon elongation occurs in a retrograde fashion, where the cell bodies are passively displaced laterally while the axon tips remain anchored at the brain surface. This suggests that extrinsic mechanical forces are required for OP morphogenesis and for the initial elongation of olfactory axons. One hypothesis for the source of these extrinsic forces is that the converging placodal cells could squeeze and push the central cell bodies laterally. The work of a former postdoc in Breau's team, Girisaran Gangatharan, tested this hypothesis and analized the movements of central OP cells when groups of cells located at the OP extremities (the converging cells) were laser

ablated. His results showed that cells located at the OP extremities and converging towards the centre are not required for the proper lateral movement of central cells, indicating that the compression potentially exerted by these cells is not responsible for the lateral movement.

Another hypothesis is that the mechanical forces driving lateral movements could originate from a surrounding tissue, namely the underlying eye. It is increasingly evident that the biomechanics of morphogenesis must be understood not only in the scope of isolated tissues, but also in the framework of interacting tissues. Indeed, evidence for extrinsic forces from surrounding tissues influencing tissue morphogenesis has been previously reported. In the next section, we will review the recent findings on mechanical interactions between developing adjacent tissues and we will focus on how these interactions contribute to morphogenesis.

C. Intertissue mechanical interactions

It is fascinating to see how the morphogenesis of different tissues is coordinated in space and time in developing organisms. Some tissues within the embryo undergo morphogenesis in a highly synchronous manner even though their movements involve different mechanisms (Lye et al., 2015). Mechanical coupling between tissues might be a major factor favouring such synchronization (Goodwin and Nelson, 2021; Villedieu et al., 2020).

A recent review proposed to use the concept of embryonic induction, formalized following Spemann and Mangold's pioneering experiments (Mangold and Spemann, 1927) as a framework for the study of tissue mechanical interactions (Villedieu et al., 2020). Embryonic induction is classically defined as the interaction between an inducer tissue and a responder tissue, where the inducer emits a chemical signal, usually a morphogen, that is received by the responder, resulting in a change in its direction of differentiation (Gurdon, 1987). According to the interesting parallel made by Villedieu *et al.*, a responder tissue deforms or flows in a non-autonomous manner due to the mechanical propagation of a deformation or flow generated in an autonomous manner in a neighbouring inducer tissue. The mechanical competence of the responder tissue relies on its way of deforming or moving under external mechanical stress, which depends, among others, on the material properties of the tissue (Figure 27).

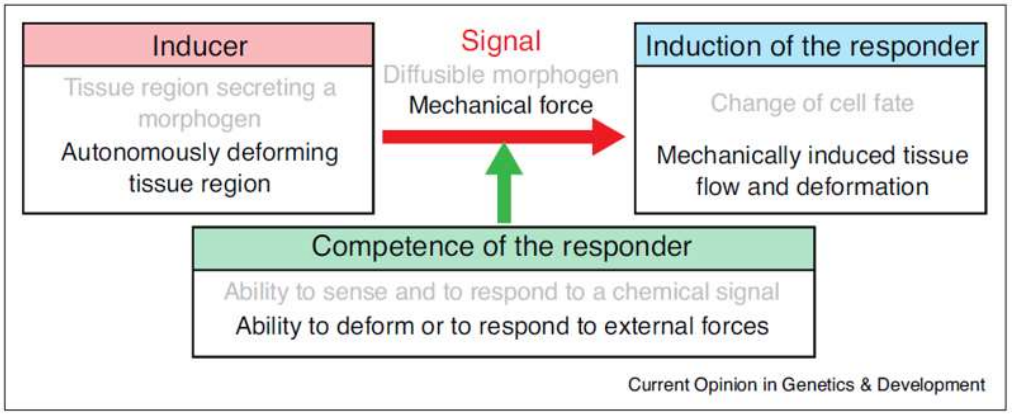

Figure 27: **Classical chemical induction versus mechanical induction.** "*This diagram illustrates the analogy between classical chemical induction (grey font) and mechanical induction (black font), whereby the signal sent by the inducer tissue (red) results in an effect in the responder tissue (blue). For classical induction the signal is a secreted morphogen, while for mechanical induction, the signal is a mechanical force. The competence of the responder (green) refers to the ability of the signal-receiving tissue to respond to the signal sent by the*

inducer. In classical induction, the secreted signal induces a cell fate change in the responder tissue, whereas in mechanical induction, the mechanical signal triggers a morphogenetic response (deformation or flows).” (Villedieu et al., 2020)

In the same review, the authors sorted interactions between two epithelial tissues based on the typology of the interface between the two tissues (Figure 28). Inducer and responder tissues can be adjacent with forces exerted on their edge: such forces can act perpendicular or tangentially to the boundary line. In the case where the inducer and the responder are on top of each other, the forces are exerted on the surface of their contact zone. Villedieu *et al.* described several types of morphogenetic movements in the inducer tissue that generate mechanical forces on the responder such as tissue invagination, contraction, elongation, spreading, etc. These different types of morphogenetic events result in various responder tissue changes depending on the typology of the interface between the two tissues (Villedieu et al., 2020).

EDGE 2 adjacent epithelial regions		**SURFACE** Not in the same plane
(A) Edge orthogonal forces	(B) Edge tangential forces	(C) Surface forces
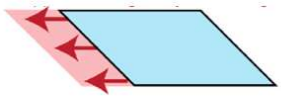	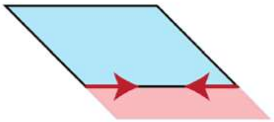	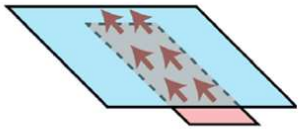
pulling forces exerted by - Invagination - Contraction - Actomyosin ring -Cell migration	- Contraction - Elongation	- Spreading - Contraction - Cell migration
- Translation - Deformation	- Swirling flow - Elongation	- Simple spreading - Swirling pattern

Inducer movements ⟶ Responder movements

Figure 28: **Classification of typologies of mechanically interacting tissues during morphogenesis.** Inducer (red) and responder (blue) tissues can be either adjacent or located in different planes (C). The forces exerted by inducer tissue on responder tissue can be perpendicular to the edge (A) or tangential (B). The two last lines of the table respectively list the inducer morphogenetic movements (red) and the consequent responder movements (blue). (adapted from (Villedieu et al., 2020))

In the following section, we will focus on examples of tissue/tissue interactions in development, trying to emphasize the evidences suggesting that these interactions are mechanical rather than chemical, a distinction which is still challenging to achieve experimentally. Here we use the nature of the interface to catalogue the reviewed examples by discriminating between interactions with presumably direct cell/cell contacts between the two tissues and interactions that are mediated by the ECM. The latter category also includes situations where the ECM plays a role in anchoring the responder to counterbalance the forces generated by the inducer, resulting in the deformation of the responder. Finally, we will discuss the general tools used in the seven upcoming examples to assess the mechanical nature of the intertissue interactions.

1. Direct contact between the two tissues

- ***Drosophila* germ band extension**

A typical example of intertissue mechanical interactions lies in the interplay between the *Drosophila* invaginating posterior midgut, also called posterior endoderm, and the extending germ band. Two main mechanisms contribute to *Drosophila* germ band extension (Collinet et al., 2015; Lye et al., 2015). At the local scale, cell intercalation by junction remodelling is essential for germ band elongation (Bertet et al., 2004). It was further found that tissue extension correlates mostly with new junction growth during the process of cell intercalation and that junction growth is due to local polarized forces generated by actomyosin contractions (Collinet et al., 2015). At the tissue scale, pulling forces from the invaginating posterior midgut contribute to tissue extension by orienting anteroposterior cell elongation and new junction growth (Collinet et al., 2015; Lye et al., 2015) (Figure 29). These studies highlighted the combination of intrinsic tissue (cell intercalation) and extrinsic (external pulling forces) mechanisms to drive the elongation of a developing tissue.

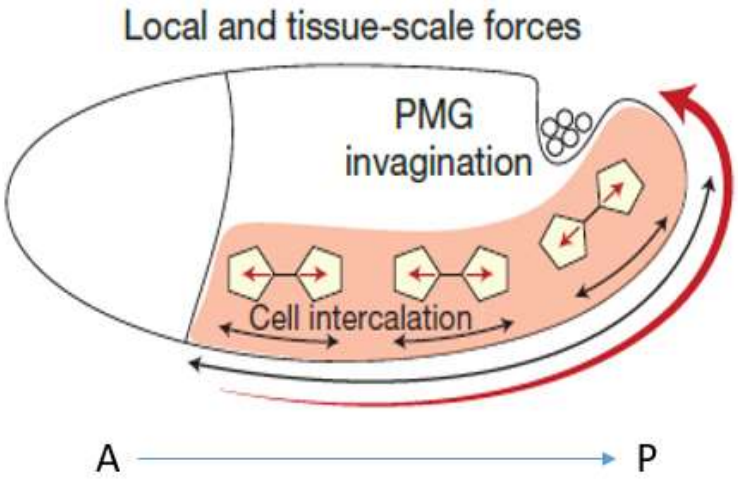

Figure 29**: Schematic of the two main mechanisms involved in germ band extension.** Cell intercalation and posterior midgut (PMG) invagination contribute to germ band extension. "*Red arrows indicate stresses and black arrows strains (cell intercalation and tissue extension). In wt embryos intrinsic forces due to MyoII promote cell intercalation and junction growth. Extrinsic forces properly orient junction growth allowing net tissue extension.*" (Collinet et al., 2015)

A further study showed that the posterior endoderm invagination is an active process driven by Rho1 and myosin II activation (Bailles et al., 2019). Such morphogenetic event is a good illustration of mechanical induction where the active inducer movements, *i.e* the endoderm invagination, induces a shape change in a responder tissue, *i.e.* an elongation of the germ band. The two tissues are adjacent, but they are rather continuous without any clear physical boundary. The authors of both studies indeed did not characterize direct cell/cell contacts between them that would transmit the forces from the posterior midgut to the germ band. Investigating the nature of the interface and how the mechanical tension is transmitted from the invaginating tissue to the expanding germ band could help to better grasp how intertissue mechanical interactions drive morphogenesis.

In both studies, the authors first show that there was an interaction between the two tissues and that the inducer movements were required for the proper extension of the responder. The former observation of a gradient of the germ band cell elongation along the anteroposterior direction suggested a role for extrinsic tensile forces (Butler et al., 2009).The loss of anteroposterior cell elongation (Lye et al., 2015) and the reduction of germ band extension (Collinet et al., 2015) in *torso-like (tsl)* mutants was attributed to the loss of endoderm invagination in this condition.

This result was confirmed in another genetic condition where the posterior mid gut invagination and its anterior movement are abolished by injection of double-stranded RNAs against *fog* (Collinet et al., 2015). These experiments demonstrate that there is an interaction between the two tissues but does not tell whether the nature of this interaction is mechanical or chemical.

Two main tools further enabled to discriminate between chemical and mechanical interactions. Numerical simulations of the germ band (based on a vertex model) showed that an actively moving posterior boundary is required for its proper extension, indicating that active forces at the posterior boundary are essential for tissue extension (Collinet et al., 2015). Finally, laser ablations within the germ band enabled to map the relative distribution of mechanical tension and showed that the tension was the highest posteriorly (close to the invaginating posterior midgut) and along the anteroposterior axis, consistent with the idea of pulling forces exerted orthogonally (Figure 29) (Collinet et al., 2015; Lye et al., 2015). Moreover, supracellular laser ablations revealed that this tension anisotropy is completely lost in *tsl* embryos, where endoderm invagination is affected (Collinet et al., 2015).

- **Zebrafish epiboly**

During zebrafish epiboly, the enveloping cell layer (EVL) progressively covers the yolk towards the vegetal pole of the embryo, a movement that is driven by pulling forces generated by the interaction between the yolk syncytial layer (YSL) and the EVL (Behrndt et al., 2012; Schwayer et al., 2019) (Figure 30). Behrndt et *al.* described how an actomyosin contractile ring in the yolk at the margin between the two tissues promotes the spreading of the EVL through two mechanisms. First, the circumferential tension produced by this contractile ring and the embryo spherical geometry engender what the authors have called a “cable-constriction motor” activity. Second, a retrograde actomyosin flow within the YSL resisted by friction creates a pulling force termed “flow friction motor” by the authors. This friction-resisted flow is sufficient to drive the EVL spreading even in the absence of the cable-constriction motor, *i.e.* in situations where the embryo geometry disables the circumferential contraction (Behrndt et al., 2012). This example illustrates how actomyosin cable and flow present in an inducer tissue (the YSL) can generate pulling forces on an adjacent responder tissue (the EVL) (Figure 28A).

A follow-up article from the same team studied in more details the nature of the interface between these two tissues. Schwayer *et al.* found that tight junctions (TJ) at the tissue boundary have a mechanosensitive role that is critical for the spreading of the EVL. The accumulation of

Zonula Occludens-1 (ZO-1) (a cytoplasmic scaffolding protein connecting the transmembrane proteins to the cytoskeleton) at TJs scales with the actomyosin tension at the EVL-YSL interface. Accumulation of junctional ZO-1b is mediated by the retrograde actomyosin flow within the yolk as it moves non-junctional ZO-1b towards the border. When the formation or the junctional incorporation of ZO-1 clusters is impaired, by expressing truncated versions of ZO-1b through RNA injections in maternal zygotic (MZ) *zo-1b/3* mutants, TJs lose their mechanosensitivity, and consequently, the EVL spreading is delayed (Schwayer et al., 2019). The role of TJ mechanosensitivity in regulating the coupling between the EVL and the YSL and in adjusting it to the mechanical force applied by the contractile actomyosin ring still needs to be explored. However, even if further investigations are required to determine whether TJs regulate intertissue coupling strength, this study is a good example where the role of cellular junctions between two tissues interacting mechanically with each other is well described.

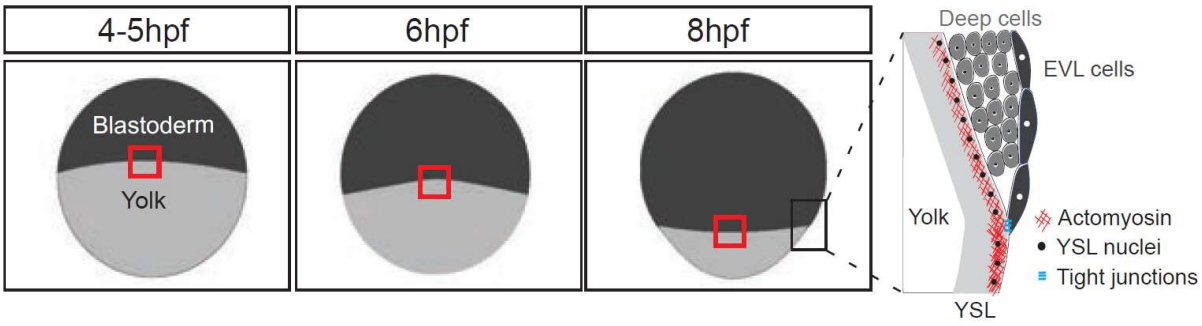

Figure 30: **Schematic representation of enveloping cell layer (EVL, black) spreading during epiboly.** *"Animal pole is to the top. Yolk cell and yolk syncytial layer (YSL), light gray; blastoderm (EVL and deep cells), dark gray. The red rectangle demarcates regions of the EVL-YSL boundary where the study focuses later on. The black rectangle demarcates the region of the enlarged sagittal view outlining the tissue structure at 8 hpf. The actomyosin network (red on the enlarged view) is denser at the EVL/YSL interface; the contact between EVL and YSL is mediated by tight junctions (blue)."* (Schwayer et al., 2019)

As in the previous example on *Drosophila* germ band extension, laser ablation was used to map tissue mechanical stress (Behrndt et al., 2012; Schwayer et al., 2019). The mechanical tension was measured in the actomyosin ring for two different orientations (parallel or orthogonal to the tissue spreading direction) and at different stages of epiboly (Behrndt et al., 2012). In order to assess the role of ZO-1 in building tension at the interface, laser ablation in the actomyosin ring was also performed in conditions where ZO-1 is disrupted at the EVL-YSL interface. In

embryos where morpholinos against *zo-1b* and *zo-3* have been injected in the YSL, the tension in the actomyosin ring was reduced indicating that proper TJs mediated by ZO-1 are required for generating tension in the actomyosin ring, which was previously shown to be required for proper EVL spreading (Schwayer et al., 2019).

A theoretical model was used to investigate the role of the "flow-friction motor" in the EVL spreading and revealed that both mechanisms, *i.e.* "cable-constriction motor" and "flow-friction motor", contribute to the total force exerted by the ring upon the EVL (Behrndt et al., 2012). Finally, changing the geometry of the embryo by constraining it in cylindrical agarose tubes whose diameters are smaller than that of the embryo hinders the "cable-constriction motor" activity, and thus enables to study the effect of the other mechanism alone. The authors found that EVL spreading occurred even in this condition indicating that flow-friction motor is sufficient to drive EVL epiboly (Behrndt et al., 2012).

- **Zebrafish neural anlage positioning**

During zebrafish epiboly, pulling forces exerted by the actomyosin ring within the YSL drive EVL migration towards the animal pole. At 50% of epiboly (5.25 hpf), the gastrulation starts with major movements in deep cells, which give rise to the mesendoderm (Figure 30 grey cells). On the anterior side of the embryo, the mesendoderm ingresses and the mesoderm leading edge, which is called the prechordal plate migrates in a group from the embryonic organizer to the animal pole (Dumortier et al., 2012) while the overlying ectoderm migrates towards the vegetal pole during epiboly. Smutny *et al.* found that these two opposing movements generate friction forces at the interface between the prechordal plate (green tissue) and the neurectoderm (dark red arrows), which gives rise to the anterior neural anlage. These friction forces lead to global rearrangement of cells within the neurectoderm and determine the final position of the neural anlage. Looking more closely at the interface, the authors found that the two tissues are in direct contact, which is mediated by E-cadherin (Smutny et al., 2017).

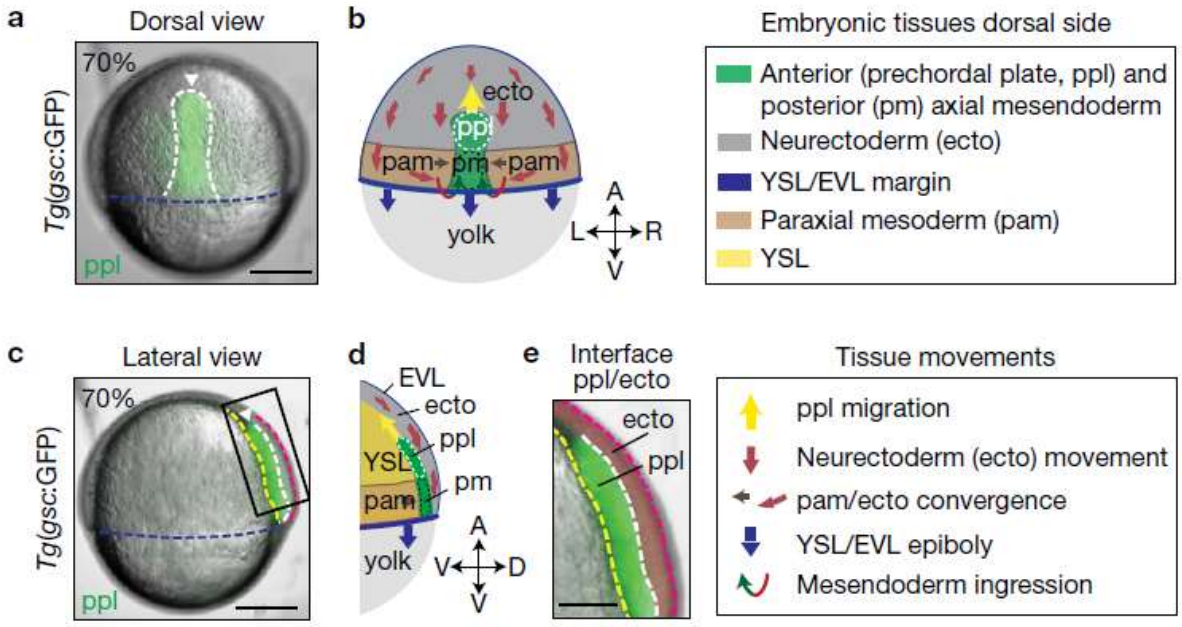

Figure 31: **interaction between neurectoderm (ecto) and prechordal plate (ppl) during zebrafish gastrulation.** *"(a,c) Bright-field/fluorescence images of a Tg(gsc:GFP) zebrafish embryo at 7 hpf; GFP-labelled prechordal plate (ppl) leading edge cells are indicated (white arrowheads); the rectangle in c marks the magnified area in e; the dashed lines in (a) indicate axial mesendoderm (white), and in (c) ectoderm/ppl (white), yolk syncytial layer (YSL)/ppl (yellow), enveloping layer (EVL)/media (pink) and EVL/YSL (blue) interfaces; embryonic axis orientation as marked in (b),(d) for same views. (b,d) Illustration of embryonic (anterior (ppl) and posterior axial mesendoderm (pm), paraxial mesoderm (pam) and ecto) and extra-embryonic (YSL, EVL, yolk) tissues, and their respective direction of movement during gastrulation at the dorsal side of the zebrafish embryo; arrows in (b),(d) indicate animal–vegetal (A–V), left–right (L–R) and dorsal–ventral (D–V) embryonic axes. (e) A magnified view of the boxed area in c showing neighbouring ppl (green) and overlying ectoderm (red pseudocoloured) tissues; dashed lines as in (c)."* (Smutny et al., 2017)

The effect of the inducer tissue, the prechordal plate, on the responder tissue, the neurectoderm, was first assessed using genetically disrupted conditions where (1) the inducer tissue was absent, as in zebrafish MZ *oep* mutant embryos, lacking much of the mesendoderm germ layers, or (2) the movements of the inducer tissue were reduced, as in *slb/wnt11* morphant embryos, in which prechordal plate cells move slower and in a less-coordinated way towards the animal pole or *cyc* mutant embryos, in which a diminished number of prechordal plate cells displayed reduced velocity and less coordination. In all these genetic conditions, the 3D velocities were

retrieved from automated cell tracking data and a directional correlation coefficient between the velocities of the two tissues was calculated. This quantitative analysis of cell movements revealed that loss of most of the mesendoderm or perturbation of movements within the mesendoderm resulted in perturbed movements of the neurectoderm and in mispositioning of the neural anlage compared to *wt* embryos.

These experiments show that the mesendoderm is required for proper mesendoderm movements but do not demonstrate the mechanical nature of this intertissue interaction. The agreement between predictions from a theoretical model and experimental data further indicated the mechanical aspect of this interaction and showed that it is the friction forces generated at the interface between the two tissues that triggers tissue deformations within the ectoderm. In addition, perturbing E-cadherin, the physical glue connecting the two tissues, using *e-cadherin* (*cdh1*) morpholinos, resulted in the loss of the correlation between the inducer and the responder tissue movements and in a further mispositioning of the responder tissue, reinforcing the idea of a physical coupling.

In order to investigate if E-cadherin-mediated friction alone is sufficient to induce a response of the neurectoderm, the authors turned up to an *in vitro* assay to mimic the friction between E-cadherin and ectodermal cells. Polystyrene beads coated with E-cadherin were positioned on top of a cluster of ectodermal cells and were sheared uniaxially in the opposite direction than the one of ectodermal cell movements. This set-up demonstrated the sufficiency of E-cadherin-mediated friction forces to reorient ectodermal cell movements. However, the exact molecular mechanism of the friction generation mediated by E-cadherin at the interface remains elusive as number, lifetime and elasticity of E-cadherin bonds at the tissue interface are unknown.

- ***C elegans* body elongation**

C elegans body elongation involves the interaction between three types of tissues: the inner muscle fibres (red on Figure 32), the lateral epidermis (yellow) and the dorsoventral epidermis (blue). A series of studies showed that muscle contractions progressively drive the extension of the overlying epidermis. During the first phase of body elongation (before the onset of muscle contractions), the combination of oriented anisotropic stiffness in dorsoventral cells and of anisotropic actomyosin stress in muscle cells ensures that the embryo only elongates along the head-to-tail axis (Vuong-Brender et al., 2017). During the second phase, muscle activity leads to cycles of contraction/elongation of the embryo and each cycle results in an irreversible

elongation of the dorsoventral cells, thus increasing the total body axis length by incremental steps. This ratchet-based mechanism relies on the progressive shortening of epidermal actin microfilaments relayed by actin-severing proteins (Lardennois et al., 2019).

The coupling between the muscles and the dorsoventral epidermis is mediated by hemidesmosomes[3] (purple on Figure 32). Moreover, this tissue coupling adapts dynamically as muscle activity triggers a mechanotransduction pathway in epidermal cells that strengthens the intercellular adhesion by promoting the maturation of these hemidesmosomes (Zhang et al., 2011). This mechanotransduction pathway also controls the establishment of bipolar planar polarity of cytoskeleton elements and therefore, controls tension orientation in the lateral epidermis (Gillard et al., 2019).

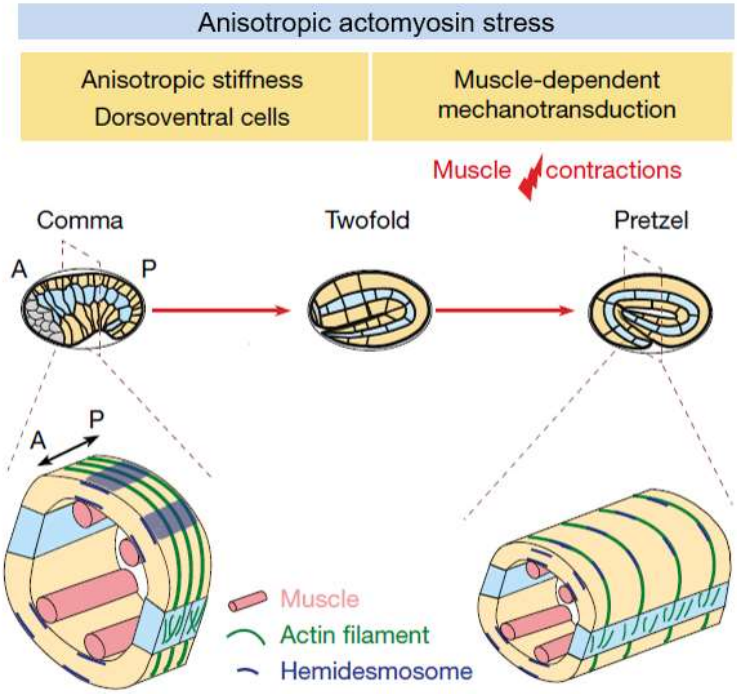

Figure 32: **Schematic view of *C elegans* embryonic elongation: during the first phase, the interplay of stiffness and force anisotropy drives embryo elongation and during the second phase, muscle contractions drive the epidermis anteroposterior extension.**

[3] Hemidesmosomes are multiprotein complexes mainly present in epithelia and facilitating the stable adhesion of cells to the basement membrane. These highly specialized integrin-mediated epithelial attachment structures make cells firmly adhere to the ECM by establishing a link between the underlying basement membrane and the internal cytoskeletal network.

Walko, G., Castanon, M.J., and Wiche, G. (2015). Molecular architecture and function of the hemidesmosome. Cell Tissue Res *360*, 363-378.

"C. elegans embryonic elongation requires an actomyosin force in lateral cells (blue) and actin-promoted stiffness in dorsoventral cells (yellow), followed by repeated muscle contractions (red), which induce mechanotransduction pathway." Adapted from (Lardennois et al., 2019)

Genetic perturbations, mainly by RNA interference, were used to either perturb the inducer tissue movement, *i.e.* the muscle contractions, by decreasing or blocking muscle contractions (Gillard et al., 2019; Lardennois et al., 2019; Vuong-Brender et al., 2017), or disturbing the interface between the muscle and the epidermis (Zhang et al., 2011). The perturbation of muscle contractions or of the muscle–epidermis interface resulted in decreased body elongation.

In order to measure the stress distribution, laser ablation experiments were performed in these studies (Gillard et al., 2019; Vuong-Brender et al., 2017). Not having the temporal resolution, Vuong-Brender *et al.* looked at the shape of the hole to access the anisotropy of the stress before the ablation (Vuong-Brender et al., 2017). The authors found a stress anisotropy along the body axis that correlates with morphological changes.

Besides, continuum models were also used to 1) show that the stress anisotropy and the stiffness anisotropy promote embryonic elongation (Vuong-Brender et al., 2017) and 2) assess the viscoplastic nature of the epidermis during embryo elongation (Lardennois et al., 2019). Finally, application of external mechanical forces on the embryo using a micromanipulator and a mobile stage enabled to partially rescue the phenotype in conditions where muscle function is abrogated and thus to confirm the mechanical role of muscles (Zhang et al., 2011).

2. Interactions mediated by the ECM

We have seen until now examples where direct cell/cell contacts between the two interacting tissues transmit the forces from the inducer to the responder through tight junctions (Schwayer et al., 2019), E-cadherin adherens junctions (Smutny et al., 2017) or hemidesmosomes (Zhang et al., 2011). In the following part, I will present two examples of intertissue mechanical interaction mediated by ECM at the interface between the two tissues, and an example where ECM anchors the responder tissue on one side while the inducer tissue pulls on the other side, which results in responder tissue spreading.

- **Zebrafish myotome morphogenesis**

During zebrafish somitogenesis (between 10.5 hpf and 22 hpf), myotomes, large muscle segments present along the trunk, in the posterior region of the embryo, acquire a characteristic chevron shape (Figure 33). Two mechanisms are at play during myotome shaping in the somites: an intrinsic mechanism, muscle cell differentiation, and an extrinsic mechanism, interaction between myotomes and their surrounding tissues (the neural tube, the notochord and ventral tissues) (Tlili et al., 2019). The mechanical coupling between the forming myotome and these adjacent tissues appears to spatially vary, resulting in spatially heterogeneous friction. Tlili et *al.* showed that the interplay between tissue spreading and friction generated by the interaction with surrounding tissues is sufficient to initiate the chevron shape formation. Further shape change into chevrons with an acute angle yet requires muscle cell differentiation which generates local anisotropic stresses within the tissue.

Here, the interface between the inducer tissues, *i.e.* the neural tube and the ventral tissues and the responder tissue, the myotome, is a surface and the authors found that ECM at the interface is critical for proper chevron shape acquisition.

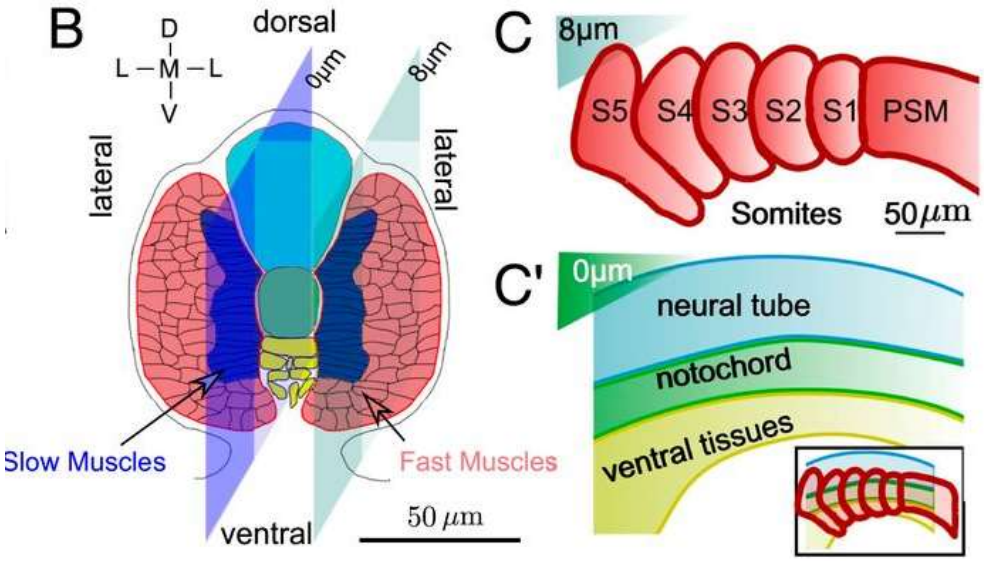

Figure 33: **Schematic representation of zebrafish myotome formation and shaping and of the adjacent tissues**. (B) transverse section with the cross-sectional views shown in (C) and (C') represented in dark and light blue. The developing somites are composed of slow muscle cells (dark blue) and fast muscle cells (red) and they progressively form from the presomitic mesoderm (PSM) and gradually acquire a chevron shape. Myotomes are adjacent to the neural

tube (light blue), the notochord (green) and ventral tissues (yellow). The mechanical coupling between the forming myotome and these adjacent tissues results in a spatially heterogeneous friction, which is sufficient to initiate myotome shape change. (Tlili et al., 2019)

What tools did the authors used to unravel the mechanical interactions with surrounding tissues? First of all, genetic conditions (mutants and morpholinos) perturbing either muscle cell differentiation or the ECM at the somite interfaces resulted in myotome shape defects, suggesting that these two processes might be involved in myotome chevron-like shape. Then, laser ablation of somites revealed the presence of a gradient of active stress with extensile stresses along the anteroposterior axis in early somites (correlating with slow muscle elongation) and tensile stresses in older somites. To note, unlike other examples presented above (I.C.1), laser ablation here was performed at the tissue scale with the ablation of a whole somite, in contrast to laser ablation of cell junctions or lines of cells performed in other studies.

Looking at the difference in velocity between the myotome and surrounding tissues further helped determining which tissue (neural tube, ventral tissues, notochord or skin) the myotome might be the more coupled with and when (before segmentation or after segmentation) this coupling might occur. This quantitative analysis revealed that after segmentation somite movements are strongly correlated to the ones of neural tube and ventral tissues.

To further test this coupling, the authors injected a mix of collagenases to degrade ECM components, as they saw that Fibronectin and Laminin displayed enrichment between the somite–neural tube and somite–ventral tissue. The quantification of somite shape 24 h post-injection revealed a defect in the chevron shape but bright-field images of these embryos also displayed visible general defects in embryo morphology, thus suggesting that the ECM degradation was global and not restricted to the injected area. To our knowledge, injection of collagenase mix in zebrafish embryo had only be done once before, in the developing eye to test whether cell/ECM interactions were involved in actin reorganization (Matejcic et al., 2018). Of note, neither of these two articles present images of the post-injection ECM components to ensure that they are well degraded and to assess the spatial specificity of ECM degradation.

Finally, vertex model simulations showed that the interplay of tissue spreading and friction is actually sufficient to drive the initial phase of chevron shape formation.

- **Zebrafish paraxial mesoderm symmetrical morphogenesis**

At the same stages, but in a more posterior location, two columns of paraxial mesoderm (light blue on Figure 34) surround the central notochord (grey) and the dorsal neural tube (purple). The interaction between the converging neural tube (black arrows) and the laterally expanding paraxial mesoderm (green arrows) are mediated by the ECM component Fibronectin (red). Indeed, Guillon *et al.* found that Fibronectin at the border between the mesoderm and the neural tube dynamically remodels as neural tube progressively converges and based on model predictions, they suggested that this remodelling enables to have higher Fibronectin density at zones of higher inter-tissue stress. This inter-tissue adhesion mechanically couples left and right mesoderms to the neural tube. Thus, the interaction between neural tube and mesoderm dynamically coordinates bilaterally symmetric morphogenesis of the paraxial mesoderms (Guillon et al., 2020).

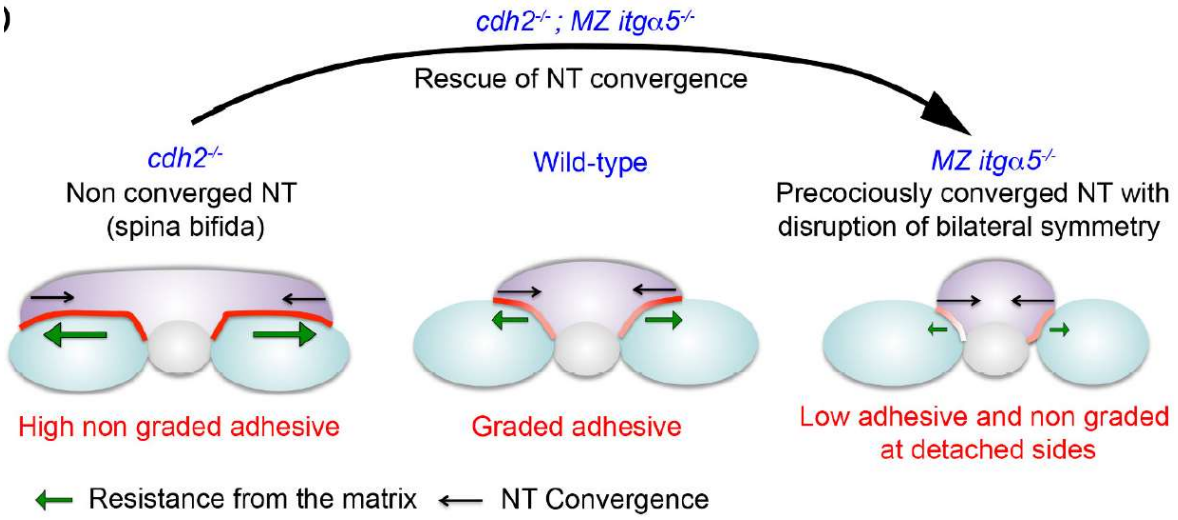

Figure 34: **Schematics of the mechanical interaction between converging neural tube (purple) and laterally expanding paraxial mesoderm (light blue).** *"Too much matrix deposition maintains the symmetry, but slows down the convergence due to high resistance, and predisposes the neural tube to spina bifida-like phenotype with an open neural tube (cdh2 mutant, left panel). Conversely, reduction in matrix deposition helps the neural tube convergence by reducing the resistance (as shown by the rescue of neural tube convergence in double cdh2; itga5 mutants), but it produces local tissue detachment and breaks the mechanical coupling between the tissues generating left-right asymmetries (itga5 mutants, right panel)."* (Guillon et al., 2020)

Genetic conditions were first used to unravel the interplay between the morphogenesis of these adjacent tissues. Reduction of cell-Fibronectin matrix adhesion in MZ *integrin a5* mutants (*itga5*$^{-/-}$) or complete loss of Fibronectin in double homozygous mutant embryos (*fn1a-/-;fn1b-/-*) enhanced neural tube convergence but abrogated bilaterally symmetric paraxial mesoderm morphogenesis (Figure 34 right). In contrast, reducing tissue surface tension as in *cadherin 2* mutants *(cdh2*$^{-/-}$*)* led to neural tube convergence failure (Figure 34 left).

Using a coarse-grained computational model that considers intertissue adhesion, surface tension and internal pressure for the 3 tissues, Guillon *et al.* were able to predict the correct tissue shapes across genotypes and to relate tissue shape changes to tissue mechanics. The computational model also predicted a gradient of tension at the interface between neural tube and mesoderm, with higher tension at the lateral edges and lower tension in the medial portion (respectively dark and light red on the central image of Figure 34), which correlates with the experimental observation of gradients of Fibronectin matrix and F-actin at the interface.

Visualisation of Fibronectin in live embryos (using a heatshock-activable transgene driving the expression of fluorescently labelled Fibronectin, *hsp70: fn1a-mKIKGR*) in the different genetic backgrounds described above revealed that Fibronectin anisotropic remodelling at the interface depends on neural tube convergence and inter-tissue adhesion. This study emphasizes the importance of tools to visualize the ECM and its remodelling to study its role at the interface of tissues mechanically interacting together.

- **Tribolium gastrulation**

During red flour beetle (*Tribolium castaneum*) gastrulation, a part of the blastoderm tissue that is destined to become the extra-embryonic serosa is pulled by the embryo contraction towards and across the posterior pole (Figure 35). Because of the adherence of the blastoderm to the vitelline envelope that surrounds the egg (red dot), these traction forces result in the blastoderm elongation (dashed arrow) (Munster et al., 2019). In this situation, the inducer is the tissue forming the embryo that exerts pulling forces on the responder tissue, the blastoderm. Interestingly, a third tissue, the vitelline envelope, is involved in counterbalancing the forces exerted by the embryo and in maintaining the anterior part of the blastoderm immobile while the posterior part moves. The contact between the vitelline envelope and the blastoderm is mediated by ECM. This process was further observed in *Drosophila* gastrulation.

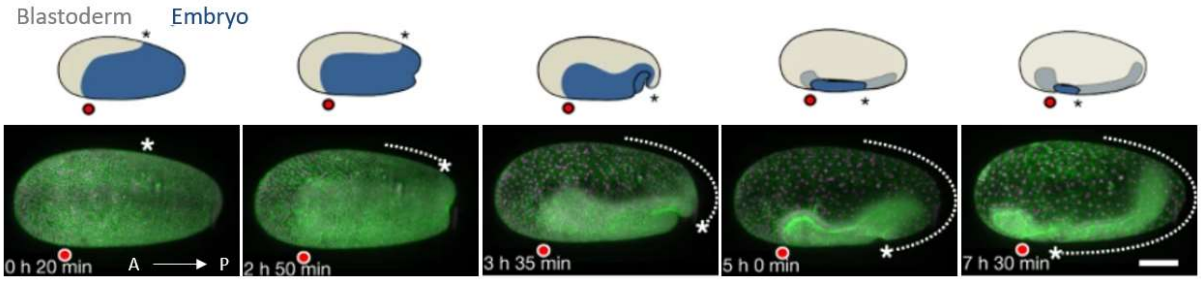

Figure 35: **Schematic representation of *Tribolium* gastrulation.** "*Lateral view of a gastrulating Tribolium embryo in a schematic (top), and in a maximum intensity projection of a line that transiently expresses LifeAct-eGFP (green), imaged by time-lapse light-sheet microscopy (bottom). The blastoderm moves unidirectionally towards and across the posterior pole (dashed arrow and asterisk) and the anterior–ventral part of the blastoderm remains stationary (red circle). Scale bar, 100 µm.*" Anterior to the left and posterior to the right. Adapted from (Munster et al., 2019).

Munster *et al.* built a theoretical model considering the tissue as an active fluid and using the myosin II distribution observed within the embryos as a proxy for the activity pattern of the tissue. They succeeded in inferring the blastoderm tissue flow. By comparing the model predictions with the tissue flow field obtained by particle image velocimetry, they found that while most of the flow patterns were predicted by their model, they did not retrieve the absence of ventral flows with this first attempt. The authors then hypothesize that the absence of ventral flow was due to the mechanical interaction between anterior–ventral blastoderm and the vitelline envelope, which would 'anchor' this region of the blastoderm in place. The addition of such an anchoring point in their model resulted in a proper simulation of the immobility of the ventral tissue.

Transmission electron tomography and the observation of the space between the vitelline envelope and the blastoderm by injecting fluorescent dextran further confirmed the attachment between the two tissues and showed that this attachment was formed dynamically over time.

Injecting the generic protease trypsin that digests ECM complexes into the perivitelline space of the egg resulted in the occurrence of a ventral flow of the anterior part of the blastoderm. This confirms that the embryo pulls on the blastoderm and that the contact between the blastoderm and vitelline envelope provides a counterforce. As in the previously described experiment where degrading enzymes were used to uncouple two mechanically interacting

tissues (Tlili et al., 2019), the proper degradation of ECM compounds was not checked and the local effect of such treatment still needs to be proven. However, this experiment of disruption of the ECM-mediated interaction was further reinforced with integrin knockdown using RNA interference. This resulted in a ventral flow of the anterior blastoderm, in agreement with the initial predictions when attachment was not considered in the model.

In this example, the anchoring of the responder tissue on one side counterbalances the forces exerted by the inducer tissue on the other side. The exact nature of the attachment of the blastoderm to the vitelline envelope remains unknown. It may be direct cell/cell contacts as transmission electron tomography revealed that some blastoderm protrusions are in direct contact with the vitelline envelope. However, ECM components might be involved as degrading them with trypsin or knocking down of *αPS2 integrin*, a transmembrane protein involved in cell-ECM contacts, resulted in a loss of attachment.

3. Key techniques

Common approaches used to assess the role of mechanical interactions between tissues in morphogenesis can be identified throughout all these examples, as summarized in Table 1, with first manipulations showing that two tissues are interacting with each other and then tools to further assess the mechanical nature of this interaction.

First, quantitative analysis of the cell movements in the two tissues either using cell tracking or flow visualization (using tools like particle image velocimetry) enables the comparison of cell motion between the responder and the inducer movements. Several quantities might be computed as the difference between the tissue velocities (Tlili et al., 2019) or the correlation between the cell trajectories (Smutny et al., 2017). Similar movements between adjacent tissues suggest a physical coupling, but without providing any indication of causality.

A widely used experiment to further test the role of the inducer movements on the responder tissue is to study the responder movements in situations where the inducer tissue is lost or its movements are affected, using genetic conditions, such as mutants, morpholinos, RNA interference, etc. The study of the effect of such manipulations can be done on fixed samples, looking at the morphology and the position of the responder tissue, or on live embryos, by quantifying changes in cell movements. In most cases, perturbing the movements of the inducer also changes its position relative to the responder or changes the shape of the inducer, and so

the effect observed on the responder could also be attributed to a defect in chemical signalling from the inducer. The only condition reported here where inducer movements are blocked without disturbing inducer shape and position is the loss of muscle contractions in *C elegans* that affects the epidermis elongation (Gillard et al., 2019; Lardennois et al., 2019; Vuong-Brender et al., 2017). Thus, in most cases, such perturbations show that the inducer movements are required for proper morphogenetic movements of the responder but do not allow to discriminate between a mechanical and a chemical interaction.

Once the interaction between two tissues has been shown, the mechanical nature of this interaction can be investigated by different methods. Physically uncoupling the two tissues by perturbing the "glue" at the interface enables to test whether this physical contact is required for the proper role of the inducer on the responder. In more than half of the cases presented above, genetic conditions affecting the protein(s) mediating the interaction, either through direct cell/cell contacts (Schwayer et al., 2019; Smutny et al., 2017; Zhang et al., 2011) or through the ECM (Guillon et al., 2020), were used to understand the mechanism of force transmission. In order to relate the defects observed in the responder tissue with the loss of contact between the two tissues, perturbing this protein(s) should not perturb the inducer movements.

When the interface is composed of ECM, enzymes degrading ECM components can be injected to uncouple the two tissues. As ECM components are involved in numerous developmental processes, it is important to have the best specificity as possible. In the two examples presented above (Munster et al., 2019; Tlili et al., 2019), the injection of ECM-degrading enzymes enables to have a temporal control of the ECM perturbation but does not seem to have a spatially restricted effect. Moreover, even with a good spatio-temporal control, the ECM might be important for the inducer morphogenesis itself, besides its potential role in force transmission. Thus, when using such tools, it is critical to check that movements in the inducer tissue are not affected. In addition, the ECM may contain secreted chemical signals that could also potentially influence a morphogenetic response in the responder. In this case, perturbing the ECM might perturb chemical signalling as well and it is important to complement ECM disruption with perturbations of the receptors involved in cell-ECM adhesion, such as integrins. This can be achieved by loss of function experiments of integrins using morpholinos or dominant negative forms (DN). Alternatively, the receptors mediating cell-ECM adhesion can be blocked with antagonists, such as Arginylglycylaspartic acid (RGD) peptides.

“Gain of force” approaches where the mechanical forces applied on the responder tissue are amplified enable to assess the sufficiency of such mechanical forces to drive responder morphological changes. This can be achieved by amplifying the inducer movements or by applying external forces. However, applying external forces specifically on the responder tissue without perturbing the integrity of the embryo remains challenging. In one example, the application of shear forces was done on cell culture to show that friction could induce cell reorganization (Smutny et al., 2017). In two examples presented here (Behrndt et al., 2012; Zhang et al., 2011), mechanical stress were applied on the whole embryo.

Theoretical modelling is useful to assess if (1) a mechanical interaction is sufficient by itself to trigger the tissue shape changes or tissue displacement (as in (Behrndt et al., 2012; Tlili et al., 2019)) or if (2) the mechanical interaction is required as an ingredient in the model to obtain the changes in the responder tissue which are observed in the experimental data. If the mechanical interaction is required, a theoretical model where this interaction is not considered will fail to predict the correct responder changes and the predictions will match experimental observations only when this interaction is an ingredient of the model. For example, adding an actively moving posterior boundary to the model predicting germ band extension resulted in higher tissue extension, in the same magnitude as what was observed in *wt* embryos, indicating that the movement of the posterior boundary, which corresponds to the interface with the posterior midgut, was required for proper germ band extension (Collinet et al., 2015).

Another approach used to demonstrate the mechanical nature of the interaction is the mapping of mechanical tension in *wt* conditions and in conditions with perturbed inducer movements. The initial velocity of wound margin retraction after a laser ablation gives an estimation of the stress (before ablation)-to-viscosity ratio within the tissue. Laser ablation experiments enable to map the distribution of mechanical tension and can be performed at the subcellular scale to measure cell junction tension (Behrndt et al., 2012; Breau et al., 2017; Vuong-Brender et al., 2017) or at the tissue scale to measure tissue stress (Tlili et al., 2019). This technique does not provide absolute values of mechanical stress and it is thus used to compare stress between different situations.

		Drosophila germ band extension	Zebrafish epiboly	Zebrafish neural anlage positioning	*C elegans* body elongation	Zebrafish myotome shaping	Zebrafish paraxial mesoderm symmetrical morphogenesis	*Tribolium* gastrulation
Tools to unravel interaction between two tissues								
Quantitative analysis of movements (*wt*)	Calculation of velocities, comparison of the movements in the 2 tissues		x	x	x		x	
Decrease or loss of inducer movements	Genetic conditions	x	x	x	x	x	x	
Approaches to test the mechanical nature of this interaction								
Uncoupling the two tissues	Genetic conditions where the physical glue between the 2 tissues is lost		x	x	x		x	
	Injection of ECM degrading enzymes at the interface					x		x
Gain of forces	Application of external mechanical forces on the developing embryo or on the responder tissue on *in vitro* assay		x	x	x			
Computationnel model		x	x	x	x	x	x	x
Mapping mechanical tension within the responder tissue	Laser ablation in wt and in conditions where the inducer movements are perturbed	x	x		x	x		

Table 1: Summary of the approaches used in the studies of intertissue mechanical interactions presented in this section.

Additional approaches could be used to map stresses in the responder tissue or at the interface between the two tissues in complement to laser ablation. Several techniques allowing to measure forces *in vivo* exist as presented in Table 2 (Sugimura et al., 2016). To name just two examples, Förster resonance energy transfer (FRET) tension sensors or liquid drops are visual sensors used to estimate respectively subcellular forces at the molecular scale or tissue stresses at the cellular scale. FRET tension sensors consist of two fluorophores: a donor and an acceptor linked by a spring-like polypeptide structure of known resistance. The length of the spring increases with pulling forces acting on it. Accordingly, the energy transfer efficiency sharply decreases with the distance between fluorophores and thus there is a scaling between the energy

transfer efficiency that can be visually measured and the molecular forces (Grashoff et al., 2010; Wang et al., 2011). This technique only gives a measurement of the amplitude of tensile stress within a molecule; the orientation of this tension or the compressive stress are not detected.

	Measured quantities	Measurable range	Time scale*	Size scale‡	Advantages	Disadvantages	Cost
Indentation/ microplates/ AFM	Cell or aggregate surface tension	0.1 Pa	s-h	1-100 µm	Absolute measurements	Contact method	€€-€€€€
Pipette aspiration	Cell or aggregate surface tension	µN/m-mN/m	>10 s	1-100 µm	Absolute measurements	Contact method	€€
Optical/magnetic tweezers	Cell junction tension	pN-nN	ms-min	0.1-10 µm	Non-contact; absolute measurements	Delicate calibration	€€€
Subcellular laser ablation	Cell junction tension to viscous drag ratio	NA	0.1 s-min	0.1-10 µm	Non-contact	Possible collateral damage	€€-€€€
Tissue-scale laser ablation	Tissue stress to viscosity ratio	NA	s-min	10 µm-1 mm	Non-contact	Requires sample and laser alignment; few experiments per sample	€€-€€€
FRET force probe	Intramolecular tension	pN	Video rate	nm	Molecular measurements	Requires different control constructs; delicate calibration	€
Liquid drops	Cell-scale stress	~0.1-60 kPa	0.1 s-h	>5 µm	Absolute measurements	Requires surface chemistry of droplets	€€
Birefringence	Tissue-scale stress	>10 kPa	Video rate	>µm	Global	Requires flat, transparent sample; delicate calibration	€
Force inference	Relative cell junction tension, cell pressure	NA	Video rate	>µm	Image based; global	Requires image segmentation	€

*Time scale of the mechanical processes that can be probed.
‡Size scale of the mechanical processes or mechanical elements that can be probed.
NA, not applicable because only relative measurements.
Cost excluding the microscopes: € (<€10,000); €€ (€10,000-50,000); €€€ (€50,000-100,000); €€€€ (€100,000-200,000).

Table 2: Comparison of several methods to measure forces and stresses *in situ* in living tissues. (Sugimura et al., 2016)

Fluorescent liquid drops and elastic beads (either compressible or not) can be injected between cells in a tissue or between tissues and their deformation gives an estimation of stress they are subjected to (Campas, 2016). For instance, fluorescent oil droplets have been used to measure mechanical stress in the presomitic mesoderm (PSM) of zebrafish embryos during body axis elongation (Campas et al., 2014; Mongera et al., 2018). The same team recently developed an analysis software for the automated geometrical characterization of deformable particles that enables the quantification of stresses in the living tissue (Gross et al., 2021). Of note, oil droplets only give the anisotropic component of the normal stresses and they do not deform under shear stress (Campas, 2016; Campas et al., 2014). The use of these *in vivo* droplet-based sensors will greatly contribute to the field of developmental mechanobiology.

The growing literature on the mechanics of developmental biology gives numerous examples of how to assess the mechanical nature of an interaction between tissues, as presented in this section. A recent study goes beyond the view of an inducer driving the morphogenetic

movements of a responder and suggests a two-way interaction where both tissues influence one another creating a mechanical feedback loop. During avian somitogenesis, the paraxial PSM expands and compresses the axial neural tube and notochord, inducing their elongation which in turn drives the lateral movement of midline PSM cells and contribute to PSM expansion (Xiong et al., 2020). This reciprocal mechanical interaction provides robustness and enables coordinated morphogenesis.

D. Zebrafish eye morphogenesis

As described in section I.B, OP axon extension initially occurs through retrograde extension where the neuron cell bodies are displaced laterally away from their axon tips. This lateral displacement of OP cell bodies appears as a passive, non-autonomous process driven by extrinsic mechanical forces. These extrinsic forces could be exerted by surrounding tissues and we saw in the previous section examples of intertissue mechanical interactions during morphogenesis.

The eye is located just underneath (more ventral to) the OP and it undergoes morphogenesis during OP coalescence, thus representing a tissue candidate that could exert extrinsic forces on OP cells and drive their lateral movement and axon extension. In the following section, we will present the known cell movements and cell shape changes driving eye morphogenesis.

1. General description of eye morphogenesis

For most animals, vision is a highly developed sense, involving the eye as a sensory organ. From deep-water marine species using bioluminescence to birds scanning the ground, the eyes of each animal are highly adapted to enable it to gather the visual information from its environment that is needed for its survival and procreation (Baden et al., 2020).

The complex cell arrangement in its mature state makes the animal eye an interesting model to understand organ morphogenesis and to decipher how single cell behaviours are coordinated at the tissue level to give rise to a complex and functional organ (Schmitt and Dowling, 1994). Moreover, a wide range of congenital eye disorders, including anophthalmia or microphthalmia, aniridia, coloboma, and retinal dysplasia, are coming from disruptions in embryonic eye development (Fuhrmann, 2010), which reinforces the importance of studying eye formation.

In order to acquire a complex organisation with different cell types functioning together for proper visual functions, animals have evolved various morphogenetic processes (Koenig and Gross, 2020). Most spiders have four pairs of eyes: primary eyes are the most complex while secondary pairs are immobile and often have specific functions, such as motion detection or depth perception. The primary eye is formed from an invagination of the prosoma, an anterior ectodermal tissue. This bending starts from the bottom of the future eye, moving upward. This

give rise to an ‘s’ shape of three layers of tissue; the most anterior generates vitreous cells, the middle generates photoreceptors and the posterior one generates pigmented cells (Figure 36E-G). In the squid, retina have placodal origins and eye organogenesis starts with the thickening of the placodal ectoderm on the two sides of the embryo. Shortly thereafter, these placodes are internalized when a lip of cells forms around the periphery of the placode and progressively closes, fusing centrally to form the optic vesicles. Once the vesicle is closed, the eye continues to grow and the retina begins to curve (Figure 36H-K) (Koenig et al., 2016).

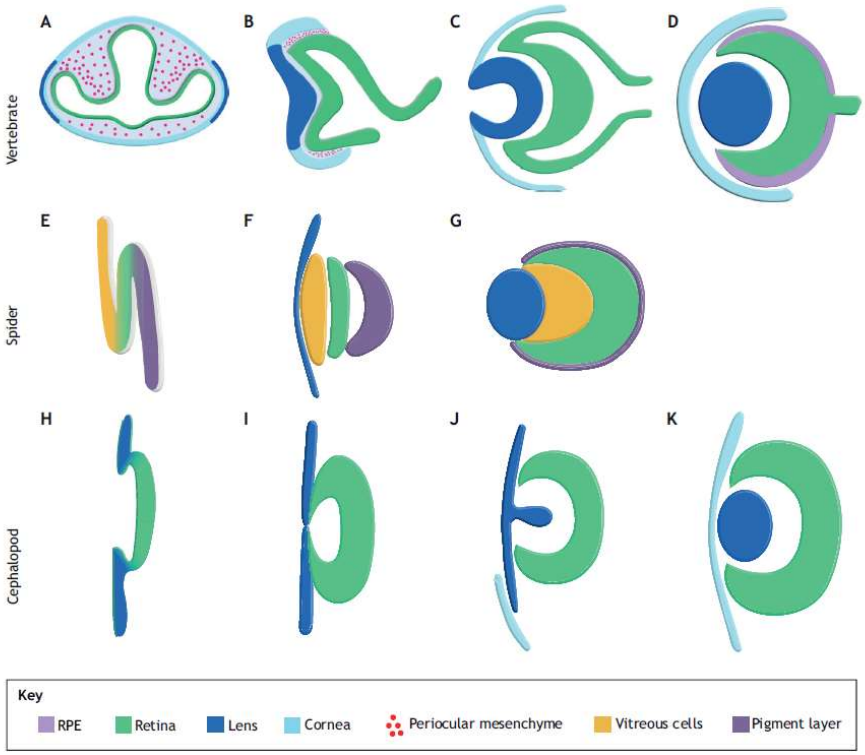

Figure 36: **Development of the vertebrate, spider and cephalopod eyes.** (Koenig and Gross, 2020)

In contrary, vertebrate eye morphogenesis starts with the formation of bilateral outgrowths from the forebrain tissue: the optic vesicles (Figure 36A-D). These optic vesicles then continue to elongate with the incoming flow of eye progenitor cells from the forebrain region. They subsequently invaginate to form optic cups (Figure 37). Prospective lens cells originate from another tissue, the lens placode, overlying the optic vesicle. During lens formation, concomitantly with eye evagination and invagination, lens cells compact dramatically.

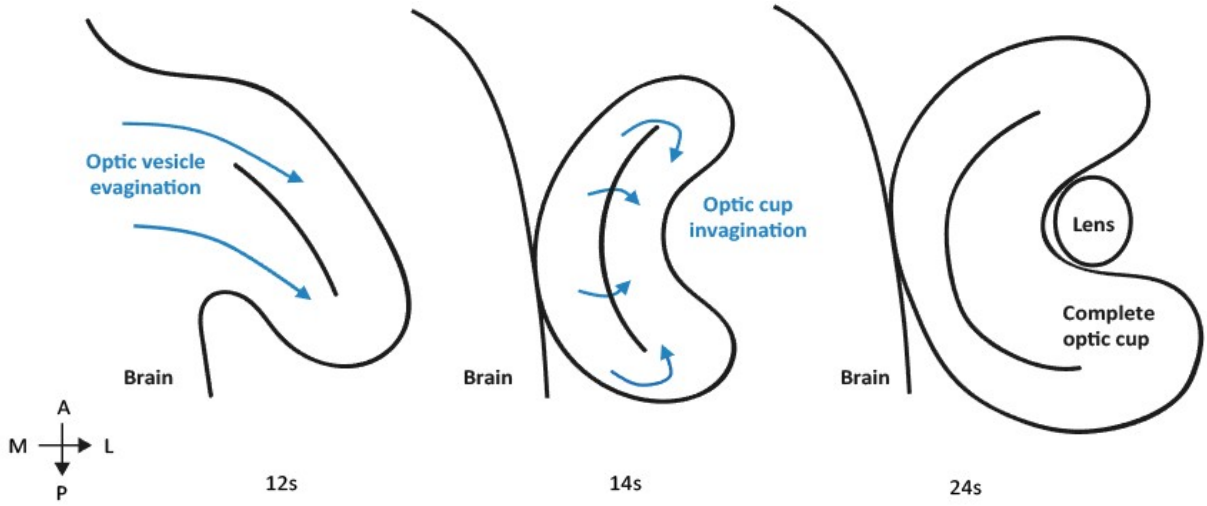

Figure 37: **Schematic view of zebrafish optic cup morphogenesis** with first the evagination of cells from the brain to form lateral optic vesicle and then the bending into an optic cup.

The vertebrate eye presents a characteristic hemispheric shape on which surface photoreceptors are arranged. The late optic cup becomes patterned into distinct ocular tissues: a spherical lens in the centre, whose role is to focus light onto photoreceptors, the hemispheric neural retina (NR), which contains photoreceptors, and in some organisms, neurons and support cells, the enveloping retinal pigment epithelium (RPE), whose function is to block light from other angles than the primary source, and the optic stalk, which connects the eye to the brain (Pei and Rhodin, 1970; Schmitt and Dowling, 1994). As represented on Figure 38, these eye tissues are surrounded by periocular mesenchyme (POM) also called extraocular mesenchyme, a heterogeneous cell population composed of cranial NC and head mesenchyme (Johnston et al., 1979).

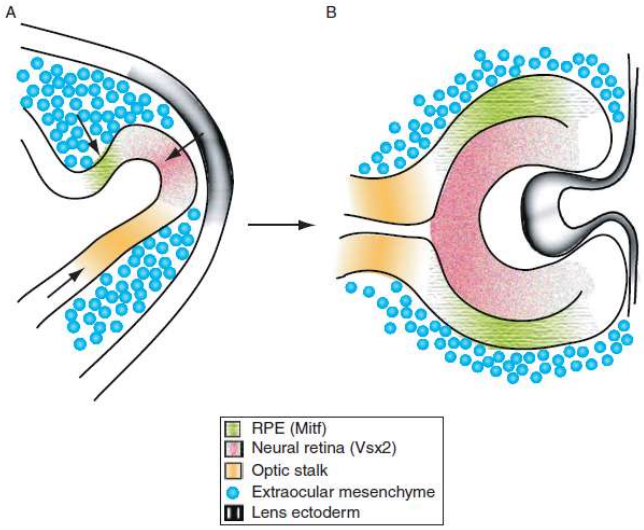

Figure 38: **Overview of vertebrate eye morphogenesis** (Fuhrmann, 2010).

Comparing morphogenesis across species reveals that there is no universal way to execute this tissue organization. One of the most widely used model to study eye morphogenesis is the tropical fish *Danio rerio* (zebrafish) (Cavodeassi, 2018). In the rest of this section, we mainly focus on eye morphogenesis in zebrafish by describing the three steps of eye formation: the evagination of the optic vesicle, the invagination of the optic cup and the coalescence of the lens.

2. Optic vesicle evagination

The evagination of the zebrafish optic vesicle starts from the beginning of somitogenesis, at 10 hpf, with the lateral displacement of retina progenitor cells from the neural keel (Varga et al., 1999). This initial process leads to the formation of two lateral eye fields that continue to elongate overtime, expanding from the forebrain.

- **Separation of the eye field from the forebrain and initiation of optic vesicle evagination**

At the end of gastrulation (9 hpf), a single field of cells, extending across the midline, is already observable in the anterior neural plate and all its cells will later contribute to one of the two eyes (pink domain in Figure 39 panel 1). At tailbud stage (11.5 hpf), the separation in two lateral domains progresses as some median cells are moving anteriorly along the midline, forming the ventral diencephalon (red domain in Figure 39 panel 2). This movement of diencephalic

precursors anteriorly along the midline is required to separate the primordial eye field into left and right eyes and this morphogenetic movement is blocked in *cyclops* mutants, thus giving rise to fused eyes (Varga et al., 1999).

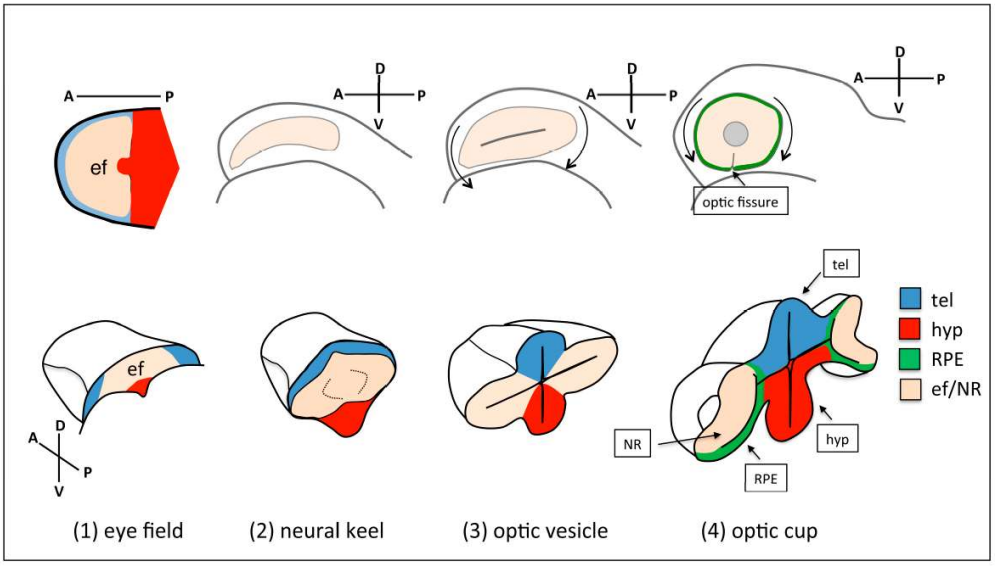

Figure 39: **Schematic representation of zebrafish eye morphogenesis.** *"Eye field specification in the anterior portion of the neural plate at 9 hpf (1) is followed by the rearrangement of the tissue as the neural plate folds into a keel at 11.5 hpf (2), and the evagination of the optic vesicles at 13 hpf (3). Subsequent folding of the optic vesicle over itself leads to the formation of the optic cup at 18 hpf (4). Top-left panel is a dorsal view with anterior to the left; the orientation of all the other panels is indicated in the figure. tel: telencephalon; hyp: hypothalamus; RPE: retinal pigment epithelium; ef: eye field; NR: neural retina."* (Cavodeassi, 2018)

During neural keel formation, all neural progenitors converge toward the midline, except the eye progenitors, which maintain their position before moving outwards, away from the rest of the forming neural tube, to form vesicles (Giger and Houart, 2018; Rembold et al., 2006) (Figure 39 panel 2-3). Two non-exclusive scenarios have been proposed to account for this opposite behaviour of eye cells compared to the rest of neural tissues. The coordinated telencephalon migration could lead to the segregative displacement of eye cells vs forebrain cells. The separation may also be driven by the maintenance of boundaries between the two tissues (Giger and Houart, 2018).

Eye field segregation from adjacent neural plate territories during forebrain morphogenesis is mediated by Eph/Ephrin signalling. Eph receptors and their Ephrin ligands are both membrane-bound proteins well characterized for their role in repulsive response and tissue boundary settings (Fagotto et al., 2014; Pasquale, 2008) as well as their role in axon guidance (see I.A.1). Several Ephrins and Ephs are expressed in complementary domains in the prospective forebrain and disruption of this signalling results in optic vesicle expansion defect and in cell intermixing from the eye territory with the adjacent telencephalon and diencephalon territories. Misexpression of Ephs or Ephrins in other forebrain regions results in segregation of the wrong domain but with maintenance of their regional cell fate. These results demonstrate that Eph/Ephrin signalling is important to maintain cell segregation between adjacent domains and that the eye field segregation from adjacent neural tissues is essential for proper eye evagination (Cavodeassi et al., 2013).

- **Process of lateral expansion**

In medaka fish, eye cells exhibit characteristics of active migration during evagination such as the formation of lamellipodia and filopodia. Thus, evagination seems to be achieved by individual active cell migration (Rembold et al., 2006). In zebrafish, evagination occurs by gradual intercalation of cells from the core of the eye field into the columnar retinal neuroepithelium. Indeed, from 4 somites (4 s) onward, marginal cells of the eye field acquire a monolayered epithelium-like type, with apico-basal polarity, while cells at the core remain mesenchymal. Afterwards, these core cells integrate into the marginal epithelium by intercalating among the marginal cells, leading to the global evagination of the tissue. At late stages of optic vesicle morphogenesis, eye cells shorten and drag their apical surfaces laterally relative to the basal lamina, resulting in further laterally directed evagination (Ivanovitch et al., 2013) (Figure 40). Moreover, the ECM component Laminin is required for this neuroepithelial organization. Laminin is the major component of basement membranes, that form barriers between different tissue compartments. Laminin proteins are heterotrimers composed of α, β and γ chains. In Lamininγ1 morphants, the evagination is perturbed and the injection of Laminin1-coated beads redirects the apicobasal orientation of eye field cells (Ivanovitch et al., 2013). In contrast to what happens in teleosts, the growing optic vesicles of mammalian and bird embryos are composed of already polarized neuroepithelial cells, which initially exhibit a cuboidal shape and then become columnar cells as the optic vesicle evaginates. When the optic

vesicle is fully formed, these epithelial cells shorten again (Martinez-Morales et al., 2017; Svoboda and O'Shea, 1987).

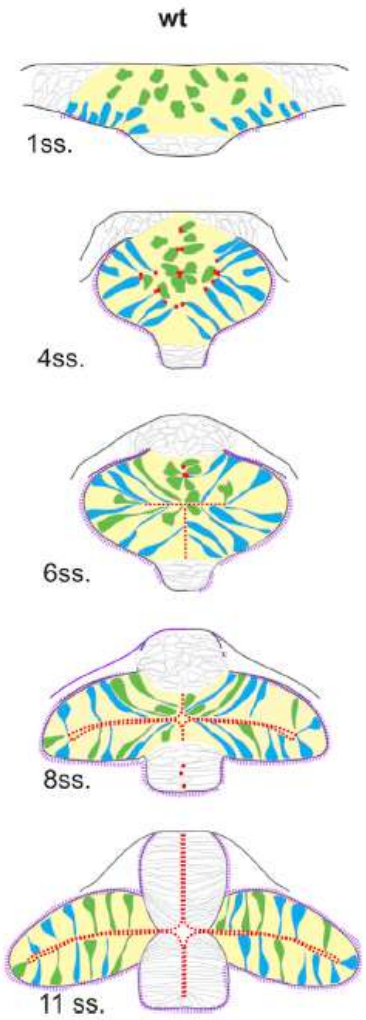

Figure 40: **Schematic frontal view of cell reorganization during optic vesicle evagination in zebrafish.** *"In the wt eye field, cells organize and polarize precociously as compared to cells in other regions of the neural plate. Cells at the margin of the eye field (blue) acquire a monolayered epithelium-like organization from 4 s (11 hpf), prior to the onset of optic vesicle evagination; subsequently, cells at the core of the eye field (green) integrate into the marginal epithelium by intercalating among the marginal cells. At late stages of optic vesicle morphogenesis, around 11 s (14.5 hpf), eye cells shorten and acquire the final dorsoventral orientation characteristic of optic vesicle neuroepithelial cells."* (Ivanovitch et al., 2013).

- **Rx3, a major regulator of eye evagination**

The Pax6, Six3, and Rx transcription factors are conserved major regulators of early eye development (Ashery-Padan and Gruss, 2001; Carl et al., 2002; Mathers and Jamrich, 2000). In zebrafish, the two *pax6* genes, that arose by duplication of an ancestral gene, are expressed in the forebrain and are involved in retinal and lens development (Nornes et al., 1998). Loss of function of Pax6 shows that it regulates eye development in a non-cell autonomous way (Lesaffre et al., 2007). Six3 loss of function in mice or medaka fish leads to severe forebrain deficiencies at early stages, thus making it hard to study its specific role in later steps of eye formation (Inbal et al., 2007). More recently, Six3 loss of function experiments in zebrafish revealed a defect in optic cup size and morphology and in optic nerve development (Samuel et al., 2016).

The retinal homeobox protein (Rx) family is a family of homeodomain-containing proteins which are essential for eye development (Mathers et al., 1997; Mathers and Jamrich, 2000). In zebrafish, *rx3* expression starts at late gastrulation (9 hpf) in the presumptive eye field (Yin et al., 2014) and at 14 hpf, it is specifically expressed in eye progenitors and in the anterior hypothalamus (Figure 41) (Loosli et al., 2003). Most zebrafish null mutations for *rx3*, as the *rx3*^{s399} mutant or the *rx3*^{ne2611} mutant, lead to an absence of eye evagination in the homozygous state (Loosli et al., 2003; Stigloher et al., 2006).

In *rx3*^{s399} mutant, the expression of Pax6 and Six3 remains unaffected indicating that retinal fate is specified normally. However, eyes are absent at all stages and neuronal differentiation is blocked, as shown by the loss of normal expression of Rx1, Rx2 and Ath5, one of the earliest markers for differentiating RGCs (Kay et al., 2001) (Figure 41). Notably, the formation of the lens looks apparently normal in these eyeless embryos (Loosli et al., 2003).

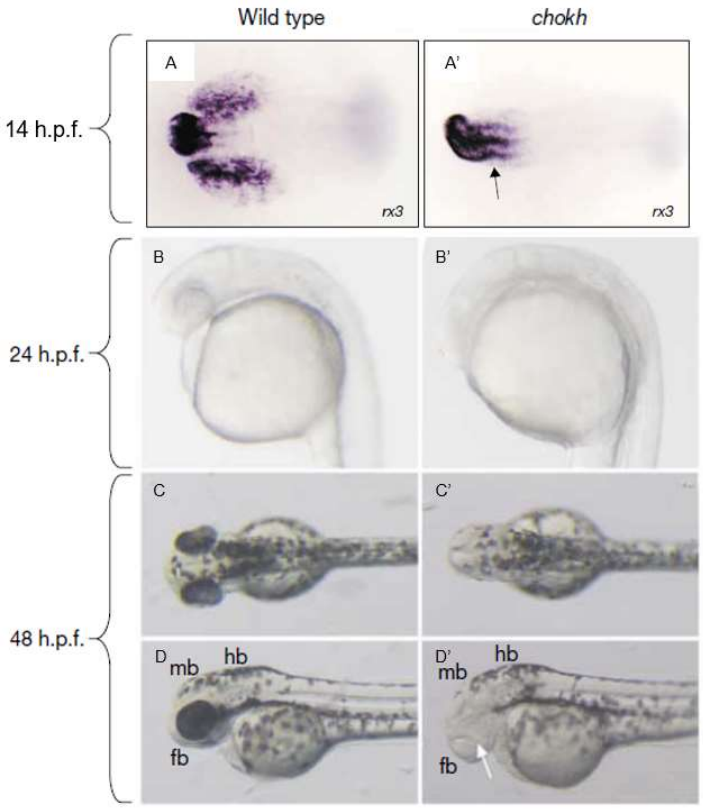

Figure 41: **Expression pattern of *rx3* and morphological analysis of the *rx3*^{s399} (*chokh*) phenotype.** (A-A') Whole-mount *in situ* hybridization analysis of *rx3* in *wt* embryos and *chokh* mutants at 14 hpf. Dorsal view. (B-D') Bright field images at 24 hpf (B-B') or at 48 hpf (C-D') in lateral view (B-C') or dorsal view (D-D'). fb, forebrain; hb, hindbrain; mb, midbrain. (adapted from (Loosli et al., 2003))

The *rx3*^{ne2611} mutant exhibits a similar phenotype, with no eye evagination and just a lens instead of a complete optic cup. Fate tracing of eye-field precursors in this mutant revealed that cells of the presumptive eye field acquire a telencephalic fate in the absence of functional Rx3 transcription factor, which is in concordance with the observation of an enlarged telencephalon and a lack of eyes. Furthermore, transplantation experiments of *wild-type* (*wt*) cells in *rx3*^{ne2611} embryos often gave rise to an evaginated retina, always fully composed of transplanted *wt* cells. This demonstrates that Rx3 controls eye field *versus* telencephalic fate in a cell-autonomous manner (Stigloher et al., 2006).

Further studies show that the morphogen Bone Morphogenetic Proteins (BMP) inhibits Rx3 in the anterior neural ectoderm during early neurulation, thus preventing future telencephalon to acquire eye-field fate (Bielen and Houart, 2012). The expression of the chemokine receptor Cxcr4a in the eye field is maintained by Rx3 while BMP acts as a repressor and prevents its

expression inside the prospective telencephalon. The precise mechanism of action of Cxcr4a in the morphogenetic segregation of eye field and telencephalon tissues remains unclear, although a lead is that Cxcr4a could promote cell adhesion within the eye field. Indeed, *in vitro* assays revealed that Cxcr4a chemokine receptor mediates cell adhesion in other contexts such as prostate cancer (Engl et al., 2006) and lung cancer (Hartmann et al., 2005).

As mentioned earlier, Eph/Ephrin signalling is involved in proper segregation of the eye and the forebrain tissues. In *rx3*^{ne2611} mutants, the failure of eye evagination is accompanied by a loss of the complementary expression of Ephs and Ephrins, suggesting that the Eph/Ephrin pathway is activated downstream of the regional fate specification machinery (Cavodeassi et al., 2013).

In order to have a complete view of Rx3 target genes, whole transcriptomic sequencing (RNA-seq) has been conducted in *rx3*^{w29} mutants, carrying a similar null mutation than *rx3*^{s399} with a premature stop codon, and morphologically *wt* siblings at around 8 s (13 hpf). Homeodomain transcription factors, such as *rx2* and *hmx1*, and genes related with retinoid-signalling, such as *rorab* and *rorb*, emerged as the two major groups of genes which are down-regulated in *rx3*^{w29} mutants. These genes, together with other down-regulated genes, such as *mab21l2*, are associated with eye development and known human eye disorders. Moreover, most of these deregulated genes are enriched with multiple consensus Rx3-binding sites on the gene promoter region, and they exhibit a transition from low levels to high levels of expression during the developmental window where Rx3 is highly expressed. These two facts suggest that they are direct Rx3 targets. On the opposite, signalling pathways and molecules that are crucial for brain development, such as Wnt, Hedgehog and p53, are upregulated in *rx3*^{w29} mutants (Yin et al., 2014) (Figure 42). This result further supports the hypothesis that Rx3 inhibits Wnt signalling within the eye field, thus preventing retinal progenitors to acquire forebrain fate and segregating the eye from the rest of the brain tissue (Giger and Houart, 2018; Stigloher et al., 2006; Yin et al., 2014).

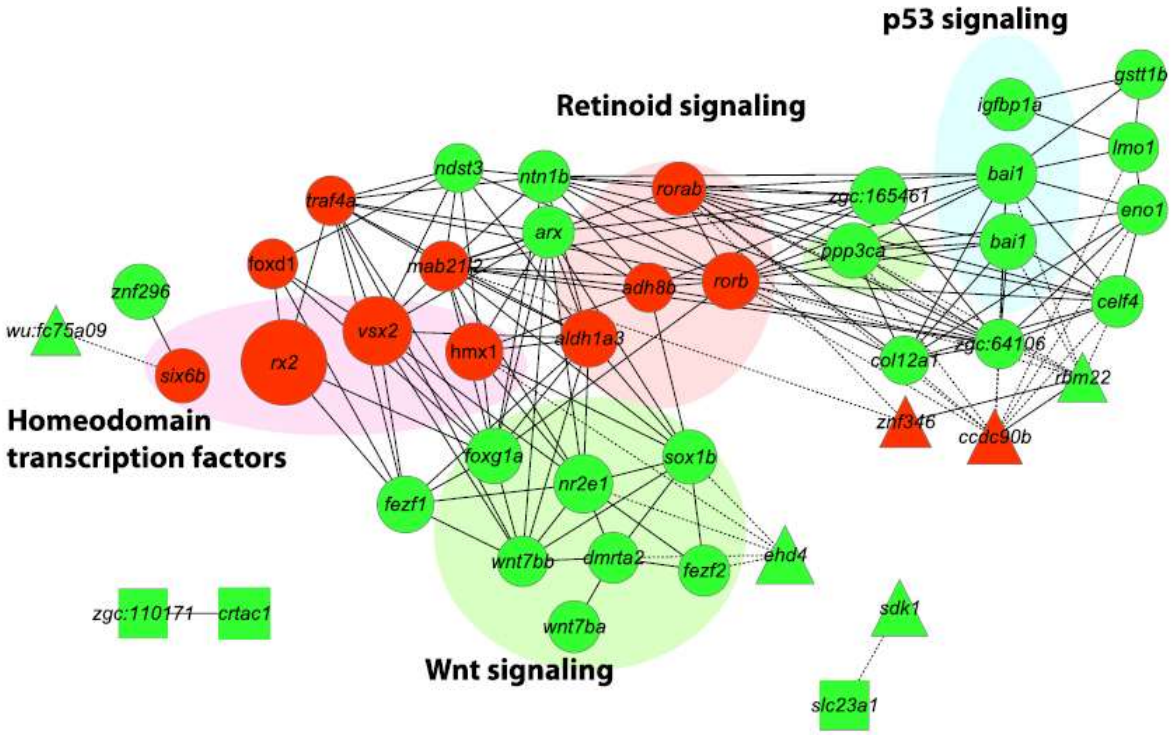

Figure 42: **Gene co-expression network of Rx3 regulated genes**. Red: downregulated in *rx3*$^{-/-}$ embryos. Green: upregulated in *rx3*$^{-/-}$ embryos. (Yin et al., 2014)

- **End of evagination**

Most of the evagination is completed by 10 s (14 hpf). However, the optic vesicle continues to grow during the following step of optic cup morphogenesis. This increase in volume and in cell number is due to proliferation (which is not necessary for proper eye morphogenesis though), but also to the continuous flow of cells from the brain to the optic vesicle until around 15 s (16.5 hpf), a process sometimes referred to as extended evagination (Kwan et al., 2012). Thus, the two steps of evagination and invagination are not strictly sequential and evagination also contributes to invagination. Indeed, the evagination movement brings retinal progenitors closer to potential sources of signalling molecules that set the dorsoventral and temporonasal axes and lead to the optic cup folding (Kruse-Bend et al., 2012; Picker et al., 2009). This process ensures a proper coupling between pattern formation and morphogenesis (Picker et al., 2009).

In this part, we have seen how the optic field emerges and segregates from the neural plate and then evaginates to form two lateral optic vesicle with neuroepithelial cell organization. How do cells reorganize from this flat structures into a folded optic cup?

3. Optic cup invagination and RPE spreading

Around 16 s (17 hpf) , the optic vesicle starts to bend into the hemispherical bi-layered cup, a process called invagination (Figure 37). At the end of this process, the outer layer of the optic cup, which faces the surface ectoderm and lens, will become the neural retina and the inner layer will become the RPE.

A broadly used method to quantify eye invagination is to measure the invagination angle defined as the angle between the inner lips of the optic cup and the centre of the neural retina (Nicolas-Perez et al., 2016; Sidhaye and Norden, 2017) (Figure 43). Before folding, this angle is constant and equal to 180°, then it progressively decreases over time to reach another plateau at 60° around 24-26 s (21-22 hpf) when the invagination is complete (our observations, (Sidhaye and Norden, 2017)).

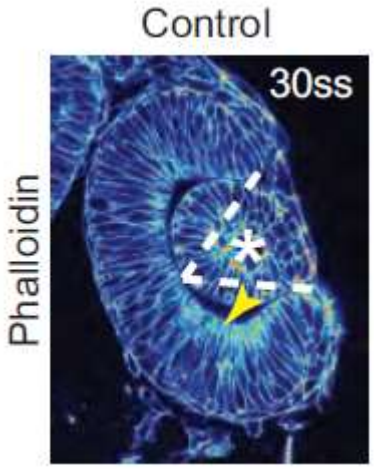

Figure 43: **Invagination angle** represented with dashed lines on a confocal scan of optic cup at 30 s stained for phalloidin. Asterisk marks the developing lens. (Sidhaye and Norden, 2017)

- **Mechanisms of invagination**

Several mechanisms are involved in eye invagination but their precise role and contribution are still unclear (Martinez-Morales et al., 2017) (Figure 44).

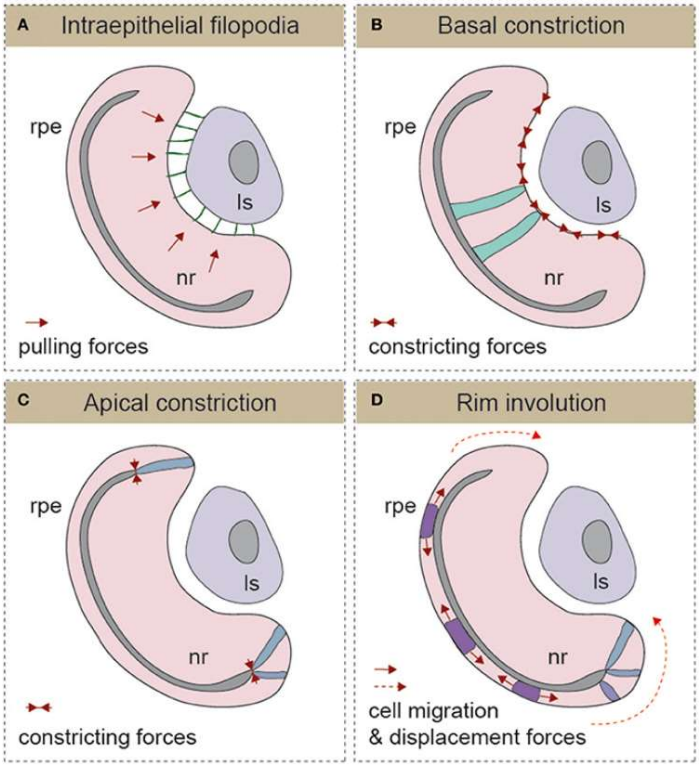

Figure 44: **Schematic representation of the different mechanisms involved in optic cup invagination** "(*A) Intraepithelial filopodia, (B) Basal constriction, (C) Apical constriction, and (D) Rim involution mechanisms are represented. In each one of the panels, the direction of morphogenetic forces is indicated with solid red arrows and cells displacement trajectories with dotted red arrows. The morphology of representative cells is also depicted. Ls, lens; nr, neural retina; rpe, retinal pigment epithelium*." (Martinez-Morales et al., 2017)

In medaka and zebrafish, invagination of the retinal neuroepithelium is associated with basal constriction of central cells (Martinez-Morales et al., 2009; Martinez-Morales and Wittbrodt, 2009; Nicolas-Perez et al., 2016; Sidhaye and Norden, 2017) (Figure 44B). This basal shrinkage seems progressive but is pulsatile and correlates with an actomyosin accumulation in basal foci (Nicolas-Perez et al., 2016). Moreover, when actomyosin is impaired by drug treatment, the basal constriction is reduced and invagination is delayed (Sidhaye and Norden, 2017) (Figure 45C i). Interestingly, analysis of tissue relaxation upon laser ablation in the basal side of the central retinal cells unveiled a developmental time window in which this ablation leads to largest tissue relaxation immediately followed by the bending of the whole retina. This particular developmental time corresponds to the time of acute constriction of the basal feet, at 20 s (19 hpf) (Nicolas-Perez et al., 2016).

Eye cell attachment to the basal ECM is essential for this basal constriction to occur properly and to induce a tissue shape change. When the transmembrane protein Opo is mutated in medaka fish, the polarized localization of focal adhesion components is impaired at the basal cell surface and the optic cup invagination is affected. This phenotype resembles the one obtained when integrin-adhesive function is impaired in the eye, by specifically expressing a dominant-negative construct in the eye anlage. This indicates that adhesion between the central retinal cells and their underlying basal lamina may be crucial for eye development (Martinez-Morales et al., 2009).

Another evidence of the role of ECM in the invagination process is the role of Laminin in both basal contractility and optic cup folding. In *lamc1* morphants (for the chain Laminin γ1), myosin II accumulation is less dynamic than in controls inducing a foci stability for longer period of time, and basal membrane shrinkage appears attenuated. This phenotype at the cell level is associated with a tissue phenotype and a reduced optic cup invagination, also observable in *lamc1*^{m86} mutants (*sly* mutant) (Nicolas-Perez et al., 2016). Similarly, in a mutant for the chain Laminin α1 (*lama1*^{UW1}), severe defects in optic cup formation, and in particular a drastically reduced invagination, are associated with focal adhesion disruption and an increase in basal endfoot width (Bryan et al., 2016). Altogether, these results indicate that the basal adhesion of retinal cells to the ECM is critical for basal constriction and thus for proper invagination. This cell/ECM adhesion is likely to contribute to the translation of the local basal constriction into tension at the tissue scale (Cavodeassi, 2018).

In addition to the central cell basal shrinkage, the cells that are in the hinge region, at the interface between the future neural retina and the future RPE, have to reduce their apical areas to allow acute bending at the tissue margin (Sidhaye and Norden, 2017) (Figure 44 C). Although this apical constriction may contribute to the whole tissue invagination, there is no *in vivo* evidence so far that apical constriction on itself is sufficient to drive the whole cup bending (Martinez-Morales et al., 2017).

This apical constriction comes with a rim movement where the cells in the proximal layer pivot at the margins of the optic vesicle on its whole circumference (Heermann et al., 2015; Kwan et al., 2012) (Figure 44D). These cells integrate the distal layer and become part of the retinal neuroepithelium, thus increasing the size of this layer (Heermann et al., 2015). Rim involution is driven by active cell migration of connected epithelial cells with the formation of actin-rich protrusions on the leading edge and with progressive cell-matrix contacts at the basal side.

Failure of this migration during neuroepithelium formation leads to ectopic determination of retinal neuroepithelium cells and consequently impairs optic cup formation (Sidhaye and Norden, 2017) (Figure 45C ii).

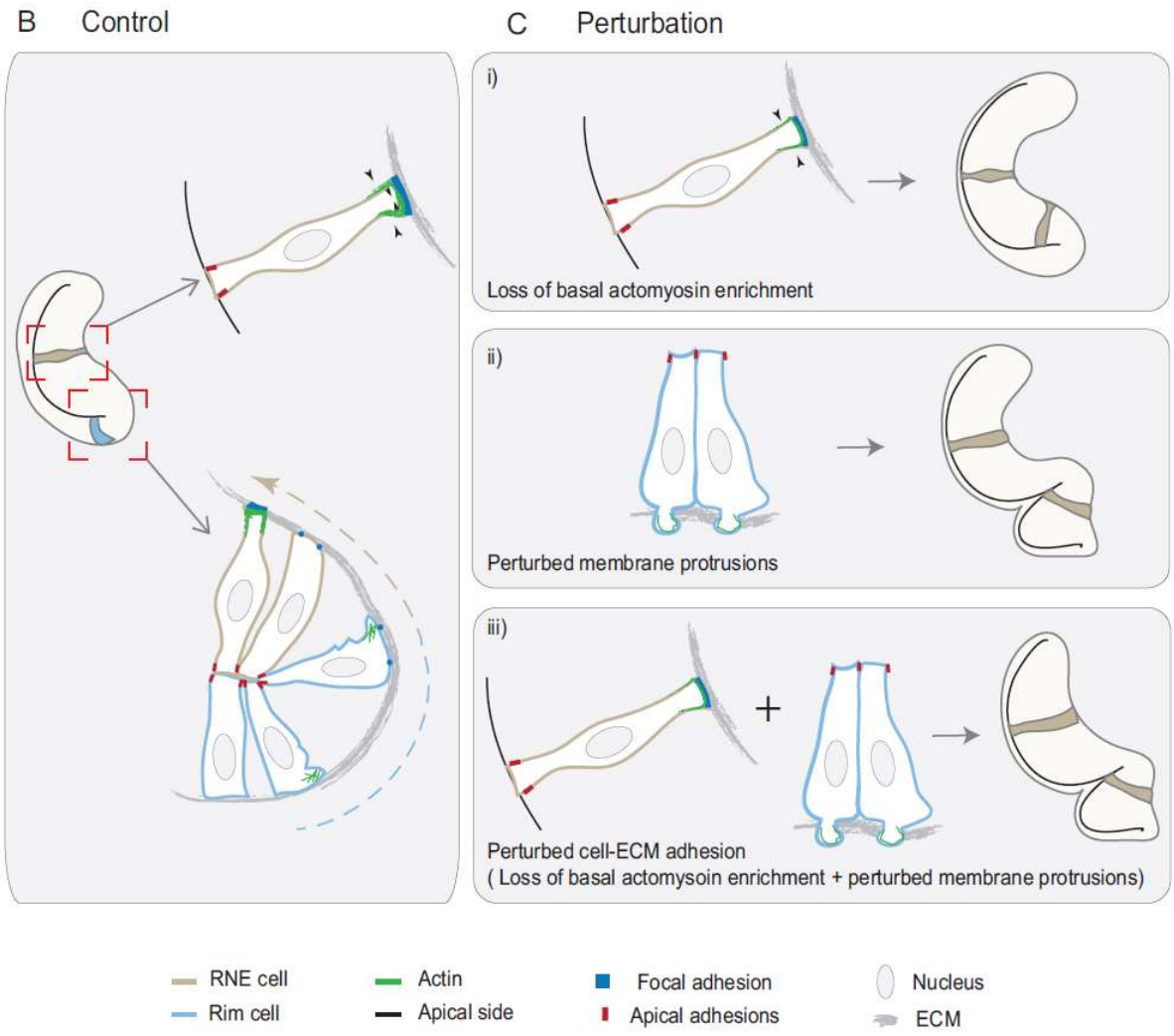

Figure 45: **Schematic of the concerted action of basal cell area shrinkage and rim involution to shape the hemispheric retinal neuroepithelium** *"(B) In control conditions, invagination is driven by basal area reduction that is guided by basally enriched actomyosin-driven constriction and overall compaction by increasing number of cells. Rim involution is driven by collective and directed migration of the epithelium at the rim of the developing optic cup. Protrusive migratory dynamics of rim cells change to adherent behaviour when cells reach the inner layer. (C) Effect of cellular perturbations on the retina neuroepithelial architecture. (i) Loss of basal actomyosin enrichment slows the invagination process, which can result in a wider optic cup. (ii) Perturbation of lamellipodial membrane protrusions affects the migratory behaviour and the optic cup architecture, resulting in an S-shaped optic cup. (iii) Perturbation*

of cell-ECM adhesion results in both loss of basal actomyosin accumulation in the invaginating zone and perturbed lamellipodial membrane protrusions in the rim zone. Such combined effect leads to a severe optic cup phenotype." (Sidhaye and Norden, 2017)

- **Stretching of the proximal layer to form the RPE**

This increase in the neural retina layer volume following the rim movement is associated with a decrease and a thinning of the proximal layer, the future RPE (Heermann et al., 2015). While the cells at the rim are turning, the central cells of the prospective RPE spread dramatically to become a flat layer surrounding and covering the entire central neural retina (Figure 44D).

Similar to the other eye cells, the cells of the optic vesicle inner layer are initially organized as a pseudostratified epithelium. Between 12 s and 16 s (15-17 hpf), the RPE progenitor domain increases mainly due to an increase in cell number and not to cell shape changes. Since preventing cell proliferation with HUA treatment does not affect this initial phase of RPE expansion, the increase in cell number is likely due to *de novo* specification (Cechmanek and McFarlane, 2017). At around 18 s (18 hpf), the central cells flatten and the distances between neighbouring nuclei increase greatly (Kwan et al., 2012). The cells start to align their nuclei and reduce their apico-basal height to form a cuboidal monolayer of cells. This results in an expansion along the dorsal, ventral and posterior directions. This flattening and cell shape change will continue until the end of somitogenesis (around 24 hpf) when the RPE has become a squamous monolayer of cells (Moreno-Marmol et al., 2018) (Figure 46).

It is tempting to think of RPE stretching as a passive process resulting from the active processes happening in the neural retina, such as the basal constriction of central cells and the rim involution. Indeed, these active morphogenetic events could generate mechanical forces on the proximal layer, leading to the elongation of central cells in the proximal layer. The mechanical stretching of the layer could result from the rim movements at its edges and from the continuity in this proximal layer probably maintained by adhesion molecules.

Another point of view is that RPE elongation is an active process that actually contributes to eye morphogenesis. Interestingly, tissue specific perturbation of actomyosin cytoskeleton at 16 s, using a photactivable myosin II inhibitor, revealed that RPE cells expand their apical and basal surfaces in a cell autonomous way, through myosin II activity. Moreover, failure of cell flattening in the photoactivated region of the RPE is consistently associated with a significant

reduction of optic cup folding, showing that RPE stretching is critical for proper invagination. On the contrary, myosin II perturbation in the neural retina by the photoactivation of the drug does not induce RPE flattening defects (Moreno-Marmol et al., 2020). Albeit additional RPE-specific perturbations are needed to determine the mechanism of this cell autonomous stretching, these results are in the favour of the second hypothesis of an active expansion of RPE contributing to optic cup invagination.

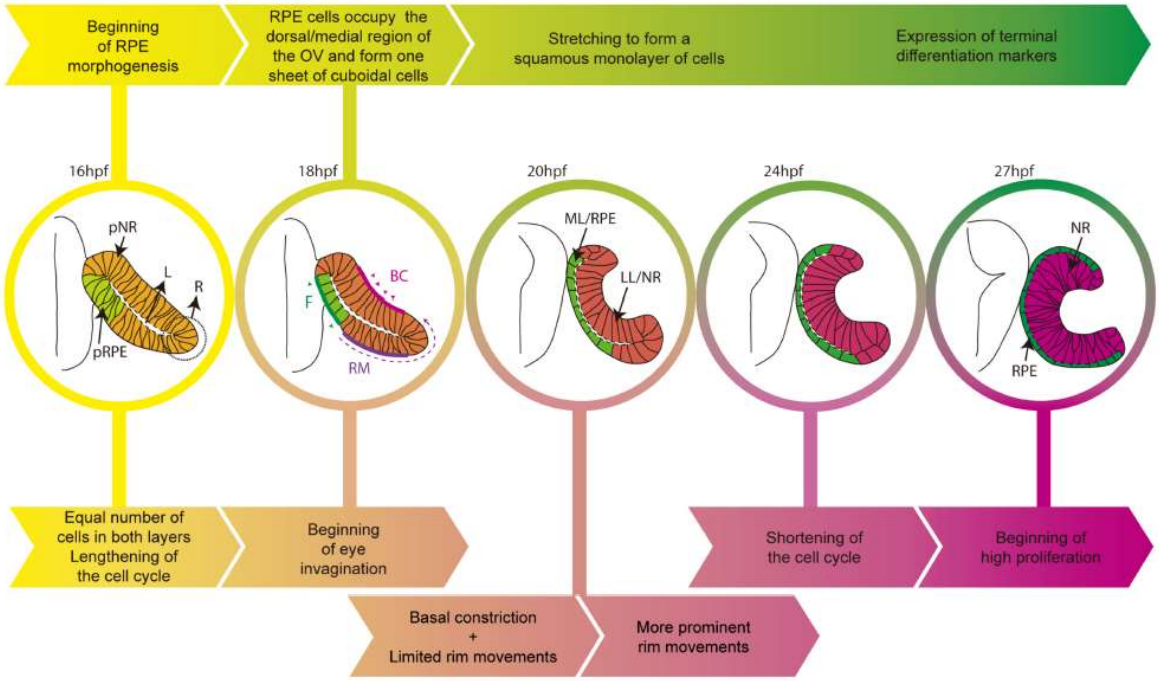

Figure 46: **Schematic diagram of the time line of RPE spreading during zebrafish eye morphogenesis.** "*The top arrows (yellow to green) indicate the salient events in RPE development whereas bottom arrows (yellow to magenta) those related to the entire eye primordium. Eye structures are color coded: progenitors, light yellow; lateral/neural retina layer, dark pink; medial/RPE layer, green. BC, basal constriction; F, flattening; L, virtual lumen; LL, lateral layer; ML, medial layer; NR, neural retina; pNR, prospective neural retina; R, rim region; RM, rim movements; RPE, retinal pigment epithelium; pRPE, prospective RPE.*" (Moreno-Marmol et al., 2018)

In addition to the role of RPE movements in neural retina folding, the retinal bending is also facilitated by cell-cell contact between these two populations mediated by a member of a key developmental signalling family, the transmembrane Semaphorin6d, and its receptor, Plexina1, that are expressed respectively in neural retinal and RPE progenitors. Loss-of-function of the

Semaphorin6d/Plexina1 pathway causes defects in temporal but not nasal optic cup morphogenesis (Cechmanek et al., 2021).

Although these studies indicate a role of RPE in neural retina folding, it seems that later on, the development into a well specified and laminated neural retina occurs independently of the RPE. Indeed, in two mutant alleles for the zebrafish gene *rx3* (*rx3*^{t25327} and *rx3*^{t25181}), optic vesicles are able to evaginate, even though they remain smaller than *wt,* and are able to give rise to a laminated neural retina composed of morphologically differentiated cell types but RPE is either reduced or absent (Rojas-Munoz et al., 2005). This points out that neural retina specification and RPE specification are two independent processes and that in addition to controlling optic vesicle evagination, the retinal homeobox gene *rx3* also regulates RPE specification.

- **End of invagination**

During the entire invagination process, the optic cup remains physically linked to the brain by the optic stalk. This structure, connecting the brain and the eye, will later remodel and give rise to cell types that ensheathe the optic nerve (Fuhrmann, 2010) (Figure 38 and Figure 47).

Following the invagination into a bilayered optic cup, the eye continues to maturate. On one hand, the retinal progenitors proliferate and differentiate into all the neuronal and glial cell types composing the final retina. On the other hand, RPE cells differentiate to give rise to a squamous pigmented epithelium, whose first pigments are observable at prim 5 (24 hpf) (Cavodeassi, 2018). While the patterning into proximal and distal domains gives rise to the separation between the RPE (proximal) and the NR (distal), the patterning into nasal and temporal domain is necessary for the subsequent morphogenetic movement of the optic cup (Figure 47). Between prim-5 and prim-25 (24-36 hpf), the optic cup undergoes a 90 ° anterior rotation and progressively align its nasal-temporal axis with the anterior-posterior axis (Schmitt and Dowling, 1994). Note that this morphogenetic movement occurs at later stages than the ones we are focusing on in my PhD work (12-24 s, 15-21 hpf) and thus will not be further described here.

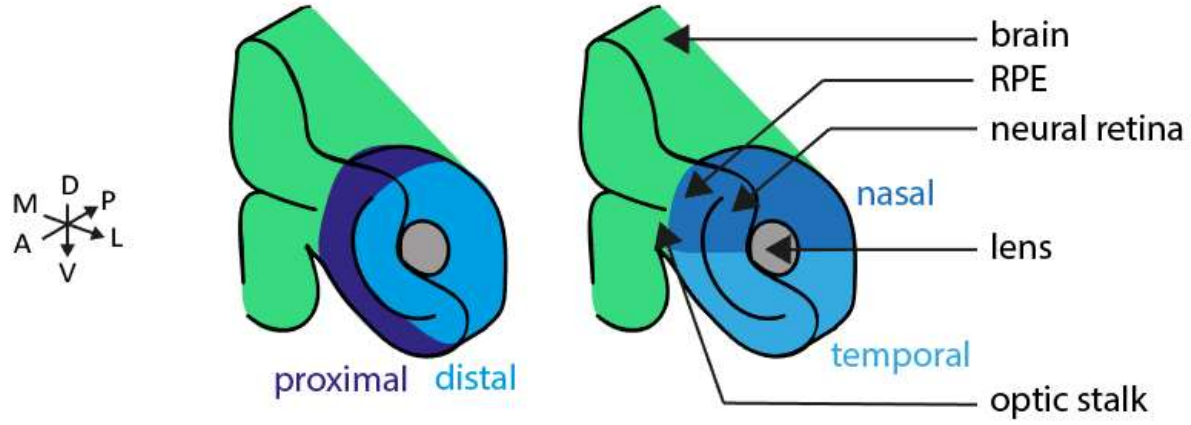

Figure 47: **Schematic 3D view of the optic cup at 24s (22hpf)** representing the patterning into proximal/distal and nasal/temporal domains.

We have seen in this section how the invagination occurs to give rise to a bended optic cup and how the RPE progressively wraps the neural retina. Zebrafish eye invagination is concomitant with the formation of another structure that is essential for the sense of sight: the placodal lens. How do the lens cells coalesce and compact into a spherical cluster at the centre of the neural retina? How do lens formation and eye invagination influence each other?

4. Lens coalescence

Prospective lens cells originate throughout the entire ectoderm overlying the optic vesicle in which they are initially intermixed with non-lens cells (Figure 48a). Between 6 and 10 s (12-14 hpf), 3D manual cell tracking shows that lens precursors converge towards the top of the retina by directed anteroposterior and postero-anterior movements. Interestingly, during this period of time, prospective lens cells follow the same trajectory as underlying retinal cells that are undergoing evagination. Despite the absence of direct contact between the two cell populations, lens progenitors move posteriorly and at the same speed as their neighbouring retinal cells (Kwan et al., 2012). From 10 s onward (14 hpf), the apicobasal height of the ectodermal cells overlying the centre of the retinal anlage increases to reach approximately twice the height as the simple cuboidal epithelium of the surface ectoderm at 14 s (16 hpf) (Greiling and Clark, 2009) (Figure 48a). At 16 s (17 hpf), the lens placode is recognizable as thickened mass of cells overlying the optic primordium (Figure 48b). Afterwards, the presumptive lens cells delaminate to form a mass filling the vitreal space. At around 22 s (20 hpf), they are elongated and radially arranged in a solid mass embedded with the ectoderm

but still connected with the rest of the ectoderm (Figure 48 c). From 26 s (22 hpf) onwards, the zebrafish lens anlage detaches from the ectoderm (Figure 48 d-e) and at prim 5 (24 hpf), it is a free nascent lens mass within the optic cup (Greiling and Clark, 2009; Schmitt and Dowling, 1994) (Figure 48 f). This free lens mass does not exhibit a vesicular organization, as opposed to mammalian lens development (Greiling and Clark, 2012; Vihtelic, 2008).

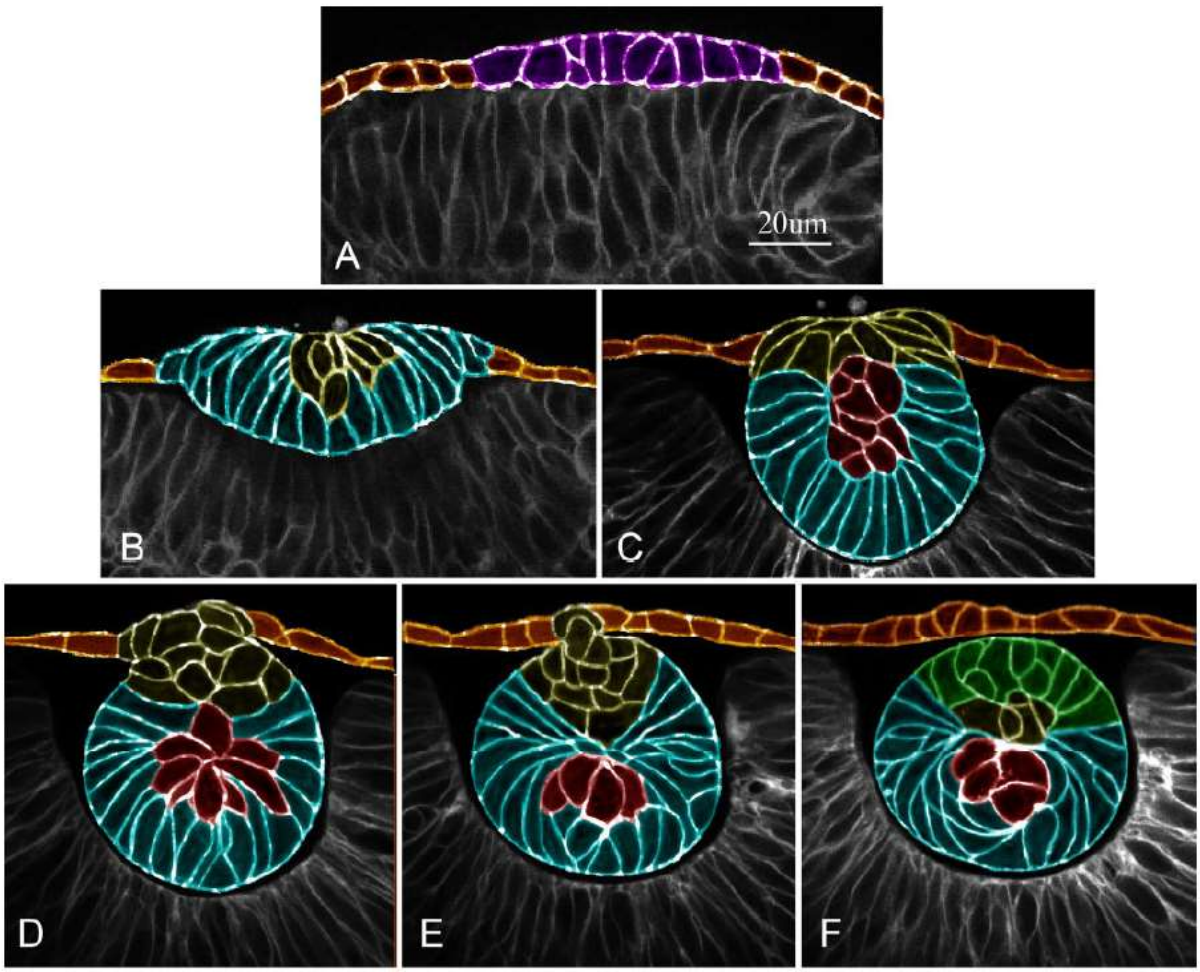

Figure 48: **Summary diagram representing the progressive stages of zebrafish lens morphogenesis**. *"Cell membranes have been pseudocolored. A: At approximately16 hpf. The cells in the surface ectoderm are represented in orange, and the cells in the lens placode in purple. B: At 18 hpf. Elongating fibre-like cells are represented in blue. C: At 20 hpf. The cells in the organizing centre (red) of the delaminating and elongated lens mass are surrounded by columnar primary fibre cells (blue). D–F: At 22 hpf, 23 hpf, and 24 hpf, respectively. Delamination completes the separation of the spherical lens from the developing cornea. Morphologically undifferentiated cells at the anterior surface of the lens mass (yellow)*

appeared to reorganize and lose adhesion contacts with the surface ectoderm." (Greiling and Clark, 2009).

As stated earlier (I.D.2), in the absence of optic vesicle evagination and subsequently optic cup invagination (*rx3* mutant), one can still observe the formation of a spherical lens, even though its dimensions have not been quantified and compared with *wt* lenses. Thus none of these two processes are essential for lens coalescence, which seems to occur independently. Interestingly, when transplanting a large number of *wt* cells into the presumptive eye domain of *rx3* mutants at shield stage, we (see III.B.1) and others (Stigloher et al., 2006) observed in most cases the formation of small but curved optic cup around the lens. The fact that these exogenous cups mostly form around the lens suggests that an interaction between the two tissues is required for proper location and coordination of retina bending and lens clustering.

In chick, optic vesicle development depends on early inductive signals emanating from the pre-lens ectoderm. In fact, when preplacodal ectoderm is surgically ablated from the optic vesicle, optic vesicle invagination, but not differentiation, is perturbed, while when surface ectoderm ablation occurs later, at the lens placode stage, an optic cup forms through proper invagination. These experiments show that in chick, retina invagination requires specific, precisely-timed interactions with the overlying surface/lens ectoderm (Hyer et al., 2003). The nature of these interactions remains however unclear.

In contrast to this situation where the lens is necessary for retina morphogenesis but not differentiation, in zebrafish, the prospective lens placode appears to be important for optic cup patterning. Indeed, the non-neural ectoderm above the eye field triggers the expression of prospective dorsal markers within the lateral presumptive retinal field during optic vesicle evagination (Kruse-Bend et al., 2012).

On top of this lens-retina chemical interaction, a physical link between the two forming tissues has been described in mouse, with the presence of F-actin-rich basal filopodia emanating from the lens and contacting the retinal epithelium. Genetic interference with filopodia formation results in perturbed foldings of lens and retinal epithelial surfaces. These transient filopodia, observed only during the invagination, could act as physical tethers that coordinate invagination by transmitting the forces from presumptive lens to retina (Chauhan et al., 2009) (Figure 44A). However, there is no evidence for the presence of such filopodial extensions in zebrafish.

Zebrafish is an amenable model to investigate the possible role of the lens in retina morphogenesis, as these two tissues can be easily imaged and micro manipulated.

In this part, we have seen how the lens placode coalesces into a compact spherical lens and how this process could be related to invagination. Later on, the lens cells mature and reorganize to form a transparent tissue whose function is to refract and focus light onto photoreceptors (Koenig and Gross, 2020). The lens is not the only tissue interacting with the retina during eye morphogenesis. How do surrounding tissues, in particular the periocular mesenchyme, influence eye morphogenesis?

5. Extrinsic influences of surrounding tissues on eye morphogenesis

While the different domains of the developing eye execute distinct morphogenetic programs, dynamic inputs are also being received from multiple extrinsic sources, including the ECM as shown in a few examples above and the POM, composed of cranial NC and head mesenchyme (Casey et al., 2021).

One example of the role of surrounding tissues in shaping the optic cup is the combined action of ligands expressed in the brain and the OPs in the nasal-temporal patterning of the retina. The fibroblast growth factors (FGF) are a family of cell signalling proteins involved in a wide variety of developmental processes, and particularly in axial patterning of the neural tube. FGFs are first involved in the posteriorization of the neural plate and then redeployed in several organizing centres where they can control cell positional identities in adjacent regions (Mason, 2007). In zebrafish embryos at 5 s (11.5 hpf), the Fgf24 ligand is expressed in the OPs and Fgf3 and Fgf8 are expressed in the brain (Figure 49A). Single *fgf8*$^{-/-}$ mutants and double *fgf3/8*$^{-/-}$ or *fgf8/24*$^{-/-}$ mutants displayed defects in expression pattern of nasal and temporal marker genes in the eye and this phenotype was enhanced in the absence of Fgf8/3/24. In this condition, there was a defect in nasal-temporal specification of retinal progenitors. Indeed, in the presumptive nasal region, misspecified retinal progenitors expressed the temporal transcription factor Foxd1 instead of the nasal one Foxg1 and started to delaminate. In the temporal region, temporal progenitors expressing Foxd1 showed increased rim movements from the inner layer to the outer layer of the optic cup (Figure 49B). This shows that combined Fgf signals fully control nasal retina identity by regulating the nasal transcription factor Foxg1.

Moreover, this nasal-temporal patterning is important for proper optic cup morphogenesis as cells in the nasal half and the temporal half undergo different types of movements, necessary for the subsequent rotation of the optic cup. This results raise the intriguing possibility of a retroactive action between pattern formation and morphogenesis. Signalling molecules present in specific locations around the optic vesicle pattern the eye and thus induce cell movements that in turn, bring these cells in closer proximity to the molecule sources and thus reinforce this patterning (Picker et al., 2009).

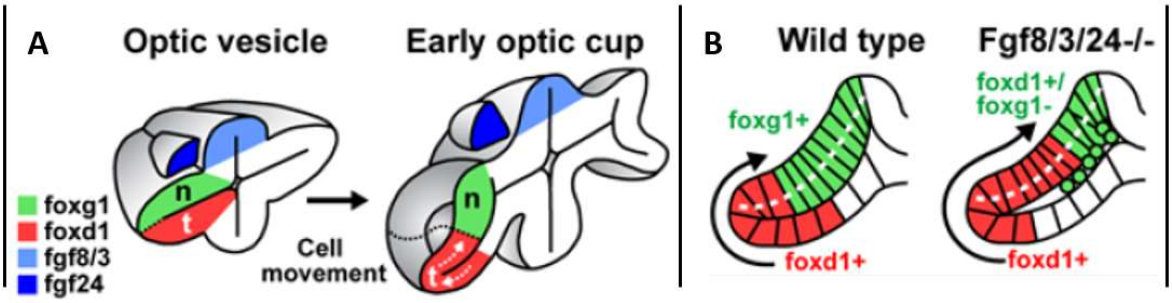

Figure 49: **Model for retinal patterning and morphogenesis along the nasal-temporal axis** n, nasal; t, temporal. Adapted from (Picker et al., 2009).

The previous example illustrates how surrounding brain and OP tissues can influence eye patterning and the following eye morphogenetic movements. The POM, and in particular the NC, can also induce cell rearrangements in the developing zebrafish optic cup. During somitogenesis (10-24 hpf), two distinct waves of cranial NCCs progressively migrate towards the anterior extremity of the embryo to surround the eye. Later on, these cranial NCCs integrate the eye and contribute to either the distal or the proximal part (Takamiya et al., 2020). In *tfap2a;foxd3* double-mutants, NCC migration around the eye is drastically impaired. In this condition, optic cup invagination is affected and temporal retina and RPE cell movements are abnormal. Most likely, NCCs influence eye morphogenetic movements by producing the basement membrane protein Nidogen. Indeed, the overexpression of Nidogen in the absence of NCCs partially restores optic cup morphogenesis. Moreover, putative quadruple mutants for Nidogen1a, Nidogen1b, Nidogen2a and Nidogen2b obtained by transient mutation for nid1a and nid2b in the double maternal zygotic mutant MZ*nid1b*; MZ*nib2a* background, displayed disrupted optic cup morphogenesis (Bryan et al., 2020) (Figure 50).

Reciprocally, the eye appears to be required for NCCs anterior migration as in *rx3*^{s399} mutant, anterior NCCs have defective migration with significantly reduced migration rates and directionality (Langenberg et al., 2008).

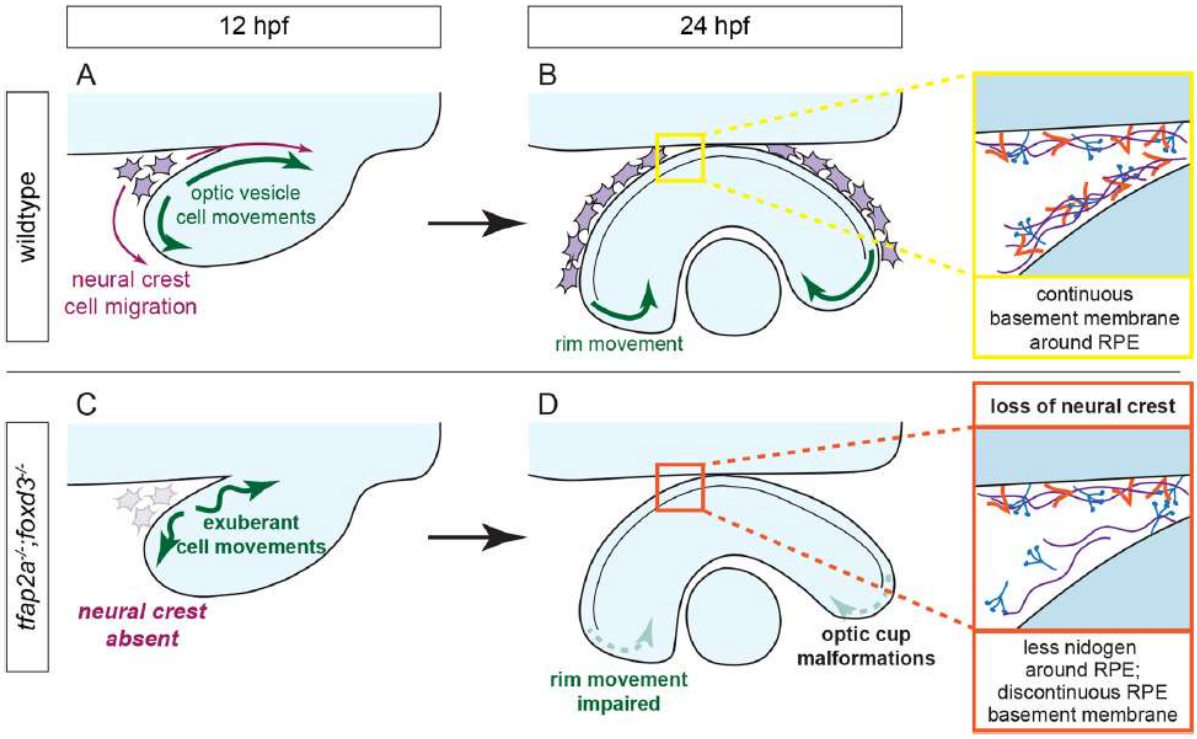

Figure 50: **Model of optic cup morphogenesis in normal condition (*wt*) and in the absence of NCC surrounding the eye (*tfap2a;foxd3* double-mutant)**. *"(A,B) Optic cup morphogenesis in a wt zebrafish embryo. NCCs migrate around the optic vesicle and enable efficient movement of optic vesicle cells (A). Cells undergo rim movement and contribute to the neural retina, partially enabled by the presence of a continuous basement membrane along the surface of the RPE (B). (C,D) Optic cup morphogenesis in a tfap2a;foxd3 double-mutant embryo. Most NCCs are absent, resulting in optic vesicle cells that move faster and farther than those in wt embryos (C). Rim movement is impaired in the absence of a complete, continuous basement membrane around the RPE, resulting in optic cup malformations (D)."* (Bryan et al., 2020)

Even though some features of *in vivo* optic cup morphogenesis such as RPE patterning and proper invagination involve surrounding tissues, the autonomous formation of an optic cup structure from a 3D culture of mouse embryonic stem cells aggregate shows that, at least in mice, basic aspects of gross optic cup morphogenesis are intrinsically programmed into neural tissues (Eiraku et al., 2011; Koenig and Gross, 2020).

In this section, we have described the main steps of eye morphogenesis with a specific focus on the zebrafish optic cup development. Initially, the eye field emerges from the forebrain tissue and evaginates laterally in two bilateral optic vesicles composed of two layers of organized neuroepithelial cells. Subsequently the optic vesicles bend and invaginate into optic cups, a process concomitant with the coalescence of the placode-derived lens tissue in the centre of the optic cup and with the progressive migration of NCCs around the cup.

II. Goals

While neuronal circuit formation has been well studied from a chemical point of view, recent studies uncovered a crucial role for mechanical signals in neuronal development. These mechanical cues include the mechanical properties of the environment (such as stiffness) and the mechanical stresses applied to growing neurons, as depicted in section I.A. My PhD project lies at the interface between biology and physics and is dedicated to investigate how mechanical forces influence neuronal movements and axon elongation to shape neuronal circuits *in vivo*.

Our model is the zebrafish olfactory circuit, which develops during the morphogenesis of the OP. As described in section I.B, OP cells are located in an elongated domain next to the brain and coalesce into a compact and spherical neuronal cluster between 12 s and 24 s (15-21 hpf). Previous work from Breau *et al.* showed that OP formation is driven by two types of cell movements. Peripheral cells migrate actively along the brain towards the centre of the placode, while central cells are displaced laterally away from the brain surface. Strikingly, axon extension occurs during these lateral movements through retrograde extension, whereby cell bodies move away from their axon tips attached to the brain's surface. Analysis of cell polarity and cell protrusions, functional perturbations, axon ablation and mapping of tension in the OP revealed that the lateral displacement of cell bodies away from axon tips is a passive, non-autonomous process driven by extrinsic mechanical forces.

What are the sources of these extrinsic forces contributing to OP morphogenesis? Previous results obtained in Breau's team showed that the convergence of cells located at the OP peripheries is not required for the proper lateral movement of central cells. We thus wondered if surrounding tissues could exert mechanical forces on the OP, resulting in cell body displacement and axon elongation. As illustrated in section I.C, the study of mechanical interactions between tissues has aroused increasing interest in recent years and it is now evident that the biomechanics of morphogenesis must be understood not only in the scope of isolated tissues, but also in the framework of interacting tissues.

The eye tissue, located underneath the OP, undergoes drastic morphogenetic movements of evagination and invagination during OP morphogenesis as shown in section I.D. Both evagination and invagination movements have lateral components and thus the eye constitutes

a potential source of forces exerted on OP cells to drive their lateral movement and axon extension.

What is the mechanical contribution of eye morphogenesis to OP cell lateral movements and axon elongation? To answer this question, my PhD project is organised around 3 aims:

Aim 1) Compare eye and placode cell movements in the *wild type* situation.

We first want to compare cell movements in the OP with those occurring in the forming eye to reveal a potential coordination between these two tissues. We will focus our analysis on their lateral component as it is along this direction that the passive movement of neuronal cell bodies and the axon retrograde extension occur.

Aim 2) Determine the role of eye morphogenesis in olfactory circuit formation using situations where eye morphogenesis is perturbed.

In order to assess the role of eye morphogenetic movements in the shaping of the olfactory circuit, we will analyse conditions where eye morphogenesis is perturbed, either lost or not complete. The quantitative analysis of the shape of the OPs, of OP cell movements and of the axon length/morphology in these situations will help us to determine if eye morphogenesis is critical for proper olfactory circuit construction. Furthermore, mapping the distribution of mechanical tension in the OP in both *wt* and affected conditions will reveal if the eye influences the distribution of mechanical stress in the OP.

Aim 3) Identify the mechanisms of force transmission at the interface between the two tissues.

Consistent with our hypothesis of extrinsic mechanical forces exerted by the eye on the OP, there should be a specific mechanism coupling the two tissues that allows force transmission at the interface. We want to investigate whether this transmission occurs through direct cell/cell contacts between the eye and the OP, *via* a third population of cells or through ECM at the interface.

III. Results

A. Scientific article

This article is available on the BioRxiv preprint server (https://www.biorxiv.org/content/10.1101/2021.03.15.435408v2) and as I write these lines, the manuscript is under consideration for publication. The first figure and the first supplementary figure of the following article present the results of Girisaran Gangatharan (former Postdoc in the Breau's team), Marie Breau and Isabelle Bonnet's work. The rest of the article corresponds to the work I carried out during my PhD.

INTERTISSUE MECHANICAL INTERACTIONS SHAPE THE OLFACTORY CIRCUIT IN ZEBRAFISH.

Monnot P[1,2,3], Gangatharan G[1], Baraban M[1,3], Pottin K[1], Cabrera M[1], Bonnet I[2*], Breau MA[1,3,4,5*]

[1]Sorbonne Université, Centre National de la Recherche Scientifique (CNRS), Institut de Biologie Paris-Seine (IBPS), Developmental Biology Laboratory, F-75005, Paris, France
[2]Institut Curie, Université PSL, Sorbonne Université, CNRS UMR168, Laboratoire Physico Chimie Curie, 75005 Paris, France
[3]Laboratoire Jean Perrin, F-75005, Paris, France
[4]Institut National de la Santé et de la Recherche Médicale (INSERM)
[5]Lead contact
[*]co-corresponding authors : Marie Anne Breau (marie.breau@sorbonne-universite.fr) and Isabelle Bonnet (isabelle.bonnet@sorbonne-universite.fr)

Key words: zebrafish, placode, olfactory, eye, mechanical force, cell movement, axon, extracellular matrix, coupling

- **Abstract**

While the chemical signals guiding neuronal migration and axon elongation have been extensively studied, the influence of mechanical cues on these processes remains poorly studied *in vivo*. Here, we investigate how mechanical forces exerted by surrounding tissues steer

neuronal movements and axon extension during OP morphogenesis of the olfactory placode in zebrafish. We mainly focus on the mechanical contribution of the adjacent eye tissue, which develops underneath the placode through extensive evagination and invagination movements. Using quantitative analysis of cell movements and biomechanical manipulations, we show that the developing eye exerts lateral traction forces on the olfactory placode through extracellular matrix, mediating proper morphogenetic movements and axon extension within the placode. Our data shed new light on the key participation of intertissue mechanical interactions in the sculpting of neuronal circuits.

- **Introduction**

Neuronal circuits develop through a series of dynamic processes including the migration of neurons to their final position and the growth of axons towards target tissues. According to the current view of neuronal development, these processes are primarily guided by chemical cues acting as traffic signs to orient the movement of neurons and of their growing projections [1–3]. In addition to the well-studied chemical signals, developing neurons are also exposed to a variety of mechanical cues, including the stiffness of the environment, and tensile or compressive stresses exerted by surrounding tissues undergoing growth or morphogenesis. Over the past decades, there has been increasing evidence of the influence of such mechanical cues in shaping neuronal morphology *in vitro* (for reviews see references[4,5]). For instance, pulling on neurites can control axon specification, growth, and pruning in neuronal cultures[6–13]. The stiffness of the dish substrate also plays a role in axon growth and branching[14–17]. In contrast, few studies have interrogated the role of such mechanical cues *in vivo*. For example, a brain stiffness gradient influences axon growth patterns in the Xenopus optic pathway[18,19] and in Drosophila, mechanical tension at the neuromuscular junction modulates vesicle accumulation and synaptic plasticity[20,21]. A better understanding of how mechanical signaling contributes to the construction of neuronal circuits is thus required.

Here, we use the development of a neurogenic placode in zebrafish to investigate how intertissue mechanical interactions influence neuronal movements and axon extension. Neurogenic placodes are transient ectodermal structures contributing sensory neurons to the cranial peripheral nervous system; they include the olfactory, otic, trigeminal and epibranchial placodes[22,23]. In the embryo, the placodes assemble through the coalescence of progenitors located in large domains of the pan-placodal region[24,25], while or soon before initiating axonal contacts with the brain[26,27]. During their assembly, neurogenic placodes are surrounded by

several non-placodal tissues undergoing morphogenetic reorganisation, including the brain[28,27,29], the optic cup[30] and neural crest cells[28,31]. The superficial location of the zebrafish neurogenic placodes, right underneath the epidermis, facilitates live imaging of cell dynamics and biomechanical manipulation. This makes them amenable models to explore the influence of pulling/pushing forces from neighbouring tissues on neuronal migration and axon growth and, more globally, the role of intertissue mechanical interactions in morphogenesis, a thriving question in developmental biology[32,33].

Our study focuses on the morphogenesis of the olfactory placode (OP), which later gives rise to the olfactory epithelium. OP cells are initially located in two elongated domains next to the brain, which both coalesce into paired ellipsoidal neuronal clusters over 7 hours of development, between 14 and 21 hours post fertilization (hpf) (corresponding to 12 somites (12 s) and 24 s stages)[27,31,34]. We previously showed that OP coalescence is driven by two types of cell movements[27] (Article figure 1A). Cells from the anterior and posterior extremities migrate actively along the brain towards the placode center, and are then displaced laterally, away from the surface of the brain. Central OP cells undergo lateral movements only, without clear anteroposterior displacement. Remarkably, axon growth initiates during lateral movements through retrograde extension, whereby cell bodies move away from their axon tips attached to the brain[27] (Article figure 1A). While the anteroposterior active convergence is guided by Cxcr4b/Cxcl12a signaling downstream of the transcription factor Neurogenin1[29,35], the mechanisms driving the lateral phase of OP cell movements, during which axons elongate, remain elusive. We previously proposed that the lateral displacement of the cell bodies is a passive, non-autonomous process, based on the following findings: (1) the lack of protrusive activity and of polarised actin and myosin II in the laterally moving cell bodies, (2) the absence of lateral movement defects upon inhibition of microtubule polymerisation or upon cell-autonomous perturbation of actomyosin activity and (3) the lack of lateral movement defects when we disrupted the axons or their attachment to the brain[27]. Altogether, these observations suggest that lateral movements and axon elongation are driven by extrinsic pushing or pulling forces exerted on the OP cell bodies by surrounding cells or tissues.

The goal of this study is to identify the source of the extrinsic mechanical forces involved. We rule out a role for actively converging placodal cells in squeezing out the neuronal cell bodies laterally, and show that the driving force comes from the morphogenesis of the adjacent eye tissue, transmitted by mutual physical interactions with the intervening ECM. This work sheds

new light on the role of mechanical forces exchanged between developing neurons and surrounding tissues in the sculpting of neuronal circuits *in vivo*, which was largely unexplored so far.

- **Results**

  - **OP cells undergoing anteroposterior convergence are not required for OP lateral movements.**

We initially hypothesised that cells from the anterior and posterior extremities of the OP - while actively converging - may compress the central cells, thereby squeezing them away from the brain and contributing to the elongation of their axons[27]. To test this, we ablated the cells that would exert this compression, using the *Tg(-8.4neurog1:*

) line[36] referred to below as the *ngn1:gfp* line, which labels the early-born neurons in the OP[27,37]. In practise, we laser ablated 10 to 20 *ngn1:gfp*$^{+}$ cells in both anterior and posterior extremities of one placode when convergence occurs, at 14-16 s (the placode typically comprising a hundred *ngn1:gfp*$^{+}$ cells at this stage[27]), the contralateral placode serving as a control (Article figure 1B,C). We then performed live imaging and 3D cell tracking of the central cells in the ablated placode, and compared their movements with those of central cells in the control placode. We focused on embryos in which ablated placodes displayed smaller volumes than contralateral placodes throughout OP morphogenesis, over 500 min after the ablation, indicating a successful ablation (N = 5 embryos; Article figure 1C,D, Article supplementary figure 1A,B and Video 1). No significant defect in the mediio displacement of central OP cells was detected in the ablated placode (nor in the anteroposterior or dorsoventral displacements, Article figure 1E,F, Article supplementary figure 1C and Video 1). These results rule out a major contribution of actively converging OP cells in mediating the lateral movements of central cells. We thus turned our attention to another potential source of extrinsic mechanical forces: the adjacent eye tissue.

  - **OP and eye cell movements are correlated along the mediolateral axis.**

The optic cup develops close to the OP in a deeper, more ventral position, through extensive evagination and invagination movements having both a strong lateral component [30,38–44] (Article figure 2A). Such morphogenetic processes may exert forces on the overlying OP neurons and contribute to their lateral movement and axon extension. To test the influence of optic cup

morphogenesis on OP formation, we first compared cell movements in the OP with those occurring in the forming eye, focusing on their lateral component. To do so, we performed live imaging using a frontal view, on embryos carrying the *ngn1:gfp* transgene, labelling the early-born neurons in the OP but also a subpopulation of neurons in the anterior brain[27], and the *Tg(rx3:GFP)* transgene (*rx3:gfp*), expressed by neural retina progenitors[45] (N = 4 embryos, Video 2). We used a biological reference time Tref, which represents the time when the eye invagination angle is equal to 120°, to synchronise the 4 embryos and analyse a common time-window around Tref (see methods and Article supplementary figure 2A,B). Taking advantage of nucleus red labelling obtained with H2B-RFP mRNA injection, we tracked individual *ngn1:gfp*$^+$ OP cells throughout OP coalescence, from 12s to 24s, and found that they recapitulate the lateral movements we previously described on dorsal views[27] (Article figure 2B and Article supplementary figure 2E). To analyse morphogenetic movements in the forming optic cup, we focused on *rx3:gfp*$^+$ eye cells populating the anterior neural retina, as their movements were shown to take place in the vicinity of the OP, as opposed to other neural retina progenitors[30,40,42,46]. Strikingly, anterior neural retina progenitors displayed mediolateral directional movements that appeared to be coordinated with those of OP cells (Article figure 2B and Article supplementary figure 2E). To evaluate the contribution of other surrounding tissues, we also tracked *ngn1:gfp*$^+$ cells in the adjacent forebrain, and skin (peridermal) cells overlying the OP and the eye. Consistent with previous findings[27,29], skin cells showed spatially limited, non-oriented displacements. Brain *ngn1:gfp*$^+$ cells did not show directed lateral movements but often moved back and forth along the mediolateral axis, akin to interkinetic nuclear migration within the brain neuroepithelium (Article figure 2B and Article supplementary figure 2E).

To further compare the movements of cells from different tissues, we computed correlation coefficients between pairs of tracks from cells belonging to the four analysed tissues (OP, eye, brain, skin). For each pair of cells, we computed the correlation coefficient of their two trajectories for a given dimension (mediolateral, anteroposterior or dorsoventral component). Correlation coefficients are dimensionless and range from -1 (anticorrelated) to +1 (correlated). Averaging correlation coefficients for pairs of cells from the same tissue reflects the cohesiveness of cell motion in this tissue, while averaging these coefficients for pairs of cells from two different tissues reflects the degree to which the motions of these tissues are correlated along the dimension of interest (see methods). In all embryos, the mean mediolateral correlation coefficient for the eye/OP tissue couple was higher than 0.7 (Article figure 2; Article

supplementary figure 2 F), close to values of OP and eye intratissue correlations (Article supplementary figure 2C), showing that eye cells populating the anterior neural retina and OP cells have coordinated displacements in the mediolateral direction. This high correlation was not solely due to the proximity between the two tissues, since the mediolateral correlation for brain/OP and skin/OP couples was lower than for the eye/OP combination (Article figure 2C; Article supplementary figure 2F). In contrast, the correlation coefficients for the anteroposterior and dorsoventral components of cell trajectories were similar for all tissue pairs, and lower than the eye/OP correlation in the mediolateral axis (Article figure 2D,E). The high correlation between eye and OP lateral movements supports the idea of a coupling between the two adjacent tissues. We thus wanted to use perturbative approaches to explore the mechanical interplay between the eye and the OP.

- **OP lateral movements are reduced in eyeless *rx3* mutant embryos.**

To analyse whether eye morphogenesis is required for OP coalescence, we used a mutant for *rx3* (*rx3*^{s399}), a transcription factor specifically expressed in eye progenitors and the anterior hypothalamus from 8 hpf, and shown to be crucial for eye development[47–53]. While embryos that are heterozygous for this mutation do not show any phenotype, the eye field progenitors in *rx3*$^{-/-}$ homozygous embryos do not evaginate to form the optic vesicles, resulting in a complete loss of optic cups[50]. We analysed the volume, the dimensions and the number of cells of the OP, in *rx3*$^{-/-}$ mutants versus control siblings at the end of OP morphogenesis (24s). *rx3*$^{-/-}$ OPs displayed normal volume and cell numbers (Article supplementary figure 3). The anteroposterior and dorsoventral dimensions of the placode were increased in *rx3*$^{-/-}$ mutants, while the mediolateral dimension was decreased, as compared with control siblings (Article figure 3A-C). To assess potential defects in the movements of OP cells during coalescence, we followed OP cells using live imaging in a dorsal view (Video 3) and 3D tracking (N = 5 mutant placodes and N = 3 control placodes). No significant change in the total anteroposterior displacements was detected (Article figure 4 and Article supplementary figure 4A). The dorsoventral movements were not affected either (Article supplementary figure 4B). By contrast, the lateral displacement of OP cells was significantly reduced in *rx3*$^{-/-}$ mutants, while there was no change in the lateral displacement of adjacent *ngn1:gfp*$^{+}$ brain cells or overlying skin cells (Article supplementary figure 4C). Thus, the absence of eyes in *rx3*$^{-/-}$ mutants mostly affects the lateral movements of OP cells. Altogether, these results show that optic cup formation is required for proper OP morphogenesis along the mediolateral axis.

- **Axons in the OP are shorter and more twisted in eyeless *rx3* mutant embryos.**

Since we previously showed that axon growth initiates during lateral movement through retrograde extension[27], we also wanted to assess the influence of optic cup morphogenesis on axon elongation. To this end, we analysed the length and shape of axons in *rx3*$^{-/-}$ mutant embryos at the end of OP coalescence (24s, Article figure 3D). Consistent with a reduced mediolateral dimension of the OP and decreased lateral movements of OP cells, the axons of acetylated-tubulin^{+} neurons (a subpopulation of *ngn1:gfp*$^{+}$ neurons) were shorter in *rx3*$^{-/-}$ embryos in comparison to control siblings (Article figure 3E). These results show that optic cup morphogenesis also contributes to the retrograde elongation of axons within the OP. Interestingly, we also observed that axons located in the central region (along the anteroposterior axis) of the OP tissue, that elongate the most parallel to the mediolateral orientation, were more twisted in *rx3*$^{-/-}$ embryos than in controls (Article figure 3F). These observations suggest that, in addition to being shorter, axons are less stretched along the mediolateral axis in the absence of optic cups. At this point, all our findings support the idea of a mechanical coupling between the eye and the OP, whereby the forming eye pulls laterally on neuronal cell bodies and their trailing axons.

- **Mechanical tension at the lateral border of the OP is decreased in eyeless *rx3* mutant embryos.**

To further probe this mechanical coupling, we used linear laser ablations. Laser ablations were initially used to sever subcellular structures that support force transmission to provoke a sudden mechanical imbalance: the initial recoil velocity of the ablated structure gives, under some assumptions, an estimation of the tension prior ablation[54–56]. Laser ablation can also be performed at tissue-scale to create a wound and estimate tissue stress[57–61]. To estimate mechanical stresses at the periphery of the *ngn1:gfp*$^{+}$ cell group within the OP, we performed linear supracellular laser cuts in anterior, lateral and posterior borders of the *ngn1:gfp*$^{+}$ cluster in control embryos and *rx3*$^{-/-}$ mutants, at 16s (as depicted in Article figure 5A, Video 4). We analysed tissue relaxation using particle image velocimetry (Article figure 5B). Assuming that the tissue material properties are homogenous, the initial retraction velocity gives a relative estimation of the tissue mechanical stress before the cut. Mechanical stress was significantly reduced at the lateral border of *rx3*$^{-/-}$ mutants compared with the controls, whereas no change was detected in anterior and posterior OP borders (Article figure 5C). These results show that the tension to which the *ngn1:gfp*$^{+}$ placodal cluster is subjected along the mediolateral axis is

reduced when the eye is absent, in agreement with the hypothesis that the developing eye exerts lateral traction forces on OP neurons during OP morphogenesis.

○ Neural crest cells populate the eye/OP interface but are not essential for OP morphogenesis.

If the eye pulls on the OP, forces must be transmitted through a physical contact, we thus decided to inspect the interface between these two tissues. To analyse whether the OP and the eye interact through direct intercellular contacts, we took advantage of the *Tg(-8.0cldnb:LY-EGFP)* line (*cldnb:lyn-gfp*), in which a membrane-targeted version of gfp is expressed in forebrain, skin (peridermal) cells, but also eye cells (in the neural retina and the retinal pigmented epithelium) and all cells of the OP[62,63]. Imaging the eye/OP interface on *cldnb:lyn-gfp* embryos showed the presence of a gfp negative gap between the two tissues, about 10-15 µm-large, demonstrating the absence of common intercellular junctions (Article supplementary figure 5A and Videos 5 and 6). Interestingly, we observed the presence of gfp negative cells progressively populating the gap between the two tissues from around 18-20s onwards (Article supplementary figure 5A). Based on the literature[64,31,28,46], we hypothesised that these cells are cranial neural crest cells (NCCs). NCCs are known to influence optic cup formation[46] and their migration is affected in *rx3* mutants[64]. To test whether NCCs are necessary for OP formation, we searched for a condition in which the migration of NCCs populating the eye/OP interface is affected, but not eye morphogenesis. This situation can be found in *foxd3*$^{-/-}$ mutants, as described in a recent study[46] and confirmed by our analysis of NCCs (Article supplementary figure 5B) and eye size and invagination in *foxd3*$^{-/-}$ mutants (Article supplementary figure 5D). The number of cells located in the gap between the two tissues was reduced in *foxd3*$^{-/-}$ mutants, confirming that these interstitial cells mostly represent migrating NCCs (Article supplementary figure 5E). The volume of the OP, as well as its anteroposterior and dorsoventral dimensions, were not affected in *foxd3*$^{-/-}$ mutants, but the mediolateral dimension was increased (Article supplementary figure 5D), showing that the NCCs are not required for, but rather prevent OP lateral movements. These results argue against a major role of these interstitial NCCs in mediating OP lateral movements.

○ The extracellular matrix establishes a physical link between the eye and the OP

From our experiments, we conclude that the OP and the eye should be tightly linked. To further identify the mechanisms underlying such mechanical coupling, we hypothesized that the two

tissues are connected by and interact through ECM. We thus analysed by immunostaining the localisation of two ECM components, Laminin and Fibronectin, at the tissue interface. Laminin displayed a basement membrane-like distribution around the OP and the eye, suggesting the presence of two basement membranes surrounding the eye and the placode respectively (Article figure 6A and Article supplementary figure 5B). Fibronectin showed a more interstitial distribution surrounding the cells located at the interface between the eye and the OP (Article figure 6A). These expression patterns were unchanged in *rx3*$^{-/-}$ mutants, except the basement membrane surrounding the forming eye, due to the lack of optic cup (Article figure 6A), suggesting that the ECM surrounding the OP is not sufficient by itself to drive proper OP morphogenesis. To test whether ECM acts as a glue physically transmitting forces between the eye and the OP, we degraded the ECM by injecting a mix of collagenases and red fluorescent dextran, as previously described in Tlili *et al.* 2020[65], close to the eye/OP interface of *ngn1:gfp; rx3:gfp* embryos. This resulted in the rapid diffusion of the fluorescent mix in all the extracellular space of the head region (Article supplementary figure 6A), and in a global perturbation of Laminin distribution (weaker, more diffuse and less continuous signal) at 24s (Article supplementary figure 6B), confirming the efficiency of the treatment. This approach thus provides a temporal control on ECM perturbation, but no precise spatial control. To specifically target the lateral movements in the OP, and not the anteroposterior convergence movements, we performed the injection at 16-18s, when most of the convergence has already occurred[29]. As expected from previous studies reporting a role for the ECM in optic cup morphogenesis[30,42,66], the collagenases injection resulted in a range of eye defects (from little or no apparent defect to strong invagination phenotypes often associated with extrusion of the lens), likely reflecting variations in the injected volume, a parameter we can not unfortunately finely tune. In order to address the role of the ECM independently from that of the eye, we selected the collagenases-injected embryos in which eye cells still displayed coherent (with a high intra-eye correlation coefficient) and directional lateral movements (Article figure 6B,C and Article supplementary figure 6C,D). Strikingly, in these embryos, the lateral movements of OP cells were perturbed, and their correlation with the lateral movements of eye cells was decreased, as compared with control embryos injected with dextran only (N = 3 collagenases-injected and N = 3 dextran-injected control embryos) (Article figure 6B,C and Article supplementary figure 6C,D). These data provide evidence that the ECM mechanically couples OP and eye morphogenesis.

- **Discussion**

Our study reveals that the developing optic cup contributes, from a mechanical point of view, to the sculpting of the OP. Our data show that eye morphogenesis steers OP lateral movements and axon extension by exerting pulling forces in the lateral direction, transmitted to OP cells by ECM located at the interface between the two tissues.

The coalescence of the OP is driven by two types of cell movements, anteroposterior convergence and lateral movement[27]. Cxcr4b/Cxcl12a chemotactic signaling has been shown to control OP coalescence downstream of the Neurogenin1 transcription factor[29,35]. While the convergence of the anterior OP cells is particularly affected in mutants for the Cxcr4b/Cxcl12a pathway, the mediolateral component of the cell movements appears to be less perturbed[29]. Conversely, the lateral movements were decreased in eyeless *rx3*$^{-/-}$ mutants, but we did not detect significant defects in anteroposterior convergence movements, although the anteroposterior OP dimension was increased at the end of OP coalescence (24s). This increase could be due to a weak perturbation of Cxcl12a/Cxcr4b signaling in *rx3*$^{-/-}$ mutants, consistent with the previously described posterior expansion of the telencephalon[67,68], known to express the Cxcl12a ligand[29,35]. Alternatively, the higher anteroposterior OP dimension in *rx3*$^{-/-}$ mutants could be a consequence of the lateral movement defects: because of the inability of OP cells to be displaced laterally by the forming eye, the converging cells would accumulate at the anterior and posterior borders of the OP, thus increasing the dimension of the OP along the anteroposterior axis. Future investigations will distinguish between these hypotheses and clarify how Cxcr4b/Cxcl12a chemotactic signaling and eye mechanical traction cooperate to orchestrate the cell movements that shape the OP.

Eye morphogenesis is a complex, multi-step process, including optic vesicle evagination, optic cup invagination, lens formation and spreading of the retinal pigmented epithelium over the forming cup [43,44]. Which of these processes is the driving force of OP morphogenesis? In *rx3*$^{-/-}$ mutants, in which OP lateral movements are affected, evagination does not occur but a lens assembles[38], suggesting that lens formation is not sufficient to drive OP morphogenesis. Evagination of the optic vesicle is proposed to be driven by active cell migration in medaka[38] and, in zebrafish, by intercalation of cells from the core of the eye field into the retinal neuroepithelium[39]. This results in a massive lateral and posterior cell flow which could act as a conveying belt dragging the overlying OP cells laterally during the early phases of OP coalescence. Later, the invagination i.e. the remodelling of the vesicle into a cup is suggested

to occur through basal constriction in the centre of the retina epithelium, which may transmit tension at the tissue scale to trigger the bending of the retina[41,42]. Rim movements of cells from the medial layer of the cup into the lateral layer[40,42], and the spreading of the retinal pigmented epithelium over the forming cup[69] have also been proposed to contribute to optic cup invagination. Most of the cell rearrangements accompanying both optic vesicle evagination and optic cup invagination display a lateral component and could contribute to the lateral movements of OP cells. However, our analysis shows that the lateral displacement of *rx3:gfp*$^{+}$ neural retina progenitors is more important after Tref (the biological reference time we used to synchronize the embryos, which corresponds to an invagination angle of 120°, see methods) when invagination rearrangements dominate. In addition, the mediolateral correlation coefficient between the eye and the OP was systematically higher after Tref than before Tref (Figure S2D). Moreover, degrading ECM from 16-18s, i.e. from the beginning of the invagination and after evagination, was sufficient to perturb lateral movements in the OP. Altogether these results suggest that optic cup invagination is the main actuator of OP's shape change along the mediolateral axis. We hypothesise that the bending of the optic cup during invagination generates laterally oriented traction forces on OP cells, resulting in their lateral movements and the elongation of their axons. Additional experiments are required to identify the precise mechanism (apical constriction and cell compaction in the centre of the retina, rim movements of retinal cells, or spreading of the RPE over the cup) which generates these traction forces.

How is force transmitted between the eye and the OP? We observed the presence of NCCs and ECM at the interface between the two tissues. Interactions between NCCs and cranial placodes are crucial for the development of both cell populations in other contexts[70,71,25]. Using the *foxd3* mutant, in which cranial NCC migration is affected but eye morphogenesis is normal[46], we demonstrate that the presence of NCCs is not required at the eye/OP interface to mediate OP lateral movements. On the contrary, degrading the ECM, which results in a physical uncoupling of the eye and the OP, clearly perturbs lateral movements in the OP. This strongly suggests that the ECM propagates the traction forces exerted by the eye to the OP. We showed the localisation of Laminin and Fibronectin at the tissue interface, but other ECM components are known to be also present in this area at similar stages[46]. Future experiments will determine whether the intertissue ECM meshwork as a whole, or a specific ECM component, transmits the forces from the eye to the OP.

It is increasingly evident that the biomechanics of morphogenesis must be understood not only in the scope of isolated tissues, but also in the framework of interacting tissues[32,33]. For instance, a recent study explained why elongation rates of paraxial and axial tissues are similar during elongation of the body axis elongation in chicken embryos. The compression of axial tissues by the flanking mesoderm leads to their elongation wich in turn promotes the mesoderm elongation too. It is tempting to imagine that such mechanical feedback loop involving adjacent tissues is a general mechanism of morphogenesis orchestration[72]. In Drosophila, endoderm invagination induces a tensile stretch contributing to germband extension[60,73], but the mechanism behind such stress transmission remains elusive. ECM-mediated differential friction between tissues is essential for myotomes to acquire a chevron shape in zebrafish[65]. In addition, Fibronectin-mediated intertissue adhesion transmits shear forces between the neural tube and the paraxial mesoderm, which ensures symmetric morphogenesis of the zebrafish spinal cord[74]. Direct cell/cell contacts mediated by cadherins have been shown to transmit forces between adjacent tissues during gastrulation morphogenetic movements[75,76] and the elongation of *C. elegans* embryos[77]. Our study adds to this emerging field by bringing new insight on how the building of neuronal circuits requires intertissue mechanical interaction, and presents an original example of a tissue elongation process resulting from the traction by an adjacent tissue which is connected by ECM.

Our results suggest a scenario in which the eye pulls on OP neuronal cells bodies, which stretches the anchored axonal protrusions that, in turn, grow in response to that tension. The retrograde axon extension in the OP could thus be seen as an *in vivo* example of stretch-induced or towed growth, in which axons grow in response to extrinsic tension without motile growth cones. This process has been hypothesised long ago by Paul Weiss to occur widely during development and body growth[78], but has been mostly studied *in vitro* so far (for reviews see references[79,4,80]). OP morphogenesis thus represents a relevant *in vivo* model to investigate the mechanotransduction mechanisms by which neurons sense and transduce extrinsic forces into axon elongation, and in particular where and how novel material (membrane, cytoskeleton) is added along the axon shaft to accommodate stretch-induced growth. Mechanotransduction pathways can also drive changes in cell fate[81–83] and could, in the OP, influence neurogenesis and neuronal differentiation, which are concomitant with OP morphogenesis[29,27,37,84].

- **Methods**

  - **Fish strains**

Wild-type, transgenic and mutant zebrafish embryos were obtained by natural spawning. In the text, the developmental times in hpf indicate hpf at 28°C. To obtain the 12s stage, embryos were collected at 10 am, incubated for 2h at 28°C before being placed overnight in a 23°C incubator. 12s corresponds to 14 hpf and 24s to 21 hpf. The OP was visualised with the *Tg(8.4neurog1:gfp)* line[36], referred to as *ngn1:gfp* in the text. The eye was visualised with the *Tg(rx3:GFP)* line[45], referred to as *rx3:gfp* in the text. The *Tg(-8.0cldnb:LY-EGFP)* line, referred to as *cldnb:lyn-gfp*, was used to label the membranes of the neural retina and the retinal pigmented epithelium, as well as all cells of the OP[62,63]. The *rx3*^{s399} mutant[50] (*chokh, chk*^{s399}), referred to as *rx3* mutant, was used to examine OP morphogenesis in the absence of eye evagination. The *foxd3*^{zdf10} mutant[85], referred to as *foxd3* mutant, was provided by the ZIRC Oregon and used to analyse OP morphogenesis when cranial NCC migration is perturbed. All our experiments were made in agreement with the European Directive 210/63/EU on the protection of animals used for scientific purposes, and the French application decree 'Décret 2013-118'. The fish facility has been approved by the French 'Service for animal protection and health', with the approval number A-75-05-25.

  - **Genotyping**

Homozygous *rx3*$^{-/-}$ embryos were identified by their morphology/phenotype as the absence of eyes was easily detectable from 8-10s. For maintaining the line, the *rx3* locus was amplified from genomic DNA of adult fish using the 5'-TTATGCAGGAGTTTGTAGG-3' (forward) and 5'-TAGTAGCCTATACTTCTCC-3' (reverse) primers. The BspeI restriction enzyme (NEB, R0540S) cuts the wild type allele, giving rise to two fragments of 172bp and 159bp, but not the *rx3*^{s399} allele (331bp). The *foxd3*^{zdf10} allele was genotyped with the CAPS (Cleaved Amplified Polymorphic Sequences) technique[86], using the SspI restriction enzyme (NEB, R132S), as described in[46].

  - **mRNA injections**

mRNAs were synthesised from linearised pCS2 vectors using the mMESSAGE mMACHINE SP6 transcription kit (Ambion). The following amounts of mRNA were injected into one-cell stage embryos: 80-100 pg for H2B-RFP, and 100 pg for mbCherry (membrane Cherry)[87].

- **Immunostainings**

For immunostaining, embryos were fixed in 4% paraformaldehyde (PFA, in PBS), blocked in 5% goat serum, 1% bovine serum albumin and 0.3% triton in PBS for 2-3h at room temperature and incubated overnight at 4°C with primary and secondary antibodies. The following primary antibodies were used: anti-acetylated-tubulin (mouse, 1/500, 6-11B-1 clone, T6793, Sigma), anti-Laminin (rabbit, 1/100, L-9393, Sigma), anti-Fibronectin (rabbit, 1/100, F3648, Sigma).

- ***In situ* hybridisation**

Partial cDNA sequences for the NCC *crestin* marker were amplified by PCR using the 5'-AAGCCCTCGAAACTCACCTG-3' (forward) and 5'-CCACTTGATTCCCACGAGCT-3' (reverse) primers. PCR products were subcloned in pGEM-T-easy (Promega) and sequenced. The Digoxigenin(DIG)-labeled riboprobe was synthetized from PCR templates. Embryos were fixed in 4% PFA in PBS and stored in methanol at − 20 °C. Embryos stored in methanol were rehydrated in a methanol/PBS series, permeabilized 1min30s with proteinase K (10 mg/ml), pre-hybridized, and hybridized overnight at 65 °C in hybridization mixture (50% formamide, 5 X standard saline citrate (SSC), 0.1% Tween 20, 100 µg/lateral heparin, 100 µg/ml tRNA in water). The embryos were subjected to a series of washes in 50% SSC/formamide and SSC/PBST, and were then incubated in the blocking solution (0.2% Tween 20, 0.2% Triton X-100, 2% sheep serum in PBST) for one hour and overnight at 4 °C with alkaline phosphatase-conjugated anti-DIG antibodies (Roche) diluted at 1:4000 in the blocking solution. Embryos were then washed in PBST, soaked in staining buffer (TMN: 0,1M NaCl, 0,1M Tris-HCl, pH 9.5, 0.1% Tween 20 in water) and incubated in NBT/BCIP (nitroblue tetrazolium/5-bromo-4-chloro-3-indolyl phosphate) solution (Roche).

- **Laser ablation of cells**

Laser ablation of anterior and posterior converging cells was performed in OPs of 14-16s *ngn1:gfp* embryos injected with H2B-RFP mRNA to label the nuclei. Embryos were mounted in 0.5% low melting agarose in 1X E3 medium, and 10-20 cells in each anteroposterior extremity were ablated using a Leica TCS SP5 MPII upright multiphoton microscope with a ×25 objective (numerical aperture (NA): 0.95), laser at 790 nm). Two successive ablations were performed when the initial ablation did not generate any cell debris.

- **Stress estimation at the OP periphery using laser ablation**

Stress at the OP periphery was assessed by performing laser ablation of a line of cells. These supracellular laser ablations were performed in OPs of 14-18s *ngn1:gfp* embryos injected with mbCherry mRNA to label the membranes. Embryos were mounted in 0.5% low melting agarose in 1X E3 medium in Ibidi dishes (81158) and imaged using an inverted laser-scanning microscope (LSM 880 NLO, Carl Zeiss) equipped with a 63x oil objective (1.4 DICII PL APO, Zeiss). The cuts (about 20-25 µm long and 2-3 µm large) were performed in anterior, lateral and posterior borders of the *ngn1:gfp*$^{+}$ cell cluster as depicted in Figure 5A. Ablations were performed using a Ti:Sapphire laser (Mai Tai, DeepSee, Spectra Physics) at 790 nm with <100 fs pulses, using a 80 MHz repetition rate, a 100% power and a number of iterations ranging between 5 and 10. Images were acquired at a frame rate of 0.46 s after ablation (the ablation itself lasted about 0.2 s). The initial velocity of wound margin retraction after ablation measures the stress-to-viscosity ratio within the tissue. To estimate the tension prior ablation, we thus measured the tissue flow by particle image velocimetry using the MatPIV toolbox for Matlab (Mathworks, US). The window size was set to 32 pixels (~ 8 µm), with an overlap of 0.5. The 2D velocity field was measured between pre-cut and 5 frames after ablation (typically 2-3 s after ablation) in two rectangles of 10 µm wide adjacent and parallel to the line of ablation, as shown in Figure 5B. The "recoil velocity" was then obtained by summing the absolute values of the two average outward velocities (component orthogonal to the line of ablation) from each side of the ablation.

- **Live imaging**

Embryos were dechorionated manually and mounted at 11-12s in 0.5% low melting agarose in E3 medium, in order to obtain a frontal or a dorsal view of the head. Movies were recorded at the temperature of the imaging facility room (21-22 °C) except for the collagenases-injection experiment (see below), on a Leica TCS SP5 AOBS upright confocal microscope or a Leica TCS SP5 MPII upright multiphoton microscope using ×25 (numerical aperture (NA) 0.95) or ×63 (NA 0.9) water lenses. At 21-22 °C, it takes around 800 min for zebrafish embryos to develop from 12s to 24 s stages. The Δt between each frame was 5 min for the analysis of cell movements in wild type embryos (Figures 2, S2) and 10 min for all the other live imaging experiments.

- **Injection of collagenases**

Embryos were injected at 1-cell stage with H2B:RFP mRNA, dechorionated manually at around 10s and mounted in 0.5% low melting agarose in E3 medium in order to obtain a dorsal view of the head. A collagenase mix was prepared with collagenase II (17101-015, Gibco) at 1000U/mL, collagenase IV (17104-019, Gibco) at 1000U/mL and Rhodamine Dextran (D1817, Invitrogen) at 5mg/mL diluted in E3 medium. Embryos were injected at 16-18s in the head region, close to the eye/OP interface, with a manual microinjector (CellTram Oil, Eppendorf). After injection, embryos were imaged using a Leica TCS SP5 MPII upright multiphoton microscope and ×25 (numerical aperture (NA) 0.95) water lens. Movies started around 30 minutes after the injection and lasted between 4 and 5 hours at 28°C. Immunostainings for Laminin were conducted on other injected embryos, kept at 28°C after injection and fixed at 24s.

- **Image analysis**

Quantification of OP volume, cell number and dimensions. To measure the volume of the OP *ngn1:gfp*$^{+}$ cluster, we manually cropped the OP using ImageJ, segmented the *ngn1:gfp*$^{+}$ cluster using median filtering and thresholding, and measured the volume of the object using the 3D ImageJ suite[88]. 3D counting of nuclei was achieved on the DAPI channel with the 3D ImageJ suite[88] and the 3D Object Counter plugin[89]. To quantify the dimension of the OP, the *ngn1:gfp*$^{+}$ segmented object was fitted with a 3D ellipsoid (see Figure 3B). A rotation of the image was applied so that the length of the ellipsoid 3D bounding box aligns with the orientation of the brain/placode interface. The lateral and anteroposterior dimensions of the OP correspond respectively to the X and Y dimensions of the 2D bounding box of the central z-slice of the ellipsoid, and the dorsoventral dimension corresponds to the Z dimension of the 3D bounding box of the whole ellipsoid.

Quantification of axon length and twisting index. Individual acetyl-tubulin positive axons were segmented manually in 3D, on images of fixed embryos at 24s, using the multiple point tool of Image J. The X,Y,Z coordinates of the resulting points were recovered and used to calculate the total 3D length of the axons and their twisting index, defined as 1 - (total 3D axon length/distance between the most proximal and the most distal point of the axon).

Manual cell tracking. Individual cells from the OP, the eye, the brain or the skin (periderm) were tracked in 3D using the Manual Tracking plugin in ImageJ. Tracked cells from the brain and the OP expressed *ngn1:gfp* at least at the end of the movie. Tracked cells from the eye expressed *rx3:gfp* at least at the end of the movie. Mediolateral cell positions were rescaled depending on the brain midline position to remove the contribution of a potential general drift of the embryo. Plots representing cell tracks merged at their origin were produced with Microsoft Excel and 2D color coded trajectories were generated in Matlab (Mathworks, US).

Time registration or synchronization. In order to compare similar stages of optic cup morphogenesis in the 4 embryos we imaged for the correlation analysis (Figure 2), we measured the invagination angle of the optic cup (θ, Figure S2A) as a function of time. We observed that θ decreases as morphogenesis goes and systematically passes through an inflection point when θ is approximately equal to 120° (Figure S2B). We used this inflexion point as a common time-coordinate in order to time-synchronize the 4 embryos. We thus fitted the invagination angle using the following equation:

$\theta(t) = \frac{\theta_i+\theta_f}{2} - \frac{\theta_i-\theta_f}{2}\ tanh\left(\frac{t-t_{ref}}{\Delta\tau}\right)$ where θ_i and θ_f are the invagination angles at 12s and 30s respectively, T_{ref} the time corresponding to an invagination angle of 120° and $\Delta\boldsymbol{\tau}$ the width of the *tanh*. We imposed the invagination angles θ_i=180° and θ_f=60°, in agreement with our observations. We thus shifted the curves of each movie in time so that their inflection points overlap for θ=120°. This enables us to set a common time window of 14h for the 4 embryos we analysed, depicted in light blue in Figure S2B.

Computation of correlation coefficients between pairs of cell tracks. The correlation coefficient R between two trajectories $\left(T^{(1)}, T^{(2)}\right)$ is the covariance of the two trajectories normalized by the variance of each trajectory: $R = \frac{Cov\left(T^{(1)},T^{(2)}\right)}{\sqrt{Var(T^{(1)})Var(T^{(2)})}}$. The 1D correlation coefficient for the mediolateral component (x component) is thus:

$$R_{lateral}\left(T^{(1)}, T^{(2)}\right) = \frac{\sum_{t_n}(x^{(1)}(t_n) - <\ x^{(1)}\ >_t)(x^{(2)}(t_n) - <\ x^{(2)}\ >_t)}{\sqrt{\sum_{t_n}(x^{(1)}(t_n) - <\ x^{(1)}\ >_t)^2}\sqrt{\sum_{t_n}(x^{(2)}(t_n) - <\ x^{(2)}\ >_t)^2}}$$

where $<>_t$ is the temporal averaging. R lies in the range [-1; 1] and R^2 approximately indicates the percentage of the variation in one variable that can be explained by the variation in the other

variable. Since the value of *R* is a function of the sample size, we consider the largest time-window common to all the embryos, which was 14h25min (depicted in light blue in Figure S2B), corresponding to 173 points.

- **Statistical analysis**

Graphs show mean ± s.e.m. (standard error of the mean), overlayed with all individual data points. The plots were generated with the GraphPad Prism software. For all figures, we checked for normality using Shapiro-Wilk normality tests, before performing parametric or non-parametric tests. The nature of the statistical test performed for each graph is indicated in the figure legends. The p values are corresponding to *$p < 0.05$, **$p < 0.01$, ***$p < 0.001$. No statistical method was used to estimate sample size and no randomisation was performed. Blinding was performed for the analysis of the supracellular laser ablation experiments

- **Figures**

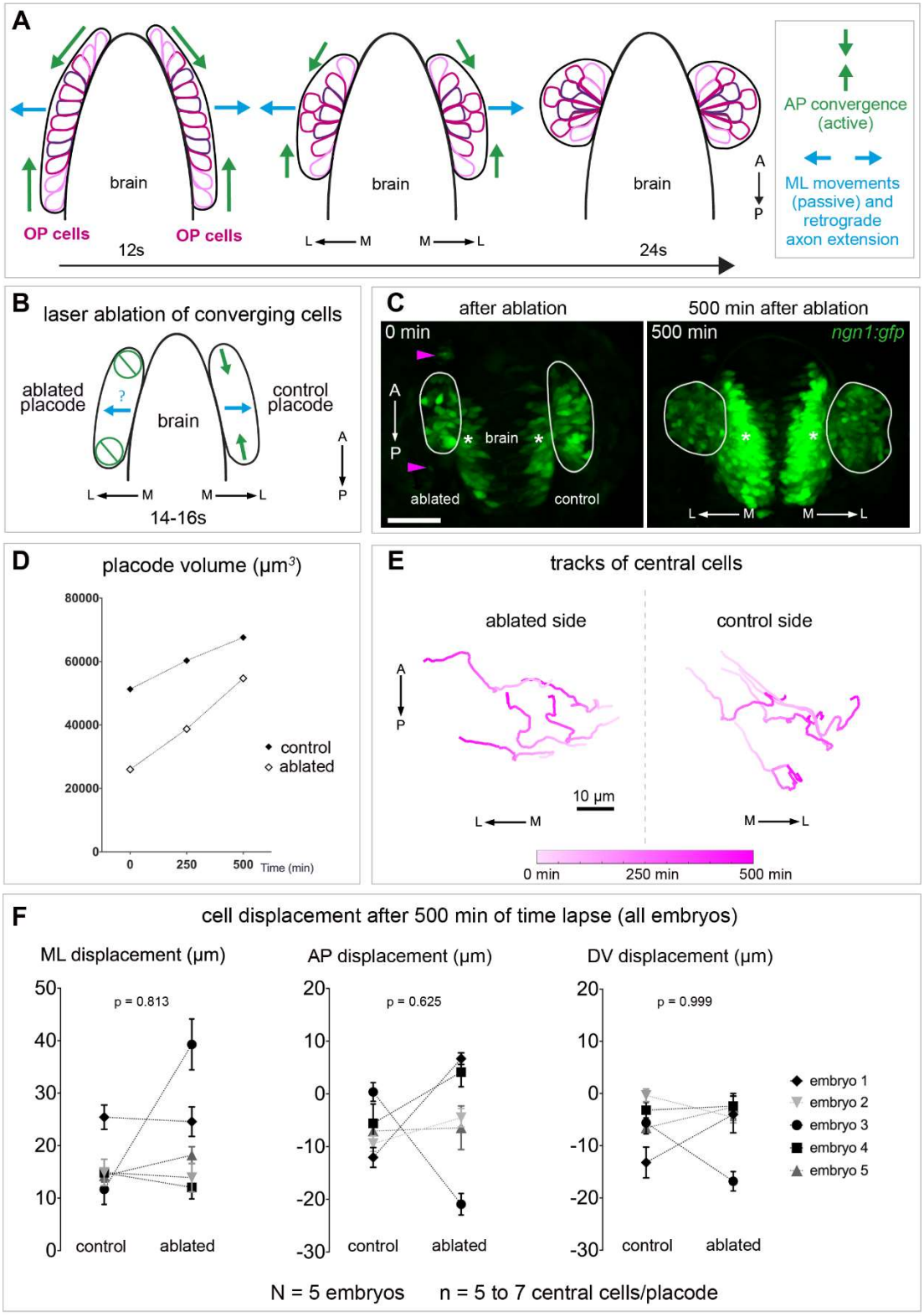

Article figure 1

Figure 1. OP cells undergoing anteroposterior convergence are not required for lateral movements. A. Schematic view of the two movements driving OP coalescence from 12s (14 hpf) to 24s (21 hpf) (dorsal view, membranes of OP cells in magenta). OP cells are initially located in two elongated domains surrounding the brain. Cells from OP extremities converge towards the centre through active migration along the brain surface (anteroposterior convergence, green arrows), while cell bodies of central cells passively move away from the brain (lateral movements, blue arrows). Axon elongation is concomitant with passive lateral movements and occurs through a retrograde mode of extension, where cell bodies move away from axon tips attached to the brain's surface. **B.** Schematic view of the laser ablation of converging cells: we used the *ngn1:gfp* transgenic line to ablate the cells undergoing anteroposterior convergence in one of the two placodes (left) at 14-16s, and tracked the central cells during the following 500 min (to reach the 24s stage). Central cells in the contralateral placode were also tracked and used as controls. Dorsal view. **C.** Images of a representative embryo (embryo 1) following the ablation (left) and 500 min later (right) (dorsal view). The ablated (left) and control (right) OPs are surrounded by white lines. Magenta arrowheads show cellular debris where cells were killed in the anterior and posterior regions of the *ngn1:gfp*$^{+}$ placodal cluster. Asterisks indicate gfp expression in the brain. Scale bar: 40 µm. See also Video 1. **D.** Graph showing the volumes of the ablated and control *ngn1:gfp*$^{+}$ placodes for 3 time-points in embryo 1, t = 0 refers to the ablation. **E.** 2D tracks of 5 central cells in the ablated and control placodes in embryo 1. The time is color-coded: light magenta at the starting of the trajectory (just after the ablation) towards dark magenta for the end of the track (500 min later). Similar data (images, volume and tracks) for embryos 2 to 5 are presented in Figure S1. **F.** Graphs showing the total mediolateral (ML), anteroposterior (AP) and dorsoventral (DV) displacements of OP central cells during the 500 min following the ablation, both in ablated and control placodes, for all embryos. N = 5 embryos from 3 independent experiments, each dot represents the mean displacement per placode (+/- sem) calculated from n = 5 to 7 cells/placode, two-tailed Wilcoxon matched-pairs signed rank test.

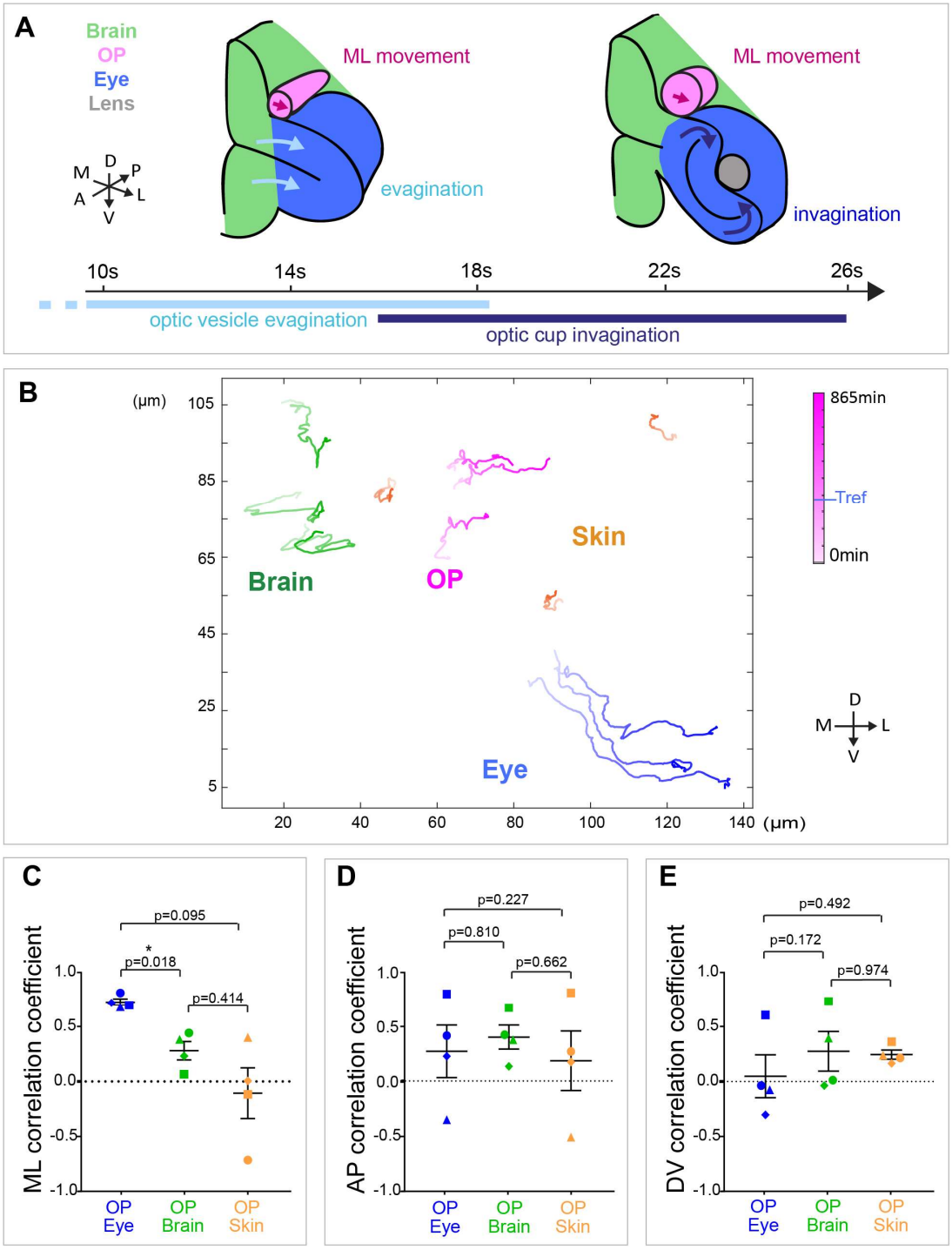

Article figure 2

Figure 2. OP and eye cell movements are correlated along the mediolateral axis. A. 3D schematic view of optic vesicle evagination and optic cup invagination, occurring during OP coalescence. The optic cup (blue) develops near the OP (pink) in a deeper, more ventral position. The brain is represented in green. Both evagination and invagination movements display a strong lateral component and may exert forces on the overlying OP neurons, contributing to their lateral movement and axon extension. **B.** Live imaging in a frontal view on *ngn1:gfp*; *rx3:gfp* double transgenic embryos injected with H2B:RFP mRNA to label cell nuclei allowed us to track individual cells in four tissues from 12s to 24s (N = 4 embryos from 2 independent experiments, the way we synchronised the 4 movies is detailed in the methods). Three representative trajectories of *ngn1:gfp*$^{+}$ OP cells (magenta), adjacent *ngn1:gfp*$^{+}$ brain cells (green), *rx3:gfp*$^{+}$ eye cells populating the anterior retina (blue) and overlying skin cells (orange) in embryo 1. The time is color-coded: light at the starting of the trajectory (12s) towards dark for the end of the track (24s, 865 min later). The reference time (Tref) when the eye invagination angle is 120° (see methods) is shown in the colorbar indicating the time. **C-E.** Mediolateral (ML), anteroposterior (AP) and dorsoventral (DV) correlation between pairs of cells belonging to different tissues. A value of 1 indicates highly correlated tracks and -1 is for anticorrelated tracks. Each dot represents the average correlation coefficient for a given pair of tissues in a given embryo (N = 4 embryos from 2 independent experiments), calculated from the tracking data of 5 to 7 cells per tissue. One-way paired ANOVA with Greenhouse-Geisser correction and Tukey's multiple comparison test. The correlation coefficients obtained of all pairs of cell trajectories for all embryos are presented in correlation matrices shown in Figure S2F.

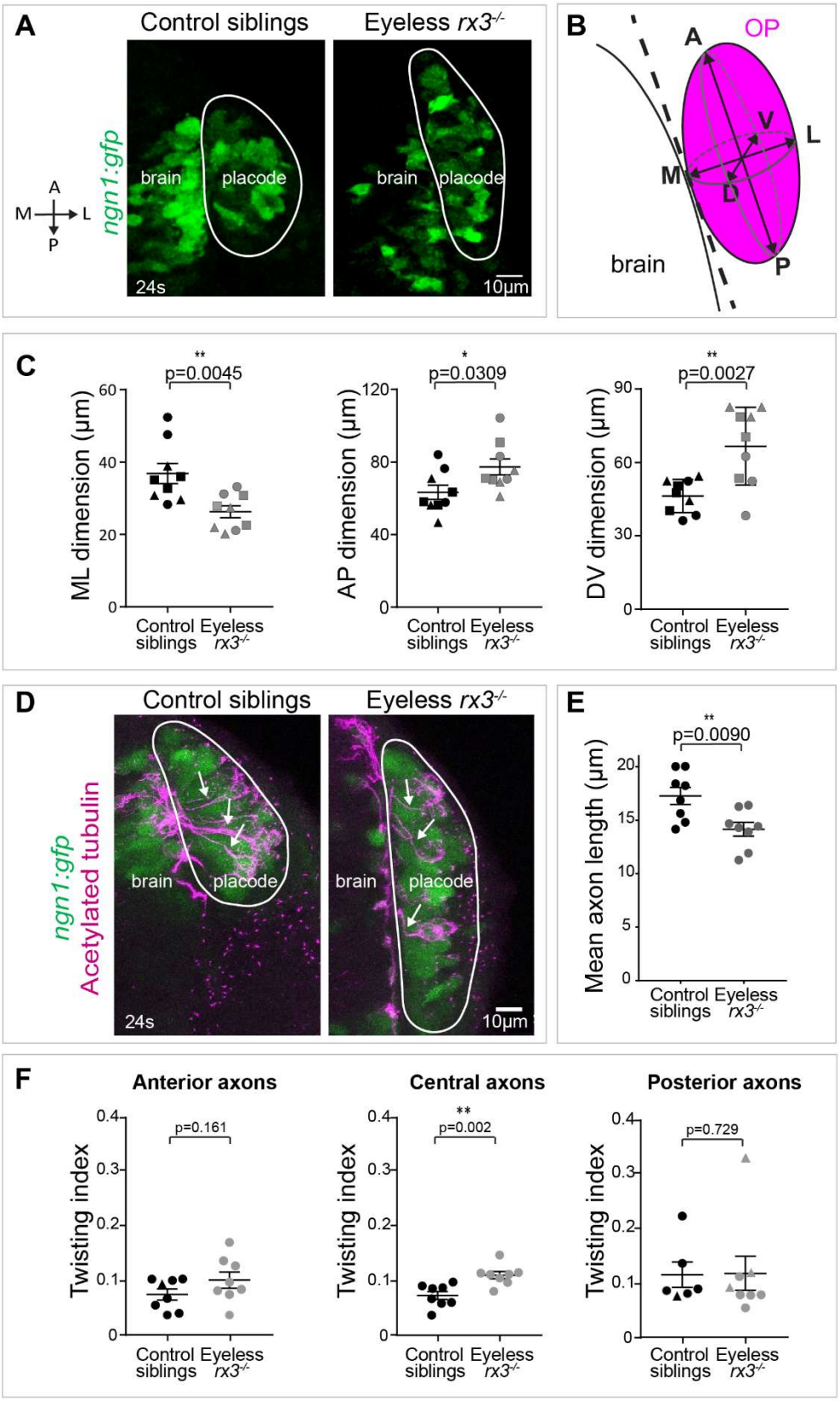

Article figure 3

Figure 3. OP shape and axon length are affected in *rx3*$^{-/-}$ eyeless embryos. A. Images (dorsal views, 1 z-section) of representative placodes from a *ngn1:gfp; rx3*$^{-/-}$ mutant (right) and a control *ngn1:gfp* sibling (left) at the end of OP coalescence (24s). The *ngn1:gfp*$^{+}$ OP clusters are surrounded by white lines. **B.** The *ngn1:gfp*$^{+}$ OP clusters were fitted with a 3D ellipsoid (pink) to estimate the mediolateral (ML), anteroposterior (AP), and dorsoventral (DV) dimensions of the placode (details in methods) at 24s. **C.** Graphs showing the mediolateral (ML), anteroposterior (AP), and dorsoventral (DV) dimensions of the OP in *rx3*$^{-/-}$ eyeless mutants (grey) and control siblings (black) at 24s (N = 9 embryos from 3 independent experiments). Embryos from the same experiment are represented with similar markers (dots, triangles or squares). Unpaired, two-tailed t test. **D.** Confocal images (dorsal views, 20 µm maximum projections) of representative placodes from a *ngn1:gfp; rx3*$^{-/-}$ eyeless mutant (right) and a control sibling (left) immunostained at 24s for acetyl-tubulin (magenta), which labels a subpopulation of *ngn1:gfp*$^{+}$ (green) neurons and their axons. The *ngn1:gfp*$^{+}$ OP clusters are surrounded by white lines. Some axons are indicated by arrows. **E.** Graph showing the length of acetyl-tubulin^{+} axons in *rx3*$^{-/-}$ mutants (grey) and control siblings (black) at 24s (N = 8 embryos from 3 independent experiments). Unpaired, two-tailed t test. **F.** Graphs showing the twisting index (see methods) of anterior, central and posterior axons in *rx3*$^{-/-}$ mutants (grey) and control siblings (black) at 24s (N = 8 embryos from 3 independent experiments). For embryos represented by a triangle, only one axon was measured. Unpaired, two-tailed t test for anterior and central axons. For the posterior axons the data did not show a normal distribution and a two-tailed Mann-Whitney test was performed.

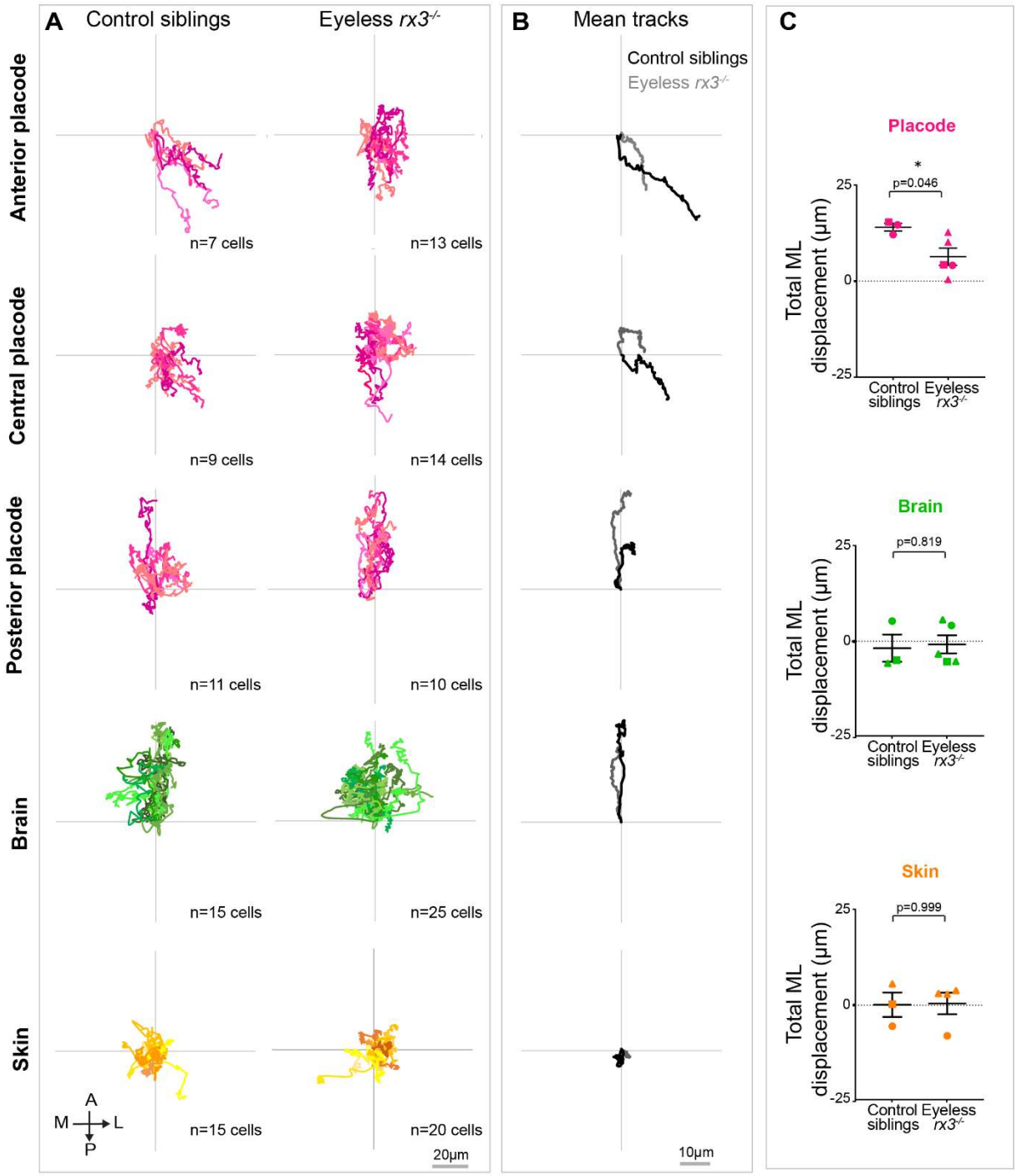

Article figure 4

Figure 4. Mediolateral movements of OP cells are reduced in *rx3*$^{-/-}$ eyeless embryos. A. 2D tracks (mediolateral along X and anteroposterior along Y), merged at their origin, of anterior, central and posterior *ngn1:gfp*$^{+}$ placodal cells (as defined in [27]) (magenta), *ngn1:gfp*$^{+}$ brain cells (green), and skin cells (orange), in control and *rx3*$^{-/-}$ eyeless mutant embryos (N = 3 control placodes and N = 5 mutant placodes from 3 independent experiments). All cells were tracked throughout the morphogenesis process, from 12s to 24s stages, during a 700 min period of time. **B.** Mean 2D trajectories for control and *rx3*$^{-/-}$ eyeless mutant embryos. **C.** Graphs showing the total mediolateral (ML) displacement of OP (magenta), brain (green) and skin (orange) cells, starting at 12s and during 700 min of time lapse in *rx3*$^{-/-}$ eyeless mutants and control embryos (N = 3 control placodes and N = 5 mutant placodes from 3 independent experiments, 5 to 7 cells per tissue per placode, unpaired, two-tailed t test).

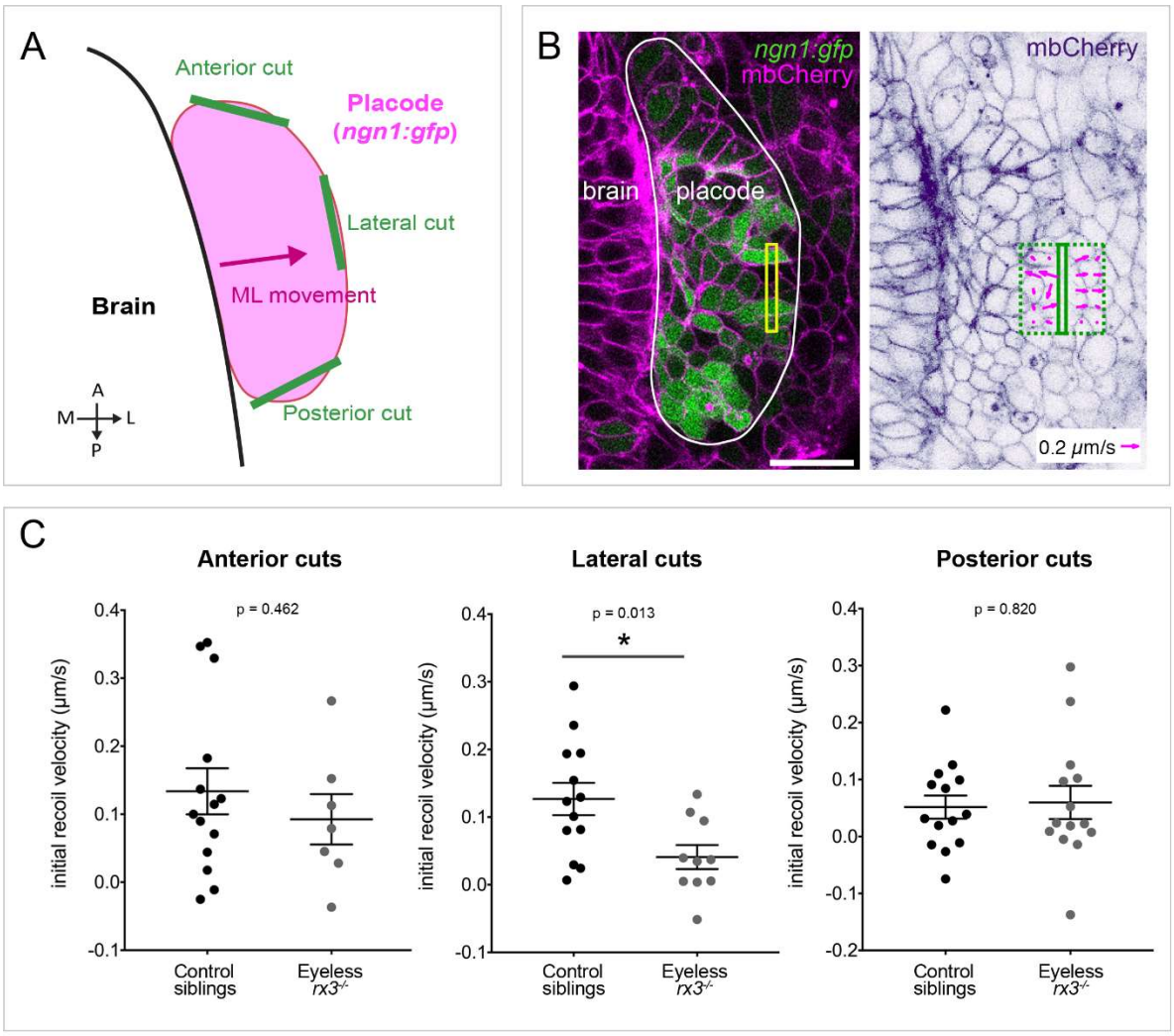

Article figure 5

Figure 5. Mechanical stress at the lateral border of the *ngn1:gfp*$^{+}$ OP cluster is reduced in eyeless embryos. **A.** Schematic view of the supracellular laser ablation experiment (dorsal view). Linear laser cuts (green segments) were performed at the anterior, lateral or posterior border of the *ngn1:gfp*$^{+}$ OP cluster at 16s, in control and *rx3*$^{-/-}$ embryos injected with mbCherry mRNA to label the membranes. **B.** Example of a lateral cut performed on a control *ngn1:gfp* (green) embryo expressing mbCherry (magenta on the left panel, and purple on the right panel). Left: image showing the position of the region of ablation (yellow), just before the ablation, the OP is delineated with a white line. Scale bar: 20 µm. Right: same image 3 s after the ablation, with tissue velocity field overimposed (magenta arrows) in rectangles of 10 µm width on both sides of the ablation line. **C.** Graphs showing the initial relaxation velocity, used as a proxy for tissue mechanical stress before the cut, following anterior, lateral or posterior cuts, in control and *rx3*$^{-/-}$ embryos (data pooled from 7 independent experiments). Unpaired, two-tailed t test.

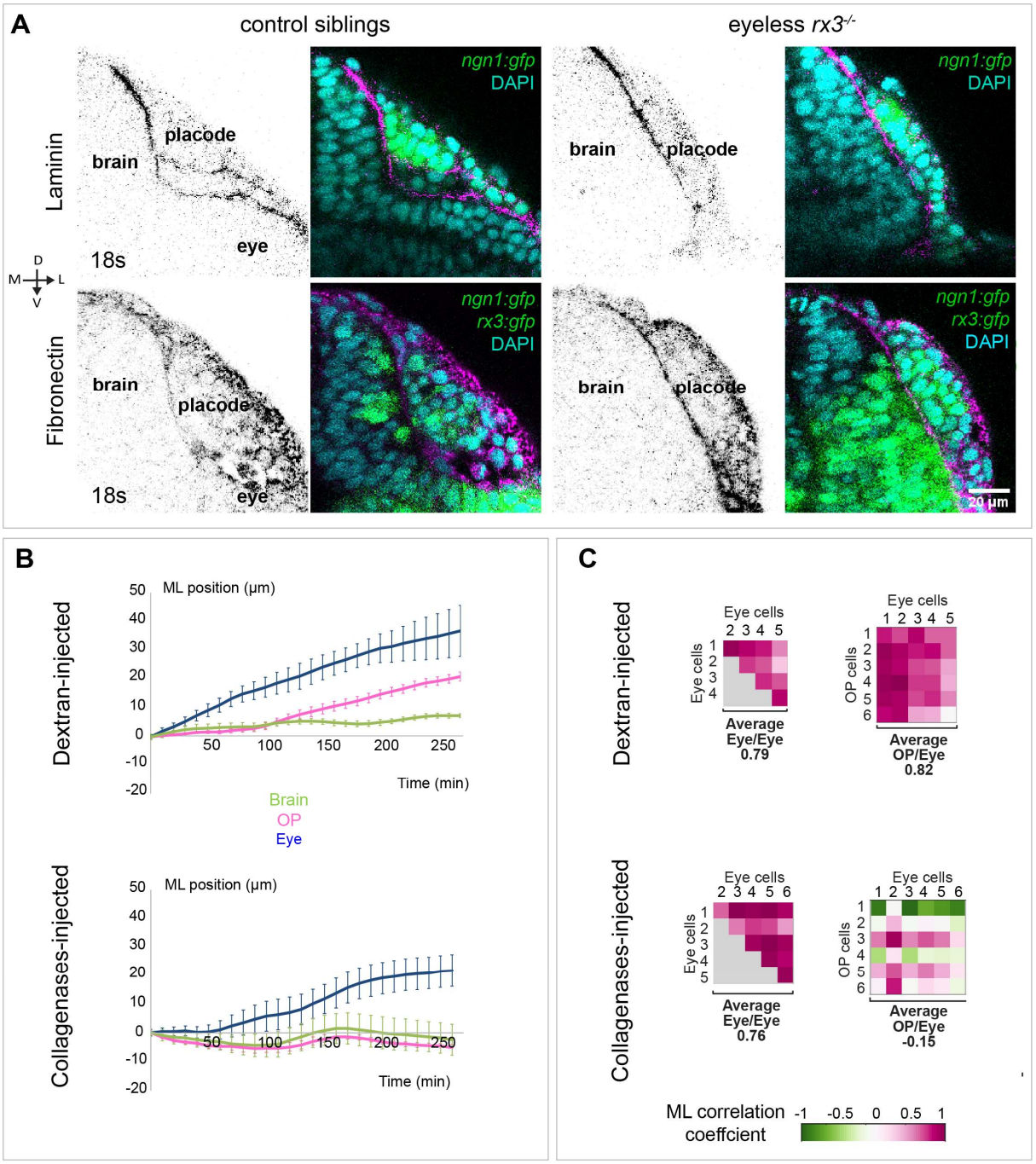

Article figure 6

Figure 6. The extracellular matrix mechanically couples the eye to the OP. **A.** Confocal images (frontal views, 1 z-section) of Laminin and Fibronectin immunostainings (black, or magenta on the merge) performed on *ngn1:gfp; rx3:gfp* control (left) and *rx3*$^{-/-}$ (right) embryos fixed at 18s. **B.** Live imaging with a dorsal view was performed on *ngn1:gfp*; *rx3:gfp* embryos expressing H2B:RFP and injected at 16s with a mixture of collagenases and red dextran or with dextran only. Individual cells were tracked in several tissues (OP, eye, brain and skin) from 16s to 24s (N = 3 collagenases-injected embryos and N = 3 dextran-injected control embryos from 3 independent experiments). To compensate for the drift often observed in injected embryos, the average displacement of skin cells was used for registration and removed from the tracking data. The graphs show the mediolateral displacement of OP (magenta), eye (blue) and brain (green) cells as a function of time (mean +/- sem from 5 to 7 cells per tissue) for one control and one collagenase-injected embryo (experiment 1). Results for experiments 2 and 3 are shown in Figure S6C. **C.** Correlation matrices presenting the intra-eye and the eye/OP mediolateral correlation coefficients, calculated from the tracking data of 5 to 7 cells per tissue (experiment 1). The average correlation coefficient for each tissue couple is indicated below the matrices. Results for experiments 2 and 3 are shown in Figure S6D.

- **Supplementary figures**

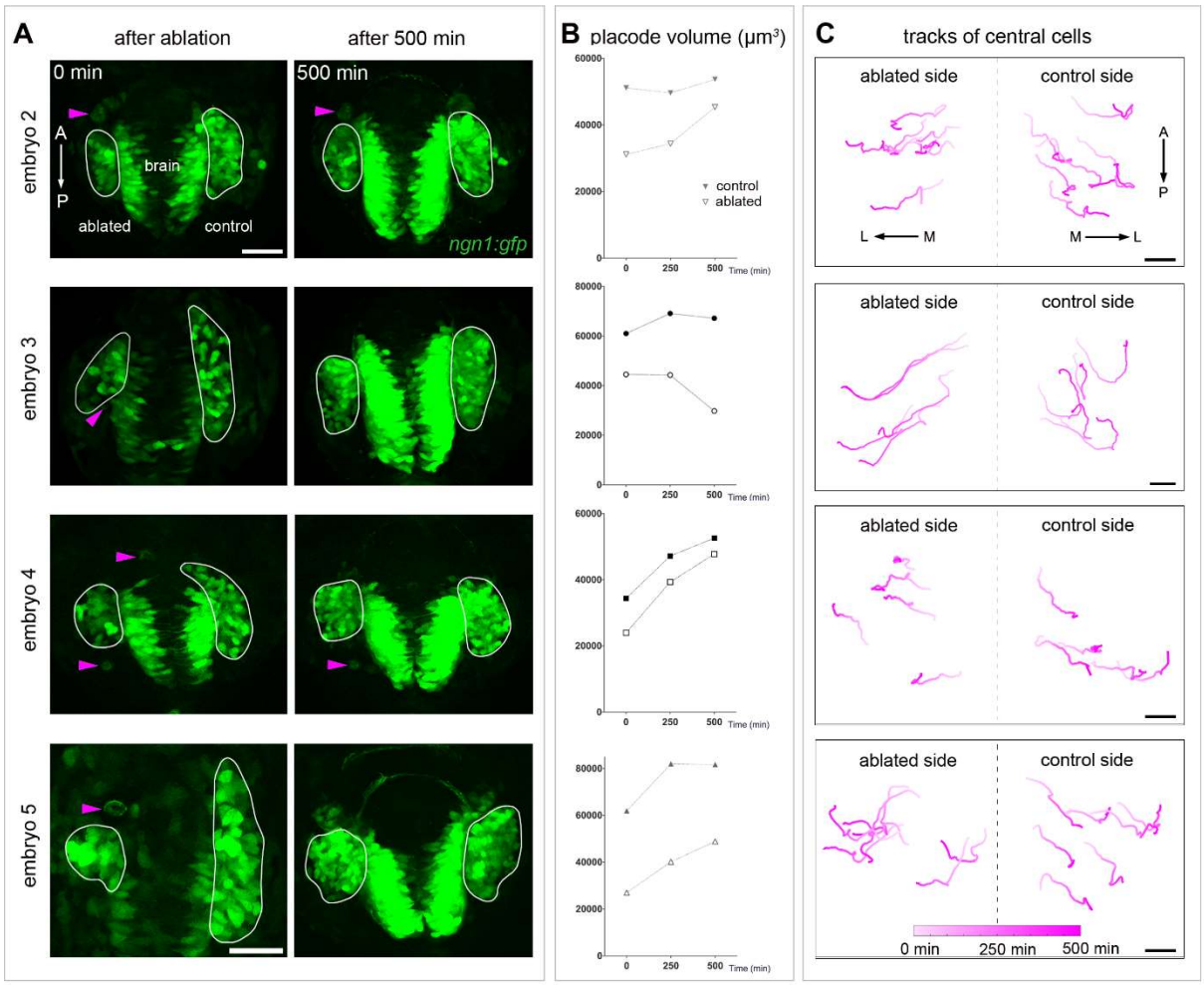

Article supplementary figure 1

Figure S1. Additional results for the laser ablation of anteroposterior converging cells. A. Images (dorsal view) of embryos 2 to 5 following the ablation (0 min) performed at 14-16s and 500 min later (24s). The OPs are surrounded by white lines. Magenta arrowheads show, when they are visible, the cellular debris resulting from cell ablation, in the anterior and/or posterior regions of the *ngn1:gfp*$^{+}$ placodal clusters. Scale bars: 40 µm. **B.** Graphs showing the volumes of the ablated and control *ngn1:gfp*$^{+}$ placodes for 3 time-points in embryos 2 to 5, t = 0 refers to the ablation. **C.** 2D-tracks of 5 to 7 OP central cells in the ablated and control placodes in embryos 2 to 5. The time is color-coded: light magenta at the starting of the trajectory (just after the ablation) towards dark magenta for the end of the track (500 min later). Scale bars: 10 µm.

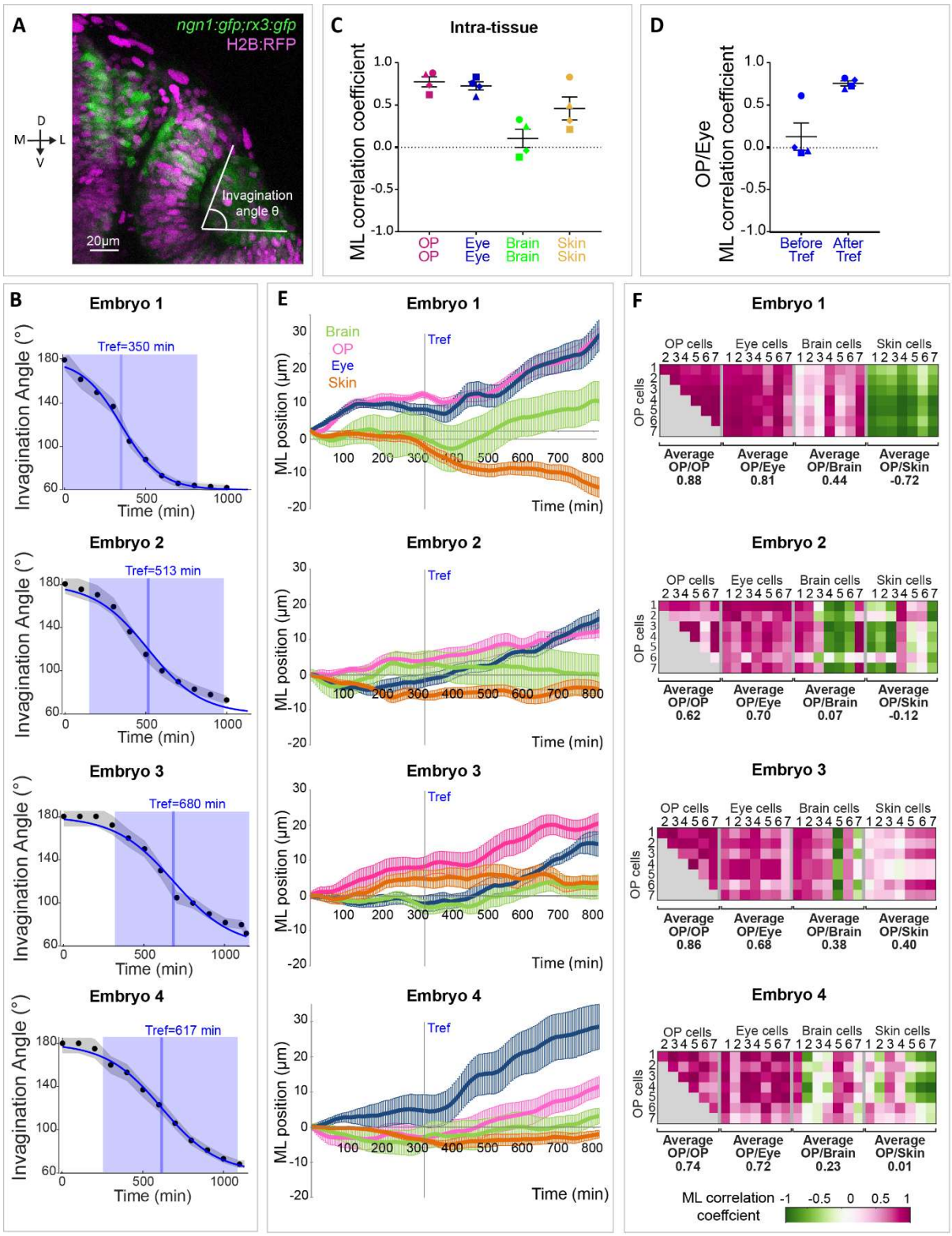

Article supplementary figure 2

Figure S2. Quantitative analysis of cell movements: time-synchronisation of the embryos and additional results for the correlation analysis. A. Confocal section of a *ngn1:gfp*; *rx3:gfp* double transgenic embryo injected with H2B:RFP mRNA, showing how the invagination angle of the optic cup (θ) was measured (shown here for embryo 1 at 24s, frontal view). B. θ decreases over time and systematically passes through an inflection point when θ is approximately equal to 120°. This inflexion point is used as a common time-coordinate (Tref) to time-synchronize the 4 embryos (see methods for more details). We shift the curves of each movie in time so that their reference times Tref overlap at θ=120°. This enables us to crop our movies in time to get a common time-window of 14h (represented in light blue on the graphs) to analyse cell movements for the 4 embryos. C. Intratissue mediolateral (ML) correlation coefficients. Each dot represents the average intratissue correlation, calculated from the tracking data of 5 to 7 cells per tissue (N = 4 embryos from 2 independent experiments). D. OP/eye mediolateral (ML) correlation coefficients for pairs of cells belonging to the placode and to the eye before and after Tref. E. Graphs showing the mediolateral (ML) displacement of OP, eye, brain and skin cells as a function of time (mean +/- sem from 5 to 7 cells per tissue). F. Correlation matrices presenting the mediolateral (ML) correlation coefficients between pairs of cell tracks. Each matrix represents the correlation coefficients for all pairs of cell tracks for a given pair of tissues in a given embryo, calculated from the tracking data of 5 to 7 cells per tissue (N = 4 embryos from 2 independent experiments). The average ML correlation coefficients (represented in Figure 2C-E for the embryo 1) for each tissue couple are indicated under the matrices.

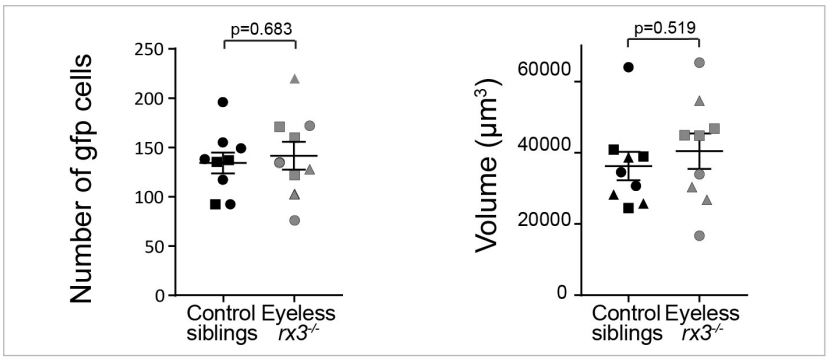

Article supplementary figure 3

Figure S3. OP volume and number of cells are not affected in *rx3*$^{-/-}$ eyeless embryos. Graphs showing the number of *ngn1:gfp*$^{+}$ placodal cells (left) and the volume of the *ngn1:gfp*$^{+}$ OP cluster (right) in *rx3*$^{-/-}$ eyeless mutant and control embryos at 24s (N = 9 embryos from 3 independent experiments). Unpaired, two-tailed t test. Embryos from the same experiment are represented with similar markers (dots, triangles or squares).

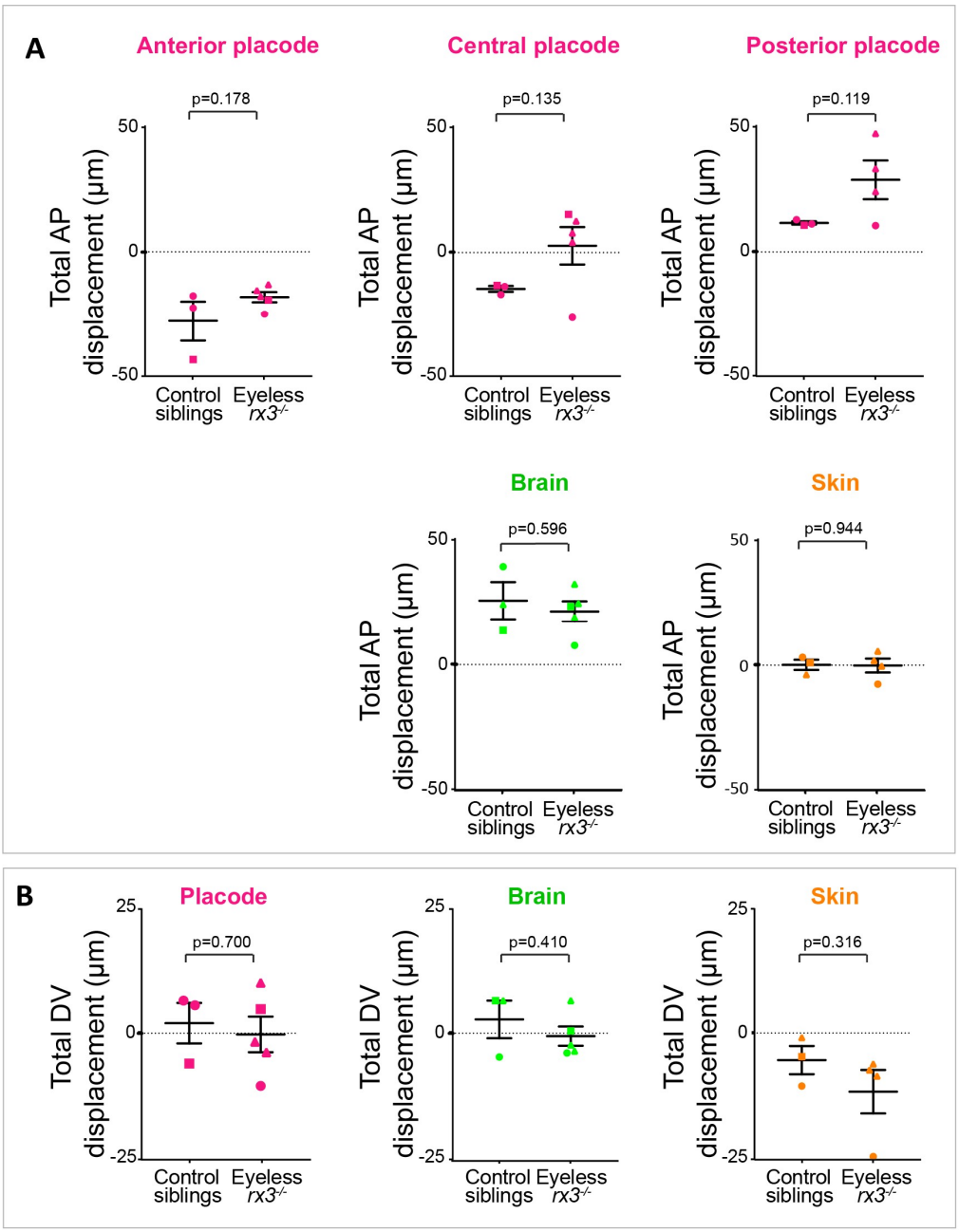

Article supplementary figure 4

Figure S4. Additional results for the analysis of cell movements in *rx3*$^{-/-}$ eyeless embryos. **A.** Graphs showing the total anteroposterior (AP) displacement of anterior, central and posterior OP cells, brain cells and skin cells, starting at 12s and during 700 min of time lapse in *rx3*$^{-/-}$ eyeless mutants and control embryos (N = 3 control placodes and N = 5 mutant placodes from 3 independent experiments, mean calculated from 5 to 7 cells per tissue, unpaired, two-tailed t test). **B.** Graphs showing the total dorsoventral (DV) displacement of OP, brain and skin cells starting at 12s and during 700 min of time lapse in *rx3*$^{-/-}$ eyeless mutants and control embryos (N = 3 control placodes and N = 5 mutant placodes from 3 independent experiments, mean calculated from 5 to 7 cells per tissue, unpaired, two-tailed t test).

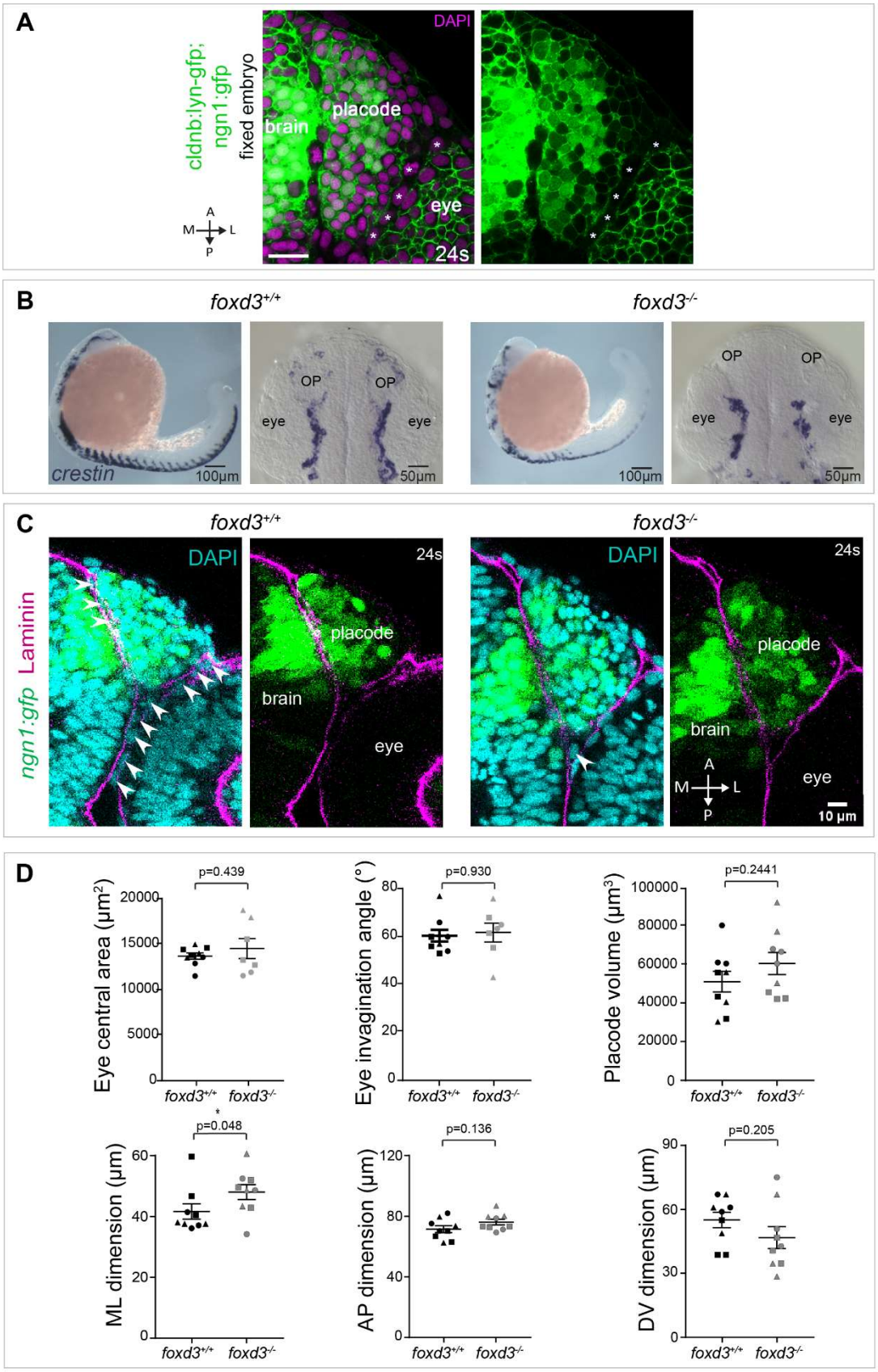

Article supplementary figure 5

Figure S5. NCCs populate the eye/OP interface but are not essential for OP morphogenesis. A. Image (dorsal view, 1 z-section) of a representative *cldnb:lyn-gfp; ngn1:gfp* double transgenic embryo fixed at 24s. The co-staining with DAPI (magenta) is shown on the left to visualise all nuclei. Note the absence of common cell/cell junctions between the eye and the OP. The white asterisks indicate the nuclei of gfp negative interstitial cells present in the gap between the eye and the OP. Scale bar: 20 µm. **B.** *In situ* hybridisation for the NCC marker *crestin*, in representative *foxd3*$^{-/-}$ mutant (right) and *foxd3*$^{+/+}$ control (left) embryos. Whole mount images and high magnifications of dorsal views on the head regions. **C.** Images (dorsal views) of representative placodes from a *ngn1:gfp; foxd3*$^{-/-}$ mutant (right) and a *ngn1:gfp; foxd3*$^{+/+}$ control sibling (left) at the end of OP coalescence (24s). The Laminin immunostaining (magenta) delineates brain, OP and eye tissues. White arrowheads indicate supposed interstitial NCC nuclei (DAPI labelling, cyan) between the basement membranes surrounding the tissues. **D.** Graphs showing, in *foxd3*$^{+/+}$ controls and *foxd3*$^{-/-}$ mutants, the area of the optic cup and its invagination angle calculated on a z-section passing through the centre of the lens (dorsal view), the OP volume, and mediolateral (ML), anteroposterior (AP), and dorsoventral (DV) dimensions of the OP at 24s, calculated as for *rx3*$^{-/-}$ mutants in Figure 2 (N = 9 embryos from 3 independent experiments). Embryos from the same experiment are represented with similar markers (dots, triangles or squares). Unpaired, two-tailed t test except for the lateral dimension (no normal distribution) where a two-tailed Mann-Whitney test was performed.

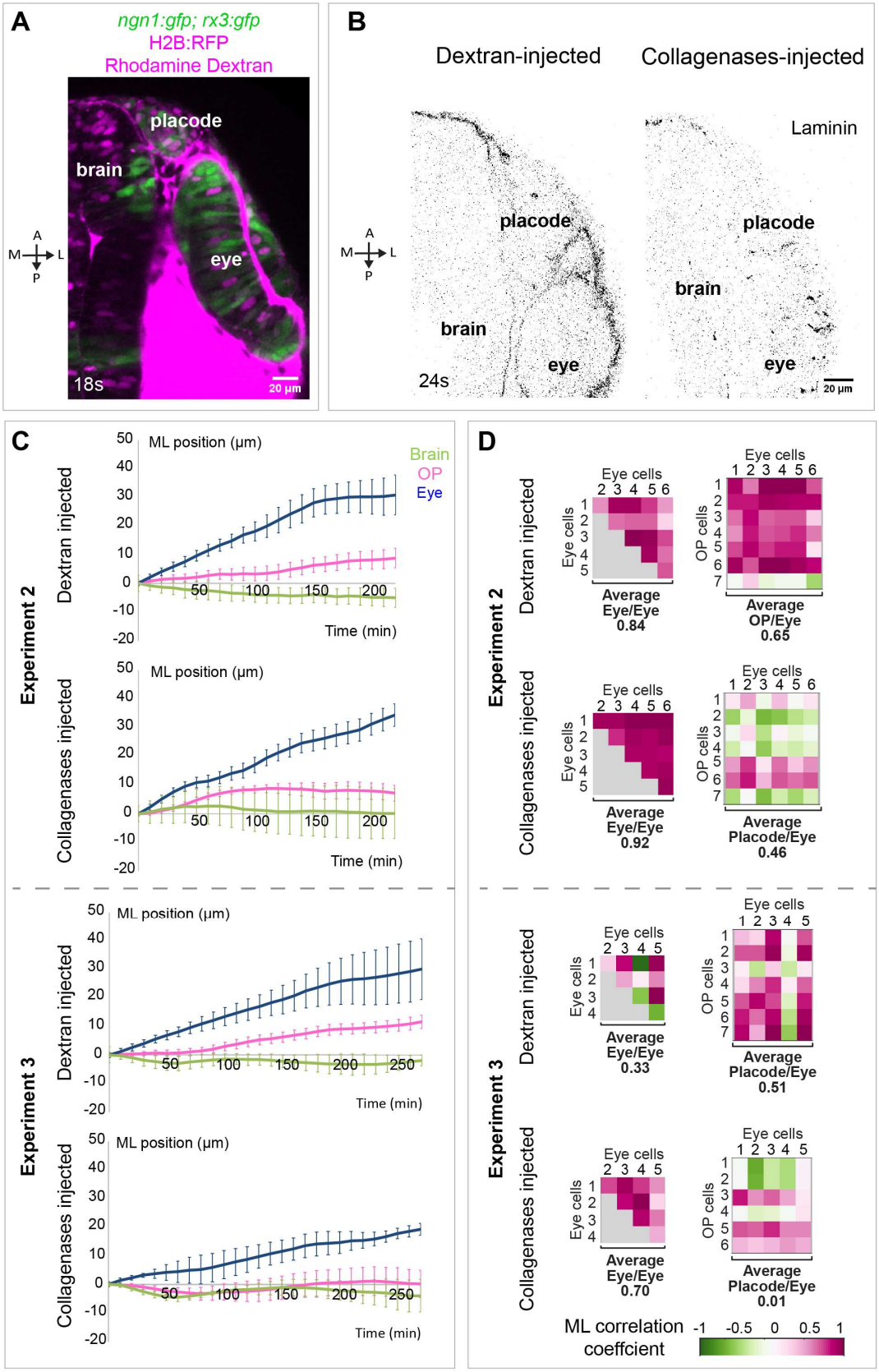

Article supplementary figure 6

Figure S6. Additional results for the collagenases injection experiment. A. Confocal image (dorsal view, 1 z-section) taken 20 min after injection of fluorescently labelled dextran (rhodamine, magenta) close to the eye/OP interface in a *ngn1:gfp; rx3:gfp* (green) embryo. The injected mix diffuses rapidly and fulfills all the space between tissues in the head region. **B.** Confocal images (dorsal views, 1 z-section) of embryos injected at 16s with collagenases and red dextran (right) or with dextran only (left), fixed at 24s and immunostained for Laminin. **C.** Graphs showing the mediolateral (ML) displacement of OP (magenta), eye (blue) and brain (green) cells as a function of time (mean +/- sem from 5 to 7 cells per tissue) for control and collagenases-injected embryos (experiments 2 and 3). To compensate for the drift often observed in injected embryos, the average displacement of skin cells was used for registration and removed from the tracking data. **D.** Correlation matrices displaying the intra-eye and the eye/OP mediolateral correlation coefficients, calculated from the tracking data of 5 to 7 cells per tissue (experiments 2 and 3). The average correlation coefficients for each tissue couple are indicated below the matrices.

- **Video legends**

Video 1. OP morphogenesis upon laser ablation of anterior and posterior OP extremities. Live imaging (dorsal view) of OP morphogenesis on a *ngn1:gfp* embryo in which laser ablation of anterior and posterior OP extremities was performed on the left placode at 16s (embryo 1). The contralateral, right placode is used as a control. In the first image, the ablated and control OPs are surrounded by white lines, and magenta arrowheads show cellular debris where cells were killed, in the anterior and posterior regions of the *ngn1:gfp*$^{+}$ OP cluster. Maximum projection of a 84 µm stack.

Video 2. Concomitant OP and eye morphogenesis. Live imaging (frontal view) of OP morphogenesis from 12s to 24s on a *ngn1:gfp*; *rx3:gfp* double transgenic embryos embryo (embryo 1). The OP is outlined in magenta on the first and the last time points. Maximum projection of a 108 µm stack.

Video 3. OP morphogenesis in *rx3*$^{-/-}$ eyeless and control embryos. Live imaging (dorsal view) of OP morphogenesis from 12s to 24s on an eyeless *rx3*$^{-/-}$ *ngn1:gfp* mutant (right) and a control *ngn1:gfp* embryo (left). The OPs are outlined in magenta on the last time point. Maximum projections of a 94 µm stack (control) and of a 56 µm stack (eyeless *rx3*$^{-/-}$ mutant).

Video 4. Example of a supracellular laser cut. Recording of the tissue response after a line laser cut performed on the lateral border of the *ngn1:gfp*$^{+}$ OP cluster in a control embryo expressing mbCherry to label the membranes (magenta). On the first time point, the region of ablation is shown in yellow (dorsal view, 1 z-section).

Video 5. Confocal z-stacks on a live *cldnb:lyn-gfp* embryo. Confocal z-stacks (dorsal view, z-step of 1 µm) on a live *cldnb:lyn-gfp* embryo at 14s (left) and 20s (right). In this transgenic line, a membrane-targeted version of gfp is expressed in the skin (periderm), the brain, in eye cells (both in the neural retina and the RPE) and in all cells of the OP. At both stages we observe the presence of a gfp negative gap between the eye and the OP (indicated by yellow arrowheads), showing the absence of shared cell/cell junctions between the two tissues.

Video 6. 3D reconstruction on a live *cldnb:lyn-gfp* embryo. 3D reconstruction of the z-stacks shown in Video 5. At both stages, 14s and 20s, we observe the presence of a clear gfp negative gap between the eye and the OP (indicated by yellow arrowheads), demonstrating the absence of shared intercellular junctions between the two tissues. Scale bar: 20 µm.

- **Acknowledgements**

This work was funded by the Agence Nationale pour la Recherche (ANR-17-CE13-0009-01 NEUROMECHANICS), the Centre National pour la Recherche Scientifique (CNRS, including the "Défi mécanobiologie" grant) and Sorbonne Université (including the Emergence 2016 grant, SU-16-R-EMR-11) and received support from the grants ANR-11-LABX-0038, ANR-10-IDEX-0001-02. M. Baraban was supported by a postdoctoral fellowship from the Fondation pour la Recherche Médicale (ARF201809006950). We also thank the imaging platform of the Institut de Biologie Paris-Seine, the Cell and Tissue Imaging core facility (PICT IBiSA), Institut Curie, member of the French National Research Infrastructure France-BioImaging (ANR10-INBS-04), and the IBPS aquatic platform for fish care. We gratefully acknowledge Oxane Divaret for her investment during her two-month internship and Pierre-Luc Bardet, Estelle Hirsinger, Julie Plastino, François Robin and Sylvie Schneider-Maunoury for insightful comments in reviewing the manuscript.

- **Author contributions**

Conceptualization: M.A.B. and I.B., Project administration: M.A.B. and I.B, Funding acquisition: M.A.B. and I.B, Methodology: M.A.B, I.B. and P.M., Software: I.B. and P.M., Investigation: P.M., G.G., M.B., K.P., M.C., Analysis: P.M., I.B, M.A.B., G.G., K.P., Supervision: M.A.B. and I.B, Writing: M.A.B, I.B. and P.M.

- **Competing Financial Interest**

The authors declare no competing financial interests.

- **References**

1. Lowery, L.A., and Van Vactor, D. (2009). The trip of the tip: understanding the growth cone machinery. Nat Rev Mol Cell Biol *10*, 332–43.

2. Kolodkin, A.L., and Tessier-Lavigne, M. (2011). Mechanisms and molecules of neuronal wiring: a primer. Cold Spring Harb Perspect Biol *3*.

3. Suter, T., and Jaworski, A. (2019). Cell migration and axon guidance at the border between central and peripheral nervous system. Science *365*.

4. Gangatharan, G., Schneider-Maunoury, S., and Breau, M.A. (2018). Role of mechanical cues in shaping neuronal morphology and connectivity. Biol Cell *110*, 125–136.

5. Abuwarda, H., and Pathak, M.M. (2020). Mechanobiology of neural development. Curr Opin Cell Biol *66*, 104–111.

6. Bray, D. (1984). Axonal growth in response to experimentally applied mechanical tension. Dev Biol *102*, 379–89.

7. Lamoureux, P., Ruthel, G., Buxbaum, R.E., and Heidemann, S.R. (2002). Mechanical tension can specify axonal fate in hippocampal neurons. J Cell Biol *159*, 499–508.

8. Dennerll, T.J., Lamoureux, P., Buxbaum, R.E., and Heidemann, S.R. (1989). The cytomechanics of axonal elongation and retraction. J Cell Biol *109*, 3073–83.

9. Zheng, J., Lamoureux, P., Santiago, V., Dennerll, T., Buxbaum, R.E., and Heidemann, S.R. (1991). Tensile regulation of axonal elongation and initiation. J Neurosci *11*, 1117–25.

10. Heidemann, S.R., Lamoureux, P., and Buxbaum, R.E. (1995). Cytomechanics of axonal development. Cell Biochem Biophys *27*, 135–55.

11. Chada, S., Lamoureux, P., Buxbaum, R.E., and Heidemann, S.R. (1997). Cytomechanics of neurite outgrowth from chick brain neurons. J Cell Sci *110 (Pt 10)*, 1179–86.

12. Anava, S., Greenbaum, A., Ben Jacob, E., Hanein, Y., and Ayali, A. (2009). The regulative role of neurite mechanical tension in network development. Biophys J *96*, 1661–70.

13. Lamoureux, P., Heidemann, S.R., Martzke, N.R., and Miller, K.E. (2010). Growth and elongation within and along the axon. Dev Neurobiol *70*, 135–49.

14. Balgude, A.P., Yu, X., Szymanski, A., and Bellamkonda, R.V. (2001). Agarose gel stiffness determines rate of DRG neurite extension in 3D cultures. Biomaterials *22*, 1077–84.

15. Flanagan, L.A., Ju, Y.E., Marg, B., Osterfield, M., and Janmey, P.A. (2002). Neurite branching on deformable substrates. Neuroreport *13*, 2411–5.

16. Georges, P.C., Miller, W.J., Meaney, D.F., Sawyer, E.S., and Janmey, P.A. (2006). Matrices with compliance comparable to that of brain tissue select neuronal over glial growth in mixed cortical cultures. Biophys J *90*, 3012–8.

17. Jiang, F.X., Yurke, B., Schloss, R.S., Firestein, B.L., and Langrana, N.A. (2010). Effect of dynamic stiffness of the substrates on neurite outgrowth by using a DNA-crosslinked hydrogel. Tissue Eng Part A *16*, 1873–89.

18. Koser, D.E., Thompson, A.J., Foster, S.K., Dwivedy, A., Pillai, E.K., Sheridan, G.K., Svoboda, H., Viana, M., Costa, L.D., Guck, J., et al. (2016). Mechanosensing is critical for axon growth in the developing brain. Nat Neurosci *19*, 1592–1598.

19. Thompson, A.J., Pillai, E.K., Dimov, I.B., Foster, S.K., Holt, C.E., and Franze, K. (2019). Rapid changes in tissue mechanics regulate cell behaviour in the developing embryonic brain. Elife *8*.

20. Siechen, S., Yang, S., Chiba, A., and Saif, T. (2009). Mechanical tension contributes to clustering of neurotransmitter vesicles at presynaptic terminals. Proc Natl Acad Sci U S A *106*, 12611–6.

21. Ahmed, W.W., Li, T.C., Rubakhin, S.S., Chiba, A., Sweedler, J.V., and Saif, T.A. (2012). Mechanical tension modulates local and global vesicle dynamics in neurons. Cell Mol Bioeng *5*, 155–164.

22. Schlosser, G. (2010). Making senses development of vertebrate cranial placodes. Int Rev Cell Mol Biol *283*, 129–234.

23. Aguillon, R., Blader, P., and Batut, J. (2016). Patterning, morphogenesis, and neurogenesis of zebrafish cranial sensory placodes. Methods Cell Biol *134*, 33–67.

24. Breau, M.A., and Schneider-Maunoury, S. (2014). Mechanisms of cranial placode assembly. Int J Dev Biol *58*, 9–19.

25. Breau, M.A., and Schneider-Maunoury, S. (2015). Cranial placodes: models for exploring the multi-facets of cell adhesion in epithelial rearrangement, collective migration and neuronal movements. Dev Biol *401*, 25–36.

26. Zecca, A., Dyballa, S., Voltes, A., Bradley, R., and Pujades, C. (2015). The Order and Place of Neuronal Differentiation Establish the Topography of Sensory Projections and the Entry Points within the Hindbrain. J Neurosci *35*, 7475–86.

27. Breau, M.A., Bonnet, I., Stoufflet, J., Xie, J., De Castro, S., and Schneider-Maunoury, S. (2017). Extrinsic mechanical forces mediate retrograde axon extension in a developing neuronal circuit. Nat Commun *8*, 282.

28. Torres-Paz, J., and Whitlock, K.E. (2014). Olfactory sensory system develops from coordinated movements within the neural plate. Dev Dyn *243*, 1619–31.

29. Aguillon, R., Madelaine, R., Aguirrebengoa, M., Guturu, H., Link, S., Dufourcq, P., Lecaudey, V., Bejerano, G., Blader, P., and Batut, J. (2020). Morphogenesis is transcriptionally coupled to neurogenesis during peripheral olfactory organ development. Development *147*.

30. Kwan, K.M., Otsuna, H., Kidokoro, H., Carney, K.R., Saijoh, Y., and Chien, C.B. (2012). A complex choreography of cell movements shapes the vertebrate eye. Development *139*, 359–72.

31. Harden, M.V., Pereiro, L., Ramialison, M., Wittbrodt, J., Prasad, M.K., McCallion, A.S., and Whitlock, K.E. (2012). Close association of olfactory placode precursors and cranial neural crest cells does not predestine cell mixing. Dev Dyn *241*, 1143–54.

32. Villedieu, A., Bosveld, F., and Bellaiche, Y. (2020). Mechanical induction and competence in epithelial morphogenesis. Curr Opin Genet Dev *63*, 36–44.

33. Goodwin, K., and Nelson, C.M. (2021). Mechanics of Development. Dev Cell *56*, 240–250.

34. Whitlock, K.E., and Westerfield, M. (2000). The olfactory placodes of the zebrafish form by convergence of cellular

fields at the edge of the neural plate. Development *127*, 3645–53.

35. Miyasaka, N., Knaut, H., and Yoshihara, Y. (2007). Cxcl12/Cxcr4 chemokine signaling is required for placode assembly and sensory axon pathfinding in the zebrafish olfactory system. Development *134*, 2459–68.

36. Blader, P., Plessy, C., and Strahle, U. (2003). Multiple regulatory elements with spatially and temporally distinct activities control neurogenin1 expression in primary neurons of the zebrafish embryo. Mech Dev *120*, 211–8.

37. Madelaine, R., Garric, L., and Blader, P. (2011). Partially redundant proneural function reveals the importance of timing during zebrafish olfactory neurogenesis. Development *138*, 4753–62.

38. Rembold, M., Loosli, F., Adams, R.J., and Wittbrodt, J. (2006). Individual cell migration serves as the driving force for optic vesicle evagination. Science *313*, 1130–4.

39. Ivanovitch, K., Cavodeassi, F., and Wilson, S.W. (2013). Precocious acquisition of neuroepithelial character in the eye field underlies the onset of eye morphogenesis. Dev Cell *27*, 293–305.

40. Heermann, S., Schutz, L., Lemke, S., Krieglstein, K., and Wittbrodt, J. (2015). Eye morphogenesis driven by epithelial flow into the optic cup facilitated by modulation of bone morphogenetic protein. Elife *4*.

41. Nicolas-Perez, M., Kuchling, F., Letelier, J., Polvillo, R., Wittbrodt, J., and Martinez-Morales, J.R. (2016). Analysis of cellular behavior and cytoskeletal dynamics reveal a constriction mechanism driving optic cup morphogenesis. Elife *5*.

42. Sidhaye, J., and Norden, C. (2017). Concerted action of neuroepithelial basal shrinkage and active epithelial migration ensures efficient optic cup morphogenesis. Elife *6*.

43. Martinez-Morales, J.R., Cavodeassi, F., and Bovolenta, P. (2017). Coordinated Morphogenetic Mechanisms Shape the Vertebrate Eye. Front Neurosci *11*, 721.

44. Cavodeassi, F. (2018). Dynamic Tissue Rearrangements during Vertebrate Eye Morphogenesis: Insights from Fish Models. J Dev Biol *6*.

45. Brown, K.E., Keller, P.J., Ramialison, M., Rembold, M., Stelzer, E.H., Loosli, F., and Wittbrodt, J. (2010). Nlcam modulates midline convergence during anterior neural plate morphogenesis. Dev Biol *339*, 14–25.

46. Bryan, C.D., Casey, M.A., Pfeiffer, R.L., Jones, B.W., and Kwan, K.M. (2020). Optic cup morphogenesis requires neural crest-mediated basement membrane assembly. Development *147*.

47. Chuang, J.C., Mathers, P.H., and Raymond, P.A. (1999). Expression of three Rx homeobox genes in embryonic and adult zebrafish. Mech Dev *84*, 195–8.

48. Winkler, S., Loosli, F., Henrich, T., Wakamatsu, Y., and Wittbrodt, J. (2000). The conditional medaka mutation eyeless uncouples patterning and morphogenesis of the eye. Development *127*, 1911–9.

49. Loosli, F., Winkler, S., Burgtorf, C., Wurmbach, E., Ansorge, W., Henrich, T., Grabher, C., Arendt, D., Carl, M., Krone, A., et al. (2001). Medaka eyeless is the key factor linking retinal determination and eye growth. Development *128*, 4035–44.

50. Loosli, F., Staub, W., Finger-Baier, K.C., Ober, E.A., Verkade, H., Wittbrodt, J., and Baier, H. (2003). Loss of eyes in zebrafish caused by mutation of chokh/rx3. EMBO Rep *4*, 894–9.

51. Bailey, T.J., El-Hodiri, H., Zhang, L., Shah, R., Mathers, P.H., and Jamrich, M. (2004). Regulation of vertebrate eye development by Rx genes. Int J Dev Biol *48*, 761–70.

52. Kennedy, B.N., Stearns, G.W., Smyth, V.A., Ramamurthy, V., van Eeden, F., Ankoudinova, I., Raible, D., Hurley, J.B., and Brockerhoff, S.E. (2004). Zebrafish rx3 and mab21l2 are required during eye morphogenesis. Dev Biol *270*, 336–49.

53. Yin, J., Morrissey, M.E., Shine, L., Kennedy, C., Higgins, D.G., and Kennedy, B.N. (2014). Genes and signaling networks regulated during zebrafish optic vesicle morphogenesis. BMC Genomics *15*, 825.

54. Ma, X., Lynch, H.E., Scully, P.C., and Hutson, M.S. (2009). Probing embryonic tissue mechanics with laser hole drilling. Phys Biol *6*, 036004.

55. Farhadifar, R., Roper, J.C., Aigouy, B., Eaton, S., and Julicher, F. (2007). The influence of cell mechanics, cell-cell interactions, and proliferation on epithelial packing. Curr Biol *17*, 2095–104.

56. Rauzi, M., Verant, P., Lecuit, T., and Lenne, P.F. (2008). Nature and anisotropy of cortical forces orienting Drosophila tissue morphogenesis. Nat Cell Biol *10*, 1401–10.

57. Bonnet, I., Marcq, P., Bosveld, F., Fetler, L., Bellaiche, Y., and Graner, F. (2012). Mechanical state, material properties and continuous description of an epithelial tissue. J R Soc Interface *9*, 2614–23.

58. Campinho, P., Behrndt, M., Ranft, J., Risler, T., Minc, N., and Heisenberg, C.P. (2013). Tension-oriented cell divisions limit anisotropic tissue tension in epithelial spreading during zebrafish epiboly. Nat Cell Biol *15*, 1405–14.

59. Porazinski, S., Wang, H., Asaoka, Y., Behrndt, M., Miyamoto, T., Morita, H., Hata, S., Sasaki, T., Krens, S.F.G., Osada, Y., et al. (2015). YAP is essential for tissue tension to ensure vertebrate 3D body shape. Nature *521*, 217–221.

60. Collinet, C., Rauzi, M., Lenne, P.F., and Lecuit, T. (2015). Local and tissue-scale forces drive oriented junction growth during tissue extension. Nat Cell Biol *17*, 1247–58.

61. Jain, A., Ulman, V., Mukherjee, A., Prakash, M., Cuenca, M.B., Pimpale, L.G., Munster, S., Haase, R., Panfilio, K.A., Jug, F., et al. (2020). Regionalized tissue fluidization is required for epithelial gap closure during insect gastrulation. Nat Commun *11*, 5604.

62. Haas, P., and Gilmour, D. (2006). Chemokine signaling mediates self-organizing tissue migration in the zebrafish lateral line. Dev Cell *10*, 673–80.

63. Picker, A., Cavodeassi, F., Machate, A., Bernauer, S., Hans, S., Abe, G., Kawakami, K., Wilson, S.W., and Brand, M. (2009). Dynamic coupling of pattern formation and morphogenesis in the developing vertebrate retina. PLoS Biol *7*, e1000214.

64. Langenberg, T., Kahana, A., Wszalek, J.A., and Halloran, M.C. (2008). The eye organizes neural crest cell migration. Dev Dyn *237*, 1645–52.

65. Tlili, S., Yin, J., Rupprecht, J.F., Mendieta-Serrano, M.A., Weissbart, G., Verma, N., Teng, X., Toyama, Y., Prost, J., and Saunders, T.E. (2019). Shaping the zebrafish myotome by intertissue friction and active stress. Proc Natl Acad Sci U S A *116*, 25430–25439.

66. Bryan, C.D., Chien, C.B., and Kwan, K.M. (2016). Loss of laminin alpha 1 results in multiple structural defects and divergent effects on adhesion during vertebrate optic cup morphogenesis. Dev Biol *416*, 324–37.

67. Stigloher, C., Ninkovic, J., Laplante, M., Geling, A., Tannhauser, B., Topp, S., Kikuta, H., Becker, T.S., Houart, C., and Bally-Cuif, L. (2006). Segregation of telencephalic and eye-field identities inside the zebrafish forebrain territory is controlled by Rx3. Development *133*, 2925–35.

68. Bielen, H., and Houart, C. (2012). BMP signaling protects telencephalic fate by repressing eye identity and its Cxcr4-dependent morphogenesis. Dev Cell *23*, 812–22.

69. Moreno-Marmol, T., Ledesma-Terron, T., Tabanera, N., Martin-Bermejo, M.J., Cardozo, M.J., Cavodeassi, F., and Bovolenta, P. (2020). Stretching of the retinal pigment epithelium contributes to zebrafish optic cup morphogenesis. BioRXiv.

70. Theveneau, E., Steventon, B., Scarpa, E., Garcia, S., Trepat, X., Streit, A., and Mayor, R. (2013). Chase-and-run between adjacent cell populations promotes directional collective migration. Nat Cell Biol *15*, 763–72.

71. Steventon, B., Mayor, R., and Streit, A. (2014). Neural crest and placode interaction during the development of the cranial sensory system. Dev Biol *389*, 28–38.

72. Xiong, F., Ma, W., Bénazéraf, B., Mahadevan, L., and Pourquié, O. (2020). Mechanical Coupling Coordinates the Co-elongation of Axial and Paraxial Tissues in Avian Embryos. Dev Cell *55*, 354-366.e5.

73. Lye, C.M., Blanchard, G.B., Naylor, H.W., Muresan, L., Huisken, J., Adams, R.J., and Sanson, B. (2015). Mechanical Coupling between Endoderm Invagination and Axis Extension in Drosophila. PLoS Biol *13*, e1002292.

74. Guillon, E., Das, D., Jülich, D., Hassan, A.R., Geller, H., and Holley, S. (2020). Fibronectin is a smart adhesive that both influences and responds to the mechanics of early spinal column development. eLife *9*.

75. Smutny, M., Akos, Z., Grigolon, S., Shamipour, S., Ruprecht, V., Capek, D., Behrndt, M., Papusheva, E., Tada, M., Hof, B., et al. (2017). Friction forces position the neural anlage. Nat Cell Biol *19*, 306–317.

76. Reig, G., Cerda, M., Sepulveda, N., Flores, D., Castaneda, V., Tada, M., Hartel, S., and Concha, M.L. (2017). Extra-embryonic tissue spreading directs early embryo morphogenesis in killifish. Nat Commun *8*, 15431.

77. Gillard, G., Nicolle, O., Brugiere, T., Prigent, S., Pinot, M., and Michaux, G. (2019). Force Transmission between Three Tissues Controls Bipolar Planar Polarity Establishment and Morphogenesis. Curr Biol *29*, 1360-1368 e4.

78. Weiss, P. (1941). Nerve patterns: the mechanics of nerve growth. Third Growth Symposium, 163–203.

79. Breau, M.A., and Schneider-Maunoury, S. (2017). [Stretch-induced axon growth: a universal, yet poorly explored process]. Biol Aujourdhui *211*, 215–222.

80. De Vincentiis, S., Falconieri, A., Mainardi, M., Cappello, V., Scribano, V., Bizzarri, R., Storti, B., Dente, L., Costa, M., and Raffa, V. (2020). Extremely Low Forces Induce Extreme Axon Growth. J Neurosci *40*, 4997–5007.

81. Maurer, M., and Lammerding, J. (2019). The Driving Force: Nuclear Mechanotransduction in Cellular Function, Fate, and Disease. Annu Rev Biomed Eng *21*, 443–468.

82. Agarwal, P., and Zaidel-Bar, R. (2021). Mechanosensing in embryogenesis. Curr Opin Cell Biol *68*, 1–9.

83. Javier-Torrent, M., Zimmer-Bensch, G., and Nguyen, L. (2021). Mechanical Forces Orchestrate Brain Development. Trends Neurosci *44*, 110–121.

84. Torres-Paz, J., Tine, E.M., and Whitlock, K.E. (2020). Dissecting the neural divide: A continuous neurectoderm gives rise to both the olfactory placode and olfactory bulb. Int J Dev Biol.

85. Stewart, R.A., Arduini, B.L., Berghmans, S., George, R.E., Kanki, J.P., Henion, P.D., and Look, A.T. (2006). Zebrafish foxd3 is selectively required for neural crest specification, migration and survival. Dev Biol *292*, 174–88.

86. Neff, M.M., Turk, E., and Kalishman, M. (2002). Web-based primer design for single nucleotide polymorphism analysis. Trends Genet *18*, 613–5.

87. Megason, S.G. (2009). In toto imaging of embryogenesis with confocal time-lapse microscopy. Methods Mol Biol *546*, 317–32.

88. Ollion, J., Cochennec, J., Loll, F., Escudé, C., and Boudier, T. (2013). TANGO: a generic tool for high-throughput 3D image analysis for studying nuclear organization. Bioinformatics *29*, 1840–1841.

89. Bolte, S., and Cordelières, F.P. (2006). A guided tour into subcellular colocalization analysis in light microscopy. J Microsc *224*, 213–232.

B. Additional results

Note to the reader: the results presented in the following section are trials of new approaches that turned out to be unadapted to our study, and preliminary results requiring more precise investigations that I did not have time to perform.

1. Additional results on the *rx3*$^{-/-}$ genetic condition

As we have seen in other studies of intertissue mechanical interactions (I.C.3), observation of the morphogenesis of a given tissue in genetic conditions where the movements of a surrounding tissue are decreased or lost helps assessing the coupling between the two tissues. In Monnot *et al.*, we used the *rx3*$^{-/-}$ mutant as a condition for the total loss of eyes and we found that in this condition, OP neuron lateral movements are actually affected and axons are also shorter. We wanted to further investigate if perturbing Rx3 function and blocking eye evagination also affects brain patterning and/or signalling pathways involved in OP morphogenesis, thus leading to the OP phenotype observed in *rx3*$^{-/-}$ mutants.

- **Expression of *cxcr4b* and *cxcl12a* in *rx3*$^{-/-}$ mutants**

A well-known pathway involved in OP morphogenesis is the Cxcr4b/Cxcl12a chemotactic signalling pathway (as described in I.B.3). The receptor Cxcr4b is expressed specifically in the OP while its ligand Cxcl12a is expressed in the telencephalon throughout OP morphogenesis. Both ligand and receptor are required for proper OP morphogenetic movements (Aguillon et al., 2020; Miyasaka et al., 2007). It was recently hypothesised that a Cxcl12a domain in the centre of the brain may act as a chemo-attractant local source that attracts OP cells towards the centre of the brain. However, because of the borders between brain and OP that act as physical borders, this attraction would result in an anteroposterior convergence movements (Figure 51) (Aguillon et al., 2020).

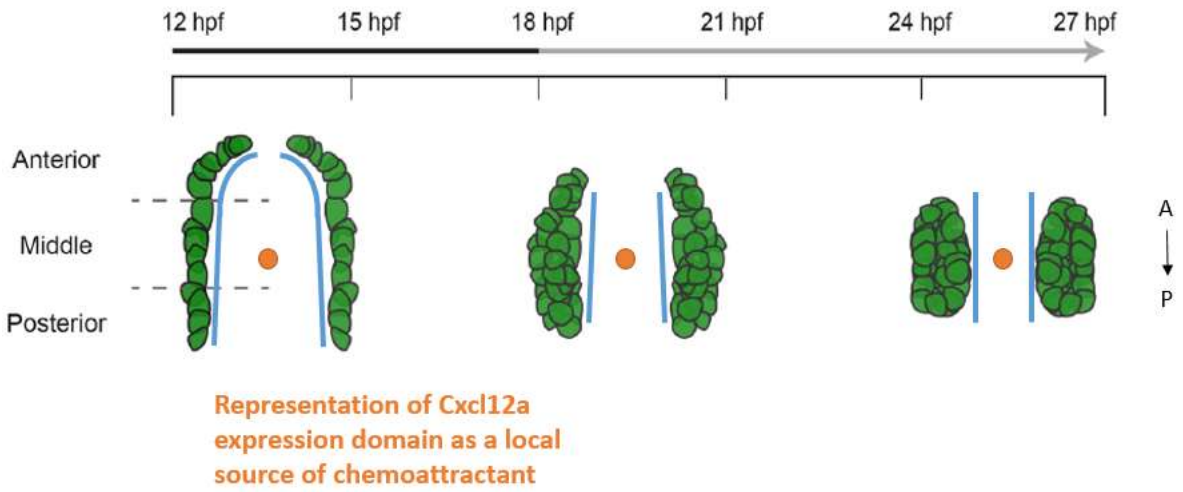

Figure 51: **Graphic representation of OP morphogenesis from 12 hpf to 27 hpf with the local source of chemo-attractant (orange) and the border with the brain (blue).** Dorsal view of the OP as visualised with the *ngn1:gfp* transgene. The early (12-18 hpf; black) and late (18-27 hpf; grey) phases of morphogenesis are noted in the time line. Adapted from (Aguillon et al., 2020).

In order to assess whether the rx3 mutation affects this signalling pathway, we looked at the expression of the receptor *cxcr4b* and its ligand *cxcl12a* in *rx3*$^{-/-}$ embryos and control siblings during OP morphogenesis (18-20 s) (Figure 52).

Figure 52: *In situ* hybridization for the ligand cxcl12a and the receptor cxcr4b in *rx3-/-* embryos and control siblings at 18-20 s (18-19 hpf). Dorsal views.

In both *rx3*$^{-/-}$ embryos and control siblings, the expression of *cxcr4b* at 18-20 s is restricted to the OP, in accordance with previous studies (Figure 21, (Miyasaka et al., 2007)). Moreover, the levels of expression of the receptor appear to be similar in both conditions. These observations show that the loss of function of Rx3 does not affect the expression of the receptor in the placode

during morphogenesis. However, the expression domain of *cxcl12a* in the forebrain appears larger along the mediolateral and anteroposterior directions in *rx3*$^{-/-}$ embryos compared to control siblings. This observation can be explained by the previous finding that cells of the presumptive eye field acquire a telencephalic fate in the absence of a functional Rx3 transcription factor (I.D.2 (Stigloher et al., 2006)). Since Cxcl12a ligand acts as a chemical guidance cue driving OP cell convergence movement (Aguillon et al., 2020), the enlargement of *cxcl12a* domain of expression in *rx3*$^{-/-}$ mutants could result in a larger attracting area, altering OP cell migration. We thus wanted to complement our results with additional conditions of perturbed eye morphogenesis (see III.B.2).

- **Transplantation of *wt* cells in *rx3*$^{-/-}$ mutants**

In order to assess the contribution of potential brain mispatterning *versus* of loss of eye morphogenetic movements in the OP defects, we tried to rescue the *rx3*$^{-/-}$ phenotype by transplanting *wt* cells specifically in the presumptive eye domain of *rx3*$^{-/-}$ mutants (Figure 53A). If rescuing the eye also rescues the OP phenotype, it means that the defects observed on the OP in *rx3*$^{-/-}$ mutants are caused by the loss of eye morphogenetic movements, and not by the defect in brain patterning. We expected to obtain a condition where there is still an expanded telencephalon domain in the brain as in *rx3*$^{-/-}$ mutants but where two optic cups form properly (from the *wt* transplanted cells) and thus could exert mechanical forces on the OP (Figure 53B).

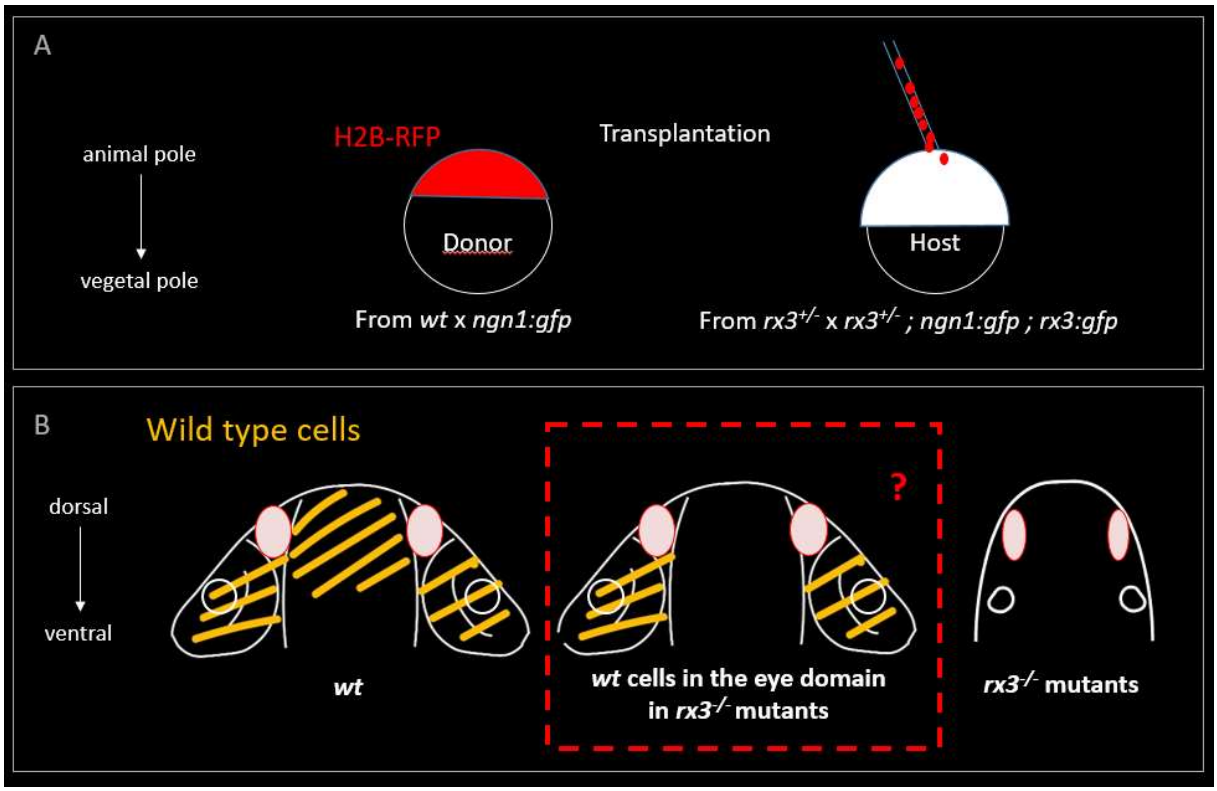

Figure 53: **Transplantation of *wt* cells in *rx3*$^{-/-}$ mutants.** (A) Schematic view of the transplantation experiments. The donor is at high stage (3.3 hpf) while the host is at shield stage (6 hpf). (B) Schematic frontal view of the expected situation obtained by transplantation of *wt* cells in *rx3*$^{-/-}$ mutant hosts. The red ovals symbolize the OPs that are thicker along the mediolateral axis in *wt* situation compared to *rx3*$^{-/-}$ mutant.

These transplantation experiments were quite fastidious and it was hard to obtain a reproducible fate of transplanted cells. Nevertheless, in a few *rx3*$^{-/-}$ embryos transplanted with *wt* cells, we could observe the formation of small retina only composed of *wt* cells (Figure 54). Interestingly, these retinas acquired a cup shape and bend around the lens, suggesting an interaction between the retina and the lens during their morphogenesis (Kruse-Bend et al., 2012; Kwan et al., 2012). However, the surface of these optic cups measured in the centre of the lens was around 3 to 4 times smaller than in the *wt*. The number of cells composing these small optic cup has not been quantified but we could observe a drastic reduction compared to *wt* embryos. The OP of transplanted embryos with small retina exhibited the same shape than the ones of *rx3*$^{-/-}$ mutants. This indicates that the formation of small optic cups is not sufficient to rescue the reduction of OP lateral movement observed in *rx3*$^{-/-}$ mutants.

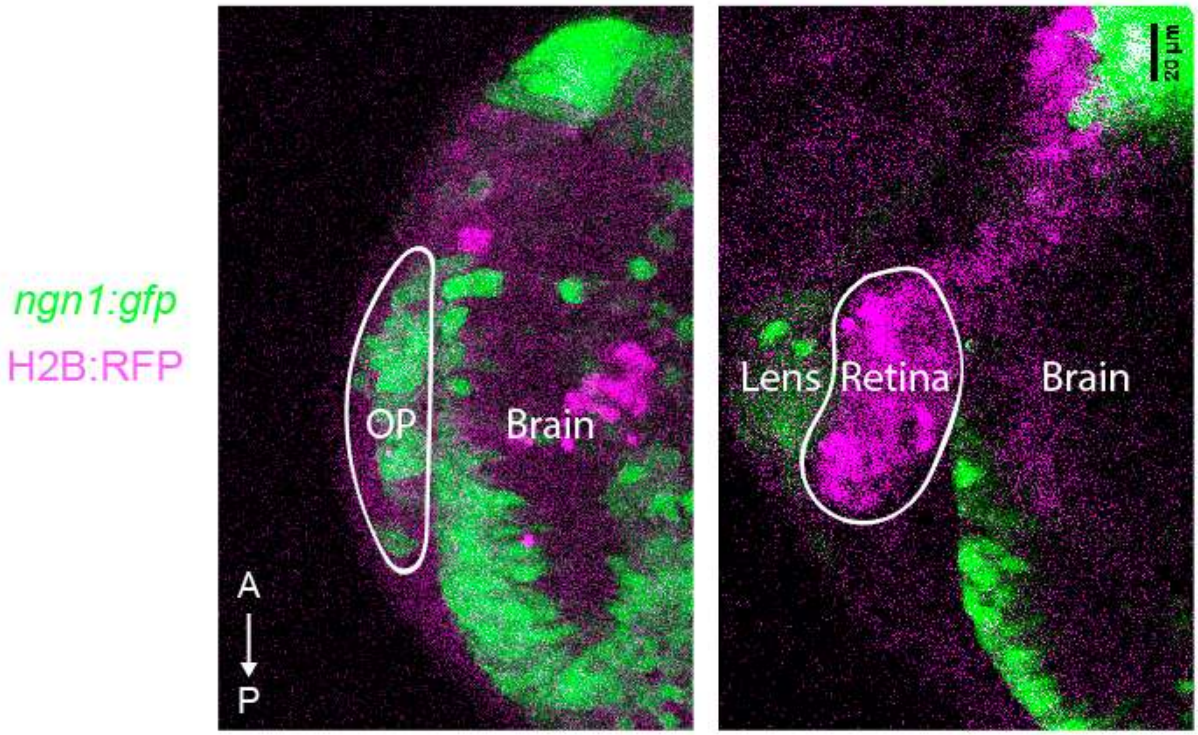

Figure 54: **Confocal images of the placode (left) and a small optic cup (right) obtained by transplantation of *wt* H2B:RFP cells in *rx3*$^{-/-}$ *ngn1:gfp* mutant.** Dorsal view, maximum projection of a 40 µm stack. The two images are taken from the same embryo at 24 s (21 hpf) at different depth within the tissues. The OP and the bended optic cup are surrounded by a white line.

In conclusion, these transplantation experiments of *wt* cells did not give rise to fully rescued eyes and even less to rescued OPs in *rx3*$^{-/-}$ mutants, probably due to the limited number of transplanted cells as we will discuss later in IV.A.

2. Perturbation of eye mechanical forces with additional conditions

Perturbing eye morphogenesis with a second condition that is independent from Rx3 would help to determine whether the OP defects observed in *rx3*$^{-/-}$ mutants are a direct consequence of the loss of eye movements. We tried to obtain conditions where the eye movements are specifically perturbed with two main methods.

- **Specific perturbation of eye movements by affecting RhoGTPases**

One way to affect eye morphogenetic movements is to perturb actomyosin dynamics specifically in eye cells, since actomyosin has been shown to be involved in eye evagination (Cavodeassi et al., 2013) and invagination (Nicolas-Perez et al., 2016; Sidhaye and Norden, 2017) in zebrafish. In order to modulate actomyosin dynamics, Hanovice *et al.* generated zebrafish transgenic lines expressing dominant negative (DN) or constitutively active (CA) forms of upstream activators of actomyosin, RhoGTPases (Hanovice et al., 2016). The CA or DN forms are placed in fusion with the self-cleaving viral peptide F2A and a fluorescent reporter, enabling the bicistronic expression of CA/DN forms of RhoGTPases and of the fluorescent reporter. This expression is under the control of an Upstream Activation Sequence (UAS), an enhancer that specifically activates gene transcription when bound by the transcription activator protein Gal4. Taking advantage of the *Tg(rx2:Gal4;myl7:GFP)* line (Di Donato et al., 2016), our strategy was to express specifically in the eye progenitors either DN forms of RhoGTPases in order to decrease cell activity or CA forms of RhoGTPases in order to increase cell activity. We thus expect to respectively impair eye morphogenetic movements or to speed up eye morphogenetic movements.

We tried this approach with *Tg(uas:EGFP-F2A-Rac1^{DN})* expecting that the expression of DN forms of the upstream activator of actin polymerization Rac1 within the eye field would lead to an impairment of eye cell movements and thus a defect in eye shape at 24 s. The level of green florescence was used as a readout of Rac1^{DN} expression levels within the different embryos of a clutch. We found a large variability in the expression levels from no fluorescence (which was expected in around 75% of the clutch) to a really mosaic expression of the GFP reporter in the majority of the other embryos and finally, a strong expression in nearly all eye cells in a very few embryos (Figure 55). At 24 s, the green fluorescence (when present) was found in the two optic cups but also in the ventral and anterior part of the telencephalon (Figure 55, right panel). We initially thought that this fluorescence was indicating RacDN cells that failed to evaginate but we found the same fluorescence pattern in *Tg(rx2:Gal4;myl7:GFP; uas:GFP)* embryos, indicating that the expression of Rac^{DN} in the brain is due to the expression pattern of the Gal4 line.

In accordance with previous studies (Sidhaye and Norden, 2017), the invagination angle at 24 s in *wt* embryos is around 60° with a variability between the two placodes of the same embryo and between embryos. This variability in invagination angle was also found in embryos

expressing DN Rac1 and even in the rare embryos with expression of GFP in almost all eye cells, we could only observe a mild eye phenotype with an invagination angle around 80°. This mild eye phenotype was associated with normal OP dimensions and thus we did not quantify further the OP phenotype in this condition.

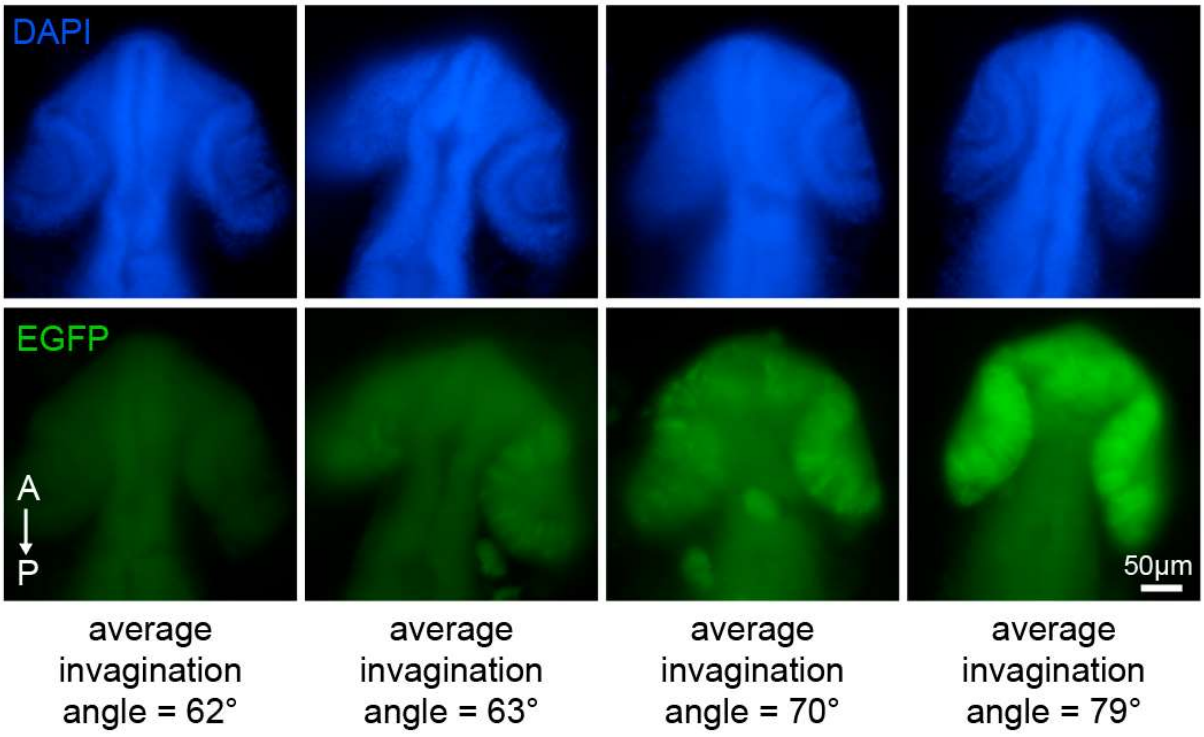

Figure 55: **Images of four embryos at 24 s (22 hpf) illustrating the variability of EGFP-F2A-Rac1^{DN} expression and the associated eye phenotype** (45 embryos analysed including 19 with GFP fluorescence).

The expression level of the DN forms of a protein has to be strong in order to interfere with the function of the endogenous product and to have a dominant negative effect. The *Tg(rx2:Gal4;myl7:GFP)* line might not induce sufficient expression of DN RhoGTPases from 12 s onwards to result in a dominant negative effect. To conclude, the issue of this approach resides in the high mosaicism and the weak expression of DN forms of RhoGTPases, which prevents to obtain a strong and reproducible effect on eye morphogenesis. The results using CA forms will be briefly mentioned in the discussion chapter.

- **Aspiration of eye progenitors with a micropipette**

The situations with transplanted *wt* cells forming a smaller but invaginated eye in *rx3*$^{-/-}$ host embryos led us to hypothesise that the size of the eye might be a critical parameter to exert enough forces on the OP and to induce OP lateral movement. We thus attempted to get experimental conditions with a variety of eye sizes in order to test if these defects scale with defects in the OP lateral movement (Figure 56B). The smaller the eye would be, the more defects we would observe on OP cells and *vice versa*. To do so, we aspirated cells in the presumptive eye domain at shield stage (6 hpf - at this stage, the eye domain has only limited overlap with progenitor domains of other tissues (Woo and Fraser, 1995)), and look at the effects at 24 s (22 hpf) (Figure 56A). In order to get a control and an "aspirated" placode within the same embryo, we tried to aspirate cells only on one side of the presumptive eye domain.

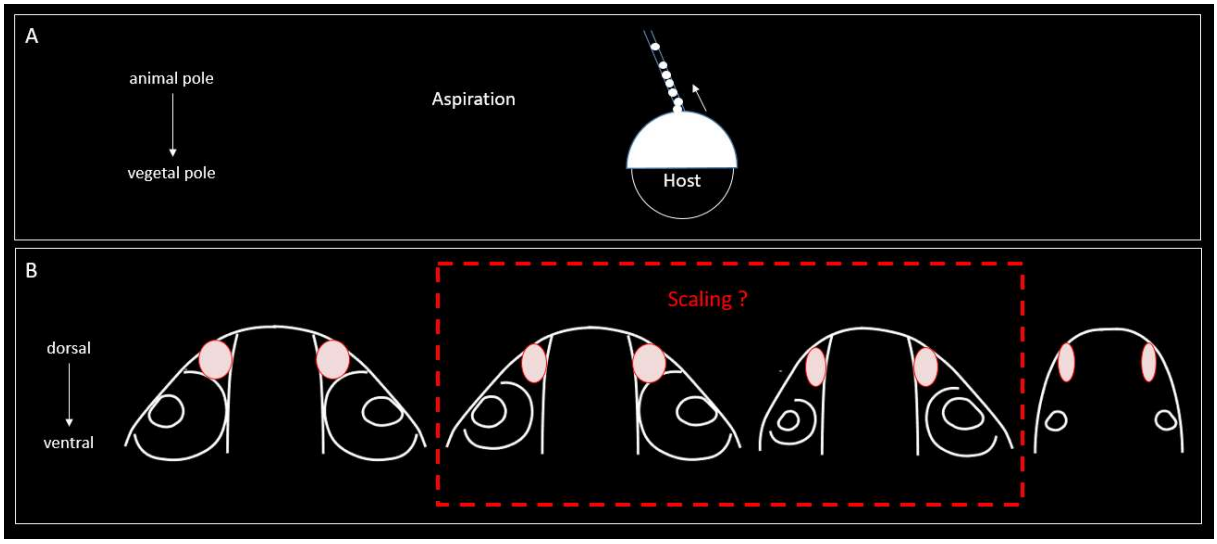

Figure 56: **Aspiration of cells in the presumptive eye domain in *wt* embryos.** (A) Schematic view of the aspiration experiments carried out at shield stage (6 hpf). (B) Schematic frontal view of the expected situations obtained by asymmetric aspiration of presumptive eye cells in *ngn1:gfp* embryos at 24 s (21 hpf). The red ovals symbolize the OPs that are thicker along the mediolateral axis in the presence of eyes than in the absence of eyes.

First of all, this technique turned out to be very challenging. The number of aspirated cells was manually controlled and was not highly reproducible from one embryo to another. Aspirating too few cells resulted in no visible eye defect, probably due to some compensation mechanisms occurring between 6 and 22 hpf, while aspirating too many cells led to embryonic death or to global embryo defects. We were however able to obtain a few situations where we could see

and measure a smaller optic cup on one side of the embryo as compared with the other side. Interestingly, in these situations, the smaller optic cup was often associated with a smaller mediolateral dimension of the placode (Figure 57). However, due to the scarcity of such situation, obtaining a good number of embryos with an asymmetry of eye size would require many experiments. We decided not to continue and not to proceed to the quantification of eye and OP defects in these situations for the time being.

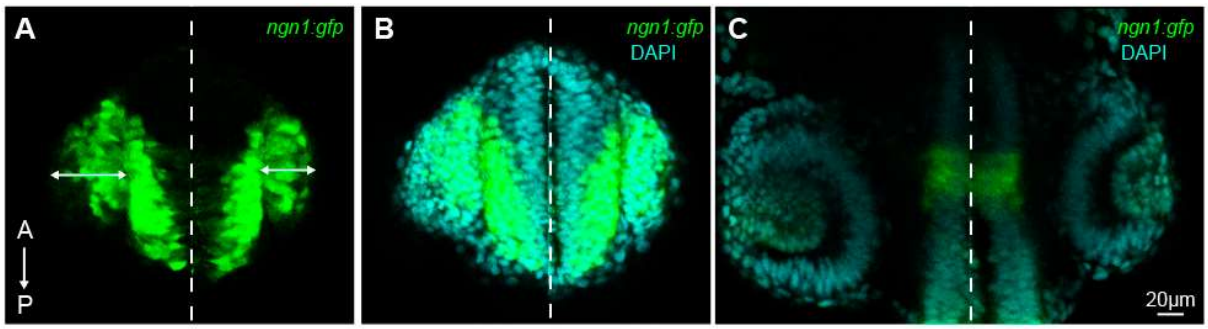

Figure 57: **Confocal images of an embryo where presumptive eye cells have been aspirated on one side, resulting in a smaller left eye.** (A, B) Z-sections in the placodes. White double arrows show the mediolateral dimension of the left and the right placodes (respectively around 52 µm and 40 µm). (C) Z-sections in the eyes (90 µm more ventral). Dorsal views. The two sides of the embryo have been imaged separately and the dashed line indicate where the two images have been combined.

The OP and telencephalic presumptive domains at shield stage (6 hpf) are in close proximity with the eye presumptive domain (Kozlowski et al., 1997). Since we do not have a highly precise control of the localization of our pipette aspiration, we cannot exclude that in some cases, we do aspirate as well some telencephalic or OP cells. In order to confirm that the effect observed on the placode is not due to an aspiration of telencephalic or OP cells, it will be important to measure and compare the volume and the dimensions of the OP, as well as the thickness of the brain, between aspirated embryos and non-aspirated siblings. To conclude, this technique, though time-consuming, remains promising and might be pursued later on to quantify the potential correlation observed so far between eye size and OP mediolateral dimension.

3. Additional Material and Methods

- ***In situ* hybridization for *cxcr4b* and *cxcl12a***

Whole-mount *in situ* hybridisation for cxcl12a and cxcr4b was performed as described in (Xu and Wilkinson, 1998) with digoxigenin-labelled RNA probes.

- **Cell transplantation and aspiration**

Cells were transplanted from sphere stage *ngn1:gfp* donors into *rx3*$^{-/-}$ *rx3:gfp ; ngn1:gfp* host embryos at shield stage, targeting the presumptive retina domain, which is close to the animal pole of the embryo but slightly in the direction of the shield (Woo and Fraser, 1995). Cells were aspirated from the same presumptive eye domain of *ngn1:gfp* embryos at shield stage. Both experiments were performed with a manual microinjector (CellTram Oil, Eppendorf). Embryos were left overnight at 23°C with100U/mL of Penicillin/Streptomycin (Gibco 15140-122) for recovery and were fixed at 24 s.

IV. Discussion and perspectives

In this last chapter (IV), we will discuss the results obtained during my PhD project, as presented in the article and in the additional results section. In the first section (IV.A), we will focus on eye development and try to identify which steps and which molecular events of eye morphogenesis are critical for OP formation. Then, in the second section (IV.B), we will review the elements that indicate the mechanical nature of eye/OP interaction and consider additional experiments that could help us to clarify the mechanisms underlying this interaction. In the third section (IV.C), we will next examine the role of the eye/OP interface and of its components (NCC, ECM) in mediating the interaction between the two tissues. Finally, in the last section (IV.D), we will debate the consequences of the extrinsic traction forces on the construction of the olfactory circuit.

A. Which steps and parameters of eye morphogenesis are critical for OP formation?

As we have seen in I.D, eye morphogenesis is a complex process involving several events. Optic vesicle evagination, optic cup invagination and lens coalescence are all at least partially concomitant with OP morphogenesis and display a mediolateral component in their movements. Hence, they are all candidate for actively generating the mediolateral traction forces exerted on the OP. Is one of these events specifically the driving force of OP morphogenesis? And if yes, which one?

- **A preponderant role for optic cup invagination**

As explained in the article, *rx3*$^{-/-}$ mutants present defects in OP cell movements and in OP axon extension despite the formation of a lens. The size, shape and number of cells of the lens formed in *rx3*$^{-/-}$ mutants should be precisely quantified to assess whether they are similar to the *wt* ones. Lens cell movements should also be characterized on live embryos to ensure that the coalescence still occurs properly in the absence of retina. In any case, our results so far indicate that the lens formation occurring in the absence of eyes is not sufficient to drive OP morphogenesis. Thus, the forces generated by lens cells during lens coalescence do not appear to be the source of the external forces driving OP lateral movement and axon extension.

The study of OP morphogenesis in *cyclops* mutants, presenting a single continuous neural retina, has often been suggested to us in order to see whether the lack of proper evagination affects OP lateral movements (Figure 58). Indeed, the lack of lateral evagination and the mislocation of the eye field occuring in this mutant may cause defects in OP coalescence. However, *cyclops* encodes for the nodal-related factor Ndr2 required for early ventral patterning in the brain (Rebagliati et al., 1998). Loss of function of Ndr2 in *cyclops* mutants also affects the movement of diencephalic precursors anteriorly along the midline, which fail to separate the primordial eye field into left and right eyes, thus giving rise to only one neural retina (Varga et al., 1999). Since the anterior region of the brain has been shown to express the ligand Cxcl12a involved in chemotactic OP coalescence (as discussed later in IV.B.4 (Aguillon et al., 2020; Miyasaka et al., 2007)), the disturbed brain patterning in *cyclops* mutants might affect OP morphogenesis. Thus, if we observe defects in OP morphogenesis in these mutants, we could not attribute them solely to the defective eye evagination.

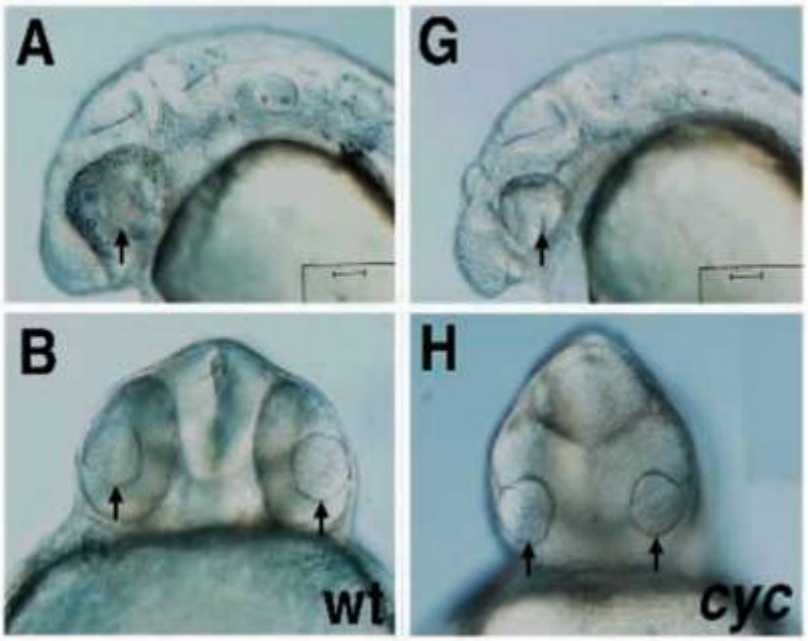

Figure 58: **Phenotypes of wild-type (WT) and *cyclops* (*cyc*^{m122}) embryos at 28 hpf.** (A,G) Lateral views. (B,H) Frontal views. Arrows indicate the position of the lens. (Schier et al., 1996)

Even though the role of evagination *versus* invagination is hard to distinguish as these two processes partially overlap in time (Kwan et al., 2012) and cannot be so strictly separated, our dynamical analysis of OP and eye cell movements brings information on their potential respective contribution. In the four *wt* embryos we studied, the rate of mediolateral displacement for both OP and eye is higher after than before the time of reference T_{ref}, which corresponds to an invagination angle of 120° (Article supplementary figure 2E). This indicates that OP lateral expansion mainly occurs after T_{ref} and from our observations and according to the literature (Kwan et al., 2012), there is no more evagination during this period of time. Moreover, comparing correlation coefficients before and after T_{ref} indicated that OP and eye cells undergo highly correlated lateral movement especially after $T_{ref,}$ (the correlation coefficient was systematically higher after T_{ref} than before T_{ref}, Article supplementary figure 2D). Strikingly, for three embryos out of four, there was almost no correlation between OP and eye cell lateral movements before T_{ref}. In addition, degrading ECM by injecting collagenases from 16-18 s, i.e. from the beginning of the invagination and after evagination, was sufficient to perturb lateral movements in the OP.

Therefore, we propose that eye invagination is the main driver of OP lateral movements and axon extension. In order to further identify which feature of eye invagination actively produces

the traction forces required for olfactory circuit formation, it would be interesting to block cell movements in specific regions of the invaginating eye, such as the centre of the neural retina where basal constriction contributes to optic cup folding (Nicolas-Perez et al., 2016; Sidhaye and Norden, 2017) (Figure 59A), the edge of the optic cup (and in particular the anterior edge, which is the closest to the OP) where the rim movement occurs (Kwan et al., 2012; Sidhaye and Norden, 2017) (Figure 59B) or the outer layer of the optic cup where the RPE spreads (Cechmanek and McFarlane, 2017; Moreno-Marmol et al., 2018) (Figure 59C).

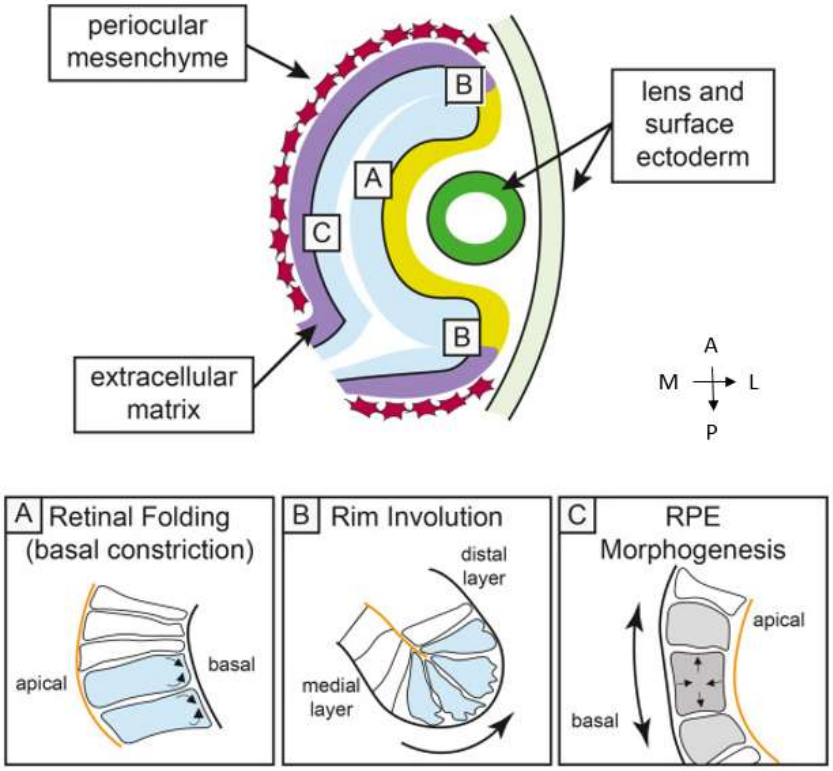

Figure 59: **Localization and description of three main processes driving optic cup invagination.** (Top) Schematic representation of an optic cup and of the localization of the different processes contributing to eye invagination (Dorsal view) (A) Cells in the centre of the distal layer of the optic vesicle undergo basal constriction. (B) Cells at the periphery move around the rim and into the distal layer. This movement is represented here at the posterior edge but also occurs at the anterior edge close to the OP. (C) Cells in the proximal layer flatten and spread to form the RPE. (Casey et al., 2021)

This could be achieved using a photoactivable myosin II inhibitor, an approach that has been employed in the zebrafish lateral line primordium (Kepiro et al., 2015) and in the developing eye (Moreno-Marmol et al., 2020). Blebbistatin is a widely used inhibitor of myosin II

(Rauscher et al., 2018) and azidoblebbistatin is a photoactivable form of blebbistatin which covalently cross-links to myosin II upon UV irradiation. Used at low doses, azidoblebbistatin does not have any effect on the cells in the absence of UV irradiation but inhibits myosin II upon UV irradiation (Kepiro et al., 2012). Using well-defined patterns of UV light, this photo-activable drug would allow us to choose the cells whose movements will be affected (in different regions of the eye). Moreover, using the UV irradiation at different developmental times would help determining which process (or processes) is (are) critical for OP cell body movement and axon elongation.

As described in the section I.D.3, RPE cells flatten and spread during optic cup invagination (Cechmanek and McFarlane, 2017; Kwan et al., 2012), a movement that may exert lateral traction forces on the OP. In order to test specifically the contribution of RPE cells on OP lateral movements, we could disturb these cells by taking advantage of the *Tg(E1-bhlhe40:GFP)* line, where GFP expression first appears in dorso-medial RPE progenitors at around 14 s (16 hpf) which then wrap around the entire retina at prim 5 (24 hpf) (Moreno-Marmol et al., 2020). A first drastic experiment would be to use this transgenic reporter to visualise RPE cells and to kill them by laser ablation at the onset of GFP expression. A second option would consist in replacing GFP by Gal4 to generate a *Tg(E1-bhlhe40:Gal4)* line using the CRISPR/Cas9 technology (Auer et al., 2014). This RPE-specific Gal4 line would be combined with transgenic lines expressing DN forms of RhoGTPases under the control of a UAS promoter (Hanovice et al., 2016). As it has been previously shown that interfering with RPE actomyosin disrupts RPE flattening and stretching around the neural retina (Moreno-Marmol et al., 2020), we expect that a strong expression of DN forms of RhoGTPases in the RPE would decrease RPE spreading movements. However, affecting RPE flattening also induces defects in neural retina invagination (Moreno-Marmol et al., 2020) and thus, it might be challenging to disentangle the different processes happening at the same time in the optic cup.

- **Eye size matters**

Our transplantation experiments of *wt* cells into *rx3*$^{-/-}$ host embryos showed that the formation of optic cups, whose sizes are around 3 to 4 times smaller than the *wt* ones, is not sufficient to rescue the OP phenotype. Note that these small optic cups seem to be properly bended around the lens (precise measurement of invagination angle must be done) (Figure 54). This suggests that the size of the eye is critical to shape the OP. This could be due to a reduced number of cells: if we consider that the traction forces exerted by the eye on the OP result from the forces

produced by each individual eye cell, then reducing the number of cells reduces the global force (schematized in blue on Figure 60). As we will discuss later, there might also be friction forces generated at the interface between the two tissues. In this case, the distance between the two tissues would be critical. Since we found that the small optic cups almost always form around the lens and are not in the close proximity with OP cells, they might be a reduction or even a loss of friction between the eye and the OP (yellow on Figure 60). Although we have not analysed the morphogenetic movements in these small optic cups, it is likely that the reduction of eye size lowers the amplitude of the movements that accompany optic cup invagination. Thus, there might be less forces generated by the movements in the small optic cups formed by transplantation of *wt* cells in *rx3*$^{-/-}$ mutants (magenta on Figure 60). Live imaging and quantitative analysis of transplanted cell movements would help to test this hypothesis.

Given the importance of eye size, a correct evagination is certainly required to ensure that there are enough cells forming the optic cup to exert traction on the OP during optic cup invagination.

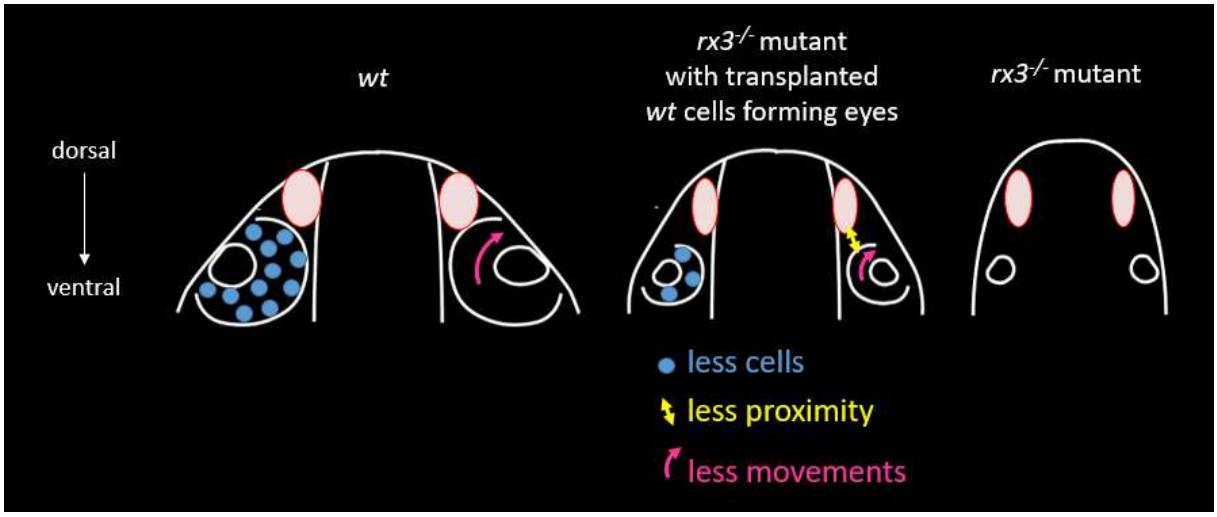

Figure 60: **Schematics of the phenotypes obtained in *wt* embryos (left), *rx3*$^{-/-}$ mutants (right) and in *rx3*$^{-/-}$ host mutants with transplanted *wt* cells forming small optic cups (middle).** The red ovals symbolize the OPs that are thicker along the mediolateral axis in *wt* situation compared to the two other situations. Different mechanisms can be suggested to explain the OP phenotype observed in the transplanted situation: a reduced eye cell number, a farther distance between the eye and the OP and a decrease in the amplitude of morphogenetic movements in the eye.

- **Potential reciprocal interaction between the eye and the OP**

Remarkably, as we saw in I.D.5 (Figure 49), expression of FGF-24 by the OP seems to play a role in nasal-temporal patterning of the optic cup, which is important for further rotation of the eye tissue (Picker et al., 2009). Interestingly, the developing eye and OP could represent a system with reciprocal interactions whereby the eye morphogenetic movements mechanically influence the OP shape and, in turn, the OP secretes a chemical signal essential for proper eye patterning.

B. The mechanical nature of the OP/eye interaction

We have discussed in the previous section the contribution of eye morphogenesis to OP lateral movements and axon extension. There are two recurrent questions which were raised throughout our study: (i) whether the eye/OP interaction is of mechanical or chemical nature and (ii) how mechanical forces exerted by the eye crosstalk with the known chemical signals involved in OP morphogenesis (Aguillon et al., 2020; Miyasaka et al., 2007). In this section, we will first focus on the evidence which are in favour of a mechanical role of eye development. We will then describe a few available techniques for measuring mechanical forces *in vivo* that could be applied to our system to further assess the mechanical interaction between the eye and the OP. Finally, we will present our current point of view about how chemical signals and extrinsic mechanical forces cooperate to orchestrate OP morphogenesis. In this discussion, since the eye generates the mechanical forces, we will refer to it as the inducer tissue while the OP will be called the responder as it deforms and flows in response to these forces (see section I.C and (Villedieu et al., 2020)).

1. Mechanical *vs.* chemical interaction

This part is dedicated to the experimental approaches that help discriminating between the mechanical or chemical nature of an interaction between two tissues. Once we have shown that eye and OP morphogenesis are coupled, how can we demonstrate that this link is mechanical rather than chemical? This question is also relevant to the other studies describing mechanical interactions between tissues (see I.C).

- **Rejecting a chemoattractive role**

A first way to try and show that two tissues interact in a mechanical manner is to demonstrate that the interaction is not mediated by chemical cues.

In case of chemotaxis, we should be able to visualize features of active cell migration in the OP. Indeed, chemotactic response of cells has been widely described as an active process involving the polymerisation of actin and the accompanying formation of protrusions at the leading edge and myosin-II-mediated contraction at the rear of the cell (Roca-Cusachs et al., 2013; Roussos et al., 2011; Shellard and Mayor, 2016). In the case of OP lateral movements, the lab has previously shown the lack of protrusive activity and of polarised actomyosin in the

moving cell bodies. Moreover, inhibition of microtubule polymerisation or cell-autonomous perturbation of actomyosin activity did not affect the OP lateral movements, indicating that these cytoskeleton elements are not required for the lateral movement. These results argue against the hypothesis of autonomous chemotaxis and supports the idea of extrinsic forces moving the responder cells. Of note, such perturbations the of intrinsic cell machinery in the responder tissue have not been used in other studies of intertissue mechanical interaction presented in I.C but it is an element which supports the mechanical role of the interaction.

Carvalho *et al.* suggested an interesting approach to test the chemo-attractive potential of a tissue A *versus* its mechanical influence on tissue B formation (Carvalho et al., 2009). The authors found that mesendodermal movements during zebrafish epiboly drive the dorsal movements of the internal YSL nuclei. They wanted to assess whether YSL nuclei respond to chemo-attractant cues secreted by the mensendoderm. To test this, they transplanted mesendodermal cells in embryos lacking mesendoderm and quantified the distance between each YSL nucleus and its closest transplanted mesendodermal cells. They argued that if the YSL nuclei had the tendency to move toward the few transplanted cells, as a result of a chemotactic signal, then the distance between the two cell types should decrease over time. They found that the distance between the two cell types was constant over time, indicating that the YSL nuclei did not move closer to the transplanted cells (Carvalho et al., 2009). They used this result to rule out the chemoattraction possibility and focus on a mechanical role played by the mesendoderm on YSL movements.

In our study, we also performed transplantation experiments of eye cells in the absence of endogenous eye formation (Figure 54). In the scenario of chemo-attraction role on OP cells by the eye cells, the small retina obtained by transplantation of *wt* cells in *rx3* mutants would act as a smaller source of chemo-attractant, as compared with the widespread source of chemo-attractant that normal eye cells would represent in the *wt* embryos. In case the eye cells would secrete attractive chemical signal (and assuming they all behave the same), we can imagine that the OP would deform in an asymmetric fashion when the retina is small. However, we did not observe specific deformation of the OP towards the small retina, suggesting that there were no directional movements of OP cells towards these transplanted *wt* eye cells. Two possibilities are still compatible with this observation and with a chemoattractive scenario: either the eye cells were too far from the OP in the transplanted embryos, preventing the chemo-attractant to reach OP cells, or the secreted signal was too weak because of the low number of *wt*

transplanted cells. Thus, we cannot firmly conclude from our transplantation experiment that there is no chemoattraction at all from the eye on the OP.

Another interesting approach to assess whether eye cells secrete a chemo-attractant acting on OP cells would be to inhibit the secretory pathway or exocytosis specifically within the eye. The secretory pathway generates, traffics and processes proteins targeted to the extracellular space or the plasma membrane, such as proteins involved in intercellular signalling, chemo-attractants or chemo-repellents or ECM components (Klee, 2008). It comprises the endoplasmic reticulum (ER), where proteins are synthesised, the Golgi complex, where glycosylation occurs, and cargo-bearing vesicles that ferry proteins between compartments of the secretory pathway (Figure 61). The proteins are then secreted by exocytosis, a process during which exocytotic vesicles carry these proteins to the cell membrane where they dock, fuse with the cell membrane and release them into the extracellular environment. Interfering with the secretory pathway or exocytosis may perturb the secretion of proteins in the extra-cellular space such as chemo-attractants. However, such approach has never been used to our knowledge to test the role of chemo-attractants and it will require precise and in-depth investigations.

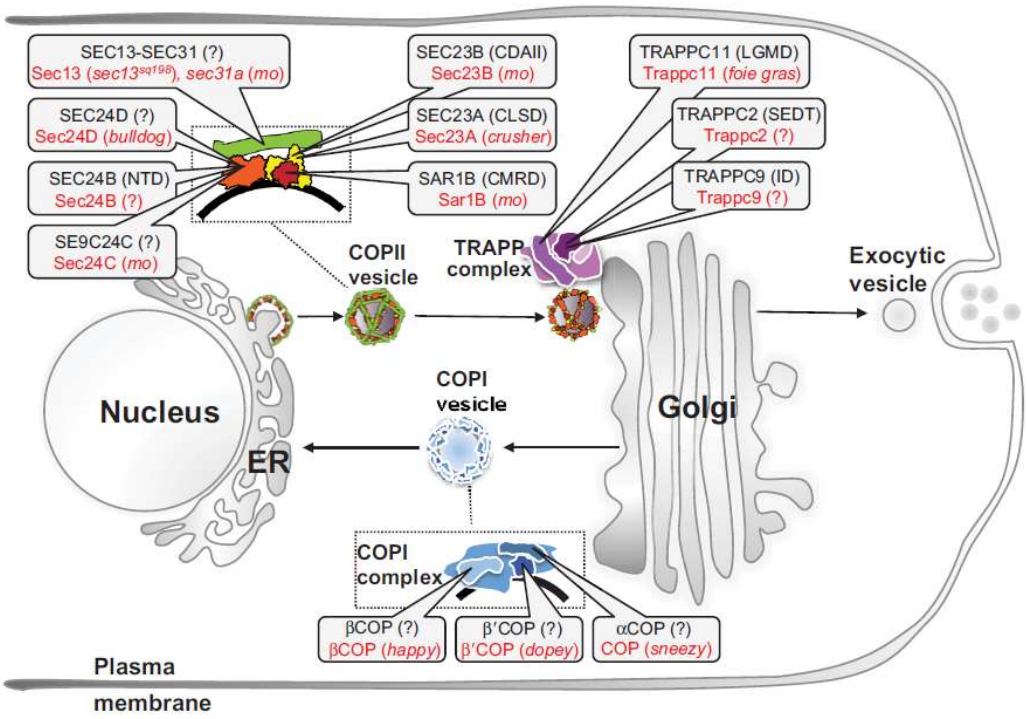

Figure 61: **Secretory pathway components studied in zebrafish.** Secretory pathway proteins implicated in human disease are shown in black with corresponding zebrafish tools to study these in red. Sec13 is a component of the outer shell of the COPII vesicle coat, involved in

vesicle trafficking from the endoplasmic reticulum (ER) to the Golgi. NTD, neural tube defects; CLSD, cranio-lenticular-sutural dysplasia; CDAII: congenital dyserythropoietic anemia II; CMRD, chylomicron retention disease; LGMD, limb girdle muscular dystrophy; SEDL, X-linked spondyloepiphyseal dysplasia tarda; ID, intellectual disability" (Vacaru et al., 2014)

Several mutants for proteins involved in the secretory pathway and especially in the transport from the ER to the Golgi complex have been identified in zebrafish (as reported in Figure 61). Although all cells secrete proteins, most of these mutants show phenotypes that are restricted to only a subset of cells (Vacaru et al., 2014). Interestingly for our study, *sec13*^{sq198} mutants display eye defects, with smaller neural retina than *wt,* disrupted retinal lamination and excessive number of apoptotic cells in the retina, but no overall general defects (Niu et al., 2012; Niu et al., 2014). Sec13 is a protein composing the COPII vesicle, which mediates protein trafficking from the ER to the Golgi apparatus (Figure 61). The eye phenotype observed in *sec13*^{sq198} mutants suggests that secretory pathway is affected specifically in the retina. Another study using morpholinos showed that for example Laminin and Collagen secretion was affected in the eye of *sec13* morphants, reinforcing the idea that Sec13 knock-down affects protein secretion in the eye (Schmidt et al., 2013). Very importantly, eye defects in both morphants and mutants become apparent after 2 dpf (Niu et al., 2014; Schmidt et al., 2013). Since Sec13 is already expressed in the eye field at 16 s (17 hpf) (Thisse et al., 2001), we can suppose that at the stages we are interested in (14-21 hpf), there is no significant defect in eye morphology but a perturbed secretion from eye cells, which would be ideal for our purpose. In order to confirm that the secretion is indeed perturbed in eye cells in these conditions, we could use a probe staining all the membranes and especially the membranes of intracellular vesicles, using for example the fluorophore BODIPY TR methyl ester (Liu et al., 2018). If the trafficking between the ER and the Golgi is perturbed, or if exocytosis is blocked, we expect to see an accumulation of vesicles inside the eye cells. If OP cells still undergo normal lateral movements in such a context, this experiment would argue against a chemo-attractive role of the eye.

Other approaches to demonstrate the mechanical nature of intertissue interactions have been discussed in I.C.3 as presented in Table 1. Below, we will see how these approaches have been or can be applied to our study.

- **Perturbing the coupling between the two tissues**

The first approach presented to assess the mechanical nature of a tissue interaction is to physically uncouple the two tissues (*i.e.* to remove the "glue" that connects the two tissues) without perturbing the inducer movements (Guillon et al., 2020; Tlili et al., 2019; Zhang et al., 2011), and to analyse the consequences on the responder movement. This physical uncoupling can be achieved using genetic conditions which affect proteins mediating the interaction, including proteins involved in direct cell/cell contacts (Schwayer et al., 2019; Smutny et al., 2017) or, if the coupling is mediated by ECM, ECM components (Guillon et al., 2020). The physical uncoupling of the two interacting tissues can be also be achieved by enzymatically degradation of the ECM present at the interface (Tlili et al., 2019).

In our case, we did not observe direct cell-cell contacts between OP and eye cells as shown in Article supplementary figure 5A where it is clear that the GFP-tagged membrane of eye and OP cells are not in contact with each other. Using immunostaining, we observed Laminin and Fibronectin enrichment at the interface between the two tissues (from 12s), as well as the presence of NCCs progressively populating the gap between the two tissues from around 18-20 s onwards. We used a genetic approach to perturb these incoming NCCs and the injection of enzymes to degrade the ECM components. We will discuss the results of these two approaches in the part IV.C dedicated to the eye/OP interface.

- **Testing the sufficiency of forces from the inducer to cause responder morphogenesis**

A way to assess whether mechanical forces exerted by the inducer are sufficient to drive the movement of the responder is to amplify the mechanical forces produced by the inducer. Indeed, if inducer forces are sufficient to generate the responder movements, we expect to also amplify the responder morphogenesis when we increase the mechanical forces produced by the inducer. This force increase can be performed in *wt* conditions or as a rescue in a condition where the inducer is absent.

In our case, we envisaged to increase forces generated by the eye using two different strategies. First, as presented in III.B, we obtained UAS transgenic lines expressing CA forms of upstream activators of actomyosin, RhoGTPases (Hanovice et al., 2016). By combining these lines with the *Tg(rx2:Gal4;myl7:GFP)* eye driver line (Di Donato et al., 2016), we expected to increase

RhoGTPases activity and thus to amplify eye morphogenetic movements. We tried this approach with $Rac1^{CA}$ but similarly to what we previously described with $Rac1^{DN}$ (III.B.2) we found that the expression of $Rac1^{CA}$ was very mosaic. At 24 s, we could not see any change in the eye morphology of embryos expressing $Rac1^{CA}$ as compared with control siblings. We thus concluded that the expression of $Rac1^{CA}$ with this combination of transgenic lines was not a suitable approach to amplify the forces associated to eye morphogenesis.

The second strategy we thought about consists in injecting small magnetic beads (smaller than one cell diameter) in the inducer tissue, and by moving these beads with a magnetic field, we could hope to pull on eye cells and thus to generate mechanical stress in the eye. Such approach has already been used *in vivo*: the injection of micro-magnetic beads in live embryonic flies in presence of a magnetic field enabled to mimic physiological tissue deformation and to study mechanotransduction within the tissue (Mitrossilis et al., 2017). To our knowledge, such tool has not been used yet to probe the mechanical nature of two interacting tissues. The bigger the beads are, the more likely they are to push the surrounding tissues or induce cell shape changes and neighbour exchange, but also, the more they aggregate and thus the harder it is to inject them. Such bead injection is thus challenging and a compromise needs to be found by testing several diameters. As a proof of concept, we succeeded in injecting beads of 500 nm diameter (MasterBeads carboxylic Acid 0215 Ademtech) into the optic vesicle of some embryos at around 16 s (17 hpf). By approaching a permanent magnet, we saw the beads reorienting and aligning in the direction of the magnetic fields. The next step would have been to use a magnetic field gradient to be able to move the beads, and subsequently to pull on the eye cells. This first attempt was very promising and further optimizations (setting a magnetic field gradient, testing other bead diameters) would be required to obtain the proper set up to induce a lateral displacement of eye cells or a deformation of the eye tissue without damaging the embryo.

These “gain of forces” approaches would enable to show the sufficiency of mechanical forces from the inducer in driving morphogenetic movements in the responder tissue. Modelling could be another way to test the sufficiency of a condition. Indeed, if model predictions are in agreement with experimental data when a unique condition is considered to be the driving mechanism (a mechanical interaction in our case), it means that this condition is a sufficient condition (as in (Behrndt et al., 2012; Tlili et al., 2019)). In our case, if we obtain more detailed measurements of the forces within the OP and the eye (see IV.B.2 for description of the tools

that could be used for this purpose), we could consider to put these values in a theoretical model to assess whether these forces amplitudes are sufficient to explain the OP shape change.

- **Measuring a change in tension distribution in the responder or at the interface when the inducer is absent**

Mapping the distribution of mechanical tension within the responder tissue in presence or in absence of the inducer tissue also enables to assess the mechanical influence of the inducer on the responder. In Breau *et al.*, (2017), laser ablation of cell/cell contacts was performed in two positions within the OP, and along two directions: at OP extremities and in the placode centre, on cell/cell contacts oriented parallel or perpendicular to the brain surface (Breau et al., 2017). For the current study, we wanted to map tension in both *wt* and *rx3*$^{-/-}$ eyeless embryos and since cell-cell junction ablations were very time-consuming, we turned to supracellular laser ablation, which has been previously used to estimate tissue stress (Bonnet et al., 2012; Campinho et al., 2013; Collinet et al., 2015; Porazinski et al., 2015). We used supracellular laser cuts in three different localizations at the border of the OP to probe stress assymetry in the OP (Article figure 5). In the *rx3*$^{-/-}$ mutants, we found a reduction of the initial recoil velocity for ablation performed at the lateral border as compared with the anterior or posterior cuts as represented on Figure 62. This result indicates that there is an asymmetry of stresses exerted at the OP periphery in eyeless embryos, with smaller stress along the mediolateral axis, which is the direction of the axon elongation. This assymetry is not present for *wt* embryos, which reinforces the idea that the eye exerts a mechanical influence on the OP.

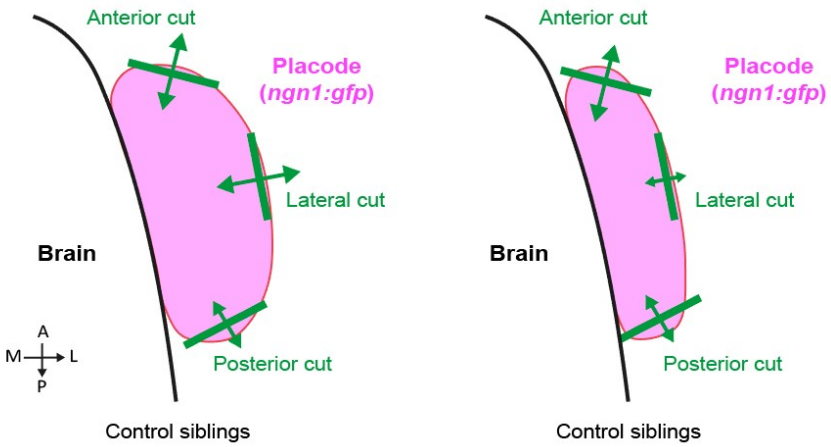

Figure 62: **Schematic view of the supracellular laser cuts (green lines) and the tension estimated from the initial recoil velocity after these cuts (green arrows)**. To note, here the

estimations of the tension are grossly represented by the length of the arrows according to the mean velocity measured (Article figure 5).

2. Measuring mechanical forces *in vivo*

In the section I.C, we presented various methods that could be used *in vivo* to probe the mechanical properties, forces and stresses of a tissue. Using them in our system would help to further assess the mechanical nature of the interaction and to gain information on the forces transmitted from the eye to the OP.

- **FRET tension sensors**

As mentioned in section I.C and in Table 2, FRET tension sensors enable to estimate intra-molecular tension. For example, a vinculin tension sensor has been described, which is composed of a protein involved in linkage of integrin adhesion molecules to the actin cytoskeleton (vinculin), in which a FRET based tension sensor module is inserted (Grashoff et al., 2010). This vinculin tension sensor is recruited to focal adhesions through which mechanical force and regulatory signals are transmitted between the ECM and the cell. Biosensors such as this one could be used to measure tensions experienced by proteins involved in cell/matrix adhesion at the eye/OP interface (refer to IV.C.2 for further discussion on this interface). This would help us to understand the mechanism of force transmission between the two tissues over time. Cadherin FRET sensors have also been described (Lagendijk et al., 2017) and could be used to map tension within the eye and/or the OP, to see how forces are propagated across the two tissues, and not only at their interface. However, the use/development of FRET sensors requires tedious optimization, consisting in generating the proper FRET sensor line, calibrating the FRET efficiency-force relationship, and setting up data acquisition and image processing to retrieve intramolecular tension from fluorescence changes. Each of these steps is technically challenging, and the approach requires adequate controls to certify that molecular tension is the only cause of FRET change (Clegg, 2009; Hildebrandt, 2013).

- **Force inference**

Force inference is a computational technique that enables to estimate the pressure of each cell and the tension of each cell/cell contact from the observed geometry of the cells. Under the assumption that the tissue is at mechanical equilibrium, cell shapes are determined by the balance between contact forces between cells, such as cell-cell junction tensions, and cell

pressures. Thus, visual measurements of cell shape and cell-cell junction curvature enables to determine tension and pressure ratios within the cells (Brodland et al., 2014; Ishihara and Sugimura, 2012; Ishihara et al., 2013). This non-invasive approach enables to have a view of mechanical forces at both the cell and the tissue level and thus is a powerful approach to link mechanics and developmental processes but it needs to be further validated for the analysis of 3D tissues (Roffay et al., 2021). Moreover, stress inference cannot be applied to tissues that deviate from mechanical equilibrium. For example, sinuous cell junctions, very acute angles or protruding cells imply that a set of tensions and pressures are not sufficient to explain the observed shapes, and such "not-regular" tissues are not compatible with tissue inference (Roffay et al., 2021). This is the case in the OP as peripheral cells display protrusions while they are actively migrating towards the centre and central cells display protrusions as they elongate their axon. Thus the OP seems to be far from mechanical equilibrium when undergoing morphogenesis.

- **Nuclei deformation as an indirect readout of mechanical forces**

In normal cells, the nucleus is stiffer than the surrounding cytoplasm: changes in nuclear shape are expected to require forces that exceed thermal forces in the cell. If a cell is under significant anisotropic forces, its nucleus should be more elongated than if the cell is at rest or subjected to isotropic stress. Thus the nuclei deformation can be used as a proxy of cells that are under significant stress (Versaevel et al., 2012; Wang et al., 2009). Previously, Breau *et al.* used OP cell nuclear morphology as a readout for mechanical stress and found that cells located in the centre of the OP close to the brain exhibit elongated nuclei along the mediolateral direction, suggesting that they undergo anisotropic mechanical stress. Moreover, in most cases observed, when these central OP cells start to move laterally, their nuclei become rounder, suggesting that lateral departure coincides with the relaxation of mechanical stress (Breau et al., 2017). It would be very interesting to analyse nuclei shape in *rx3*$^{-/-}$ mutants to test whether the absence of eye decreases the anisotropy in nuclei shape that central OP cells display. We would expect to see less nuclei deformation in central OP cells in *rx3*$^{-/-}$ mutants compared to *wt* embryos, in agreement with the loss of mechanical forces exerted by the eye on the OP cells.

- **Injection of oil droplets in zebrafish tissues**

Fluorescent oil droplets can be used as force sensors and enable to directly quantify the anisotropic part of the normal mechanical stresses within developing tissues *in vivo* (Campas et

al., 2014; Gross et al., 2021; Mongera et al., 2018). Thanks to a collaboration with Lea-Laetitia Pontani and Iaroslava Golovkova (Laboratoire Jean Perrin) and to the previous work of Girisaran Gangatharan, we were able to successfully inject and image naked (*i.e.* non functionalized) oil droplets in the OP, without affecting OP morphogenesis (Figure 63). The further analysis of their deformation enabled to estimate stress field in *wt* embryos in the middle of OP morphogenesis. This analysis showed that there were no significant compressive stresses exerted in the OP at these stages. Moreover, oil droplets injected in the presomitic mesoderm were deformed and elongated along the anteroposterior axis, in agreement with what has already been published in this tissue (Mongera et al., 2018), which validates our oil droplet technique.

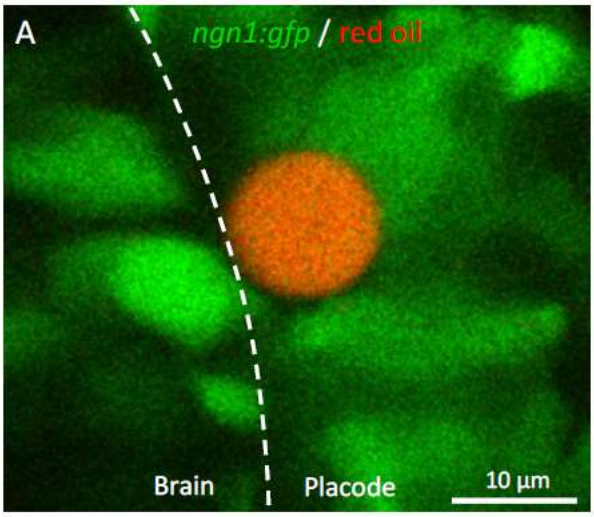

Figure 63: **Confocal image of a 10 µm fluorescent oil droplet injected in the OP centre of a *ngn1:gfp* embryo and imaged at 14 s** (G. Gangatharan and P. Monnot).

However, naked oil droplets only enable to measure the anisotropic part of compressive stresses and do not deform under traction stresses. Engineering new droplets that would deform upon both compression and traction will enable to map both compression and traction forces in the OP. These new oil droplets have to adhere to the surrounding cells or ECM so that pulling forces are transmitted through the cell/droplet adhesions. A way to make these droplets adhere is to functionalize them with adhesion proteins such as Cadherins for adhesion with surrounding cells (Pontani et al., 2016; Pontani et al., 2012) or Collagen for adhesion with ECM. These functionalized droplets could then be injected within the OP but also at the eye/OP interface of *wt* embryos and of *rx3*$^{-/-}$ mutants. As our preliminary results indicated that there were no significant compressive stresses in the OP, we could attribute the deformation of the

functionalized droplets to traction stresses. We expect to detect traction stress anisotropy with higher stress along the mediolateral direction in *wt* OP, which would be reduced in *rx3*$^{-/-}$ mutants.

3. Comparison with other examples of intertissue interactions

In this part, we will compare our model system with other systems of mechanical interaction between developing tissues.

- **Intertissue surface interaction and orientation of the forces.**

As represented on Figure 64 and on article movies 5 and 6, the interface between the eye and the OP is a curved surface, whose size and curvature change over time during OP morphogenesis. As presented in IV.A, different types of movements and cell shape changes occurring in specific regions of the invaginating eye could generate the mechanical stresses that are exerted on the OP at the eye/OP interface. Basal constriction at the centre of the neural retina would mainly exert orthogonal stresses with respect to the eye/OP interface (Figure 64 blue arrows). This gradual constriction of NR basal end feet in the centre of the retina is likely translated into tension at the tissue level (as suggested by Cavodeassi (Cavodeassi, 2018)) and thus orthogonal forces could be transmitted to the OP. By contrast, rim movements and RPE spreading at the edge of the optic cup would exert mainly tangential stresses with respect to the interface (Figure 64 white arrows). The resulting force of both components would align along the mediolateral direction.

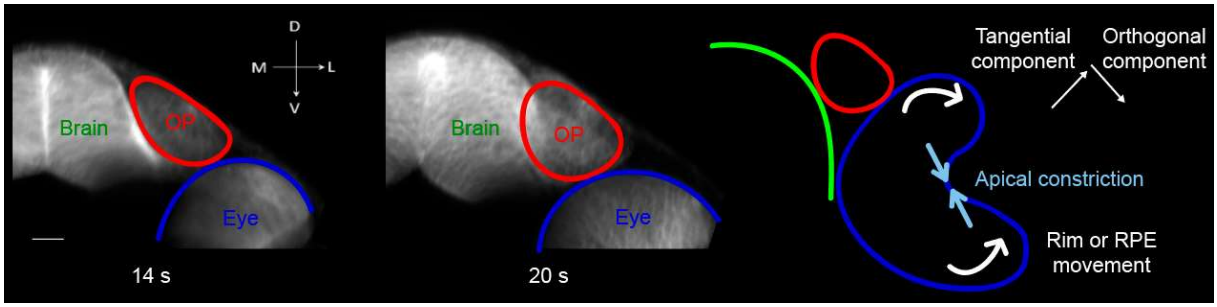

Figure 64: **Eye/OP surface of interaction and direction of the forces exerted**. (Left) Confocal images (frontal view) on a live *cldnb:lyn-gfp* embryo at 14 s and 20 s from the same embryo imaged in live. Note the curved interface between eye and OP. (Right) Schematic outline of the three tissues (brain in green, OP in red, eye in blue) and of the two types of eye cell movements that could exert forces on the OP in a frontal view.

Our results suggest that the developing optic cup exerts mechanical forces on the OP, providing a frictional drive that induces lateral movements and axon extension. Quantifying the relative movement between the two tissues would help assessing the frictional resisting forces between the eye and the OP. No relative movement, indicating that both tissues move exactly at the same speed, would signify that there is no friction and that the two tissues move together laterally. On the contrary, we could observe on three out of the four *wt* embryos we studied, that the speed of mediolateral displacement was higher in the eye than in the OP after T_{ref} (slopes on Article supplementary figure 2E), suggesting that there could be friction between the eye and the OP.

- **Competence of the OP**

In their review, Villedieu *et al.* described the competence of the responder tissue as its ability to deform or move under extrinsic mechanical stress exerted by the inducer. Under extrinsic forces, the tissue can be deformed like a solid (either reversibly and elastically, or irreversibly and plastically) or like a fluid (Villedieu et al., 2020). Biological tissues are usually described as viscoelastic, where the tissue behaves as an elastic solid over short timescales, rapidly coming back to its original shape when the force is released, and as a viscous fluid over long timescales due to cell rearrangement, molecular turnover, or cell division and death (Tlili et al., 2020). The typical timescale characterizing the crossover from elastic to viscous behavior is a material parameter specific for each tissue (Schotz et al., 2013) and depends, amongst others, on the type of cells, the type of tissue, the development stage, the speed of the strain applied, etc., but is in the order of magnitude of an hour.

On one hand, cell neighbor exchanges enable plastic and fluid tissue deformations, and thus contribute to the permissiveness for the induced deformation (Villedieu et al., 2020). Cell rearrangement can be favored by low level of intercellular adhesion, cell division and decreased cortical contractility which decreases cell/cell adhesion. Even though OP cells migrate in a coherent fashion, there are some short-range cell intermixing during OP morphogenesis (Breau et al., 2017). Moreover, around half of OP cells undergo cell division during this period (Breau et al., 2017). Our observations so far support the idea that the OP behaves at the timescale of morphogenesis more like a viscous fluid (rather than like a plastic solid) tissue, making the OP a competent tissue for deformation. These observations could be complemented by the study of the speed profile of cell movements within the OP: no gradient of mediolateral velocity would indicate cells move as a whole, *i.e.* that the OP undergoes a solid-like movement, while a speed

gradient with higher velocities close to the interface with the eye would suggest a fluid-like deformation. This analysis would require to have the position of the eye/OP boundary at all time points, a parameter which is not easily accessible.

On the other hand, Villedieu *et al.* defined local adhesion of the responder tissue with a rigid substratum as resisting to the induced deformation (Villedieu et al., 2020). This is the case for example during *Tribolium* gastrulation where the region of the blastoderm that is attached to the vitelline envelop resists to flows induced by the embryo contraction (Munster et al., 2019). In our case, the attachment of OP neurons to the brain through their axonal processes or through cell/matrix adhesion could anchor the OP tissue to the brain, thus promoting tissue elongation instead of simple lateral tissue flow. Further investigations are required to characterize in detail the connection between the brain and the OP.

~~4.~~ Cooperation of traction forces with chemokine signalling

The coalescence of the OP is driven by two types of cell movements, the active anteroposterior convergence and the lateral movement which appears to be passive (Breau et al., 2017). Cxcr4b/Cxcl12a chemotactic signalling has been shown to control OP coalescence downstream of the Ngn1 transcription factor (Aguillon et al., 2020; Miyasaka et al., 2007). In mutants for the Cxcr4b/Cxcl12a pathway or for Ngn1 transcription factor, the convergence of the anterior OP cells is particularly affected but the mediolateral component of cell movements appears to be less perturbed (Aguillon et al., 2020). On the contrary, in eyeless *rx3*$^{-/-}$ mutants, the lateral movement of anterior and central OP cells is reduced but on our movies the anteroposterior displacement remains similar to control siblings: in both control and *rx3*$^{-/-}$ embryos, anterior OP cells undergo a posterior movement and posterior OP cells move anteriorly (Article figure 4 and Article supplementary figure 4). This supports a scenario in which Cxcr4b/Cxcl12a chemical signalling controls anteroposterior convergence movements, while mechanical forces exerted by the neighbouring eye morphogenesis mediate lateral movements.

Surprisingly however, the anteroposterior dimension of *rx3*$^{-/-}$ OP measured on fixed embryos at the end of OP morphogenesis (77.3 ± 13.3 µm, n=9 embryos) was higher than in control OP (63.3 ± 11.7 µm, n=9 embryos) (Figure 3C). Several elements could account for this difference, knowing that there was no difference between both conditions in the OP volume and in the number of *ngn:gfp*$^{+}$ cells (Article supplementary figure 3). First, this increase could be due to a weak perturbation of Cxcl12a/Cxcr4b signalling in *rx3*$^{-/-}$ mutants, consistent with our finding

that the domain of expression of the ligand is larger in *rx3*$^{-/-}$ mutants compared to controls (III.B). Besides, we did not analyse the anteroposterior dimension of the OP at the beginning of morphogenesis (12s) between *rx3*$^{-/-}$ and control embryos and it is possible that OP cells undergo similar anteroposterior movements between 12 and 24 s in both situations but that *rx3*$^{-/-}$ cells start this convergence movement from a more scattered position along the anteroposterior axis. Alternatively, the higher anteroposterior OP dimension in *rx3*$^{-/-}$ mutants could be a consequence of the lateral movement defects and of a crowding in the central OP area. Because of the inability of OP cells to be displaced laterally by the forming eye, the converging cells would accumulate at the anterior and posterior borders, thus increasing the OP dimension along the anteroposterior axis.

Future investigations are necessary to distinguish between these hypotheses. First, we can try and analyse OP dimensions at 12 s, similarly to what we did at 24 s, to assess whether the OP domain is more spread along the anteroposterior axis in *rx3*$^{-/-}$ compared to control embryos. However, this could be challenging as 12 s corresponds to the onset of expression of the *ngn1:gfp* reporter line in the OP, so the GFP signal is weak and mosaic at these early stages. In order to test whether OP cells accumulate on the anteroposterior borders because the central placode is crowded with cells that did not move laterally, we could try to laser ablate central cells in *rx3*$^{-/-}$ mutants and see if this is sufficient to increase the convergence of cells located at the extremities.

Next, I want to discuss how we could clarify how Cxcr4b/Cxcl12a chemotactic signalling and eye mechanical traction cooperate to orchestrate the cell movements that shape the OP. As described previously (I.B.3 and III.B.1), the receptor Cxcr4b is expressed in OP cells while the ligand Cxcl12a is expressed in the brain, and both are required for proper OP morphogenesis (Aguillon et al., 2020; Miyasaka et al., 2007). The coordination between the role of this chemical pathway and the role of mechanical forces could be the following: Cxcr4b/Cxcl12a signalling in OP cells may be initially required for the proper anteroposterior convergence towards the centre of the OP and then inhibited to let the cells be displaced laterally by extrinsic mechanical forces. The inhibition of the Cxcr4b/Cxcl12a pathway could occur at the level of gene expression and interestingly, from 24 hpf onwards, we can observe, on data published by another group, a decrease in the expression level of the Cxcr4b receptor in at least some central OP cells (Miyasaka et al., 2007). The inhibition of Cxcr4b/Cxcl12a signalling could also occur at the post-translational level through the internalization of Cxcr4b specifically in the central

OP cells. Indeed, the role of Cxcr4b internalization in inhibiting cell migration in response to the Cxcl12a chemo-attractive cue has been previously reported in zebrafish primordial germ cells. Primordial germ cells express Cxcr4b and migrate towards sites in the embryo where the ligand Cxcl12a is expressed. While *wt* migration speed was reduced as they approach their target, cells expressing a non-internalizable Cxcr4b mutant, lacking the carboxyl-terminal region, failed to down-regulate signalling and exhibited longer runs and less precise targeting (Minina et al., 2007). Cxcr4b internalization also occurs in the migrating primordium of the lateral line where Cxcl12a ligand binding causes Cxcr4b receptor internalization, but this internalization is dispensable for primordium migration, as opposed to the internalization and sink activity of the Cxcr7 receptor which is crucial for the process (Dona et al., 2013; Venkiteswaran et al., 2013). We can think that such post-translational regulation of Cxcr4b also occurs in central cells of the OP, thus inhibiting Cxcr4b-mediated chemical signalling during the second phase of lateral movements. We could test this hypothesis for instance by expressing a non-internalizable Cxcr4b mutant form in OP cells and see how it affects lateral movements.

C. Role of the eye/OP interface

The third goal of my PhD project is to identify the mechanisms of force transmission at the interface between the two tissues. We observed the presence of NCCs and of ECM between the eye and the OP. In the following part, we will discuss the role of these two elements in transmitting forces from the eye to the OP.

1. Role of the NCCs

As described in chapter I.B, neural crest and cranial placodes are transient vertebrate tissues arising at the border of the neural plate in close proximity to each other: neural crest is located close to the neural plate while the large domain giving rise to the placodes (the PPR) originates from an adjacent and more lateral tissue. Throughout their development, neural crest and placode remain in close proximity and interact frequently (as reviewed by (Steventon et al., 2014)). As examples of these interactions during development, we saw in the section I.B, how the interactions between NCCs and epibranchial placode cells lead to the coordinated migration of both populations (I.B.1) (Theveneau et al., 2013) and how cranial NCCs surround the OP it without intermixing of the two cell populations (I.B.3) (Aguillon et al., 2016; Harden et al., 2012).

From around 18-20 s onwards, we observed the presence of cells progressively populating the gap between the two tissues (Article supplementary figure 5A), that we identified as cranial NCCs based on the literature (Bryan et al., 2020; Harden et al., 2012; Langenberg et al., 2008; Torres-Paz and Whitlock, 2014). These NCCs might play a role in the coupling between the two tissues. This third cell population could for instance increase the adhesion between the eye and the OP by establishing concomitant cellular contacts with both tissues and thus increase the transmission of traction forces from the eye to the OP. On the contrary, they could also lower intertissue adhesion and friction by increasing the distance between the two tissues or degrading the intersticial ECM.

In order to assess the role of NCC in transmitting forces from the eye to the placode, *foxd3*$^{-/-}$ mutants appeared as an ideal condition as NCC migration between the two tissues is affected but eye evagination and eye invagination occur normally, as estimated respectively by our measurements of the eye size and the eye invagination angle (Article supplementary figure 5B-D). Our analysis of OP shape at 24 s in *foxd3*$^{-/-}$ mutants showed that the absence of NCCs

between the eye and the placode does not change the OP volume, the OP dimension along the anteroposterior axis and the OP dimension along the dorsoventral axis. Interestingly, *foxd3*$^{-/-}$ mutants exhibit a slightly higher dimension along the mediolateral axis (48.0 ± 7.4 µm, n=9 embryos) compared to control siblings (41.6 ± 7.5 µm, n=9 embryos) (Article supplementary figure 5D). This difference of 6.4 µm is in the same magnitude as the width of a raw of cells.

As said earlier, an interesting hypothesis would be that the presence of NCCs between the eye and the placode, instead of promoting force transmission, rather uncouples the two tissues either just by being physically present or by degrading the ECM. This second eventuality seems less probable though, as our immunostaining for Laminin did not reveal any difference in presence or in absence of NCCs at the interface. However, Laminin is the only ECM component we looked at in *foxd3*$^{-/-}$ mutants and we cannot exclude that other ECM components would be degraded by NCCs. The physical presence of NCCs between the two tissues could dampen down intertissue adhesion and thus force transmission from the eye to the placode and thus results in less lateral movement in the placode. To test this idea, it would be necessary to look at the dynamics of cell movements to quantify if there is an increase of OP lateral movements and OP/eye correlation in the *foxd3*$^{-/-}$ situation, and to perform supracellular laser ablations to estimate if there is an increase in the mechanical tension anisotropy in the *foxd3*$^{-/-}$ situation.

Even if more experiments are required to confirm a potential role of NCCs in uncoupling the two tissues, our data indicate so far that NCCs between the eye and the placode are not required for the proper lateral movements of OP cells.

2. Role of the ECM

As we have seen in I.C.2, the injection of enzymes degrading the ECM enables to physically uncouple two tissues and to assess the role of ECM in mediating their interaction (Tlili et al., 2019). An ideal way to test whether ECM acts as a glue transmitting forces between the eye and the OP would have been a condition where the matrix is degraded only between the two tissues, while the matrix surrounding the brain or the rest of the eye tissue remains intact. This is important, since ECM has been shown to play a role in eye morphogenesis (Bryan et al., 2020; Bryan et al., 2016; Martinez-Morales et al., 2009; Nicolas-Perez et al., 2016). Compared with genetic conditions such as mutants for Laminin, the injection of collagenases enables to have a temporal control of the ECM degradation. However, the mix of collagenases and red

fluorescent dextran we injected diffused rapidly within the whole head of the embryo and it was not possible to get a precise spatial restriction of matrix perturbation (Article supplementary figure 6A). Unlike other studies where collagenases injection was used in zebrafish embryos (Matejcic et al., 2018; Tlili et al., 2019), here, we confirmed the efficiency of this approach by performing immunostaining for Laminin at 24 s, showing the successful degradation of this component of the ECM.

Since we could not finely tune the injected volume, it was not surprising to observe a high variability in the induced eye phenotypes. As ECM is necessary for proper eye formation, the degradation of the ECM resulted in a range of eye defects from little or no apparent defect to strong invagination phenotypes often associated with extrusion of the lens. By selecting only the embryos in which eye cells still displayed directional lateral movements with a high intra-eye correlation coefficient (Article figure 6B,C and Article supplementary figure 6C,D), we ensured that the defects observed on the OP are not due to highly perturbed eye movements. Yet, we cannot exclude that the perturbed OP cell movements observed in these embryos are caused by the general loss of ECM in the head. For instance, disrupting basement membrane all around the OP may affect tissue cohesion and lead to a reduction of lateral movements.

A future perspective of this work would be to focus on the eye/OP interface with greater details and to decipher the molecular mechanisms of force transmission. The first aim would consist in characterizing in more details the organisation and topology of the ECM meshwork present between the two tissues. During my PhD, we performed immunostainings for two components of the ECM, Laminin and Fibronectin, but other ECM components are known to be also present in this area at similar stages such as the ECM crosslinking protein Nidogen (Bryan et al., 2020) or Collagen XII which does not form supramolecular aggregates by itself but bridges collagen fibrils (Bader et al., 2009). Using available antibodies on samples fixed at different stages in combination with super resolution microscopy will enable to get a spatial and temporal map of the ECM topology. We could also use the *Tg(hsp70:fn1a-mKIKGR)* reporter line generated by Guillon *et al.* to dynamically visualize Fibronectin at the interface between the two tissues (Guillon et al., 2020). Preliminary tests showed that upon heat shock, Fn1a-mKIKGR does accumulate at the interface between the two tissues during OP morphogenesis and further experiments of photoconversion of the mKIKGR reporter fused to Fn1a will enable to observe the dynamics of Fibronectin remodelling (collaboration with Scott Holley, Yale University).

A second aim would be to further map the mechanical forces around the interface. As presented earlier (IV.B.2), the design of functionalized oil droplets coated with Collagen and their injection at the eye/OP interface would enable to map both compression and traction forces between the two tissues, but also on both sides of this border. By following these droplets during OP morphogenesis, we could identify specific time windows when they deform more, indicating a higher force anisotropy. This experiment might help determining specific eye morphogenetic events that induce more traction forces at the interface.

The third aim would consist in perturbing ECM or cell/ECM interactions with two novel strategies. The first strategy is still based on enzymatic degradation of ECM components but achieved in a tissue-specific manner, using genetic conditions. A challenging but exciting possibility would be to overexpress enzymes degrading ECM components, such as matrix metalloproteinases (MMP), specifically in the eye tissue (Pedersen et al., 2015). MMP2 appears as a good candidate as it cleaves type IV Collagen, denatured Collagen and other ECM components such as Fibronectin, Laminin, Aggrecan, Elastin, large Tenasin-C, and Collagen I, V, VII and X (Nagase and Woessner, 1999; Zhang et al., 2003). To our knowledge MMP overexpression has never been done in zebrafish and this strategy would require the cloning of the MMP gene under the control of a promoter specific for the eye such as the *rx3* promoter or under the control of a UAS, allowing the combination with different Gal4 lines. With this strategy, we expect to degrade only the ECM surrounding the eye and not the basement membrane between the brain and the OP. We would still have to check that eye movements are not perturbed in this condition.

The second approach would consist in perturbing the main receptors involved in cell-ECM adhesion, the Integrins. We speculate that cells at the periphery of the OP, and in particular in the region close to the eye, might adhere to the ECM through Integrins and that this cell/matrix adhesion might transmit forces from the eye to the OP. Thus, perturbing integrin function might affect the force transmission between the two tissues. Integrin receptors mediating cell-ECM adhesion can be blocked with antagonists, such as the RGD peptide or the disintegrin echistatin, which have already been used in zebrafish to perturb integrin/ECM interactions upon injection (Becker et al., 2003; Chiu et al., 2012) or by bathing the embryos in a medium containing RGD peptides (Nair and Schilling, 2008). However, such experiments would not give rise to a restricted effect on the interface between the eye and the OP. As an alternative, loss of function of Integrins can be achieved by overexpression of DN forms, using for example the

Tg(UAS:mCherry-itgb1aDN) line. In this line, the cytoplasmic domain of Integrin β1 is used as a DN form as it sequesters intracellular cytoskeleton proteins that are essential for the function of endogenous β1 Integrins. It is expressed under the control of an UAS promoter, enabling to have a temporal and spatial control of its expression with adequate Gal4 driver lines (Iida et al., 2018). We could combine this line with the *Tg(ngn1:KalTA4)* line recently generated by the lab (Baraban, unpublished data) to interfere with integrins in the OP.

These two strategies (degradation of ECM with MMPs or perturbation of integrins) would complement our collagenases injection experiments and help confirming the role of ECM in transmitting the forces from the eye to the OP. However, they require time-consuming optimization and thus could not be used in the scope of my PhD work.

D. Functional neuronal circuit formation

Here, we will discuss the potential consequences of the extrinsic traction forces on the formation of the olfactory circuit, focusing first at the subcellular scale on OP axon growth and then at the organism-scale on the functionality of olfactory circuit.

1. Mechanisms of stretch-induced axon growth

As stated in the article, our results suggest a scenario in which the eye pulls on OP neuronal cells bodies, which stretches the anchored axonal protrusions that, in turn, grow in response to that tension. This retrograde extension of neurites contrasts with the classical view of axon elongation as a growth-cone-driven process, in which the axon extremity moves progressively further away from a static cell body (Polleux and Snider, 2010). Similar retrograde mode of extension have also been identified in dendrites of *C. elegans* neurons as described previously in I.B.3 (Cebul et al., 2020; Fan et al., 2019b; Heiman and Shaham, 2009). These *in vivo* situations are good examples of the stretch-growth or towed growth mechanism suggested by Weiss (Weiss, 1941), by which axons grow in response to extrinsic tension without motile growth cones (for Weiss, the tension comes from growth of the organism). However, this process has been mostly studied *in vitro* so far (Bray, 1984; De Vincentiis et al., 2020a; Loverde and Pfister, 2015; Loverde et al., 2020; Pfister et al., 2006; Pfister et al., 2004).

An interesting perspective of my PhD work is to understand how OP neurons sense extrinsic traction forces and adapt their architecture to grow in response to these forces. A first step would be to characterize the axon structure throughout OP morphogenesis. This could be achieved by high-resolution imaging of cytoskeleton components visualized by immunostaining at different stages with antibodies as for example acetylated Tubulin (Breau et al., 2017) or phosphorylated Myosin II (Sidhaye and Norden, 2017). The axon structure can also be characterized in live embryos using mRNA injection of probes such as Doublecortin–GFP or Utrophin–GFP used to visualize respectively microtubules and actin (Breau et al., 2017) or transgenic lines such as the *Tg(actb1:myl12.1-eGFP)* line used to visualize Myosin II dynamics (Maitre et al., 2012). Looking at axon diameter and ultrastructure using electron microscopy at different stages will also help identifying changes in axon organization over time during stretch-growth. Moreover, in order to try and localize the site of new material addition along the axon shaft, we could use a photoconvertible protein fused to a cytoskeleton probe. The photoconversion of this probe at a given time in discrete locations along the shaft, followed by the tracking of the photoconverted

and non photoconverted regions, would enable to determine the sites of addition of new cytoskeleton material. In order to generate such a tool, we could for example design a probe by fusing the monomeric photoswitchable fluorescent protein mKikGR (Habuchi et al., 2008) with the Doublecortin sequence of Doublecortin–GFP, previously used to look at microtubule dynamics in OP axons (Breau et al., 2017).

We could next use the same tools (immunostainings, live imaging of probes and transgenes, electron microscopy, photoconversion experiments) to characterize axon organisation in the absence of extrinsic forces exerted by the eye, namely in eyeless *rx3*$^{-/-}$ embryos. We have observed that axons are shorter in *rx3*$^{-/-}$ mutants, and that the axons in the centre of the OP appear more twisted than in controls (Article figure 3E,F). We could determine if this change of morphology correlates with a change in cytoskeleton organization and material addition. Another approach to understand how OP axons grow upon forces would be to culture OP neurons and apply finely tuned forces on their cell bodies *in vitro.* This approach would require to set up primary cultures of zebrafish OP neurons, which appears for the moment really challenging, and then to develop a micromachine to perform stretching of the cultured axons. This is technically complicated but would enable to complete our *in vivo* data with an understanding of how the intracellular machinery reorganises, and where/when new material is added during OP axon extension in a simpler system.

Finally, the third step would be to dissect the molecular mechanisms of neuronal mechanotransduction*, i.e.* how neurons detect the traction forces and transmit the signal to the growth machinery, by focusing for instance on mechanosensitive channels known to be important in neuronal development in other contexts (Franze et al., 2009; Koser et al., 2016). In summary, this work would help determining the molecular cascade by which the neurons sense the forces and reorganize their internal architecture to grow their axon, during an unclassical mode of axon extension.

Moreover, mechanotransduction pathways can also drive changes in cell fate in numerous developmental situations (Agarwal and Zaidel-Bar, 2021; Maurer and Lammerding, 2019). For example, the contribution of gastrulation forces to the determination of mesodermal cell fate seems to be a conserved mechanism in bilaterians (Brunet et al., 2013) and mechanical pressure can ectopically activate or restore expression of mesoderm fate determinants (Pukhlyakova et al., 2018). As neurogenesis and morphogenesis occur concomitantly in the zebrafish OP

(Aguillon et al., 2020), we can envisage that mechanotransduction in the OP also influences neurogenesis and neuronal differentiation.

2. Olfactory circuit formation in the absence of eye

We found that in the absence of eyes in *rx3*$^{-/-}$ embryos, the OPs at 24 s are thinner along the mediolateral dimension and longer along the two other dimensions, and that OP axons are shorter and less straight compared to the control situation. Do these defects have consequences on olfactory circuit formation?

First, we wondered whether the defects we observe on OPs of eyeless *rx3*$^{-/-}$ embryos are simply due to a developmental delay. Eyeless *rx3*$^{-/-}$ embryos did not present general developmental delay compared to their control siblings. Indeed, at a given time, there was no differences in the number of somites formed between eyeless and control embryos from the same clutch. Moreover, the onset of *ngn1:gfp* expression in the OP and the brain appeared similar in both populations. However, independently of a general delay in development, the OP morphogenesis solely could be delayed in eyeless *rx3*$^{-/-}$ embryos and the defect of OP lateral movements could be subsequently remedied at later stages of olfactory epithelium formation. In order to test this hypothesis, we should analyse OP shape and perform live imaging of cell movements at later stages. Preliminary observations a few hours after 24 s (the latest stage of our initial analysis of OP morphogenesis) indicated that *rx3*$^{-/-}$ OPs shape was still affected and that their mediolateral dimension was shorter than control siblings, but this requires additional characterisation.

Since OP axons exhibit defects in the absence of eyes at the end of OP coalescence, we could first check whether these axons can properly exit the OP, bundle in the brain, grow and reach the olfactory bulb during the steps of axon growth (22 hpf-32 hpf) and protoglomeruli innervation (32 hpf-72 hpf) (Figure 25). The *Tg(omp:yfp)* reporter line specifically labels OSNs and their axons at these later stages (Celik et al., 2002) and could be used in the *rx3*^{s399} background. The 3D quantification of OP dimensions and axon bundle size on eyeless *Tg(omp:yfp) rx3*$^{-/-}$ and control *Tg(omp:yfp) rx3*$^{+/\Delta}$ fixed embryos at different stages would enable to evaluate potential later defects in olfactory circuit formation.

The defects we observed at earlier stages of olfactory circuit formation in the absence of eyes might affect the later function of this circuit. For instance, an intriguing possibility is that the axon initial segment (AIS) is affected in eyeless mutants. Indeed, the proximal axonal portion

that forms within the OP through retrograde extension may correspond to the AIS, a specialized structure in neurons that resides in between axonal and somatodendritic domains (Jones and Svitkina, 2016). The AIS is a segment of about 20 to 60 µm (which is close to the length of the proximal portion of the axons forming within the OP, which we measured at 24 s: 17 µm) which serves two functions essential for proper neuronal activity: to generate action potentials and to maintain neuron polarity (Jones and Svitkina, 2016; Leterrier, 2018). At the molecular level, the AIS is characterized by the accumulation of specific ion channels at the membrane and by the presence of ankyrinG (AnkG also called Ank3), a multidomain scaffolding protein that functions as a master organizer of the AIS structure. Ank3 protein concentrates specifically at the AIS and nodes of Ranvier (Leterrier, 2018). The AIS cytoskeleton is built during early neuronal development, as soon as neuron breaks symmetry, with the clustering of Ank3 in the proximal axonal region (Galiano et al., 2012). Using antibodies against Ank3 and sodium channels (Voas et al., 2009) would enable us to assess whether the axonal portion that assembles through retrograde extension during OP morphogenesis corresponds to the AIS. Interestingly, it has recently been shown that AIS assembly and plasticity can change upon manipulation of tension along axons (Berger et al., 2018; Evans et al., 2019). We can thus hypothesize that the establishment of the AIS is affected in the absence of eye pulling forces, which can be easily tested by using the antibodies mentioned above in *rx3*$^{-/-}$ mutants.

Finally, an evident readout to assess whether the absence of eye affects olfactory circuit function would be to analyse whether eyeless *rx3*$^{-/-}$ embryos are able to smell chemical compounds using behavioural tests. During development, behavioral responses to odorants have first been detected shortly after hatching: zebrafish larvae at 3-4 dpf responded to amino acid odors and to nucleotides with increased swimming activity (Lindsay and Vogt, 2004; Wakisaka et al., 2017). The analysis of odor-mediated behaviors of zebrafish can be accomplished by recording and comparing swimming movements of individual zebrafish larvae before and after odorant exposure in an experimental tank (Calvo-Ochoa and Byrd-Jacobs, 2019; Whitlock, 2008). If olfactory circuit function is affected in the absence of eye morphogenesis, then we should see different behavioural responses to chemical odorants between *rx3*$^{-/-}$ mutants and control larvae, with *rx3*$^{-/-}$ mutants swimming less towards the chemo-attractant odorant.

Loosli *et al.* reported that *rx3*$^{-/-}$ mutants do not show visual responses and die at ~3–4 week but the exact causes of this death remain unknown (Loosli et al., 2003). Zebrafish *rx3*$^{-/-}$ larvae could

die solely from the lack of vision that would affect their foraging behaviours. A good method to assess whether vision is critical for survival above 3–4 weeks would be to raise control siblings in the complete dark for the same period and see if they survive. However, this experiment raises obvious ethical questions and requires to perform experiments on fish above the legal stage of 5 dpf, which cannot be achieved without a specific authorisation. Interestingly, it has been shown that zebrafish of all ages have the ability to forage in the dark (Carrillo and McHenry, 2016), suggesting that the lack of vision might not be the direct cause of *rx3*$^{-/-}$ death. Another hypothesis could be that, in addition to the lack of vision, *rx3*$^{-/-}$ mutants sense of olfaction is also affected, thus preventing them from foraging and progressively leading to the death of the larvae.

To conclude this section, the work carried during my PhD suggests that the developing eye exert traction forces, probably mediated by friction, on the OP neurons, enabling the movement of neuronal cell bodies and the elongation of axons. Our study adds to the emerging field of study of intertissue mechanical interaction by bringing new insights on how the building of neuronal circuits requires mechanical forces from surrounding tissues, and presents an original example of a tissue elongation process resulting from the traction by an adjacent tissue which is connected by ECM.

Conclusion

The animal nervous system is a complex network of neurons and glial cells and their surrounding matrix that encodes, processes, stores and transmits information to and from different parts of the body. The correct wiring of the nervous system is essential for its proper function and relies on the neuron ability to move to its final position and to grow neurites towards its appropriate synaptic partners. Numerous studies focused on the chemical cues enabling developing neurons to migrate to their proper location, extend their axon in the correct direction and reach their target through their complex *in vivo* environment. Recent studies *in vitro* suggest that physical cues play a central role in neuronal development, either through the mechanical properties of the environment or through the mechanical stresses applied to the growing neurons. However, little is known about the role of mechanical forces in shaping neuronal circuits *in vivo*.

In order to investigate how mechanical forces influence neuronal movements and axon elongation, I used the zebrafish olfactory circuit, which develops during OP morphogenesis, as a model. Previous work from Breau *et al.* showed that OP formation from an elongated domain into a compact and spherical neuronal cluster is driven by two types of cell movements. Peripheral cells migrate actively along the brain towards the centre of the placode and central cells are displaced laterally away from the brain surface while the tip of their axon remains anchored at the brain surface, thus leading to a retrograde axon extension. Functional perturbations, axon ablation and mapping of tension in the OP revealed that the lateral displacement of cell bodies away from axon tips is a passive, non-autonomous process driven by extrinsic mechanical forces. In parallel, the optic cup develops ventrally and laterally to the OP, through large-scale evagination and invagination rearrangements and thus the eye appears as a candidate to exert these extrinsic forces. What is the mechanical contribution of eye morphogenesis in OP lateral movement and axon elongation?

Using live imaging and quantitative analysis of cell movements, we showed that OP and eye cells undergo correlated movements in the lateral direction, supporting the idea of a coupling between the two tissues. In embryos lacking eyes, OP lateral cell movements were affected, resulting in thinner placodes and shorter axons, indicating that eye morphogenesis is required for lateral cell movements and axon extension in the OP. Laser ablation revealed that mechanical tension at the lateral border of the OP is reduced in the absence of eyes, supporting

the hypothesis of the developing eye pulling on OP neurons and their axons. We next sought to perturb the interface between the two tissues, which contains both ECM and migrating NCCs. While OP morphogenesis was unaffected in a mutant where NCC migration is affected, ECM enzymatic degradation affected lateral movements in the OP and perturbed their correlation with eye cell movements, indicating that the ECM establishes a physical link between the eye and the OP.

Altogether, these results suggest that the developing eye exerts traction forces on the OP through ECM, mediating proper neuronal movements and axon extension. It would be interesting to further test the mechanical contribution of other surrounding tissues and in particular of the brain as the brain/OP attachment might play a role in counterbalancing the forces exerted by the eye on the OP.

This work sheds new light on the role of mechanical forces exchanged between developing neurons and surrounding tissues in the sculpting of neuronal circuits *in vivo*, which was largely unexplored so far. Beyond its importance for basic neuroscience, my work will turn attention to the contribution of mechanics, so far neglected, in neurodevelopmental disorders associated with abnormal neuronal migration and axon growth, including malformations of the brain cortex (Barkovich et al., 2012; Budday et al., 2015).

The identified mechanical signals could also be exploited to improve *in vitro* models of neuro-degenerative diseases, such as Alzheimer's disease (Ranjan et al., 2018) or Parkinson's disease (Salari and Bagheri, 2019). 3D scaffolds in which mechanical properties can be spatially controlled and mechanical stresses can be externally applied would enable to better mimic the endogenous intricate environment of these cultured neurons. By taking into account the complexity of their environment, these novel scaffolds will allow better investigation of the mechanisms involved in these diseases.

Mechanical cues could also be used to design innovative strategies to repair brain and spinal cord injuries. Current practice in nerve injury treatment is based on the combination of biomaterials, stem cells, growth factors, and rehabilitation trainings such as electrical stimulation (Yang et al., 2020). In combination with these approaches, exploiting mechanical stimuli might help to induce axon elongation in the lesion site. Providing proper mechanical cues in addition to chemical stimuli would offer a beneficial environment for neurons and glial cells to develop after an injury (Franze et al., 2013). Moreover, the integration of mechanical

cues in tissue engineering strategies might be used create transplantable axonal scaffolds adapted to neuronal regeneration (De Vincentiis et al., 2020b; Franze et al., 2013). The lack of methodologies to apply research results to clinical practice might be a reason why the therapeutic potential of mechanical force as an inducer of axon outgrowth has been neglected so far (De Vincentiis et al., 2020b). However, future advances in biomedical engineering and nanotechnology will open up new perspectives and may make these innovative strategies possible.

Bibliography

Agarwal, P., and Zaidel-Bar, R. (2021). Mechanosensing in embryogenesis. Curr Opin Cell Biol *68*, 1-9.

Aguillon, R., Blader, P., and Batut, J. (2016). Patterning, morphogenesis, and neurogenesis of zebrafish cranial sensory placodes. Methods Cell Biol *134*, 33-67.

Aguillon, R., Madelaine, R., Aguirrebengoa, M., Guturu, H., Link, S., Dufourcq, P., Lecaudey, V., Bejerano, G., Blader, P., and Batut, J. (2020). Morphogenesis is transcriptionally coupled to neurogenesis during peripheral olfactory organ development. Development *147*.

Ahmed, W.W., Li, T.C., Rubakhin, S.S., Chiba, A., Sweedler, J.V., and Saif, T.A. (2012). Mechanical tension modulates local and global vesicle dynamics in neurons. Cell Mol Bioeng *5*, 155-164.

Ahmed, W.W., and Saif, T.A. (2014). Active transport of vesicles in neurons is modulated by mechanical tension. Sci Rep *4*, 4481.

Ahmed, W.W., Williams, B.J., Silver, A.M., and Saif, T.A. (2013). Measuring nonequilibrium vesicle dynamics in neurons under tension. Lab Chip *13*, 570-578.

Ahrens, K., and Schlosser, G. (2005). Tissues and signals involved in the induction of placodal Six1 expression in Xenopus laevis. Dev Biol *288*, 40-59.

Ambrosini, A., Gracia, M., Proag, A., Rayer, M., Monier, B., and Suzanne, M. (2017). Apoptotic forces in tissue morphogenesis. Mech Dev *144*, 33-42.

Anava, S., Greenbaum, A., Ben Jacob, E., Hanein, Y., and Ayali, A. (2009). The regulative role of neurite mechanical tension in network development. Biophys J *96*, 1661-1670.

Anthonisen, M., Rigby, M., Sangji, M.H., Chua, X.Y., and Grutter, P. (2019). Response of mechanically-created neurites to extension. J Mech Behav Biomed Mater *98*, 121-130.

Ashery-Padan, R., and Gruss, P. (2001). Pax6 lights-up the way for eye development. Curr Opin Cell Biol *13*, 706-714.

Auer, T.O., Duroure, K., Concordet, J.P., and Del Bene, F. (2014). CRISPR/Cas9-mediated conversion of eGFP- into Gal4-transgenic lines in zebrafish. Nat Protoc *9*, 2823-2840.

Baden, T., Euler, T., and Berens, P. (2020). Understanding the retinal basis of vision across species. Nat Rev Neurosci *21*, 5-20.

Bader, H.L., Keene, D.R., Charvet, B., Veit, G., Driever, W., Koch, M., and Ruggiero, F. (2009). Zebrafish collagen XII is present in embryonic connective tissue sheaths (fascia) and basement membranes. Matrix Biol *28*, 32-43.

Bailles, A., Collinet, C., Philippe, J.M., Lenne, P.F., Munro, E., and Lecuit, T. (2019). Genetic induction and mechanochemical propagation of a morphogenetic wave. Nature *572*, 467-473.

Baker, C.V., and Bronner-Fraser, M. (2001). Vertebrate cranial placodes I. Embryonic induction. Dev Biol *232*, 1-61.

Baker, C.V., Stark, M.R., Marcelle, C., and Bronner-Fraser, M. (1999). Competence, specification and induction of Pax-3 in the trigeminal placode. Development *126*, 147-156.

Balgude, A.P., Yu, X., Szymanski, A., and Bellamkonda, R.V. (2001). Agarose gel stiffness determines rate of DRG neurite extension in 3D cultures. Biomaterials *22*, 1077-1084.

Barkovich, A.J., Guerrini, R., Kuzniecky, R.I., Jackson, G.D., and Dobyns, W.B. (2012). A developmental and genetic classification for malformations of cortical development: update 2012. Brain *135*, 1348-1369.

Becker, T., McLane, M.A., and Becker, C.G. (2003). Integrin antagonists affect growth and pathfinding of ventral motor nerves in the trunk of embryonic zebrafish. Mol Cell Neurosci *23*, 54-68.

Behrndt, M., Salbreux, G., Campinho, P., Hauschild, R., Oswald, F., Roensch, J., Grill, S.W., and Heisenberg, C.P. (2012). Forces driving epithelial spreading in zebrafish gastrulation. Science *338*, 257-260.

Berger, S.L., Leo-Macias, A., Yuen, S., Khatri, L., Pfennig, S., Zhang, Y., Agullo-Pascual, E., Caillol, G., Zhu, M.S., Rothenberg, E.*, et al.* (2018). Localized Myosin II Activity Regulates Assembly and Plasticity of the Axon Initial Segment. Neuron *97*, 555-570 e556.

Bernal, R., Melo, F., and Pullarkat, P.A. (2010). Drag force as a tool to test the active mechanical response of PC12 neurites. Biophys J *98*, 515-523.

Bernal, R., Pullarkat, P.A., and Melo, F. (2007). Mechanical properties of axons. Phys Rev Lett *99*, 018301.

Bertet, C., Sulak, L., and Lecuit, T. (2004). Myosin-dependent junction remodelling controls planar cell intercalation and axis elongation. Nature *429*, 667-671.

Bhat, N., and Riley, B.B. (2011). Integrin-alpha5 coordinates assembly of posterior cranial placodes in zebrafish and enhances Fgf-dependent regulation of otic/epibranchial cells. PLoS One *6*, e27778.

Bhattacharyya, S., Bailey, A.P., Bronner-Fraser, M., and Streit, A. (2004). Segregation of lens and olfactory precursors from a common territory: cell sorting and reciprocity of Dlx5 and Pax6 expression. Dev Biol *271*, 403-414.

Bhattacharyya, S., and Bronner-Fraser, M. (2008). Competence, specification and commitment to an olfactory placode fate. Development *135*, 4165-4177.

Bhattacharyya, S., and Bronner, M.E. (2013). Clonal analyses in the anterior pre-placodal region: implications for the early lineage bias of placodal progenitors. Int J Dev Biol *57*, 753-757.

Bielen, H., and Houart, C. (2012). BMP signaling protects telencephalic fate by repressing eye identity and its Cxcr4-dependent morphogenesis. Dev Cell *23*, 812-822.

Blader, P., Fischer, N., Gradwohl, G., Guillemot, F., and Strahle, U. (1997). The activity of neurogenin1 is controlled by local cues in the zebrafish embryo. Development *124*, 4557-4569.

Blader, P., Plessy, C., and Strahle, U. (2003). Multiple regulatory elements with spatially and temporally distinct activities control neurogenin1 expression in primary neurons of the zebrafish embryo. Mech Dev *120*, 211-218.

Bonnet, I., Marcq, P., Bosveld, F., Fetler, L., Bellaiche, Y., and Graner, F. (2012). Mechanical state, material properties and continuous description of an epithelial tissue. J R Soc Interface *9*, 2614-2623.

Brankatschk, M., and Dickson, B.J. (2006). Netrins guide Drosophila commissural axons at short range. Nat Neurosci *9*, 188-194.

Braubach, O.R., Fine, A., and Croll, R.P. (2012). Distribution and functional organization of glomeruli in the olfactory bulbs of zebrafish (Danio rerio). J Comp Neurol *520*, 2317-2339, Spc2311.

Bray, D. (1979). Mechanical tension produced by nerve cells in tissue culture. J Cell Sci *37*, 391-410.

Bray, D. (1984). Axonal growth in response to experimentally applied mechanical tension. Dev Biol *102*, 379-389.

Breau, M.A., Bonnet, I., Stoufflet, J., Xie, J., De Castro, S., and Schneider-Maunoury, S. (2017). Extrinsic mechanical forces mediate retrograde axon extension in a developing neuronal circuit. Nat Commun *8*, 282.

Breau, M.A., and Schneider-Maunoury, S. (2014). Mechanisms of cranial placode assembly. Int J Dev Biol *58*, 9-19.

Breau, M.A., and Schneider-Maunoury, S. (2017). [Stretch-induced axon growth: a universal, yet poorly explored process]. Biol Aujourdhui *211*, 215-222.

Breau, M.A., Wilson, D., Wilkinson, D.G., and Xu, Q. (2012). Chemokine and Fgf signalling act as opposing guidance cues in formation of the

lateral line primordium. Development *139*, 2246-2253.

Brodland, G.W., Veldhuis, J.H., Kim, S., Perrone, M., Mashburn, D., and Hutson, M.S. (2014). CellFIT: a cellular force-inference toolkit using curvilinear cell boundaries. PLoS One *9*, e99116.

Brugmann, S.A., Pandur, P.D., Kenyon, K.L., Pignoni, F., and Moody, S.A. (2004). Six1 promotes a placodal fate within the lateral neurogenic ectoderm by functioning as both a transcriptional activator and repressor. Development *131*, 5871-5881.

Brunet, T., Bouclet, A., Ahmadi, P., Mitrossilis, D., Driquez, B., Brunet, A.C., Henry, L., Serman, F., Bealle, G., Menager, C.*, et al.* (2013). Evolutionary conservation of early mesoderm specification by mechanotransduction in Bilateria. Nat Commun *4*, 2821.

Bryan, C.D., Casey, M.A., Pfeiffer, R.L., Jones, B.W., and Kwan, K.M. (2020). Optic cup morphogenesis requires neural crest-mediated basement membrane assembly. Development *147*.

Bryan, C.D., Chien, C.B., and Kwan, K.M. (2016). Loss of laminin alpha 1 results in multiple structural defects and divergent effects on adhesion during vertebrate optic cup morphogenesis. Dev Biol *416*, 324-337.

Budday, S., Steinmann, P., and Kuhl, E. (2015). Physical biology of human brain development. Front Cell Neurosci *9*, 257.

Buitrago-Delgado, E., Nordin, K., Rao, A., Geary, L., and LaBonne, C. (2015). NEURODEVELOPMENT. Shared regulatory programs suggest retention of blastula-stage potential in neural crest cells. Science *348*, 1332-1335.

Butcher, D.T., Alliston, T., and Weaver, V.M. (2009). A tense situation: forcing tumour progression. Nat Rev Cancer *9*, 108-122.

Butler, L.C., Blanchard, G.B., Kabla, A.J., Lawrence, N.J., Welchman, D.P., Mahadevan, L., Adams, R.J., and Sanson, B. (2009). Cell shape changes indicate a role for extrinsic tensile forces in Drosophila germ-band extension. Nat Cell Biol *11*, 859-864.

Cajal, S. (1909). Histologie du Système Nerveux de l´Homme et des Vertèbres (Paris).

Calvo-Ochoa, E., and Byrd-Jacobs, C.A. (2019). The Olfactory System of Zebrafish as a Model for the Study of Neurotoxicity and Injury: Implications for Neuroplasticity and Disease. Int J Mol Sci *20*.

Campas, O. (2016). A toolbox to explore the mechanics of living embryonic tissues. Semin Cell Dev Biol *55*, 119-130.

Campas, O., Mammoto, T., Hasso, S., Sperling, R.A., O'Connell, D., Bischof, A.G., Maas, R., Weitz, D.A., Mahadevan, L., and Ingber, D.E. (2014). Quantifying cell-generated mechanical forces within living embryonic tissues. Nat Methods *11*, 183-189.

Campbell, D.S., Regan, A.G., Lopez, J.S., Tannahill, D., Harris, W.A., and Holt, C.E. (2001). Semaphorin 3A elicits stage-dependent collapse, turning, and branching in Xenopus retinal growth cones. J Neurosci *21*, 8538-8547.

Campinho, P., Behrndt, M., Ranft, J., Risler, T., Minc, N., and Heisenberg, C.P. (2013). Tension-oriented cell divisions limit anisotropic tissue tension in epithelial spreading during zebrafish epiboly. Nat Cell Biol *15*, 1405-1414.

Carl, M., Loosli, F., and Wittbrodt, J. (2002). Six3 inactivation reveals its essential role for the formation and patterning of the vertebrate eye. Development *129*, 4057-4063.

Carrillo, A., and McHenry, M.J. (2016). Zebrafish learn to forage in the dark. J Exp Biol *219*, 582-589.

Carvalho, L., Stuhmer, J., Bois, J.S., Kalaidzidis, Y., Lecaudey, V., and Heisenberg, C.P. (2009). Control of convergent yolk syncytial layer nuclear movement in zebrafish. Development *136*, 1305-1315.

Casey, M.A., Lusk, S., and Kwan, K.M. (2021). Build me up optic cup: Intrinsic and extrinsic mechanisms of vertebrate eye morphogenesis. Dev Biol.

Cavodeassi, F. (2018). Dynamic Tissue Rearrangements during Vertebrate Eye Morphogenesis: Insights from Fish Models. J Dev Biol *6*.

Cavodeassi, F., Ivanovitch, K., and Wilson, S.W. (2013). Eph/Ephrin signalling maintains eye field segregation from adjacent neural plate territories during forebrain morphogenesis. Development *140*, 4193-4202.

Cebul, E.R., McLachlan, I.G., and Heiman, M.G. (2020). Dendrites with specialized glial attachments develop by retrograde extension using SAX-7 and GRDN-1. Development *147*.

Cechmanek, P.B., Hehr, C.L., and McFarlane, S. (2021). Retinal Pigment Epithelium and Neural Retinal Progenitors Interact Via Semaphorin 6D to Facilitate Optic Cup Morphogenesis. eNeuro.

Cechmanek, P.B., and McFarlane, S. (2017). Retinal pigment epithelium expansion around the neural retina occurs in two separate phases with distinct mechanisms. Dev Dyn *246*, 598-609.

Celik, A., Fuss, S.H., and Korsching, S.I. (2002). Selective targeting of zebrafish olfactory receptor neurons by the endogenous OMP promoter. Eur J Neurosci *15*, 798-806.

Chauhan, B.K., Disanza, A., Choi, S.Y., Faber, S.C., Lou, M., Beggs, H.E., Scita, G., Zheng, Y., and Lang, R.A. (2009). Cdc42- and IRSp53-dependent contractile filopodia tether presumptive lens and retina to coordinate epithelial invagination. Development *136*, 3657-3667.

Chisholm, A.D., and Hardin, J. (2005). Epidermal morphogenesis. WormBook, 1-22.

Chiu, C.H., Chou, C.W., Takada, S., and Liu, Y.W. (2012). Development and fibronectin signaling requirements of the zebrafish interrenal vessel. PLoS One *7*, e43040.

Clegg, R. (2009). Förster resonance energy transfer—FRET what is it, why do it, and how it's done. In Laboratory Techniques in Biochemistry and Molecular Biology (Elsevier), pp. 1-57.

Collas, P. (2010). The current state of chromatin immunoprecipitation. Mol Biotechnol *45*, 87-100.

Collinet, C., Rauzi, M., Lenne, P.F., and Lecuit, T. (2015). Local and tissue-scale forces drive oriented junction growth during tissue extension. Nat Cell Biol *17*, 1247-1258.

Couly, G., Grapin-Botton, A., Coltey, P., Ruhin, B., and Le Douarin, N.M. (1998). Determination of the identity of the derivatives of the cephalic neural crest: incompatibility between Hox gene expression and lower jaw development. Development *125*, 3445-3459.

Couly, G., and Le Douarin, N.M. (1990). Head morphogenesis in embryonic avian chimeras: evidence for a segmental pattern in the ectoderm corresponding to the neuromeres. Development *108*, 543-558.

Cummings, D.M., and Belluscio, L. (2010). Continuous neural plasticity in the olfactory intrabulbar circuitry. J Neurosci *30*, 9172-9180.

Dance, A. (2021). The secret forces that squeeze and pull life into shape. Nature *589*, 186-188.

De Vincentiis, S., Falconieri, A., Mainardi, M., Cappello, V., Scribano, V., Bizzarri, R., Storti, B., Dente, L., Costa, M., and Raffa, V. (2020a). Extremely Low Forces Induce Extreme Axon Growth. J Neurosci *40*, 4997-5007.

De Vincentiis, S., Falconieri, A., Scribano, V., Ghignoli, S., and Raffa, V. (2020b). Manipulation of Axonal Outgrowth via Exogenous Low Forces. Int J Mol Sci *21*.

Dennerll, T.J., Lamoureux, P., Buxbaum, R.E., and Heidemann, S.R. (1989). The cytomechanics of axonal elongation and retraction. J Cell Biol *109*, 3073-3083.

Dent, E.W., and Gertler, F.B. (2003). Cytoskeletal dynamics and transport in growth cone motility and axon guidance. Neuron *40*, 209-227.

Dhande, O.S., and Huberman, A.D. (2014). Retinal ganglion cell maps in the brain: implications for visual processing. Curr Opin Neurobiol *24*, 133-142.

Di Donato, V., De Santis, F., Auer, T.O., Testa, N., Sanchez-Iranzo, H., Mercader, N., Concordet, J.P., and Del Bene, F. (2016). 2C-Cas9: a versatile

tool for clonal analysis of gene function. Genome Res *26*, 681-692.

Dickson, B.J. (2002). Molecular mechanisms of axon guidance. Science *298*, 1959-1964.

Dona, E., Barry, J.D., Valentin, G., Quirin, C., Khmelinskii, A., Kunze, A., Durdu, S., Newton, L.R., Fernandez-Minan, A., Huber, W.*, et al.* (2013). Directional tissue migration through a self-generated chemokine gradient. Nature *503*, 285-289.

Dotti, C.G., and Banker, G.A. (1987). Experimentally induced alteration in the polarity of developing neurons. Nature *330*, 254-256.

Drescher, U., Kremoser, C., Handwerker, C., Loschinger, J., Noda, M., and Bonhoeffer, F. (1995). In vitro guidance of retinal ganglion cell axons by RAGS, a 25 kDa tectal protein related to ligands for Eph receptor tyrosine kinases. Cell *82*, 359-370.

Dubois, E.A., Zandbergen, M.A., Peute, J., and Goos, H.J. (2002). Evolutionary development of three gonadotropin-releasing hormone (GnRH) systems in vertebrates. Brain Res Bull *57*, 413-418.

Dumortier, J.G., Martin, S., Meyer, D., Rosa, F.M., and David, N.B. (2012). Collective mesendoderm migration relies on an intrinsic directionality signal transmitted through cell contacts. Proc Natl Acad Sci U S A *109*, 16945-16950.

Dutta, S., Dietrich, J.E., Aspock, G., Burdine, R.D., Schier, A., Westerfield, M., and Varga, Z.M. (2005). pitx3 defines an equivalence domain for lens and anterior pituitary placode. Development *132*, 1579-1590.

Eiraku, M., Takata, N., Ishibashi, H., Kawada, M., Sakakura, E., Okuda, S., Sekiguchi, K., Adachi, T., and Sasai, Y. (2011). Self-organizing optic-cup morphogenesis in three-dimensional culture. Nature *472*, 51-56.

Elosegui-Artola, A., Oria, R., Chen, Y., Kosmalska, A., Perez-Gonzalez, C., Castro, N., Zhu, C., Trepat, X., and Roca-Cusachs, P. (2016). Mechanical regulation of a molecular clutch defines force transmission and transduction in response to matrix rigidity. Nat Cell Biol *18*, 540-548.

Engl, T., Relja, B., Marian, D., Blumenberg, C., Muller, I., Beecken, W.D., Jones, J., Ringel, E.M., Bereiter-Hahn, J., Jonas, D.*, et al.* (2006). CXCR4 chemokine receptor mediates prostate tumor cell adhesion through alpha5 and beta3 integrins. Neoplasia *8*, 290-301.

Evans, M.G., Al-Shakli, A., and Chari, D.M. (2019). Electrophysiological properties of neurons grown on soft polymer scaffolds reveal the potential to develop neuromimetic culture environments. Integr Biol (Camb) *11*, 395-403.

Fagotto, F., Winklbauer, R., and Rohani, N. (2014). Ephrin-Eph signaling in embryonic tissue separation. Cell Adh Migr *8*, 308-326.

Fan, A., Joy, M.S.H., and Saif, T. (2019a). A connected cytoskeleton network generates axonal tension in embryonic Drosophila. Lab Chip *19*, 3133-3139.

Fan, A., Tofangchi, A., Kandel, M., Popescu, G., and Saif, T. (2017). Coupled circumferential and axial tension driven by actin and myosin influences in vivo axon diameter. Sci Rep *7*, 14188.

Fan, L., Kovacevic, I., Heiman, M.G., and Bao, Z. (2019b). A multicellular rosette-mediated collective dendrite extension. Elife *8*.

Flanagan, L.A., Ju, Y.E., Marg, B., Osterfield, M., and Janmey, P.A. (2002). Neurite branching on deformable substrates. Neuroreport *13*, 2411-2415.

Franze, K. (2020). Integrating Chemistry and Mechanics: The Forces Driving Axon Growth. Annu Rev Cell Dev Biol *36*, 61-83.

Franze, K., Gerdelmann, J., Weick, M., Betz, T., Pawlizak, S., Lakadamyali, M., Bayer, J., Rillich, K., Gogler, M., Lu, Y.B.*, et al.* (2009). Neurite branch retraction is caused by a threshold-dependent mechanical impact. Biophys J *97*, 1883-1890.

Franze, K., Janmey, P.A., and Guck, J. (2013). Mechanics in neuronal development and repair. Annu Rev Biomed Eng *15*, 227-251.

Fritzsch, B., Elliott, K.L., and Pavlinkova, G. (2019). Primary sensory map formations reflect unique needs and molecular cues specific to each sensory system. F1000Res *8*.

Fuhrmann, S. (2010). Eye morphogenesis and patterning of the optic vesicle. Curr Top Dev Biol *93*, 61-84.

Fuller, C.L., and Byrd, C.A. (2005). Ruffed cells identified in the adult zebrafish olfactory bulb. Neurosci Lett *379*, 190-194.

Fuller, C.L., Yettaw, H.K., and Byrd, C.A. (2006). Mitral cells in the olfactory bulb of adult zebrafish (Danio rerio): morphology and distribution. J Comp Neurol *499*, 218-230.

Galiano, M.R., Jha, S., Ho, T.S., Zhang, C., Ogawa, Y., Chang, K.J., Stankewich, M.C., Mohler, P.J., and Rasband, M.N. (2012). A distal axonal cytoskeleton forms an intra-axonal boundary that controls axon initial segment assembly. Cell *149*, 1125-1139.

Gangatharan, G., Schneider-Maunoury, S., and Breau, M.A. (2018). Role of mechanical cues in shaping neuronal morphology and connectivity. Biol Cell *110*, 125-136.

Garcia-Marin, V., Garcia-Lopez, P., and Freire, M. (2009). The growth cone as seen through Cajal's original histological preparations and publications. J Hist Neurosci *18*, 197-210.

Georges, P.C., Miller, W.J., Meaney, D.F., Sawyer, E.S., and Janmey, P.A. (2006). Matrices with compliance comparable to that of brain tissue select neuronal over glial growth in mixed cortical cultures. Biophys J *90*, 3012-3018.

Giger, F.A., and Houart, C. (2018). The Birth of the Eye Vesicle: When Fate Decision Equals Morphogenesis. Front Neurosci *12*, 87.

Gillard, G., Nicolle, O., Brugiere, T., Prigent, S., Pinot, M., and Michaux, G. (2019). Force Transmission between Three Tissues Controls Bipolar Planar Polarity Establishment and Morphogenesis. Curr Biol *29*, 1360-1368 e1364.

Glavic, A., Maris Honore, S., Gloria Feijoo, C., Bastidas, F., Allende, M.L., and Mayor, R. (2004). Role of BMP signaling and the homeoprotein Iroquois in the specification of the cranial placodal field. Dev Biol *272*, 89-103.

Goodwin, K., and Nelson, C.M. (2021). Mechanics of Development. Dev Cell *56*, 240-250.

Grabe, V., and Sachse, S. (2018). Fundamental principles of the olfactory code. Biosystems *164*, 94-101.

Graham, A., Blentic, A., Duque, S., and Begbie, J. (2007). Delamination of cells from neurogenic placodes does not involve an epithelial-to-mesenchymal transition. Development *134*, 4141-4145.

Grashoff, C., Hoffman, B.D., Brenner, M.D., Zhou, R., Parsons, M., Yang, M.T., McLean, M.A., Sligar, S.G., Chen, C.S., Ha, T.*, et al.* (2010). Measuring mechanical tension across vinculin reveals regulation of focal adhesion dynamics. Nature *466*, 263-266.

Greiling, T.M., and Clark, J.I. (2009). Early lens development in the zebrafish: a three-dimensional time-lapse analysis. Dev Dyn *238*, 2254-2265.

Greiling, T.M., and Clark, J.I. (2012). New insights into the mechanism of lens development using zebra fish. Int Rev Cell Mol Biol *296*, 1-61.

Gross, B., Shelton, E., Gomez, C., and Campas, O. (2021). STRESS, an automated geometrical characterization of deformable particles for in vivo measurements of cell and tissue mechanical stresses. BioRxiv.

Groves, A.K., and Bronner-Fraser, M. (2000). Competence, specification and commitment in otic placode induction. Development *127*, 3489-3499.

Guillon, E., Das, D., Jülich, D., Hassan, A.R., Geller, H., and Holley, S. (2020). Fibronectin is a smart adhesive that both influences and responds to the mechanics of early spinal column development. Elife *9*.

Gupta, M., Doss, B., Lim, C.T., Voituriez, R., and Ladoux, B. (2016). Single cell rigidity sensing: A complex relationship between focal adhesion dynamics and large-scale actin cytoskeleton remodeling. Cell Adh Migr *10*, 554-567.

Gurdon, J.B. (1987). Embryonic induction--molecular prospects. Development *99*, 285-306.

Habuchi, S., Tsutsui, H., Kochaniak, A.B., Miyawaki, A., and van Oijen, A.M. (2008). mKikGR, a monomeric photoswitchable fluorescent protein. PLoS One *3*, e3944.

Handorf, A.M., Zhou, Y., Halanski, M.A., and Li, W.J. (2015). Tissue stiffness dictates development, homeostasis, and disease progression. Organogenesis *11*, 1-15.

Hanovice, N.J., McMains, E., and Gross, J.M. (2016). A GAL4-inducible transgenic tool kit for the in vivo modulation of Rho GTPase activity in zebrafish. Dev Dyn *245*, 844-853.

Hansen, A., and Zeiske, E. (1993). Development of the olfactory organ in the zebrafish, Brachydanio rerio. J Comp Neurol *333*, 289-300.

Hansen, A., and Zeiske, E. (1998). The peripheral olfactory organ of the zebrafish, Danio rerio: an ultrastructural study. Chem Senses *23*, 39-48.

Harden, M.V., Pereiro, L., Ramialison, M., Wittbrodt, J., Prasad, M.K., McCallion, A.S., and Whitlock, K.E. (2012). Close association of olfactory placode precursors and cranial neural crest cells does not predestine cell mixing. Dev Dyn *241*, 1143-1154.

Hartmann, T.N., Burger, J.A., Glodek, A., Fujii, N., and Burger, M. (2005). CXCR4 chemokine receptor and integrin signaling co-operate in mediating adhesion and chemoresistance in small cell lung cancer (SCLC) cells. Oncogene *24*, 4462-4471.

Hashiguchi, Y., and Nishida, M. (2007). Evolution of trace amine associated receptor (TAAR) gene family in vertebrates: lineage-specific expansions and degradations of a second class of vertebrate chemosensory receptors expressed in the olfactory epithelium. Mol Biol Evol *24*, 2099-2107.

Hedgecock, E.M., Culotti, J.G., and Hall, D.H. (1990). The unc-5, unc-6, and unc-40 genes guide circumferential migrations of pioneer axons and mesodermal cells on the epidermis in C. elegans. Neuron *4*, 61-85.

Heermann, S., Schutz, L., Lemke, S., Krieglstein, K., and Wittbrodt, J. (2015). Eye morphogenesis driven by epithelial flow into the optic cup facilitated by modulation of bone morphogenetic protein. Elife *4*.

Heiman, M.G., and Shaham, S. (2009). DEX-1 and DYF-7 establish sensory dendrite length by anchoring dendritic tips during cell migration. Cell *137*, 344-355.

Herculano-Houzel, S. (2009). The human brain in numbers: a linearly scaled-up primate brain. Front Hum Neurosci *3*, 31.

Hildebrandt, N. (2013). How to Apply FRET: From Experimental Design to Data Analysis. In FRET – Förster Resonance Energy Transfer, I. Medintz, and N. Hildebrandt, eds.

Hill, A., Howard, C.V., Strahle, U., and Cossins, A. (2003). Neurodevelopmental defects in zebrafish (Danio rerio) at environmentally relevant dioxin (TCDD) concentrations. Toxicol Sci *76*, 392-399.

Hoijman, E., Fargas, L., Blader, P., and Alsina, B. (2017). Pioneer neurog1 expressing cells ingress into the otic epithelium and instruct neuronal specification. Elife *6*.

Honig, M.G., Petersen, G.G., Rutishauser, U.S., and Camilli, S.J. (1998). In vitro studies of growth cone behavior support a role for fasciculation mediated by cell adhesion molecules in sensory axon guidance during development. Dev Biol *204*, 317-326.

Hyer, J., Kuhlman, J., Afif, E., and Mikawa, T. (2003). Optic cup morphogenesis requires pre-lens ectoderm but not lens differentiation. Dev Biol *259*, 351-363.

Iida, A., Wang, Z., Hirata, H., and Sehara-Fujisawa, A. (2018). Integrin beta1 activity is required for cardiovascular formation in zebrafish. Genes Cells *23*, 938-951.

Inbal, A., Kim, S.H., Shin, J., and Solnica-Krezel, L. (2007). Six3 represses nodal activity to establish early brain asymmetry in zebrafish. Neuron *55*, 407-415.

Ishihara, S., and Sugimura, K. (2012). Bayesian inference of force dynamics during morphogenesis. J Theor Biol *313*, 201-211.

Ishihara, S., Sugimura, K., Cox, S.J., Bonnet, I., Bellaiche, Y., and Graner, F. (2013). Comparative study of non-invasive force and stress inference methods in tissue. Eur Phys J E Soft Matter *36*, 9859.

Ivanovitch, K., Cavodeassi, F., and Wilson, S.W. (2013). Precocious acquisition of neuroepithelial character in the eye field underlies the onset of eye morphogenesis. Dev Cell *27*, 293-305.

Javier-Torrent, M., Zimmer-Bensch, G., and Nguyen, L. (2021). Mechanical Forces Orchestrate Brain Development. Trends Neurosci *44*, 110-121.

Jessen, K.R. (2004). Glial cells. Int J Biochem Cell Biol *36*, 1861-1867.

Jiang, F.X., Yurke, B., Schloss, R.S., Firestein, B.L., and Langrana, N.A. (2010). Effect of dynamic stiffness of the substrates on neurite outgrowth by using a DNA-crosslinked hydrogel. Tissue Eng Part A *16*, 1873-1889.

Johnston, M.C., Noden, D.M., Hazelton, R.D., Coulombre, J.L., and Coulombre, A.J. (1979). Origins of avian ocular and periocular tissues. Exp Eye Res *29*, 27-43.

Jones, S.L., and Svitkina, T.M. (2016). Axon Initial Segment Cytoskeleton: Architecture, Development, and Role in Neuron Polarity. Neural Plast *2016*, 6808293.

Kaeppler, K., and Mueller, F. (2013). Odor classification: a review of factors influencing perception-based odor arrangements. Chem Senses *38*, 189-209.

Kay, J.N., Finger-Baier, K.C., Roeser, T., Staub, W., and Baier, H. (2001). Retinal ganglion cell genesis requires lakritz, a Zebrafish atonal Homolog. Neuron *30*, 725-736.

Kennedy, T.E., Serafini, T., de la Torre, J.R., and Tessier-Lavigne, M. (1994). Netrins are diffusible chemotropic factors for commissural axons in the embryonic spinal cord. Cell *78*, 425-435.

Kepiro, M., Varkuti, B.H., Bodor, A., Hegyi, G., Drahos, L., Kovacs, M., and Malnasi-Csizmadia, A. (2012). Azidoblebbistatin, a photoreactive myosin inhibitor. Proc Natl Acad Sci U S A *109*, 9402-9407.

Kepiro, M., Varkuti, B.H., Rauscher, A.A., Kellermayer, M.S.Z., Varga, M., and Malnasi-Csizmadia, A. (2015). Molecular tattoo: subcellular confinement of drug effects. Chem Biol *22*, 548-558.

Kermen, F., Franco, L.M., Wyatt, C., and Yaksi, E. (2013). Neural circuits mediating olfactory-driven behavior in fish. Front Neural Circuits *7*, 62.

Kidd, T., Bland, K.S., and Goodman, C.S. (1999). Slit is the midline repellent for the robo receptor in Drosophila. Cell *96*, 785-794.

Klee, E.W. (2008). The zebrafish secretome. Zebrafish *5*, 131-138.

Knaut, H., Blader, P., Strahle, U., and Schier, A.F. (2005). Assembly of trigeminal sensory ganglia by chemokine signaling. Neuron *47*, 653-666.

Koch, D., Rosoff, W.J., Jiang, J., Geller, H.M., and Urbach, J.S. (2012). Strength in the periphery: growth cone biomechanics and substrate rigidity response in peripheral and central nervous system neurons. Biophys J *102*, 452-460.

Koenig, K.M., and Gross, J.M. (2020). Evolution and development of complex eyes: a celebration of diversity. Development *147*.

Koenig, K.M., Sun, P., Meyer, E., and Gross, J.M. (2016). Eye development and photoreceptor differentiation in the cephalopod Doryteuthis pealeii. Development *143*, 3168-3181.

Kolodkin, A.L., Matthes, D.J., O'Connor, T.P., Patel, N.H., Admon, A., Bentley, D., and Goodman, C.S. (1992). Fasciclin IV: sequence, expression, and function during growth cone guidance in the grasshopper embryo. Neuron *9*, 831-845.

Kolodkin, A.L., and Tessier-Lavigne, M. (2011). Mechanisms and molecules of neuronal wiring: a primer. Cold Spring Harb Perspect Biol *3*.

Koser, D.E., Thompson, A.J., Foster, S.K., Dwivedy, A., Pillai, E.K., Sheridan, G.K., Svoboda, H., Viana, M., Costa, L.D., Guck, J.*, et al.* (2016). Mechanosensing is critical for axon growth in the developing brain. Nat Neurosci *19*, 1592-1598.

Kozlowski, D.J., Murakami, T., Ho, R.K., and Weinberg, E.S. (1997). Regional cell movement and tissue patterning in the zebrafish embryo revealed by fate mapping with caged fluorescein. Biochem Cell Biol *75*, 551-562.

Kretzschmar, K., and Watt, F.M. (2012). Lineage tracing. Cell *148*, 33-45.

Kruse-Bend, R., Rosenthal, J., Quist, T.S., Veien, E.S., Fuhrmann, S., Dorsky, R.I., and Chien, C.B. (2012). Extraocular ectoderm triggers dorsal retinal fate during optic vesicle evagination in zebrafish. Dev Biol *371*, 57-65.

Kwan, K.M., Otsuna, H., Kidokoro, H., Carney, K.R., Saijoh, Y., and Chien, C.B. (2012). A complex choreography of cell movements shapes the vertebrate eye. Development *139*, 359-372.

Lagendijk, A.K., Gomez, G.A., Baek, S., Hesselson, D., Hughes, W.E., Paterson, S., Conway, D.E., Belting, H.G., Affolter, M., Smith, K.A.*, et al.* (2017). Live imaging molecular changes in junctional tension upon VE-cadherin in zebrafish. Nat Commun *8*, 1402.

Lakhina, V., Marcaccio, C.L., Shao, X., Lush, M.E., Jain, R.A., Fujimoto, E., Bonkowsky, J.L., Granato, M., and Raper, J.A. (2012). Netrin/DCC signaling guides olfactory sensory axons to their correct location in the olfactory bulb. J Neurosci *32*, 4440-4456.

Lamoureux, P., Buxbaum, R.E., and Heidemann, S.R. (1989). Direct evidence that growth cones pull. Nature *340*, 159-162.

Lamoureux, P., Heidemann, S.R., Martzke, N.R., and Miller, K.E. (2010). Growth and elongation within and along the axon. Dev Neurobiol *70*, 135-149.

Lamoureux, P., Ruthel, G., Buxbaum, R.E., and Heidemann, S.R. (2002). Mechanical tension can specify axonal fate in hippocampal neurons. J Cell Biol *159*, 499-508.

Langenberg, T., Kahana, A., Wszalek, J.A., and Halloran, M.C. (2008). The eye organizes neural crest cell migration. Dev Dyn *237*, 1645-1652.

Lantoine, J., Grevesse, T., Villers, A., Delhaye, G., Mestdagh, C., Versaevel, M., Mohammed, D., Bruyere, C., Alaimo, L., Lacour, S.P.*, et al.* (2016). Matrix stiffness modulates formation and activity of neuronal networks of controlled architectures. Biomaterials *89*, 14-24.

Lardennois, A., Pasti, G., Ferraro, T., Llense, F., Mahou, P., Pontabry, J., Rodriguez, D., Kim, S., Ono, S., Beaurepaire, E.*, et al.* (2019). An actin-based viscoplastic lock ensures progressive body-axis elongation. Nature *573*, 266-270.

Lassiter, R.N., Reynolds, S.B., Marin, K.D., Mayo, T.F., and Stark, M.R. (2009). FGF signaling is essential for ophthalmic trigeminal placode cell delamination and differentiation. Dev Dyn *238*, 1073-1082.

Lassiter, R.N., Stark, M.R., Zhao, T., and Zhou, C.J. (2014). Signaling mechanisms controlling cranial placode neurogenesis and delamination. Dev Biol *389*, 39-49.

Lecuit, T., and Le Goff, L. (2007). Orchestrating size and shape during morphogenesis. Nature *450*, 189-192.

Lecuit, T., Lenne, P.F., and Munro, E. (2011). Force generation, transmission, and integration during cell and tissue morphogenesis. Annu Rev Cell Dev Biol *27*, 157-184.

Lesaffre, B., Joliot, A., Prochiantz, A., and Volovitch, M. (2007). Direct non-cell autonomous Pax6 activity regulates eye development in the zebrafish. Neural Dev *2*, 2.

Leterrier, C. (2018). The Axon Initial Segment: An Updated Viewpoint. J Neurosci *38*, 2135-2145.

Lewellis, S.W., Nagelberg, D., Subedi, A., Staton, A., LeBlanc, M., Giraldez, A., and Knaut, H. (2013). Precise SDF1-mediated cell guidance is achieved through ligand clearance and microRNA-mediated decay. J Cell Biol *200*, 337-355.

Lindsay, S.M., and Vogt, R.G. (2004). Behavioral responses of newly hatched zebrafish (Danio rerio) to amino acid chemostimulants. Chem Senses *29*, 93-100.

Litsiou, A., Hanson, S., and Streit, A. (2005). A balance of FGF, BMP and WNT signalling positions the future placode territory in the head. Development *132*, 4051-4062.

Liu, T.L., Upadhyayula, S., Milkie, D.E., Singh, V., Wang, K., Swinburne, I.A., Mosaliganti, K.R., Collins, Z.M., Hiscock, T.W., Shea, J.*, et al.* (2018). Observing the cell in its native state: Imaging subcellular dynamics in multicellular organisms. Science *360*.

Loosli, F., Staub, W., Finger-Baier, K.C., Ober, E.A., Verkade, H., Wittbrodt, J., and Baier, H. (2003). Loss of eyes in zebrafish caused by mutation of chokh/rx3. EMBO Rep *4*, 894-899.

Loverde, J.R., and Pfister, B.J. (2015). Developmental axon stretch stimulates neuron growth while maintaining normal electrical activity, intracellular calcium flux, and somatic morphology. Front Cell Neurosci *9*, 308.

Loverde, J.R., Tolentino, R.E., Soteropoulos, P., and Pfister, B.J. (2020). Biomechanical Forces Regulate Gene Transcription During Stretch-Mediated Growth of Mammalian Neurons. Front Neurosci *14*, 600136.

Lowery, L.A., and Van Vactor, D. (2009). The trip of the tip: understanding the growth cone machinery. Nat Rev Mol Cell Biol *10*, 332-343.

Lye, C.M., Blanchard, G.B., Naylor, H.W., Muresan, L., Huisken, J., Adams, R.J., and Sanson, B. (2015). Mechanical Coupling between Endoderm Invagination and Axis Extension in Drosophila. PLoS Biol *13*, e1002292.

Madelaine, R., Garric, L., and Blader, P. (2011). Partially redundant proneural function reveals the importance of timing during zebrafish olfactory neurogenesis. Development *138*, 4753-4762.

Maharana, S.K., and Schlosser, G. (2018). A gene regulatory network underlying the formation of pre-placodal ectoderm in Xenopus laevis. BMC Biol *16*, 79.

Maiorana, V.C., and Van Valen, L.M. (2020). Animal - Nervous System. In Encyclopedia Britannica.

Maitre, J.L., Berthoumieux, H., Krens, S.F., Salbreux, G., Julicher, F., Paluch, E., and Heisenberg, C.P. (2012). Adhesion functions in cell sorting by mechanically coupling the cortices of adhering cells. Science *338*, 253-256.

Mangold, O., and Spemann, H. (1927). Wilhelm Roux Arch Entwickl Mech Org *111*, 341-422.

Martinez-Morales, J.R., Cavodeassi, F., and Bovolenta, P. (2017). Coordinated Morphogenetic Mechanisms Shape the Vertebrate Eye. Front Neurosci *11*, 721.

Martinez-Morales, J.R., Rembold, M., Greger, K., Simpson, J.C., Brown, K.E., Quiring, R., Pepperkok, R., Martin-Bermudo, M.D., Himmelbauer, H., and Wittbrodt, J. (2009). ojoplano-mediated basal constriction is essential for optic cup morphogenesis. Development *136*, 2165-2175.

Martinez-Morales, J.R., and Wittbrodt, J. (2009). Shaping the vertebrate eye. Curr Opin Genet Dev *19*, 511-517.

Mason, I. (2007). Initiation to end point: the multiple roles of fibroblast growth factors in neural development. Nat Rev Neurosci *8*, 583-596.

Matejcic, M., Salbreux, G., and Norden, C. (2018). A non-cell-autonomous actin redistribution enables isotropic retinal growth. PLoS Biol *16*, e2006018.

Mathers, P.H., Grinberg, A., Mahon, K.A., and Jamrich, M. (1997). The Rx homeobox gene is essential for vertebrate eye development. Nature *387*, 603-607.

Mathers, P.H., and Jamrich, M. (2000). Regulation of eye formation by the Rx and pax6 homeobox genes. Cell Mol Life Sci *57*, 186-194.

Maurer, M., and Lammerding, J. (2019). The Driving Force: Nuclear Mechanotransduction in Cellular Function, Fate, and Disease. Annu Rev Biomed Eng *21*, 443-468.

Minina, S., Reichman-Fried, M., and Raz, E. (2007). Control of receptor internalization, signaling level, and precise arrival at the target in guided cell migration. Curr Biol *17*, 1164-1172.

Mitrossilis, D., Roper, J.C., Le Roy, D., Driquez, B., Michel, A., Menager, C., Shaw, G., Le Denmat, S., Ranno, L., Dumas-Bouchiat, F.*, et al.* (2017). Mechanotransductive cascade of Myo-II-dependent mesoderm and endoderm invaginations in embryo gastrulation. Nat Commun *8*, 13883.

Miyasaka, N., Knaut, H., and Yoshihara, Y. (2007). Cxcl12/Cxcr4 chemokine signaling is required for placode assembly and sensory axon pathfinding in the zebrafish olfactory system. Development *134*, 2459-2468.

Miyasaka, N., Sato, Y., Yeo, S.Y., Hutson, L.D., Chien, C.B., Okamoto, H., and Yoshihara, Y. (2005). Robo2 is required for establishment of a precise glomerular map in the zebrafish olfactory system. Development *132*, 1283-1293.

Miyasaka, N., Wanner, A.A., Li, J., Mack-Bucher, J., Genoud, C., Yoshihara, Y., and Friedrich, R.W. (2013). Functional development of the olfactory system in zebrafish. Mech Dev *130*, 336-346.

Mongera, A., Rowghanian, P., Gustafson, H.J., Shelton, E., Kealhofer, D.A., Carn, E.K., Serwane, F., Lucio, A.A., Giammona, J., and Campas, O. (2018). A fluid-to-solid jamming transition underlies vertebrate body axis elongation. Nature *561*, 401-405.

Monier, B., and Suzanne, M. (2015). The Morphogenetic Role of Apoptosis. Curr Top Dev Biol *114*, 335-362.

Moreno-Marmol, T., Cavodeassi, F., and Bovolenta, P. (2018). Setting Eyes on the Retinal Pigment Epithelium. Front Cell Dev Biol *6*, 145.

Moreno-Marmol, T., Ledesma-Terron, T., Tabanera, N., Martin-Bermejo, M.J., Cardozo, M.J., Cavodeassi, F., and Bovolenta, P. (2020). Stretching of the retinal pigment epithelium contributes to zebrafish optic cup morphogenesis. BioRXiv.

Mori, K., and Sakano, H. (2011). How is the olfactory map formed and interpreted in the mammalian brain? Annu Rev Neurosci *34*, 467-499.

Mortimer, D., Fothergill, T., Pujic, Z., Richards, L.J., and Goodhill, G.J. (2008). Growth cone chemotaxis. Trends Neurosci *31*, 90-98.

Munster, S., Jain, A., Mietke, A., Pavlopoulos, A., Grill, S.W., and Tomancak, P. (2019). Attachment of the blastoderm to the vitelline envelope affects gastrulation of insects. Nature *568*, 395-399.

Nagase, H., and Woessner, J.F., Jr. (1999). Matrix metalloproteinases. J Biol Chem *274*, 21491-21494.

Nair, S., and Schilling, T.F. (2008). Chemokine signaling controls endodermal migration during zebrafish gastrulation. Science *322*, 89-92.

Nguyen, H., Boix-Fabres, J., Peyrieras, N., and Kardash, E. (2019). 3D + Time Imaging and Image Reconstruction of Pectoral Fin During Zebrafish Embryogenesis. Methods Mol Biol *2040*, 135-153.

Nicolas-Perez, M., Kuchling, F., Letelier, J., Polvillo, R., Wittbrodt, J., and Martinez-Morales, J.R. (2016). Analysis of cellular behavior and cytoskeletal dynamics reveal a constriction mechanism driving optic cup morphogenesis. Elife *5*.

NIH-Website, N.C.I. (2021). Nerve tissue.

Niu, X., Gao, C., Jan Lo, L., Luo, Y., Meng, C., Hong, J., Hong, W., and Peng, J. (2012). Sec13 safeguards the integrity of the endoplasmic reticulum and organogenesis of the digestive system in zebrafish. Dev Biol *367*, 197-207.

Niu, X., Hong, J., Zheng, X., Melville, D.B., Knapik, E.W., Meng, A., and Peng, J. (2014). The nuclear pore complex function of Sec13 protein is required for cell survival during retinal development. J Biol Chem *289*, 11971-11985.

Nornes, S., Clarkson, M., Mikkola, I., Pedersen, M., Bardsley, A., Martinez, J.P., Krauss, S., and Johansen, T. (1998). Zebrafish contains two pax6 genes involved in eye development. Mech Dev *77*, 185-196.

Ortiz, A., Kardash, E., and Peyrieras, N. (2019). 3D+time imaging of normal and twin sea urchin embryos for the reconstruction of their cell lineage. Methods Cell Biol *151*, 399-418.

Pakkenberg, B., Pelvig, D., Marner, L., Bundgaard, M.J., Gundersen, H.J., Nyengaard, J.R., and Regeur, L. (2003). Aging and the human neocortex. Exp Gerontol *38*, 95-99.

Pasquale, E.B. (2008). Eph-ephrin bidirectional signaling in physiology and disease. Cell *133*, 38-52.

Paulus, J.D., Willer, G.B., Willer, J.R., Gregg, R.G., and Halloran, M.C. (2009). Muscle contractions guide rohon-beard peripheral sensory axons. J Neurosci *29*, 13190-13201.

Pedersen, M.E., Vuong, T.T., Ronning, S.B., and Kolset, S.O. (2015). Matrix metalloproteinases in fish biology and matrix turnover. Matrix Biol *44-46*, 86-93.

Pei, Y.F., and Rhodin, J.A. (1970). The prenatal development of the mouse eye. Anat Rec *168*, 105-125.

Petridou, N.I., and Heisenberg, C.P. (2019). Tissue rheology in embryonic organization. EMBO J *38*, e102497.

Pfister, B.J., Bonislawski, D.P., Smith, D.H., and Cohen, A.S. (2006). Stretch-grown axons retain the ability to transmit active electrical signals. FEBS Lett *580*, 3525-3531.

Pfister, B.J., Iwata, A., Meaney, D.F., and Smith, D.H. (2004). Extreme stretch growth of integrated axons. J Neurosci *24*, 7978-7983.

Picker, A., Cavodeassi, F., Machate, A., Bernauer, S., Hans, S., Abe, G., Kawakami, K., Wilson, S.W., and Brand, M. (2009). Dynamic coupling of pattern formation and morphogenesis in the developing vertebrate retina. PLoS Biol *7*, e1000214.

Pieper, M., Ahrens, K., Rink, E., Peter, A., and Schlosser, G. (2012). Differential distribution of competence for panplacodal and neural crest induction to non-neural and neural ectoderm. Development *139*, 1175-1187.

Piper, M., Anderson, R., Dwivedy, A., Weinl, C., van Horck, F., Leung, K.M., Cogill, E., and Holt, C. (2006). Signaling mechanisms underlying Slit2-induced collapse of Xenopus retinal growth cones. Neuron *49*, 215-228.

Polleux, F., and Snider, W. (2010). Initiating and growing an axon. Cold Spring Harb Perspect Biol *2*, a001925.

Pontani, L.L., Jorjadze, I., and Brujic, J. (2016). Cis and Trans Cooperativity of E-Cadherin Mediates Adhesion in Biomimetic Lipid Droplets. Biophys J *110*, 391-399.

Pontani, L.L., Jorjadze, I., Viasnoff, V., and Brujic, J. (2012). Biomimetic emulsions reveal the effect of mechanical forces on cell-cell adhesion. Proc Natl Acad Sci U S A *109*, 9839-9844.

Porazinski, S., Wang, H., Asaoka, Y., Behrndt, M., Miyamoto, T., Morita, H., Hata, S., Sasaki, T., Krens, S.F.G., Osada, Y.*, et al.* (2015). YAP is essential for tissue tension to ensure vertebrate 3D body shape. Nature *521*, 217-221.

Pukhlyakova, E., Aman, A.J., Elsayad, K., and Technau, U. (2018). beta-Catenin-dependent mechanotransduction dates back to the common ancestor of Cnidaria and Bilateria. Proc Natl Acad Sci U S A *115*, 6231-6236.

Rajagopalan, J., Tofangchi, A., and MT, A.S. (2010). Drosophila neurons actively regulate axonal tension in vivo. Biophys J *99*, 3208-3215.

Ranade, S.S., Syeda, R., and Patapoutian, A. (2015). Mechanically Activated Ion Channels. Neuron *87*, 1162-1179.

Ranjan, V.D., Qiu, L., Tan, E.K., Zeng, L., and Zhang, Y. (2018). Modelling Alzheimer's disease: Insights from in vivo to in vitro three-dimensional culture platforms. J Tissue Eng Regen Med *12*, 1944-1958.

Rauscher, A.A., Gyimesi, M., Kovacs, M., and Malnasi-Csizmadia, A. (2018). Targeting Myosin by Blebbistatin Derivatives: Optimization and Pharmacological Potential. Trends Biochem Sci *43*, 700-713.

Rauzi, M., Lenne, P.F., and Lecuit, T. (2010). Planar polarized actomyosin contractile flows control epithelial junction remodelling. Nature *468*, 1110-1114.

Rebagliati, M.R., Toyama, R., Haffter, P., and Dawid, I.B. (1998). cyclops encodes a nodal-related factor involved in midline signaling. Proc Natl Acad Sci U S A *95*, 9932-9937.

Reiten, I., Uslu, F.E., Fore, S., Pelgrims, R., Ringers, C., Diaz Verdugo, C., Hoffman, M., Lal, P., Kawakami, K., Pekkan, K.*, et al.* (2017). Motile-Cilia-Mediated Flow Improves Sensitivity and Temporal Resolution of Olfactory Computations. Curr Biol *27*, 166-174.

Rembold, M., Loosli, F., Adams, R.J., and Wittbrodt, J. (2006). Individual cell migration serves as the driving force for optic vesicle evagination. Science *313*, 1130-1134.

Rhinn, M., Lun, K., Ahrendt, R., Geffarth, M., and Brand, M. (2009). Zebrafish gbx1 refines the midbrain-hindbrain boundary border and mediates the Wnt8 posteriorization signal. Neural Dev *4*, 12.

Roca-Cusachs, P., Sunyer, R., and Trepat, X. (2013). Mechanical guidance of cell migration: lessons from chemotaxis. Curr Opin Cell Biol *25*, 543-549.

Roellig, D., Tan-Cabugao, J., Esaian, S., and Bronner, M.E. (2017). Dynamic transcriptional signature and cell fate analysis reveals plasticity of individual neural plate border cells. Elife *6*.

Roffay, C., Chan, C.J., Guirao, B., Hiiragi, T., and Graner, F. (2021). Inferring cell junction tension and pressure from cell geometry. Development *148*.

Rojas-Munoz, A., Dahm, R., and Nusslein-Volhard, C. (2005). chokh/rx3 specifies the retinal pigment epithelium fate independently of eye morphogenesis. Dev Biol *288*, 348-362.

Roussos, E.T., Condeelis, J.S., and Patsialou, A. (2011). Chemotaxis in cancer. Nat Rev Cancer *11*, 573-587.

Salari, S., and Bagheri, M. (2019). In vivo, in vitro and pharmacologic models of Parkinson's disease. Physiol Res *68*, 17-24.

Samuel, A., Rubinstein, A.M., Azar, T.T., Ben-Moshe Livne, Z., Kim, S.H., and Inbal, A. (2016). Six3 regulates optic nerve development via multiple mechanisms. Sci Rep *6*, 20267.

Sato, Y., Miyasaka, N., and Yoshihara, Y. (2005). Mutually exclusive glomerular innervation by two distinct types of olfactory sensory neurons revealed in transgenic zebrafish. J Neurosci *25*, 4889-4897.

Sato, Y., Miyasaka, N., and Yoshihara, Y. (2007). Hierarchical regulation of odorant receptor gene choice and subsequent axonal projection of olfactory sensory neurons in zebrafish. J Neurosci *27*, 1606-1615.

Saxena, A.K., Singh, D., and Gupta, J. (2010). Role of stem cell research in therapeutic purpose--a hope for new horizon in medical biotechnology. J Exp Ther Oncol *8*, 223-233.

Scheib, J.J., Pozzuto, J.M., and Byrd-Jacobs, C.A. (2019). Reversible deafferentation of the zebrafish olfactory bulb with wax plug insertion. J Neurosci Methods *311*, 47-56.

Schier, A.F., Neuhauss, S.C., Harvey, M., Malicki, J., Solnica-Krezel, L., Stainier, D.Y., Zwartkruis, F., Abdelilah, S., Stemple, D.L., Rangini, Z.*, et al.* (1996). Mutations affecting the development of the embryonic zebrafish brain. Development *123*, 165-178.

Schlosser, G. (2010). Making senses development of vertebrate cranial placodes. Int Rev Cell Mol Biol *283*, 129-234.

Schlosser, G. (2014). Early embryonic specification of vertebrate cranial placodes. Wiley Interdiscip Rev Dev Biol *3*, 349-363.

Schmidt, K., Cavodeassi, F., Feng, Y., and Stephens, D.J. (2013). Early stages of retinal development depend on Sec13 function. Biol Open *2*, 256-266.

Schmitt, E.A., and Dowling, J.E. (1994). Early Eye Morphogenesis in the Zebrafish,

Brachydanio rerio. The Journal of Comparative Neurology, 532-542.

Schotz, E.M., Lanio, M., Talbot, J.A., and Manning, M.L. (2013). Glassy dynamics in three-dimensional embryonic tissues. J R Soc Interface *10*, 20130726.

Schreiner, C.E., and Winer, J.A. (2007). Auditory cortex mapmaking: principles, projections, and plasticity. Neuron *56*, 356-365.

Schwayer, C., Shamipour, S., Pranjic-Ferscha, K., Schauer, A., Balda, M., Tada, M., Matter, K., and Heisenberg, C.P. (2019). Mechanosensation of Tight Junctions Depends on ZO-1 Phase Separation and Flow. Cell *179*, 937-952 e918.

Seo, J., Youn, W., Choi, J.Y., Cho, H., Choi, H., Lanara, C., Stratakis, E., and Choi, I.S. (2020). Neuro-taxis: Neuronal movement in gradients of chemical and physical environments. Dev Neurobiol *80*, 361-377.

Shao, X., Lakhina, V., Dang, P., Cheng, R.P., Marcaccio, C.L., and Raper, J.A. (2017). Olfactory sensory axons target specific protoglomeruli in the olfactory bulb of zebrafish. Neural Dev *12*, 18.

Shellard, A., and Mayor, R. (2016). Chemotaxis during neural crest migration. Semin Cell Dev Biol *55*, 111-118.

Shi, P., and Zhang, J. (2009). Extraordinary diversity of chemosensory receptor gene repertoires among vertebrates. Results Probl Cell Differ *47*, 1-23.

Short, C.A., Onesto, M.M., Rempel, S.K., Catlett, T.S., and Gomez, T.M. (2021). Familiar growth factors have diverse roles in neural network assembly. Curr Opin Neurobiol *66*, 233-239.

Sidhaye, J., and Norden, C. (2017). Concerted action of neuroepithelial basal shrinkage and active epithelial migration ensures efficient optic cup morphogenesis. Elife *6*.

Siechen, S., Yang, S., Chiba, A., and Saif, T. (2009). Mechanical tension contributes to clustering of neurotransmitter vesicles at presynaptic terminals. Proc Natl Acad Sci U S A *106*, 12611-12616.

Smit, D., Fouquet, C., Pincet, F., Zapotocky, M., and Trembleau, A. (2017). Axon tension regulates fasciculation/defasciculation through the control of axon shaft zippering. Elife *6*.

Smutny, M., Akos, Z., Grigolon, S., Shamipour, S., Ruprecht, V., Capek, D., Behrndt, M., Papusheva, E., Tada, M., Hof, B.*, et al.* (2017). Friction forces position the neural anlage. Nat Cell Biol *19*, 306-317.

Steventon, B., Mayor, R., and Streit, A. (2012). Mutual repression between Gbx2 and Otx2 in sensory placodes reveals a general mechanism for ectodermal patterning. Dev Biol *367*, 55-65.

Steventon, B., Mayor, R., and Streit, A. (2014). Neural crest and placode interaction during the development of the cranial sensory system. Dev Biol *389*, 28-38.

Stigloher, C., Ninkovic, J., Laplante, M., Geling, A., Tannhauser, B., Topp, S., Kikuta, H., Becker, T.S., Houart, C., and Bally-Cuif, L. (2006). Segregation of telencephalic and eye-field identities inside the zebrafish forebrain territory is controlled by Rx3. Development *133*, 2925-2935.

Stoeckli, E.T. (2018). Understanding axon guidance: are we nearly there yet? Development *145*.

Streit, A. (2002). Extensive cell movements accompany formation of the otic placode. Dev Biol *249*, 237-254.

Stundl, J., Bertucci, P.Y., Lauri, A., Arendt, D., and Bronner, M.E. (2021). Evolution of new cell types at the lateral neural border. Curr Top Dev Biol *141*, 173-205.

Sugimura, K., Lenne, P.F., and Graner, F. (2016). Measuring forces and stresses in situ in living tissues. Development *143*, 186-196.

Suter, T., and Jaworski, A. (2019). Cell migration and axon guidance at the border between central and peripheral nervous system. Science *365*.

Svoboda, K.K., and O'Shea, K.S. (1987). An analysis of cell shape and the neuroepithelial basal lamina during optic vesicle formation in the mouse embryo. Development *100*, 185-200.

Takamiya, M., Stegmaier, J., Kobitski, A.Y., Schott, B., Weger, B.D., Margariti, D., Cereceda Delgado, A.R., Gourain, V., Scherr, T., Yang, L., *et al.* (2020). Pax6 organizes the anterior eye segment by guiding two distinct neural crest waves. PLoS Genet *16*, e1008774.

Theveneau, E., Steventon, B., Scarpa, E., Garcia, S., Trepat, X., Streit, A., and Mayor, R. (2013). Chase-and-run between adjacent cell populations promotes directional collective migration. Nat Cell Biol *15*, 763-772.

Thiery, A., Buzzi, A.L., and Streit, A. (2020). Cell fate decisions during the development of the peripheral nervous system in the vertebrate head. Curr Top Dev Biol *139*, 127-167.

Thisse, B., Pflumio, S., Fürthauer, M., Loppin, B., Heyer, V., Degrave, A., Woehl, R., Lux, A., Steffan, T., Charbonnier, X.Q., *et al.* (2001). Expression of the zebrafish genome during embryogenesis. (ZFIN Direct Data Submission.).

Thompson, A.J., Pillai, E.K., Dimov, I.B., Foster, S.K., Holt, C.E., and Franze, K. (2019). Rapid changes in tissue mechanics regulate cell behaviour in the developing embryonic brain. Elife *8*.

Tlili, S., Durande, M., Gay, C., Ladoux, B., Graner, F., and Delanoe-Ayari, H. (2020). Migrating Epithelial Monolayer Flows Like a Maxwell Viscoelastic Liquid. Phys Rev Lett *125*, 088102.

Tlili, S., Yin, J., Rupprecht, J.F., Mendieta-Serrano, M.A., Weissbart, G., Verma, N., Teng, X., Toyama, Y., Prost, J., and Saunders, T.E. (2019). Shaping the zebrafish myotome by intertissue friction and active stress. Proc Natl Acad Sci U S A *116*, 25430-25439.

Tofangchi, A., Fan, A., and Saif, M.T.A. (2016). Mechanism of Axonal Contractility in Embryonic Drosophila Motor Neurons In Vivo. Biophys J *111*, 1519-1527.

Torres-Paz, J., Tine, E.M., and Whitlock, K.E. (2020). Dissecting the neural divide: A continuous neurectoderm gives rise to both the olfactory placode and olfactory bulb. Int J Dev Biol.

Torres-Paz, J., and Whitlock, K.E. (2014). Olfactory sensory system develops from coordinated movements within the neural plate. Dev Dyn *243*, 1619-1631.

Trevers, K.E., Prajapati, R.S., Hintze, M., Stower, M.J., Strobl, A.C., Tambalo, M., Ranganathan, R., Moncaut, N., Khan, M.A.F., Stern, C.D., *et al.* (2018). Neural induction by the node and placode induction by head mesoderm share an initial state resembling neural plate border and ES cells. Proc Natl Acad Sci U S A *115*, 355-360.

Vacaru, A.M., Unlu, G., Spitzner, M., Mione, M., Knapik, E.W., and Sadler, K.C. (2014). In vivo cell biology in zebrafish - providing insights into vertebrate development and disease. J Cell Sci *127*, 485-495.

Van Essen, D.C. (1997). A tension-based theory of morphogenesis and compact wiring in the central nervous system. Nature *385*, 313-318.

Varga, Z.M., Wegner, J., and Westerfield, M. (1999). Anterior movement of ventral diencephalic precursors separates the primordial eye field in the neural plate and requires cyclops. Development *126*, 5533-5546.

Venkiteswaran, G., Lewellis, S.W., Wang, J., Reynolds, E., Nicholson, C., and Knaut, H. (2013). Generation and dynamics of an endogenous, self-generated signaling gradient across a migrating tissue. Cell *155*, 674-687.

Versaevel, M., Grevesse, T., and Gabriele, S. (2012). Spatial coordination between cell and nuclear shape within micropatterned endothelial cells. Nat Commun *3*, 671.

Vihtelic, T.S. (2008). Teleost lens development and degeneration. Int Rev Cell Mol Biol *269*, 341-373.

Villedieu, A., Bosveld, F., and Bellaiche, Y. (2020). Mechanical induction and competence in epithelial morphogenesis. Curr Opin Genet Dev *63*, 36-44.

Voas, M.G., Glenn, T.D., Raphael, A.R., and Talbot, W.S. (2009). Schwann cells inhibit ectopic clustering of axonal sodium channels. J Neurosci *29*, 14408-14414.

Vuong-Brender, T.T., Ben Amar, M., Pontabry, J., and Labouesse, M. (2017). The interplay of stiffness and force anisotropies drives embryo elongation. Elife *6*.

Wakisaka, N., Miyasaka, N., Koide, T., Masuda, M., Hiraki-Kajiyama, T., and Yoshihara, Y. (2017). An Adenosine Receptor for Olfaction in Fish. Curr Biol *27*, 1437-1447 e1434.

Walko, G., Castanon, M.J., and Wiche, G. (2015). Molecular architecture and function of the hemidesmosome. Cell Tissue Res *360*, 363-378.

Wang, K.H., Brose, K., Arnott, D., Kidd, T., Goodman, C.S., Henzel, W., and Tessier-Lavigne, M. (1999). Biochemical purification of a mammalian slit protein as a positive regulator of sensory axon elongation and branching. Cell *96*, 771-784.

Wang, N., Tytell, J.D., and Ingber, D.E. (2009). Mechanotransduction at a distance: mechanically coupling the extracellular matrix with the nucleus. Nat Rev Mol Cell Biol *10*, 75-82.

Wang, Y., Meng, F., and Sachs, F. (2011). Genetically encoded force sensors for measuring mechanical forces in proteins. Commun Integr Biol *4*, 385-390.

Weiss, P. (1941). Nerve patterns: the mechanics of nerve growth;. Third Growth Symposium *5*, 163-203.

Whitlock, K.E. (2006). The sense of scents: olfactory behaviors in the zebrafish. Zebrafish *3*, 203-213.

Whitlock, K.E. (2008). Developing a sense of scents: plasticity in olfactory placode formation. Brain Res Bull *75*, 340-347.

Whitlock, K.E., and Westerfield, M. (1998). A transient population of neurons pioneers the olfactory pathway in the zebrafish. J Neurosci *18*, 8919-8927.

Whitlock, K.E., and Westerfield, M. (2000). The olfactory placodes of the zebrafish form by convergence of cellular fields at the edge of the neural plate. Development *127*, 3645-3653.

Whitlock, K.E., Wolf, C.D., and Boyce, M.L. (2003). Gonadotropin-releasing hormone (GnRH) cells arise from cranial neural crest and adenohypophyseal regions of the neural plate in the zebrafish, Danio rerio. Dev Biol *257*, 140-152.

Woo, K., and Fraser, S.E. (1995). Order and coherence in the fate map of the zebrafish nervous system. Development *121*, 2595-2609.

Wu, Z., Makihara, S., Yam, P.T., Teo, S., Renier, N., Balekoglu, N., Moreno-Bravo, J.A., Olsen, O., Chedotal, A., Charron, F.*, et al.* (2019). Long-Range Guidance of Spinal Commissural Axons by Netrin1 and Sonic Hedgehog from Midline Floor Plate Cells. Neuron *101*, 635-647 e634.

Xiong, F., Ma, W., Benazeraf, B., Mahadevan, L., and Pourquie, O. (2020). Mechanical Coupling Coordinates the Co-elongation of Axial and Paraxial Tissues in Avian Embryos. Dev Cell *55*, 354-366 e355.

Xu, H., Dude, C.M., and Baker, C.V. (2008). Fine-grained fate maps for the ophthalmic and maxillomandibular trigeminal placodes in the chick embryo. Dev Biol *317*, 174-186.

Xu, Q., and Wilkinson, D.G. (1998). In situ hybridization of mRNA with hapten labelled probes. . In In Situ Hybridization: A Practical Approach, W.D. G, ed. (Oxford: Oxford University Press), pp. 87-106.

Yang, B., Zhang, F., Cheng, F., Ying, L., Wang, C., Shi, K., Wang, J., Xia, K., Gong, Z., Huang, X.*, et al.* (2020). Strategies and prospects of effective neural circuits reconstruction after spinal cord injury. Cell Death Dis *11*, 439.

Yin, J., Morrissey, M.E., Shine, L., Kennedy, C., Higgins, D.G., and Kennedy, B.N. (2014). Genes and signaling networks regulated during zebrafish optic vesicle morphogenesis. BMC Genomics *15*, 825.

Yoshihara, Y. (2014). Zebrafish Olfactory System. In The Olfactory System., M. K., ed. (Tokyo: Springer).

Zhang, H., Landmann, F., Zahreddine, H., Rodriguez, D., Koch, M., and Labouesse, M. (2011). A tension-induced mechanotransduction

pathway promotes epithelial morphogenesis. Nature *471*, 99-103.

Zhang, J., Bai, S., Zhang, X., Nagase, H., and Sarras, M.P., Jr. (2003). The expression of gelatinase A (MMP-2) is required for normal development of zebrafish embryos. Dev Genes Evol *213*, 456-463.

Zheng, J., Lamoureux, P., Santiago, V., Dennerll, T., Buxbaum, R.E., and Heidemann, S.R. (1991). Tensile regulation of axonal elongation and initiation. J Neurosci *11*, 1117-1125.

List of Figures

Legends coming from the initial article of the figure are indicated with brackets and in italics.

Figure 1: **Structure of a typical neuron** with the cell body (soma) and the neurites, comprising the dendrites and axon covered with myelin sheaths. (NIH-Website, 2021) 14

Figure 2 : **Schematic illustration of the diversity of neuronal guidance mechanisms**. Neuronal processes are guided by chemical cues that can function at long and short distances to mediate either attractive or repulsive guidance. (Kolodkin and Tessier-Lavigne, 2011) 16

Figure 3: **Conserved families of guidance molecules (A) and their receptors (B)**. (Dickson, 2002)..... 18

Figure 4: **Structure of the growth cone and origin of forces**. (a) Schematic drawing of a neuronal growth cone and its cytoskeleton divided in the P domain (periphery), the T domain (transition zone) and the C domain (central zone). "*Actin filaments (red) are connected to the extracellular environment via molecular clutches, which are assembled in point contacts (green). Point contacts are found mainly in the P domain, while myosin II motors (cyan) are localized in the C domain*." (b) Schematic drawing of force generation within growth cones. (c) Schematic drawing of forces acting in growth cones. The length of the arrows correspond to the strength of the represented forces. (Franze, 2020) 20

Figure 5: **Schematic representation for the neuronal movements in the environmental gradients**. (Seo et al., 2020) 22

Figure 6: **Examples of mechanical cues involved in axon and synapse development**. (Gangatharan et al., 2018) 23

Figure 7: **Cultured neurons from different neuronal tissues respond differently to the stiffness of the substrate.** *"(A) Dorsal root ganglion (DRG) and hippocampal neurons grown on soft (300 Pa), intermediate (1000 Pa), and rigid substrates (5000 Pa), fixed and stained for actin filaments at 8 h (DRG) or 24 h (hippocampal). Scale bars are 10 mm. (B and C) Neurite outgrowth of hippocampal (B) and DRG (C) neurons on Laminin-coated polyacrylamide substrates of different stiffness. Total neurite length is normalized to the mean value at 1000 Pa to allow for comparison between independent experiments. Values represent the mean of at*

least three independent experiments. Error bars indicate the standard errors." (Koch et al., 2012)..... 25

Figure 8: **Elongation of a minor process induced by experimentally applied tensile force**. *"(A) Neuron immediately before needle application. Arrowhead marks short process to which needle was attached. (B) Same neuron 30 min later during early stage of neurite towing. (C) 5 h 40 min after B, at the end of towing. The scale bar is 20 µm."* (Lamoureux et al., 2002) 27

Figure 9: **Axon tracts grown to 5 cm long by artificial stretch growth.** *"Axon tracts (middle) bridge two populations of neurons (left and right). Before the initiation of stretch growth, the two populations of neurons were adjacent and the bridging axons were only about 100 µm long. Progressively separating the neuron populations induced mechanical tension on the axon tracts, resulting in enormous and rapid growth (colors are inverted to highlight axon tracts)."* Adapted from (Pfister et al., 2004)..... 29

Figure 10: **Mechanical forces influence every phase of neuronal growth**. (De Vincentiis et al., 2020b)..... 30

Figure 11: **Schematics of the proposed mechanism for axon pathfinding depending on surrounding brain stiffness.** (a) Outline of a Xenopus brain and the optic tract. (b) *"Schematic illustration of a mechanism by which axon bundles encountering a perpendicular stiffness gradient might turn toward the softer side of the substrate."* (Koser et al., 2016)..... 32

Figure 12: **Schematic view of the proposed mechanism connecting tension, cytoskeleton dynamics, vesicle transport and accumulation.** *"(A) A schematic diagram of an axon in its normal resting state. Microtubules (green) extend along the axon and are crosslinked (black) together to form a network. Vesicles (cyan) are attached to molecular motors (brown) that transport them along the microtubule network and some accumulate in the actin scaffolding (red) at the synapse. (B) Microtubules depolymerize under compression leading to disrupted vesicle transport while maintaining normal vesicle accumulation at the synapse. (C) A stretched axon exhibits increased vesicle accumulation at the synapse due to tension induced actin polymerization creating more vesicle binding sites."* (Ahmed et al., 2012)..... 34

Figure 13: **Schematic illustrating the variety of vertebrate cranial placodes and of their cellular derivatives.** (Schlosser, 2010) 37

Figure 14: **Schematic representation of the position of placodal precursors and placodal structures respectively before and after placode assembly.** *"(A) Schematic view of placode progenitors scattered and intermixed within the pan-placodal region (PPR) surrounding the anterior neural plate at the 1s stage (dorsal view of a theoretical vertebrate). (B) Compact and individualised placodes occupying specific positions along the anteroposterior axis of the embryo from mid-somitogenesis stages onwards (dorsal view, the ventral position of the adenohypophysis is indicated by the dotted line surrounding the placode). Anterior to the left."* (Breau and Schneider-Maunoury, 2014) 38

Figure 15: **Schematic representation of the two models for the induction of the PPR at the neural plate border.** (Left) Neural plate border model with the common neural plate border region represented in purple, the signals from adjacent epidermis by red arrows and the signals from the adjacent neural plate by red arrows. (Right) Binary competence model with neural and nonneural competence territory represented respectively in light green and light yellow. (Schlosser, 2014) 40

Figure 16: **Placode assembly seen as a two-step developmental process**. "*Fate map studies suggest two sequential steps in placode formation: segregation of intermingled placodal precursors into immiscible but still juxtaposed placodal domains (initial segregation), and further compaction resulting in discrete and condensed placodes separated by non-placodal tissues (secondary coalescence). In the upper panel, the coloured balls represent progenitors of adjacent placodes, whether or not they are specified."* (Breau and Schneider-Maunoury, 2014) 41

Figure 17: **Schematics describing the models that lead to initial segregation of the PPR domain.** *"(Model 1). Large-scale sorting out of early-specified intermingled placodal precursors. Specified placodal precursors initially present a high degree of intermixing and actively sort-out from each other by differential adhesion (Model 1a) or directional migration (Model 1b). (Model 2). Random movements preceding specification of placodal identities by surrounding signalling centres. Unspecified progenitors undergo random movements within the PPR before being specified by environmental signals. Further patterning mechanisms (cross-repression of transcription factors) lead to the formation of a sharp boundary between placodal domains. Grey and coloured balls represent unspecified and specified placodal progenitors, respectively."* (Breau and Schneider-Maunoury, 2014) 42

Figure 18**: Scanning electron microscopy image of the left side of an adult zebrafish head showing the eye (e), the incurrent (in) and excurrent (ex) nostril** and the openings of the cephalic lateral line system (l l). Scale bar = 0.5mm. (Hansen and Zeiske, 1993) 45

Figure 19: **Schematic representation of the organization of the zebrafish olfactory system.** *"(A) Localization of the olfactory system in zebrafish. Dorsal side is shown; rostral side is located upwards. (B) Olfactory organ morphology. Olfactory sensory epithelium forming a rosette structure arranged in lamellae is shown in black. (C) Olfactory epithelium (OE) composed of the following sensory neurons (OSNs): microvillous (mv), ciliated (cl), crypt (cr), kappe (kp) and pear (pr) OSNs. OSNs extend their axons to the olfactory bulb via the olfactory nerve (ON) to form discrete glomeruli. (D) olfactory bulb organization in three laminae: olfactory nerve layer (ONL); glomerular layer (GL) and intracellular layer (ICL).*" Adapted from (Calvo-Ochoa and Byrd-Jacobs, 2019) 47

Figure 20: **Representation of the olfactory placode and telencephalon fields lineage tracing at 4-5 s (11-11.5 hpf) and the corresponding cell locations at 50 hpf.** *"(A) Schematized dorsal view of the anterior end of 12 h embryo with anterior towards the top of the page. The blackened border extending along the anteroposterior axis approximately represents the border between the fields of cells giving rise to olfactory organ and those giving rise to telencephalon. The transverse blackened border represents the anterior limits of premigratory cranial NC. (B) Schematized ventral view of a 50 h zebrafish head with anterior towards the top of the page. Right-hand olfactory organ: the olfactory organ has been subdivided into four coloured areas. Clones in these areas were colour coded in diagram A. Left hand olfactory organ: sensory neurons with axons extending into the CNS at 50 h come predominantly from red cells, pioneer neurons come from orange cells but only in the region abutting the telencephalic field anteriorly. The pituitary clones come from the non-coloured cells most anterior in the neural plate between the two blackened borders."* The cells are colour coded with respect to their future fates in the developing olfactory organ and bulb at 50 h: red, orange, green and blue cells contribute to the olfactory organ, yellow cells give rise to clones in the telencephalon. (Whitlock and Westerfield, 2000)..... 49

Figure 21: **Whole-mount *in situ* hybridization analysis of *cxcr4b* and *cxcl12a* expression during development of the OP in zebrafish**. From 14 to 16 hpf (10 s to 14 s), *cxcr4b* is expressed bilaterally along the lateral edge of developing neural tube (C,E), whereas *cxcl12a* is expressed medially, in the anterior brain (telencephalon), adjacent to the *cxcr4b*-expressing

bilateral stripes (D,F). Progressive convergence of *cxcr4b*-expressing domains occurs between 16 and 20 hpf (14-22 s) (E,G,I) to form the OPs. *cxcr4b* expression in the OP persists during the initial phase of axon pathfinding (K). At the same period, *cxcl12a* expression is detected at the OP-telencephalon border (J, arrowheads in L), as well as in the anterior tip of the telencephalon. Adapted from (Miyasaka et al., 2007). 51

Figure 22: **Schematic description of the two movements sculpting OP morphogenesis.** *"Cells from OP extremities converge towards the centre through active migration along the brain surface (red arrows), while cell bodies of central cells passively move away from the brain (blue arrows). As they move laterally, central neurons keep contact with the brain surface through long cytoplasmic protrusions, thereby initiating the elongation of their axons (blue cells). Axons thus extend through movements of cell bodies away from static axon tips, a process referred to as retrograde axon extension. The red circle indicates the future entry point of axons in the brain."* Adapted from (Breau et al., 2017)..... 52

Figure 23: **Schematic representation of the suggested models for the mechanical forces driving passive retrograde axon extension in the OP** Compression exerted by actively converging cells from placode extremities is represented with red arrows while traction force exerted by eye morphogenetic movements is represented with cross-hatched green arrow. Adapted from (Breau et al., 2017)..... 54

Figure 24: ***Tg(8.4neurog1:gfp)*** **line as a marker of a subpopulation of zebrafish OP neurons**. *"(A-F) Single confocal sections of OPs showing co-expression of HuC/D (A-C) or Zns-2 (D-F) with GFP from the Tg(8.4neurog1:gfp) transgene at 24 hpf. (G-L) Single confocal sections of OPs showing immunolabelling of HuC/D (G-I) or in situ hybridisation and immunolabelling of Omp (J-L) and GFP from the Tg(8.4neurog1:gfp) transgene at 48 hpf. Whereas all GFP-positive cells in the placode are HuC/D- and Zns-2-positive at 24 hpf, at 48 hpf HuC/D+/GFP– cells are present; little, if any, overlap is detected between the expression of omp transcripts and GFP at 48 hpf. (M,N) Schematics of OPs at 24 hpf (M) or 48 hpf (N). EONs are shown in green and OSNs in red. A, anterior; L, lateral; M, medial; P, posterior; T, telencephalon. The scale bars are 10 µm."* (Madelaine et al., 2011)..... 57

Figure 25: **Schematic representation of the OSN rosette and the pioneer neurons, and of the chemical cues involved in pathfinding of OSN axons towards their target glomeruli.** *"(A) Cxcl12a/Cxcr4b signalling guides the pioneer axons to exit the OP. (B) Slit/Robo2*

repulsive signalling guides the pioneer axons toward the presumptive olfactory bulb (OB) by preventing them from entering into inappropriate area. Slit/Robo2 signalling and Anosmin-1a are required for fasciculation of olfactory axons before entering into the OB. Netrin1/DCC attractive signalling draws the pioneer/OSN axons into the OB. (C) Netrin1/DCC signalling guides the axons of OSNs expressing particular ORs to terminate on a specific glomerular cluster." (Miyasaka et al., 2013)..... 59

Figure 26: **Time lapse images showing the migration of cranial NCCs (sox10:EGFP line; green) and the coalescence of OP precursors (six4b:mCherry line, red).** Dorsal views with anterior to the left. (Harden et al., 2012)..... 60

Figure 27: **Classical chemical induction versus mechanical induction.** "*This diagram illustrates the analogy between classical chemical induction (grey font) and mechanical induction (black font), whereby the signal sent by the inducer tissue (red) results in an effect in the responder tissue (blue). For classical induction the signal is a secreted morphogen, while for mechanical induction, the signal is a mechanical force. The competence of the responder (green) refers to the ability of the signal-receiving tissue to respond to the signal sent by the inducer. In classical induction, the secreted signal induces a cell fate change in the responder tissue, whereas in mechanical induction, the mechanical signal triggers a morphogenetic response (deformation or flows)."* (Villedieu et al., 2020)..... 63

Figure 28: **Classification of typologies of mechanically interacting tissues during morphogenesis.** Inducer (red) and responder (blue) tissues can be either adjacent or located in different planes (C). The forces exerted by inducer tissue on responder tissue can be perpendicular to the edge (A) or tangential (B). The two last lines of the table respectively list the inducer morphogenetic movements (red) and the consequent responder movements (blue). (adapted from (Villedieu et al., 2020))..... 64

Figure 29**: Schematic of the two main mechanisms involved in germ band extension.** Cell intercalation and posterior midgut (PMG) invagination contribute to germ band extension. "*Red arrows indicate stresses and black arrows strains (cell intercalation and tissue extension). In wt embryos intrinsic forces due to MyoII promote cell intercalation and junction growth. Extrinsic forces properly orient junction growth allowing net tissue extension.*" (Collinet et al., 2015)..... 66

Figure 30: **Schematic representation of enveloping cell layer (EVL, black) spreading during epiboly.** *"Animal pole is to the top. Yolk cell and yolk syncytial layer (YSL), light gray; blastoderm (EVL and deep cells), dark gray. The red rectangle demarcates regions of the EVL-YSL boundary where the study focuses later on. The black rectangle demarcates the region of the enlarged sagittal view outlining the tissue structure at 8 hpf. The actomyosin network (red on the enlarged view) is denser at the EVL/YSL interface; the contact between EVL and YSL is mediated by tight junctions (blue)."* (Schwayer et al., 2019) 68

Figure 31: **interaction between neurectoderm (ecto) and prechordal plate (ppl) during zebrafish gastrulation.** *"(a,c) Bright-field/fluorescence images of a Tg(gsc:GFP) zebrafish embryo at 7 hpf; GFP-labelled prechordal plate (ppl) leading edge cells are indicated (white arrowheads); the rectangle in c marks the magnified area in e; the dashed lines in (a) indicate axial mesendoderm (white), and in (c) ectoderm/ppl (white), yolk syncytial layer (YSL)/ppl (yellow), enveloping layer (EVL)/media (pink) and EVL/YSL (blue) interfaces; embryonic axis orientation as marked in (b),(d) for same views. (b,d) Illustration of embryonic (anterior (ppl) and posterior axial mesendoderm (pm), paraxial mesoderm (pam) and ecto) and extra-embryonic (YSL, EVL, yolk) tissues, and their respective direction of movement during gastrulation at the dorsal side of the zebrafish embryo; arrows in (b),(d) indicate animal–vegetal (A–V), left–right (L–R) and dorsal–ventral (D–V) embryonic axes. (e) A magnified view of the boxed area in c showing neighbouring ppl (green) and overlying ectoderm (red pseudocoloured) tissues; dashed lines as in (c)."* (Smutny et al., 2017)..... 70

Figure 32: **Schematic view of *C elegans* embryonic elongation: during the first phase, the interplay of stiffness and force anisotropy drives embryo elongation and during the second phase, muscle contractions drive the epidermis anteroposterior extension.** *"C. elegans embryonic elongation requires an actomyosin force in lateral cells (blue) and actin-promoted stiffness in dorsoventral cells (yellow), followed by repeated muscle contractions (red), which induce mechanotransduction pathway."* Adapted from (Lardennois et al., 2019)..... 72

Figure 33: **Schematic representation of zebrafish myotome formation and shaping and of the adjacent tissues**. (B) transverse section with the cross-sectional views shown in (C) and (C') represented in dark and light blue. The developing somites are composed of slow muscle cells (dark blue) and fast muscle cells (red) and they progressively form from the presomitic mesoderm (PSM) and gradually acquire a chevron shape. Myotomes are adjacent to the neural

tube (light blue), the notochord (green) and ventral tissues (yellow). The mechanical coupling between the forming myotome and these adjacent tissues results in a spatially heterogeneous friction, which is sufficient to initiate myotome shape change. (Tlili et al., 2019) 74

Figure 34: **Schematics of the mechanical interaction between converging neural tube (purple) and laterally expanding paraxial mesoderm (light blue).** *"Too much matrix deposition maintains the symmetry, but slows down the convergence due to high resistance, and predisposes the neural tube to spina bifida-like phenotype with an open neural tube (cdh2 mutant, left panel). Conversely, reduction in matrix deposition helps the neural tube convergence by reducing the resistance (as shown by the rescue of neural tube convergence in double cdh2; itga5 mutants), but it produces local tissue detachment and breaks the mechanical coupling between the tissues generating left-right asymmetries (itga5 mutants, right panel)."* (Guillon et al., 2020) 76

Figure 35: **Schematic representation of *Tribolium* gastrulation.** "*Lateral view of a gastrulating Tribolium embryo in a schematic (top), and in a maximum intensity projection of a line that transiently expresses LifeAct-eGFP (green), imaged by time-lapse light-sheet microscopy (bottom). The blastoderm moves unidirectionally towards and across the posterior pole (dashed arrow and asterisk) and the anterior–ventral part of the blastoderm remains stationary (red circle). Scale bar, 100 μm*." Anterior to the left and posterior to the right. Adapted from (Munster et al., 2019). 78

Figure 36: **Development of the vertebrate, spider and cephalopod eyes.** (Koenig and Gross, 2020) 86

Figure 37: **Schematic view of zebrafish optic cup morphogenesis** with first the evagination of cells from the brain to form lateral optic vesicle and then the bending into an optic cup. .. 87

Figure 38: **Overview of vertebrate eye morphogenesis** (Fuhrmann, 2010) 88

Figure 39: **Schematic representation of zebrafish eye morphogenesis.** *"Eye field specification in the anterior portion of the neural plate at 9 hpf (1) is followed by the rearrangement of the tissue as the neural plate folds into a keel at 11.5 hpf (2), and the evagination of the optic vesicles at 13 hpf (3). Subsequent folding of the optic vesicle over itself leads to the formation of the optic cup at 18 hpf (4). Top-left panel is a dorsal view with anterior to the left; the orientation of all the other panels is indicated in the figure. tel: telencephalon;*

hyp: hypothalamus; RPE: retinal pigment epithelium; ef: eye field; NR: neural retina." (Cavodeassi, 2018) 89

Figure 40: **Schematic frontal view of cell reorganization during optic vesicle evagination in zebrafish.** *"In the wt eye field, cells organize and polarize precociously as compared to cells in other regions of the neural plate. Cells at the margin of the eye field (blue) acquire a monolayered epithelium-like organization from 4 s (11 hpf), prior to the onset of optic vesicle evagination; subsequently, cells at the core of the eye field (green) integrate into the marginal epithelium by intercalating among the marginal cells. At late stages of optic vesicle morphogenesis, around 11 s (14.5 hpf), eye cells shorten and acquire the final dorsoventral orientation characteristic of optic vesicle neuroepithelial cells."* (Ivanovitch et al., 2013). .. 91

Figure 41: **Expression pattern of *rx3* and morphological analysis of the *rx3*^{s399} (*chokh*) phenotype.** (A-A') Whole-mount *in situ* hybridization analysis of *rx3* in *wt* embryos and *chokh* mutants at 14 hpf. Dorsal view. (B-D') Bright field images at 24 hpf (B-B') or at 48 hpf (C-D') in lateral view (B-C') or dorsal view (D-D'). fb, forebrain; hb, hindbrain; mb, midbrain. (adapted from (Loosli et al., 2003)) 93

Figure 42: **Gene co-expression network of Rx3 regulated genes**. Red: downregulated in *rx3*$^{-/-}$ embryos. Green: upregulated in *rx3*$^{-/-}$ embryos. (Yin et al., 2014)..... 95

Figure 43: **Invagination angle** represented with dashed lines on a confocal scan of optic cup at 30 s stained for phalloidin. Asterisk marks the developing lens. (Sidhaye and Norden, 2017) 96

Figure 44: **Schematic representation of the different mechanisms involved in optic cup invagination** "(*A) Intraepithelial filopodia, (B) Basal constriction, (C) Apical constriction, and (D) Rim involution mechanisms are represented. In each one of the panels, the direction of morphogenetic forces is indicated with solid red arrows and cells displacement trajectories with dotted red arrows. The morphology of representative cells is also depicted. Ls, lens; nr, neural retina; rpe, retinal pigment epithelium*." (Martinez-Morales et al., 2017)..... 97

Figure 45: **Schematic of the concerted action of basal cell area shrinkage and rim involution to shape the hemispheric retinal neuroepithelium** *"(B) In control conditions, invagination is driven by basal area reduction that is guided by basally enriched actomyosin-driven constriction and overall compaction by increasing number of cells. Rim involution is*

driven by collective and directed migration of the epithelium at the rim of the developing optic cup. Protrusive migratory dynamics of rim cells change to adherent behaviour when cells reach the inner layer. (C) Effect of cellular perturbations on the retina neuroepithelial architecture. (i) Loss of basal actomyosin enrichment slows the invagination process, which can result in a wider optic cup. (ii) Perturbation of lamellipodial membrane protrusions affects the migratory behaviour and the optic cup architecture, resulting in an S-shaped optic cup. (iii) Perturbation of cell-ECM adhesion results in both loss of basal actomyosin accumulation in the invaginating zone and perturbed lamellipodial membrane protrusions in the rim zone. Such combined effect leads to a severe optic cup phenotype." (Sidhaye and Norden, 2017) 99

Figure 46: **Schematic diagram of the time line of RPE spreading during zebrafish eye morphogenesis.** "*The top arrows (yellow to green) indicate the salient events in RPE development whereas bottom arrows (yellow to magenta) those related to the entire eye primordium. Eye structures are color coded: progenitors, light yellow; lateral/neural retina layer, dark pink; medial/RPE layer, green. BC, basal constriction; F, flattening; L, virtual lumen; LL, lateral layer; ML, medial layer; NR, neural retina; pNR, prospective neural retina; R, rim region; RM, rim movements; RPE, retinal pigment epithelium; pRPE, prospective RPE.*" (Moreno-Marmol et al., 2018)..... 101

Figure 47: **Schematic 3D view of the optic cup at 24s (22hpf)** representing the patterning into proximal/distal and nasal/temporal domains..... 103

Figure 48: **Summary diagram representing the progressive stages of zebrafish lens morphogenesis**. *"Cell membranes have been pseudocolored. A: At approximately16 hpf. The cells in the surface ectoderm are represented in orange, and the cells in the lens placode in purple. B: At 18 hpf. Elongating fibre-like cells are represented in blue. C: At 20 hpf. The cells in the organizing centre (red) of the delaminating and elongated lens mass are surrounded by columnar primary fibre cells (blue). D–F: At 22 hpf, 23 hpf, and 24 hpf, respectively. Delamination completes the separation of the spherical lens from the developing cornea. Morphologically undifferentiated cells at the anterior surface of the lens mass (yellow) appeared to reorganize and lose adhesion contacts with the surface ectoderm."* (Greiling and Clark, 2009)..... 104

Figure 49: **Model for retinal patterning and morphogenesis along the nasal-temporal axis** n, nasal; t, temporal. Adapted from (Picker et al., 2009). 107

Figure 50: **Model of optic cup morphogenesis in normal condition (*wt*) and in the absence of NCC surrounding the eye (*tfap2a;foxd3* double-mutant)**. *"(A,B) Optic cup morphogenesis in a wt zebrafish embryo. NCCs migrate around the optic vesicle and enable efficient movement of optic vesicle cells (A). Cells undergo rim movement and contribute to the neural retina, partially enabled by the presence of a continuous basement membrane along the surface of the RPE (B). (C,D) Optic cup morphogenesis in a tfap2a;foxd3 double-mutant embryo. Most NCCs are absent, resulting in optic vesicle cells that move faster and farther than those in wt embryos (C). Rim movement is impaired in the absence of a complete, continuous basement membrane around the RPE, resulting in optic cup malformations (D)."* (Bryan et al., 2020)..... 108

Figure 51: **Graphic representation of OP morphogenesis from 12 hpf to 27 hpf with the local source of chemo-attractant (orange) and the border with the brain (blue).** Dorsal view of the OP as visualised with the *ngn1:gfp* transgene. The early (12-18 hpf; black) and late (18-27 hpf; grey) phases of morphogenesis are noted in the time line. Adapted from (Aguillon et al., 2020)..... 160

Figure 52: *In situ* hybridization for the ligand cxcl12a and the receptor cxcr4b in *rx3-/-* embryos and control siblings at 18-20 s (18-19 hpf). Dorsal views. 160

Figure 53: **Transplantation of *wt* cells in *rx3*$^{-/-}$ mutants.** (A) Schematic view of the transplantation experiments. The donor is at high stage (3.3 hpf) while the host is at shield stage (6 hpf). (B) Schematic frontal view of the expected situation obtained by transplantation of *wt* cells in *rx3*$^{-/-}$ mutant hosts. The red ovals symbolize the OPs that are thicker along the mediolateral axis in *wt* situation compared to *rx3*$^{-/-}$ mutant. 162

Figure 54: **Confocal images of the placode (left) and a small optic cup (right) obtained by transplantation of *wt* H2B:RFP cells in *rx3*$^{-/-}$ *ngn1:gfp* mutant.** Dorsal view, maximum projection of a 40 µm stack. The two images are taken from the same embryo at 24 s (21 hpf) at different depth within the tissues. The OP and the bended optic cup are surrounded by a white line..... 163

Figure 55: **Images of four embryos at 24 s (22 hpf) illustrating the variability of EGFP-F2A-Rac1^{DN} expression and the associated eye phenotype** (45 embryos analysed including 19 with GFP fluorescence)..... 165

Figure 56: **Aspiration of cells in the presumptive eye domain in *wt* embryos.** (A) Schematic view of the aspiration experiments carried out at shield stage (6 hpf). (B) Schematic frontal view of the expected situations obtained by asymmetric aspiration of presumptive eye cells in *ngn1:gfp* embryos at 24 s (21 hpf). The red ovals symbolize the OPs that are thicker along the mediolateral axis in the presence of eyes than in the absence of eyes. 166

Figure 57: **Confocal images of an embryo where presumptive eye cells have been aspirated on one side, resulting in a smaller left eye.** (A, B) Z-sections in the placodes. White double arrows show the mediolateral dimension of the left and the right placodes (respectively around 52 µm and 40 µm). (C) Z-sections in the eyes (90 µm more ventral). Dorsal views. The two sides of the embryo have been imaged separately and the dashed line indicate where the two images have been combined. 167

Figure 58: **Phenotypes of wild-type (WT) and *cyclops* (*cyc^{m122}*) embryos at 28 hpf.** (A,G) Lateral views. (B,H) Frontal views. Arrows indicate the position of the lens. (Schier et al., 1996) 171

Figure 59: **Localization and description of three main processes driving optic cup invagination.** (Top) Schematic representation of an optic cup and of the localization of the different processes contributing to eye invagination (Dorsal view) (A) Cells in the centre of the distal layer of the optic vesicle undergo basal constriction. (B) Cells at the periphery move around the rim and into the distal layer. This movement is represented here at the posterior edge but also occurs at the anterior edge close to the OP. (C) Cells in the proximal layer flatten and spread to form the RPE. (Casey et al., 2021) 172

Figure 60: **Schematics of the phenotypes obtained in *wt* embryos (left), *rx3$^{-/-}$* mutants (right) and in *rx3$^{-/-}$* host mutants with transplanted *wt* cells forming small optic cups (middle).** The red ovals symbolize the OPs that are thicker along the mediolateral axis in *wt* situation compared to the two other situations. Different mechanisms can be suggested to explain the OP phenotype observed in the transplanted situation: a reduced eye cell number, a farther distance between the eye and the OP and a decrease in the amplitude of morphogenetic movements in the eye. 174

Figure 61: **Secretory pathway components studied in zebrafish.** Secretory pathway proteins implicated in human disease are shown in black with corresponding zebrafish tools to study

these in red. Sec13 is a component of the outer shell of the COPII vesicle coat, involved in vesicle trafficking from the endoplasmic reticulum (ER) to the Golgi. NTD, neural tube defects; CLSD, cranio-lenticular-sutural dysplasia; CDAII: congenital dyserythropoietic anemia II; CMRD, chylomicron retention disease; LGMD, limb girdle muscular dystrophy; SEDL, X-linked spondyloepiphyseal dysplasia tarda; ID, intellectual disability" (Vacaru et al., 2014) 178

Figure 62: **Schematic view of the supracellular laser cuts (green lines) and the tension estimated from the initial recoil velocity after these cuts (green arrows)**. To note, here the estimations of the tension are grossly represented by the length of the arrows according to the mean velocity measured (Article figure 5). 182

Figure 63: **Confocal image of a 10 µm fluorescent oil droplet injected in the OP centre of a *ngn1:gfp* embryo and imaged at 14 s** (G. Gangatharan and P. Monnot). 185

Figure 64: **Eye/OP surface of interaction and direction of the forces exerted**. (Left) Confocal images (frontal view) on a live *cldnb:lyn-gfp* embryo at 14 s and 20 s from the same embryo imaged in live. Note the curved interface between eye and OP. (Right) Schematic outline of the three tissues (brain in green, OP in red, eye in blue) and of the two types of eye cell movements that could exert forces on the OP in a frontal view. 186

List of Tables

Table 1: Summary of the approaches used in the studies of intertissue mechanical interactions presented in this section. 82

Table 2: Comparison of several methods to measure forces and stresses *in situ* in living tissues. (Sugimura et al., 2016) 83

Rôle des interactions mécaniques entre tissus dans la mise en place du circuit olfactif du poisson-zèbre

Résumé :

Alors que les signaux biochimiques impliqués dans la croissance axonale et la migration neuronale sont largement étudiés, la contribution des signaux mécaniques dans la formation des circuits neuronaux reste peu explorée *in vivo*. Nous cherchons à étudier comment les forces mécaniques contribuent à la formation du circuit olfactif du poisson-zèbre. Ce circuit se développe durant la morphogénèse de la placode olfactive (PO), par le mouvement passif des corps cellulaires qui s'éloignent de l'extrémité de leurs axones. Mes travaux de thèse s'intéressent à la contribution mécanique de l'œil, qui se forme sous la PO par des mouvements d'évagination et d'invagination, à cette migration passive des neurones et à l'extension de leurs axones.

L'analyse quantitative des mouvements cellulaires a tout d'abord révélé que les mouvements des cellules de la PO et de l'œil sont corrélés. Chez des embryons dans lesquels l'œil ne se développe pas, les mouvements des cellules de la PO sont affectés, ce qui produit des PO plus fines et des axones plus courts, et la tension mécanique dans la direction d'élongation des axones dans la PO est réduite. Enfin, la matrice extracellulaire s'accumule à l'interface œil/PO et sa dégradation enzymatique réduit la corrélation entre les mouvements des cellules de la PO et de l'œil. Ces résultats suggèrent que l'œil en formation exerce des forces de traction sur la PO, transmises par la matrice, entrainant le mouvement des neurones et l'extension des axones.

Ce travail apporte un éclairage nouveau sur le rôle des forces mécaniques échangées entre les neurones en développement et les tissus environnants dans la formation des circuits neuronaux *in vivo*.

Mots clés : [Développent neuronal ; Morphogénèse ; Forces mécaniques ; Circuit Olfactif ; Interactions entre tissus ; Croissance axonale ; Poisson-zèbre]

Role of intertissue mechanical interactions in the formation of the zebrafish olfactory circuit

Abstract:

Whereas the biochemical signals guiding axon growth and neuronal migration are extensively studied, the contribution of mechanical cues in neuronal circuit formation is still poorly explored *in vivo*. We aim at investigating how mechanical forces influence the construction of the zebrafish olfactory circuit. This circuit forms during the morphogenesis of the olfactory placode (OP) by the passive displacement of neuronal cell bodies away from the tip of their axons. My PhD work focuses on the mechanical contribution of the adjacent eye tissue, which develops underneath the OP through extensive evagination and invagination movements, to this passive neuronal migration and to their associated axon elongation.

Quantitative live cell imaging analysis during OP morphogenesis first revealed that OP and eye cells undergo correlated movements. In embryos lacking eyes, the movements of OP cell bodies are affected, resulting in thinner placodes and shorter axons, and the mechanical stress along the direction of axon elongation within the OP is reduced. Finally, extracellular matrix was observed to accumulate at the eye/OP interface, and its enzymatic degradation decreased the correlation between OP and eye cell movements. Altogether, these results suggest that the developing eye exerts traction forces on the OP through extracellular matrix, mediating proper neuronal movements and axon extension.

This work sheds new light on the role of mechanical forces exchanged between developing neurons and surrounding tissues in the sculpting of neuronal circuits *in vivo*.

Keywords: [Neuronal development; Morphogenesis; Mechanical forces; Olfactory circuit; Tissue interactions; Axon growth; Zebrafish]